Analysis of transgenic mouse models of Huntington's disease

by

Mia Deschepper

A thesis submitted to Cardiff University
for the degree of
Doctor of Philosophy

September 2008

Department of Psychological Medicine
Wales School of Medicine
Cardiff University
Heath Park
Cardiff CF14 4XN

ProQuest LLC
789 East Eisenhower Parkway
P.O. Box 1346
Ann Arbor, MI 48106-1346

DECLARATION

This work has not previously been accepted in substance for any degree and is not concurrently submitted in candidature for any degree.

Signed ..... (candidate) Date 25.09.2008

STATEMENT 1

This thesis is being submitted in partial fulfillment of the requirements for the degree of PhD.

Signed ..... (candidate) Date 25.09.2008

STATEMENT 2

This thesis is the result of my own independent work/investigation, except where otherwise stated. Other sources are acknowledged by explicit references.

Signed ..... (candidate) Date 25.09.2008

STATEMENT 3

I hereby give consent for my thesis, if accepted, to be available for photocopying and for inter-library loan, and for the title and summary to be made available to outside organisations.

Signed ..... (candidate) Date 25.09.2008

Acknowledgements

I am most grateful to Dr Lesley Jones for supervising my work, for the inspiration and encouragement she gave me, and for her unfailing faith in me.

I must also thank Dr Bastiaan Hoogendoorn for supervising the SELDI work, and for his valuable support and lab training, at a time I knew very little about it all.

Many others deserve thanks. I must mention particularly Simon Brooks for performing far more micro-dissections that he had originally agreed to, and Sharon Pitts for her extremely valuable assistance with the DIGE experiments.

I especially want to say thanks to Amanda and Lynn who were always ready to help, who gave me the moral support and the courage to keep going, and made me laugh often.

I also want to remember Alan Williams for help with some drawings, which he performed to perfection, as always.

And last, but not least, my long-suffering family, Dickon, Cleo, Thetis and my PhD-baby Flora, who are so relieved that the work is finished, and are still wondering how it can take so long to write a book that so few people will read!

My thanks to you all.

Summary

Huntington's disease (HD) is an autosomal dominant neurodegeneration, characterised by a movement disorder, complex cognitive disturbances and psychiatric problems. The disease is caused by the expansion of a CAG repeat in the HD gene on chromosome 4, giving rise to an expanded glutamine tract in the encoded protein, huntingtin.

Microarray studies have already found substantial changes in gene expression in HD individuals and in transgenic mouse models of HD. However, it was important to determine whether a similar pattern of differential expression could be found at the protein level, in order to assess the significance of the observed gene expression changes to the disease process. For this, the Surface-Enhanced Laser Desorption Ionization - Time Of Flight (SELDI-TOF) system was used to analyse brain protein extracts from genetic mouse models of HD, both from whole brain and microdissected brain samples. Several brain regions and different timepoints of transgenic R6/1 and knock-in Hdh^{Q92} and Hdh^{Q150} mouse models were analysed. To analyse a wider range of the HD mouse brain proteome, Hdh^{Q150} mouse caudate-putamen was analysed using the 2-D fluorescence Difference Gel Electrophoresis (DIGE) system.

Differentially expressed proteins have been detected in brain samples from HD mice, and sixteen of these have been identified using Tandem Mass Spectrometry. Western blot analysis confirmed results for some of the proteins.

The majority of the proteins identified as changed in expression had earlier been reported as changed in gene expression in human HD and mouse HD brain. In general, there is a high degree of agreement between the protein and the gene expression data. Some of the proteins identified in this study have been implicated in HD pathogenesis, and many are part of a pathogenic mechanism recognised to contribute to HD, such as mitochondrial dysfunction and deficient energy metabolism, oxidative stress and aberrant calcium signalling.

Table of contents

List of abbreviations

2-DE	2-D electrophoresis
3-NP	3-nitropropionic acid
ACN	acetonitrile
AD	Alzheimer's disease
ADP	adenosine diphosphate
APOE	apolipoprotein E
appr.	approximate
ATP	adenosine triphosphate
av.	average
bp	base pair
BDNF	brain-derived neurotrophic factor
BP	band pass
BVA	Biological Variation Analysis
CA2	carbonic anhydrase II
CaM	calmodulin
CaN	calcineurin
CaN-A	calcineurin A
CB	cerebellum
CBP	CREB-binding protein
CHAPS	3-[(3-cholamidopropyl)dimethylammonio]-1-propane sulphonate
CHCA	α-cyano-4-hydroxycinnamic acid
CI	confidence interval
CK	creatine kinase
CKB	creatine kinase – brain type

COX	cytochrome C oxidase
COX-VIb	cytochrome C oxidase polypeptide VIb
CP	caudate-putamen
Cyt c	cytochrome c
Da	dalton
dH_2O	distilled water
DIA	Differential In-gel Analysis
DNA	deoxyribonucleic acid
DTT	dithiothreitol
E.	expectation
EAM	energy absorbing molecules
FC	fold change
FKBP12	12 kDa FK506-binding protein
g/l	gram(s) per litre
GLT1	astroglial glutamate transporter 1
GS	glutamine synthetase
h	hour(s)
HAP1	huntingtin-associated protein-1
HC	hippocampus
HD	Huntington's disease
HEPES	4-(2-hydroxyethyl)-1-piperazineethanesulfonic acid
HET	heterozygote
HIP1	huntingtin interacting protein 1
HOM	homozygote
HSP10	10 kDa heat shock protein

HSP60	60 kDa heat shock protein
HSPs	heat shock proteins
HYPB	huntingtin yeast partner B
IAA	iodoacetamide
IEF	isoelectric focusing
Inc.	Incorporated
kb	kilo base pairs
kDa	kilodalton
kVh	kilovolts per hour
L.I.	laser intensity
M	molar
mA	milliampere
MALDI	Matrix-assisted laser desorption/ionization
max.	maximum
MBP	myelin basic protein
MC	motor cortex
mg	milligram
min	minute(s)
ml	millilitre
mm	millimetre
mM	millimolar
MRI	magnetic resonance imaging
MS	mass spectrometry
MSN	medium spiny neurons
MW	molecular weight

m/z	mass-to-charge ratio
NCBI	National Center for Biotechnology Information
NCoR	nuclear co-repressor
NIIs	neuronal intranuclear inclusions
nm	nanometer
NMDA	N-methyl-d-aspartate
nr	number
NRSE	neuron restrictive silencer element
OXPHOS	oxidative phosphorylation
PBS	phosphate buffered saline
PBS-T	phosphate buffered saline + tween
PFC	prefrontal cortex
pI	isoelectric point
pmol	picomolar
PSD-95	postsynaptic density protein 95
PMT	photomultiplier tube
ROS	reactive oxygen species
rpm	rotations per minute
SDS	sodium dodecyl sulphate
sec	second(s)
SELDI	surface-enhanced laser desorption/ionization
SOD	superoxide dismutase
Sp1	specificity protein 1
SPA	sinapinic acid
STMN	stathmin

T	transgenic
TFA	trifluoroacetic acid
T-MS	tanden mass spectrometry
TOF	time of flight
Tpr	translocated promoter region
UPS	ubiquitin proteasome system
μm	micrometre
μl	microlitre
V	volt(s)
v/v	volume per volume
WT	wild type
w/v	weight per volume

Chapter 1. Introduction

1.1 Historical background of Huntington's disease

A disease similar to Huntington's disease has been clinically described for several centuries. George Huntington was, however, the first person to recognise and publicly record the salient features of the disease in 1872. George Huntington recognised the three foremost features of the disease: its hereditary nature, the late onset in life and the psychological consequences (Huntington 1872). The condition he described became known as Huntington's disease (HD). The Mendelian dominant inheritance of HD was recognised by 1908, but it took another 85 years to identify the genetic cause for the disease (Harper 2002a).

1.2 Epidemiology of Huntington's disease

The incidence of HD varies between countries and between ethnic groups. The overall prevalence in the Caucasian population worldwide is estimated at about 4-10 per 100,000. Prevalence in Japan, and probably in most of the Asian populations, is an order of magnitude lower that in the Caucasian population. The same trend is observed in sub-Saharan Africa. One of the reasons for this might be the higher frequency of alleles in the upper normal range (section 1.5.3), which could be subject to expansion between generations, in the Caucasian compared with the Asian and African populations (Harper 2002b). However, these estimates were made before HD genetic testing became available. More recent studies documented an increased prevalence over earlier estimates (Siesling *et al.* 2000;

Almqvist *et al.* 2001; Ramos-Arroyo *et al.* 2005). On the other hand, a study of the HD mortality rate in Austria failed to observe any difference after diagnostic testing became available, although this might have been on account of the low number of requests for predictive testing (Ekestern & Lebhart 2005).

1.3 Clinical features of Huntington's disease

HD is characterised by a variety of features, not all of which are present in every patient and particularly not to the same degree. The motor symptoms are certainly the most distinctive feature of the disease. The majority of HD sufferers display chorea of the body and face, although the intensity of it can vary widely between patients. Chorea tends to feature mainly during the first phase of the illness, often replaced by a more disabling motor disorder later on. Bradykinesia, rigidity and dystonia gradually take over from the involuntary motor dysfunction, and often dominate the later stages of the disease. The majority of patients also suffer from a variety of other motor abnormalities, such as oculomotor disturbances, impairment of voluntary movements, hyperactive reflexes and gait disturbances. Most patients have a degree of speech abnormality as well (Kremer 2002).

Although the motor abnormalities are the hallmark of the disorder, the cognitive and psychiatric symptoms are often far more intrusive in the daily lives of patients. Cognitive changes can frequently be detected before any of the motor symptoms become clear. The cognitive decline is progressive over the course of the disease, although the rate of decline varies widely between patients. The psychiatric aspects of HD include depression, anxiety, irritability, social

withdrawal, apathy and various sexual disorders. Again, the degree to which patients suffer from these is variable. In some cases, acute irritability can bring about severe aggression, and in others, depression and anxiety can become so severe that it leads to acts of suicide (Craufurd & Snowden 2002).

The age of onset of HD can vary widely. The youngest person described with HD was 2 years old, while some patients only develop the first symptoms in their eighties. However, the majority of HD patients are between 40 and 50 years old when the first signs are noticed. A number of patients develop the disease before the age of 20 and are classified as suffering from juvenile HD, as opposed to adult onset HD. Although the symptoms in juvenile HD are often more severe, disease progression and time from onset until death do not differ much. Death generally follows 15 to 20 years after onset and can be brought about by a wide range of associated causes, the principal one being pneumonia (Kremer 2002).

1.4 The neuropathology of Huntington's disease

Final stage human HD brain shows a 10-20% weight loss compared with controls (Vonsattel *et al.* 1985). The most characteristic neuropathological element of HD is the gradual atrophy of the caudate nucleus and the putamen in the striatum. The striatum is part of the basal ganglia, a brain structure present in both hemispheres, that is associated with motor control, cognition, emotions, and learning. The two areas in the striatum are the dorsal striatum, comprising the caudate nucleus and the putamen, and the ventral striatum, which corresponds to the olfactory tubercle and the nucleus accumbens (Figure 1.1). The principal functions of the striatum involve planning and modulation of movement and a

variety of cognitive processes. The striatal neuronal population consists primarily of medium spiny neurons (MSN) and a relatively small number of different aspiny neurons. The striatal atrophy in HD is for the greater part caused by the degeneration of the MSN, while the aspiny interneurons are largely unchanged.

Vonsattel *et al.* (1985) developed a classification system to assess pathological severity in the human brain, based on the pattern of striatal degeneration. The system consists of five grades, designated in ascending order of severity, ranging from no discernible neuropathological abnormalities in grade 0 to very severe atrophy in grade 4. Further assessment of the severity of the disease in HD patients correlated the grades in Vonsattel's classification closely with the degree of physical disability (Vonsattel *et al.* 1985; Myers *et al.* 1988). Structural imaging and functional studies established significant correlations between the changing striatal morphology described in this classification system and the development of cognitive deficits in HD (Montoya *et al.* 2006).

The cerebral atrophy in HD is not confined to the striatum, however. As the disease progresses, the pathological process involves other areas in the brain. In the basal ganglia other than the striatum, various degrees of neurodegeneration and neuronal loss have been reported in the globus pallidus, the ansae penducularis, the subthalamus and the substantia nigra (Gutekunst *et al.* 2002). Generalised atrophy was also described in the cerebral cortex in the end stages of the disease, with significant reductions seen in the prefrontal cortex (Sotrel *et al.* 1991), the angular gyrus (Macdonald *et al.* 1997; Ruocco *et al.* 2008), the post-central gyrus (Jech *et al.* 2007) and the cingulate cortex (Ruocco *et al.* 2008). The hippocampus displayed a substantial amount of atrophy, although it was suggested that the changes might be region specific (Spargo *et al.* 1993; Jech *et*

al. 2007). The cerebellum is generally considered to be an area with minimal atrophy, and only a few studies reported some change (Jeste *et al.* 1984; Jech *et al.* 2007; Ruocco *et al.* 2008). Loss of neurones has also been described in the hypothalamus (Kremer *et al.* 1991; Kassubek *et al.* 2004a) and the thalamus (Heinsen *et al.* 1996; Heinsen *et al.* 1999). Little is known about the pathology of the brainstem, although some change has been noted in the posterior brainstem during MRI (Jech *et al.* 2007). For a long time, the research into HD neuropathology has for the greater part concentrated on the basal ganglia, and very few studies have looked at the rest of the brain. The majority of the brain regions mentioned in this section are indicated on Figure 1.1.

The number of CAG repeats has been positively correlated with the degree of selected but not global cerebral atrophy (Vonsattel & DiFiglia 1998; Kassubek *et al.* 2004b; Jech *et al.* 2007). A positive correlation was also found between the number of repeats and progressive atrophy over time as well as the rate of progression (Ruocco *et al.* 2008).

Neuronal atrophy occurs not only at the level of complete neuronal structures. Various morphological alterations have been seen in dendritic and axonal structures some time before the cell dies (Gutekunst *et al.* 2002).

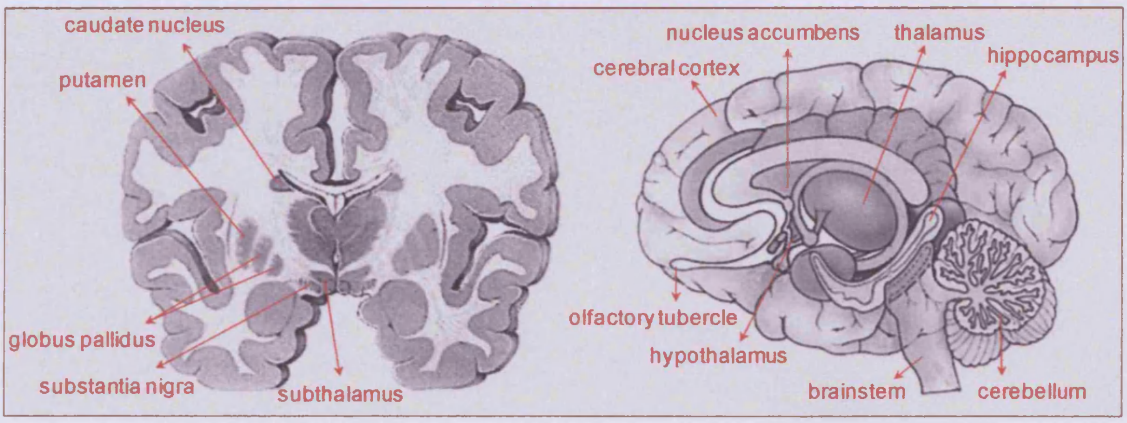

Figure 1.1 Schematic drawing of a coronal section and a parasagittal section of the complete human brain. Regions known to be affected by HD pathology are specified.

1.5 The genetics of Huntington's disease

1.5.1 The HD gene

The genetic cause of HD has been known since 1993, when the HD gene was located in a region of 4p16.3 (Huntington's Disease Collaborative Research Group 1993) to which it had been previously mapped by linkage analysis (Gusella *et al.* 1983). The gene was cloned and designated IT15 (Huntington's Disease Collaborative Research Group 1993). It is translated into a large 348 kDa protein named huntingtin, the function of which is still unclear today. The HD mutation involves an unstable DNA segment with a polymorphic variation of a CAG trinucleotide repeat near the 5' end of the gene. While the HD gene in the healthy population is polymorphic for the CAG repeat region too, the number of repeats is generally below 30, whereas an HD individual has 36 or more repeats. Initially the range between 30 and 40 repeats was considered the intermediate range with an uncertain outcome (Huntington's Disease Collaborative Research Group 1993). Subsequent studies narrowed the intermediate range down to 36-41 repeats by

ascertaining that there were no HD individuals with less than 36 CAG repeats (Rubinsztein *et al.* 1996; Brinkman *et al.* 1997).

The HD locus spans 180 kb of genomic DNA and consists of 67 exons, ranging in size from 48 bp to 341 bp. The gene is ubiquitously expressed, although not in equal abundance in different tissues (Strong *et al.* 1993; Ambrose *et al.* 1994). Differential polyadenylation results in a 13.7 kb transcript, predominantly expressed in adult and foetal brain, and a smaller 10.3 kb transcript, which is the predominant mRNA species in other tissues (Lin *et al.* 1993). Huntingtin mRNA is ubiquitously expressed in all human tissues with highest levels found in the brain, where the expression dominates in neurons over glial cells (Li *et al.* 1993; Strong *et al.* 1993).

HD is a Mendelian autosomal dominant disorder (Harper & Jones 2002), which was thought to show true dominance (Durr *et al.* 1999). However, this idea has been questioned, supported by evidence from *in vitro* investigation (Narain *et al.* 1999) and genetic mouse models of HD (described later in this chapter).

1.5.2 CAG repeat size and age of onset

Being able to measure the CAG repeats in all individuals with HD, or at risk of it, made it possible for studies to define the relationship between CAG size and various disease characteristics. The most obvious aspect of this relationship was the inverse correlation between age of onset and CAG repeat size (Andrew *et al.* 1993; Duyao *et al.* 1993). It was suggested that CAG size alone could account for up to 70% of the variance in age of onset. A study of large cohorts even allowed for the determination of a probability of onset at different ages for a given CAG size. It became clear that the difference of a single CAG repeat could have a

significant effect on the expected age of onset for a carrier (Brandt *et al.* 1996; Brinkman *et al.* 1997; Rosenblatt *et al.* 2001). Although an association of CAG repeat length with clinical progression and age of death was first postulated, this correlation disappeared once age of onset had been controlled for (Andrew *et al.* 1993; Brandt *et al.* 1996). A recent longitudinal MRI study of a cohort of patients over a period of one year indicated, however, that patients with higher numbers of repeats show faster developing and more widespread atrophy (Ruocco *et al.* 2008).

1.5.3 Germline CAG instability

It was soon discovered that the HD repeat was unstable during meiosis, changing in length, with generally either small increases or small decreases in CAG number. Although CAG expansion is rare on normal chromosomes, it was discovered that approximately 70% of meiosis on HD chromosomes introduced a change in CAG number, 73% of these involving expansions. The largest increases appeared to occur in cases where the mutation was paternally transmitted (Duyao *et al.* 1993; Kremer *et al.* 1995), and occasionally large jumps in size occur. It was further noted that juvenile HD was inherited primarily from the father, and it was determined that the sex of the transmitting parent was the key factor in expansion of the CAG repeat (Telenius *et al.* 1993). Germline instability was also detected in knock-in HD mouse models, with a direct correlation between the number of repeats and the magnitude of the instability (Mangiarini *et al.* 1996; Shelbourne *et al.* 1999).

1.5.4 Somatic CAG instability

In conjunction with germline instability, several studies have also shown somatic instability of the CAG repeat, both in humans and in HD mouse models (Aronin *et al.* 1995; Manley *et al.* 1999; Kennedy & Shelbourne 2000; Kennedy *et al.* 2003; Gonitel *et al.* 2008). The somatic heterogeneity appeared to be more pronounced in patients with juvenile HD than in late onset cases, denoting a correlation between progenitor CAG size and level of instability. Furthermore, CAG instability was more evident in the cortex and striatum and least of all in the cerebellum (Aronin *et al.* 1995). Subsequent research confirmed these early findings, showing higher somatic instability in striatal tissue in HD mouse models. A hypothesis of CAG somatic expansion steered by the mismatch repair system has been put forward (Manley *et al.* 1999), particularly in the presence of the mismatch repair protein MSH3 (Gonitel *et al.* 2008). Increasing CAG expansion was also correlated with advancing age in HD mouse models (Kennedy & Shelbourne 2000; Kennedy *et al.* 2003).

1.5.5 Genetic modifiers

Although the variation in age of onset of HD is determined partly by the polymorphism in the CAG repeat of the HD gene (section 1.3.2), it cannot all be attributed to the HD locus. Studies in various HD populations suggested that the CAG repeat length determines up to 70% of the variance in age of onset (Ranen *et al.* 1995; Brinkman *et al.* 1997; Rosenblatt *et al.* 2001). Additional genetic and environmental factors which may modify the variance in onset have been suggested. The age of onset and the sex of the affected parent are thought to

contribute significantly to the variance in age of onset of the offspring (Ranen *et al.* 1995; Rosenblatt *et al.* 2001). Other studies also suggested an effect of the normal HD allele on age of onset and disease progression (Snell *et al.* 1993; Kehoe *et al.* 1999; Leavitt *et al.* 2001).

Polymorphisms in various huntingtin interacting or associated genes have been found, and were put forward as modifiers of the course of the disease. The presence of the APOE ε2ε3 allele (Kehoe *et al.* 1999), a polymorphism in the ubiquitin carboxy-terminal hydrolase L1 gene (Naze *et al.* 2002; Metzger *et al.* 2006), variations in the GluR6 kainate receptor gene (Rubinsztein *et al.* 1997; Chattopadhyay *et al.* 2003), a polymorphism in the transcriptional coactivator CA150 (TCERG1) (Holbert *et al.* 2001; Chattopadhyay *et al.* 2003), polymorphisms in the gene coding for the homocysteine metabolising enzyme methyltetrahydrofolate reductase (Brune *et al.* 2004), variations in *GRIN2A* and *GRIN2B*, the genes coding for the NR2A and NR2B glutamate receptor subunits (Arning *et al.* 2005) and the M441 polymorphism in the human huntingtin-associated protein-1 (HAP1) (Metzger *et al.* 2008), have all been linked to the variation in age of onset in HD. However, only the GRIN2A and the TCERG1 results were replicated and may show true association with residual age of onset in HD (Andresen *et al.* 2007).

Recently, a high-throughput screen identified a large number of huntingtin interacting proteins, many of them not recognised before. A number of these were tested in a *Drosophila* model for HD and the larger proportion was found either to enhance or to suppress HD neurodegeneration in the *Drosophila* eye (Kaltenbach *et al.* 2007). This demonstrates again that the development of pathology in HD is

a much more complex process than was first anticipated, and there is much that still needs to be learned.

1.6 Huntingtin

1.6.1 The structure of huntingtin

The HD gene encodes a 348 kDa protein called huntingtin. When the HD gene was cloned, there were no known protein homologues in the databases (Huntington's Disease Collaborative Research Group 1993), and this remains largely true today.

Some sequence motifs have been identified in huntingtin, indicated on the schematic in Figure 1.2. The polyglutamine repeat starts at amino acid 18 (Huntington's Disease Collaborative Research Group 1993) and it has been suggested that this construct binds to other polyglutamine stretches to form a polar zipper structure, which might cause the protein to bind with other proteins (Perutz *et al.* 1994; Li & Li 2004), as well as accumulate into huntingtin aggregates (Wanker & Droge 2002). The polyglutamine region is followed by a polyproline stretch, which might be involved in the solubility of the protein (Steffan *et al.* 2004), and which is a common motif in transcription factors. Huntingtin also contains a considerable number of tandem arrays of HEAT repeats. Several other known proteins containing HEAT repeats appear to be regulatory proteins involved in cytoplasmic transport (Andrade & Bork 1995). A recent model even proposed that the entire huntingtin protein is made up of numerous HEAT repeats which interact to form an elongated superhelix (Li *et al.* 2006). A highly conserved nuclear export signal is located at the carboxy-terminal third of the huntingtin

protein, suggesting a possible role for huntingtin in exporting proteins from the nucleus (Xia *et al.* 2003). A number of caspase (Goldberg *et al.* 1996; Wellington *et al.* 1998; Wellington *et al.* 2000) and calpain (Gafni & Ellerby 2002; Gafni *et al.* 2004) cleavage sites, where cleavage generates huntingtin fragments, have been located. In addition, huntingtin is also subject to caspase-independent proteolytic cleavage (Ratovitski *et al.* 2007), and to post-translational modifications such as SUMOylation (Steffan *et al.* 2004), ubiquitination (Kalchman *et al.* 1996; Steffan *et al.* 2004) and phosphorylation (Humbert *et al.* 2002; Luo *et al.* 2005; Schilling *et al.* 2006).

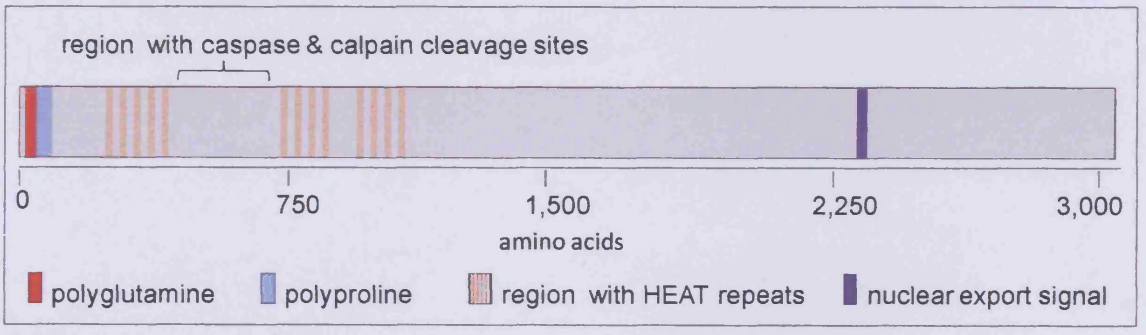

Figure 1.2 Schematic of the huntingtin amino acid sequence.

1.6.2 The localisation of huntingtin

In parallel with its mRNA, huntingtin is ubiquitously expressed, in both brain and peripheral tissue. Although higher levels of huntingtin are present in the brain compared with other tissues, the widespread expression of the protein throughout the body raises the question of why the disease results in selective neuronal loss. (Hoogeveen *et al.* 1993; Sharp *et al.* 1995; Wood *et al.* 1996).

The first studies of the cellular localisation of huntingtin detected the protein only in the cytoplasm (DiFiglia *et al.* 1995; Gutekunst *et al.* 1995). Subsequent reports placed huntingtin in the nucleus, but suggested that the distribution of huntingtin between the cytoplasm and the nucleus was cell type specific. While huntingtin was contained within the cytoplasm in most somatic cells, it was detected in both the cytoplasm and the nucleus in neurons, spermatocytes and lymphoblastoid cells (Hoogeveen *et al.* 1993; De Rooij *et al.* 1996; Hilditch-Maguire *et al.* 2000). Further studies found only a low level of full-length huntingtin but a much higher level of huntingtin N-terminal and C-terminal fragments in the nucleus (Tao & Tartakoff 2001; Kegel *et al.* 2002; Cornett *et al.* 2005).

In the cytoplasm, huntingtin was found in close proximity to mitochondria, endoplasmic reticulum, Golgi and recycling endosomes (Hilditch-Maguire *et al.* 2000; Tao & Tartakoff 2001). Within neurons, huntingtin was placed in neuronal cell bodies, dendrites, axons and pre- and post-synaptic regions, where it appeared to be highly expressed (DiFiglia *et al.* 1995; Gutekunst *et al.* 1995; Sharp *et al.* 1995). Small N-terminal huntingtin fragments were found to interact with the nuclear pore protein translocated promoter region (Tpr), involved in nuclear export. Expansion of the polyglutamine region or increased length of the entire huntingtin protein reduced the level of binding to Tpr (Cornett *et al.* 2005).

1.6.3 The proposed functions of huntingtin

Huntingtin during development

Knock-out mice, nullizygous for *Hdh*, died before gastrulation and the development of the nervous system, demonstrating that huntingtin is essential for embryonic and probably for neuronal development (Duyao *et al.* 1995; Nasir *et al.* 1995; Zeitlin *et al.* 1995). However, these studies failed to provide any further insight into the function of the protein. Subsequent research in mice showed that decreased levels of huntingtin in the embryonic brain lead to reduced neurogenesis and profound cortical and striatal abnormalities, implying that huntingtin is involved in the development of the central nervous system (White *et al.* 1997). A similar outcome was obtained with embryonic HD stem cells, which showed that the expression of huntingtin follows the pattern of neurogenesis, although it did not seem to be required for neuronal differentiation (Metzler *et al.* 1999; Metzler *et al.* 2000). In chimeric mice, many brain regions did not appear to require huntingtin for normal development, although it did seem to have a region-specific role in neuronal survival in the cortex and the basal ganglia (Reiner *et al.* 2001; Reiner *et al.* 2003).

There is some indication that huntingtin might be essential in the postnatal brain too, as the site specific elimination of huntingtin in large proportions of the brain leads to neuronal degeneration and certain aspects of disease, while it affects spermatogenesis when being knocked out in the testis (Dragatsis *et al.* 2000).

The neuroprotective role of huntingtin

A number of studies have indicated the neuroprotective effect of wild-type huntingtin in brain cells that are exposed to various apoptotic stimuli. Some attribute this to the anti-apoptotic property of huntingtin, which may be able to inhibit caspase-3 (Rigamonti *et al.* 2000) and caspase-9 (Rigamonti *et al.* 2001) activation. In the case of caspase-3, this may be achieved through the direct interaction with huntingtin (Zhang *et al.* 2006).

Huntingtin is also known to interact with numerous proteins, some of which are involved in pathways leading to neuroprotection or neuronal death. One of these is brain-derived neurotrophic factor (BDNF), a neurotrophin particularly important for the survival of striatal neurons. It was demonstrated that huntingtin facilitating BDNF transport, and in this way supports neuronal survival (Gauthier *et al.* 2004). It was also suggested that huntingtin regulates the BDNF promoter by inhibiting the neuron restrictive silencer element (NRSE), and in this way enhances transcription of BDNF (Zuccato *et al.* 2001; Zuccato *et al.* 2003).

Huntingtin also exerts its anti-apoptotic influence by binding huntingtin interacting protein (HIP1) (Wanker *et al.* 1997). HIP1 is thought to be involved in apoptosis through the caspase-1 and caspase-3 pathway, and high levels of the unbound form of this protein in the cell lead to increased neuronal death (Majumder *et al.* 2006). Huntingtin was also recognised as a substrate for Akt, a pro-survival serine-threonine kinase that exerts its protective function by phosphorylating several substrates (Colin *et al.* 2005).

The role of huntingtin in intracellular transport

The association of huntingtin with BDNF, as discussed earlier, is one example of huntingtin as promoter of intracellular transport. Huntingtin acts as a processivity factor that facilitates the transport of BDNF-containing vesicles along the microtubules (Gauthier *et al.* 2004). Huntingtin-associated protein 1 (HAP1), the first huntingtin interacting protein identified, is associated with this transport enhancing capacity of huntingtin. HAP1 is enriched in neurons and is probably involved in axonal transport (McGuire *et al.* 2006). This putative role of huntingtin in mitochondrial trafficking has recently been demonstrated by showing that the absence of normal huntingtin in HD can impair this process (Trushina *et al.* 2004; Orr *et al.* 2008).

Huntingtin in synaptic signalling

Huntingtin is highly expressed in presynaptic nerve terminals (DiFiglia *et al.* 1995) and is involved in synaptic transmission. Exactly how huntingtin contributes to this process is not yet clear, although various theories have been put forward, many of which probably hold a piece of the puzzle. First, direct interaction between huntingtin and proteins involved in vesicle transport, release or uptake could exert some level of control, and several of these proteins have been found to interact with huntingtin. It is also known that huntingtin can affect transcription (see below) and in this way it could impact on the level of proteins involved in synaptic transport and postsynaptic transduction present in the cell (Smith *et al.* 2005). One of the key proteins in synaptic transmission is postsynaptic density protein 95 (PSD-95). PSD-95 is located almost exclusively in the post synaptic density of neurons, and is involved in anchoring synaptic proteins. PSD-95

binding partners include N-methyl-d-aspartate (NMDA) receptors and kainate receptors, and huntingtin is associated with these through binding with PSD-95 (Sun *et al.* 2001).

Huntingtin as transcriptional regulator

There is increasing evidence that an important role of huntingtin is in mediating transcription. Recent studies confirmed this by identifying strong transcriptional dysregulation in HD (section 1.7.7). Huntingtin accomplishes this transcriptional regulation in various ways. Huntingtin can act as a direct transcriptional regulator by binding transcription factors. It has been suggested that the glutamine repeats present in huntingtin serve to interact with other polyglutamine containing proteins. Long glutamine repeats occur in many proteins, especially among transcription factors. For that reason it has been proposed that huntingtin might function as a transcriptional regulator (Perutz *et al.* 1994). By now, a vast number of proteins involved in transcriptional regulation have been found to interact with huntingtin. Some of these are transcription factors, such as huntingtin yeast partner B (HYPB), specificity protein 1 (Sp1) and p53; others are transcriptional co-regulators, such as nuclear co-repressor (NCoR) and CREB-binding protein (CBP) (Luthi-Carter & Cha 2003).

The regulation of gene expression can also be accomplished through the interaction between huntingtin and histone modifying proteins. Histones are subjected to several types of post-translational modifications, including acetylation, methylation, phosphorylation, ubiquitination and SUMOylation, all of which can affect transcription. Many of the huntingtin interacting proteins display histone modifying activity (Luthi-Carter & Cha 2003). Although the role of

huntingtin in histone modification is not at all clear, some research indicates that mutant huntingtin interferes with the activity of histone acetyltransferase (Sadri-Vakili & Cha 2006a; Anderson *et al.* 2008). It has also been suggested that huntingtin is involved in histone methylation by means of HYPB, which has been found to possess histone methyltransferase activity (Sun *et al.* 2005).

Huntingtin can also interact directly with RNA polymerases or with proteins acting on RNA polymerases. In this respect, huntingtin was found to interact with polyglutamine binding protein-1 (PQBP-1), which binds RNA pol II, and with TAF_{II} 130, which binds to the TATA-binding protein (Luthi-Carter & Cha 2003).

In conclusion, a picture has emerged of huntingtin as a participant in a wide range of molecular pathways through its interaction with a large number of proteins. Numerous studies have provided pieces in this puzzle (Jones 2002; Li & Li 2004; Li *et al.* 2007). However, the Kaltenback study (2007) showed that the manner in which these interactions have an impact on pathology in HD is still uncertain, and that many more direct and indirect interactions probably exist and have an impact on the pathophysiology of HD.

1.6.4 Aggregation of mutant huntingtin

A great deal of research has been carried out to determine the significance of aggregates of mutant huntingtin in HD. For a long time, the appearance of aggregates in HD brain was considered to be the signature of HD pathology, and aggregate formation was thought to set off the sequence of events culminating in cell death and generalised neurodegeneration. Mutant huntingtin undergoes

cleavage and some of these N-terminal fragments form aggregates. Several models have been suggested to explain this aggregation event. One of these is the polar zipper model, according to which the expanded CAG repeat destabilises the tertiary structure of the protein, which leads to interactions by hydrogen bonding with other polyglutamine proteins, including other N-terminal huntingtin fragments. This can ultimately result in insoluble formations of ß-pleated sheets (Perutz *et al.* 1994; Li & Li 2004). The transglutaminase model proposes that aggregates are formed by the increased transglutaminase activity caused by the expansion of the glutamine repeat. Transglutaminases catalyse the formation of covalent bonds between glutamine residues, and bonds formed in this fashion exhibit a high resistance to proteolytic degradation. It has been demonstrated that huntingtin is a substrate of transglutaminase and that the transglutaminase reaction increases in proportion to the length of the polyglutamine stretch (Kahlem *et al.* 1998).

Accumulation of mutant huntingtin aggregates has been seen in human brain (DiFiglia *et al.* 1997; Becher *et al.* 1998) and can be found in any part of the neuron, including the nucleus, perikaryon, dendrites and axons. Aggregates are found in most brain areas that show neurodegeneration, with largest numbers in areas of the cerebral cortex, but very few in the striatum. N-terminal fragments of nuclear huntingtin can enter the nucleus where they aggregate to form intranuclear inclusions. However the majority of aggregates are found in the neuropil, where they appear in different forms (Gutekunst *et al.* 1999).

The parallel between the distribution of aggregates and the pattern of neurodegeneration fuelled the notion that aggregation was the initial step in HD pathology. However, this theory has been fiercely debated. The presence of

aggregates and nuclear inclusions could just be a secondary effect of the pathological process, or incidental to it. By and large it is agreed that soluble N-terminal fragments of huntingtin in the nucleus play a role in cellular toxicity. However, this is not so with regards to nuclear inclusions. The presence of nuclear inclusions did not correlate with neurodegeneration in cell models (Saudou *et al.* 1998; Arrasate *et al.* 2004). This outcome was also observed in the shortstop mouse model of HD, which displayed extensive nuclear inclusions but no neurodegeneration (Slow *et al.* 2005). Notably, exposing cells to conditions that suppressed the formation of inclusions accelerated cell death, suggesting a protective effect of aggregates during the early stages of the disease (Saudou *et al.* 1998; Arrasate *et al.* 2004), possibly through the sequestration of the toxic soluble fragments, which could be more harmful.

1.6.5 Gain of function or loss of function?

Despite concerted efforts to explain the method by which mutant huntingtin brings about HD, the answer is still unclear. Two theories exist and they are probably complementary. One is explained by the gain of function mechanism of mutant huntingtin mediated pathology, which is based on the acquisition of a toxic function, imparted to the huntingtin protein by the expansion of the polyglutamine stretch. It is generally recognised that a large number of consecutive glutamines convey some toxic property to the protein it is part of, born out by the numerous polyglutamine diseases, each characterised by a distinct pattern of neurodegeneration (Taylor *et al.* 2002). Some features of this common pathological pattern are protein misfolding, followed by proteolytic processing with the formation of soluble protein fragments, which might be toxic in their own right,

and possibly subsequent aggregation of these fragments into insoluble constructs. In turn, these aggregates can sequester other proteins and as a result deplete the cell of vital components (Kazantsev *et al.* 1999).

On the other hand, the loss of function theory recognises the potential toxicity of the loss of wild-type huntingtin, given the many functions it most likely performs in the brain (section 1.6.3). Decreased activity of wild-type huntingtin could theoretically lead to impaired neural development, activation of proteases, disruption of intracellular transport, synaptic dysfunction and transcriptional dysregulation. On the other hand, it was demonstrated that mutant huntingtin can perform at least some of the functions of the normal protein (White *et al.* 1997).

Finally, the gain of function of mutant huntingtin could lead to the loss of wild-type huntingtin function by the sequestration of the normal protein into mutant huntingtin aggregates, and it is certainly possible that a combination of the two mechanisms is closer to the truth.

1.7 Mechanisms of pathology in Huntington's disease

The progression of HD pathology is complex. Various pathways leading to cell death are activated and a number of vital cellular support systems are impaired. All of these pathological mechanisms gradually develop during the course of the disease and may act synergistically. Some of these mechanisms are discussed below.

1.7.1 Excitotoxicity

Excitotoxicity is the pathological process by which nerve cells are damaged and killed by excitatory neurotransmitters, such as glutamate. This occurs when receptors for these neurotransmitters, such as the NMDA receptor, are overactivated by pathologically high levels of neurotransmitters, allowing high levels of Ca^{2+} to enter the cell. In turn, this can activate phospholipases, endonucleases and proteases, as well as generate reactive oxygen species (ROS), all of which will damage and eventually destroy the cell.

The selective vulnerability of the MSN in the striatum has been intriguing, particularly considering the ubiquitous distribution of both wild-type and mutant huntingtin in the brain. Excitotoxicity is thought to be a substantial contributor to this discriminating susceptibility. Within the basal ganglia, MSN are part of several complex neuronal circuits. MSN are GABAergic neurons and hence have an inhibitory impact on the neurons they project to. In turn, MSN receive a vast amount of excitatory glutamatergic input from various brain regions, predominantly from the entire cerebral cortex. In addition, MSN express high levels of NMDA type glutamate receptors, particularly NR1 and NR2B subtypes,

which contribute to excitatory synaptic transmission. This huge amount of glutamatergic input has been held responsible for the vulnerability of the MSN in HD, particularly as striatal interneurons, which are mostly spared in HD, have fewer excitatory inputs and express lower levels of NMDA receptors than the MSN projection neurons.

In vitro studies agree with this concept by showing that the co-expression of NMDA receptor subunits NR1 and NR2B with mutant huntingtin enhances excitotoxicity (Chen *et al.* 1999; Zeron *et al.* 2001). Transgenic YAC72 and CAG94 HD mice also exhibited hyperactive NMDA receptors in the brain, suggesting that mutant huntingtin can cause sensitisation and activation of NMDA receptors (Hodgson *et al.* 1999; Levine *et al.* 1999; Cepeda *et al.* 2001; Zeron *et al.* 2002; Tang *et al.* 2005). Similar results were obtained in transgenic R6/2 mice, where enhanced currents induced by selective activation of NMDA receptors and increased Ca^{2+} movement were recorded (Cepeda *et al.* 2001). In addition, while wild-type huntingtin inhibits NMDA receptor activity by the sequestration of PSD-95 in normal circumstances, it has been suggested that the polyglutamine expansion impedes mutant huntingtin binding to PSD-95. This would mark PSD-95 and mutant huntingtin as mediators in NMDA related neuronal toxicity (section 1.6.3); (Sun *et al.* 2001).

There is also evidence to suggest that nigrostriatal dysfunction plays a part in excitotoxicity. The nigrostriatal neural pathway connects the substantia nigra with the striatum and is one of the major dopamine conduits in the brain. Nigrostriatal dysfunction has been implicated in HD, with a downregulation of the dopamine transporter and D1 and D2 dopamine receptors linked to motor and cognitive deficits in HD (Backman & Farde 2001). The dopaminergic input from

the substantia nigra was shown to contribute to striatal excitotoxicity, and it was suggested that the dopamine signalling pathway acts synergistically with the glutamate pathway (Meldrum *et al.* 2001; Tang *et al.* 2007). Moreover, only low doses of dopamine were needed in the presence of mutant huntingtin to initiate apoptosis and the production of ROS (Charvin *et al.* 2005).

Numerous studies have indicated that the nuclear accumulation of mutant huntingtin interferes with transcriptional events (section 1.7.7). With regard to excitotoxicity, this effect on genes encoding neurotransmitter receptor proteins, especially those involved in glutamatergic neurotransmission, as well as on any proteins involved in the glutamate excitatory pathway, is of particular importance. Changes in these receptors may bring about a level of chronic excitotoxicity in the projection neurons of the striatum, which could ultimately lead to cell death (Sieradzan & Mann 2001). Examples of this are the significant decrease in the mRNA levels of the astroglial glutamate transporter GLT1 and the astroglial enzyme glutamine synthetase in the striatum and cerebral cortex of transgenic R6/2 mice. This would almost certainly result in a decrease in glutamate uptake from the synaptic cleft, which could contribute to a chronic excitotoxic insult on the MSN (Lievens *et al.* 2001).

Some corroboration of the glutamate-dopamine mediated excitotoxic mechanism in HD neurodegeneration was presented by Stack *et al.* (2007), when they demonstrated that lesions introduced in the corticostriatal and nigrostriatal pathways of transgenic R6/2 extended survival and ameliorated both the behavioural and neuropathological phenotype (Stack *et al.* 2007).

1.7.2 Mitochondrial dysfunction

Mitochondrial dysfunction and a deficient energy metabolism have been recognised as early events in HD pathology. Significantly decreased activity of mitochondrial complexes was found in post-mortem brain tissue of HD patients (Brennan *et al.* 1985; Gu *et al.* 1996; Browne *et al.* 1997). Defects of energy metabolism have been demonstrated *in vivo* in skeletal muscle in both symptomatic and presymptomatic HD patients, suggesting mitochondrial dysfunction as an early component of HD pathophysiology (Tabrizi *et al.* 2000; Saft *et al.* 2005). Changes in the activity of complexes II and III in skeletal muscle of HD patients were subsequently correlated with disease duration (Turner *et al.* 2007). An inverse relationship was also identified between the length of the CAG repeat and the ATP/ADP ratio in human HD lymphoblasts, demonstrating a regulatory role for the polyglutamine tract in oxidative phosphorylation (Seong *et al.* 2005). Morphological changes and decreased membrane potential were also seen in human HD lymphoblasts, with an exacerbated condition in homozygote individuals (Squitieri *et al.* 2006).

In addition, it has been demonstrated that it is possible to curb metabolic energy insufficiency in HD by promoting the activity of complex III. The administration of coenzyme Q10 supplements enhanced mitochondrial activity in HD patients and as such reduced impaired energy metabolism (Koroshetz *et al.* 1997; Andrich *et al.* 2004). A similar effect was found in rats treated with 3-nitropropionic acid (3-NP), where the energy deficit was reduced by increasing the concentration of coenzyme Q10 in the brain (Kasparova *et al.* 2006). In transgenic R6/2 mice, high doses of coenzyme Q10 significantly improved motor deficits, reduced brain atrophy and inclusion formation, and prolonged survival (Smith *et*

al. 2006). The beneficial effect of coenzyme Q was enhanced when it was administered in combination with the tetracycline antibiotic drug minocycline (Stack *et al.* 2006) and the antioxidant vitamin E (Kasparova *et al.* 2006).

Consistent with this, biochemical analysis of R6/2 mouse brain demonstrated a significant reduction in mitochondrial complex IV activity in the striatum and some decrease in the cerebral cortex (Tabrizi *et al.* 2000). Mitochondrial dysfunction was also detected in muscle and muscle mitochondria of R6/2 mice, with a 15% reduction of complex IV in HD muscle (Gizatullina *et al.* 2006). A recent study identified a depletion of mitochondrial DNA in leucocytes of HD patients and the degree of the reduction was negatively correlated with the number of CAG repeats (Liu *et al.* 2008).

The dysfunction of the oxidative phosphorylation (OXPHOS) pathway may be the result of OXPHOS inhibitors, of mutations in genes encoding OXPHOS subunits (Leonard & Schapira 2000a; Leonard & Schapira 2000b), or of transcriptional dysregulation through the interference of mutant huntingtin with transcription factors involved with mitochondrial biogenesis and function. Mutant huntingtin was shown to interfere with the transcriptional coactivator PGC-1α in the nucleus. PGC-1α regulates several metabolic processes, including mitochondrial biogenesis and oxidative phosphorylation, and repression of PGC-1α and its targets may contribute to mitochondrial dysfunction and striatal degeneration in HD (Cui *et al.* 2006; Weydt *et al.* 2006).

Another mechanism by which mutant huntingtin could bring about mitochondrial dysfunction is through direct interaction with mitochondria. Mutant huntingtin was found to associate with neuronal mitochondrial membranes in YAC72 mice (Panov *et al.* 2002), Hdh^{Q111} mice (Choo *et al.* 2004) and Hdh^{Q150}

mice (Orr *et al.* 2008). In Hdh^{Q111} mice, a truncated mutant huntingtin fragment could directly induce the opening of the mitochondrial permeability pore, accompanied by the release of a considerable amount of cytochrome c (cyt c) (Choo *et al.* 2004). In turn, cyt c can lead to caspase activation, which can cleave mutant huntingtin and thus promote its entry into the nucleus, where it can interfere with transcription. One of these transcription factors is p53, a tumour suppressor known to regulate genes involved in mitochondrial function and oxidative stress. Mutant huntingtin was shown to bind p53 and increase p53 levels and transcriptional activity in neuronal cultures, in HD transgenic mice and in HD patients, leading to mitochondrial membrane depolarisation (Bae *et al.* 2005) and further mitochondrial abnormalities.

Cyt c as caspase activator can also promote cell death (section 1.7.4); (Green & Reed 1998). A significant release of cyt c was observed in mitochondria isolated from Hdh^{Q150} mouse liver cells after a calcium-induced increase of mitochondrial permeability (Choo *et al.* 2004) and upon glutamate-induced apoptosis in YAC128 mice (Tang *et al.* 2005).

1.7.3 Oxidative stress

While mitochondria are a major source of ROS production, they also contain various antioxidants, such as coenzyme Q10 and superoxide dismutase (SOD), to protect the cell against oxidative damage. ROS levels can accumulate in the cell, particularly in case of respiratory chain dysfunction or when SOD function is altered (Raha & Robinson 2000). For that reason, mitochondrial dysfunction in HD may lead to accumulation of ROS, which can reach toxic levels in conjunction with ROS generated during glutamate-dopamine mediated

excitotoxicity, and result in significant damage to the cell. This condition is known as oxidative stress and it may play a significant part in HD neurodegeneration. Supporting this, reduced expression of nitric oxide synthase was found in transgenic R6/2 (Deckel *et al.* 2001; Deckel *et al.* 2002) and decreased SOD was observed in transgenic R6/1, in a 3-NP acid rat model of HD (Santamaria *et al.* 2001), and in peripheral blood of HD patients (Chen *et al.* 2007). In cells expressing mutant huntingtin, oxidative stimuli enhanced the aggregation of truncated N-terminal mutant huntingtin, proteasomal malfunction and cell death, while overexpression of SOD reversed these detrimental processes (Goswami *et al.* 2006).

Interestingly, analysis of the localisation of the cytosolic SOD1 and the mitochondrial SOD2 in different types of striatal neurons in normal rhesus monkey indicated that the striatal projection neurons express only low levels of both SOD1 and SOD2, which might explain to some extent why projection neurons are particularly vulnerable to neurodegenerative processes, and confirm the notion that superoxide free radicals are at least partly involved in the differential neuronal loss observed in the striatum in HD (Medina *et al.* 1996).

1.7.4 Pathways to cell death

In recent years a number of findings suggested a role for apoptosis in HD (Friedlander 2003). Apoptosis is a form of programmed cell death which involves characteristic cell morphology, including blebbing, nuclear condensation, cell shrinkage and DNA fragmentation. Many chemical signals may lead to apoptosis, after which a cell will undergo organised degradation of cellular organelles by activated proteolytic caspases. Numerous studies have recognised huntingtin as a

substrate for caspase activity, and a number of caspase binding sites have been identified on the protein (section 1.6.1). This has led to the suggestion that caspase-mediated cleavage of huntingtin generated the toxic mutant huntingtin fragments crucial to the development of neurodegeneration in HD.

Throughout HD disease progression, caspase 1 and caspase 3 were found to be increasingly upregulated, coinciding with the release of excessive cyt c and eventually leading to neuronal dysfunction and cell death (Friedlander 2003). Increased levels of cyt c and caspases, associated with cell death and disease progression, have also been observed in cell cultures of HD patients, including unaffected mutation carriers, as well as in genetic mouse models (Li *et al.* 2000; Kiechle *et al.* 2002; Wang *et al.* 2003; Ciammola *et al.* 2006). In addition, research in transgenic YAC72 mice demonstrated that caspase cleavage of mutant huntingtin precedes the onset of neurodegeneration in HD (Wellington *et al.* 2002). Recent work has suggested, however, that it might not be caspase 3 but caspase 6 which is the key player in the damaging proteolytic process (Warby *et al.* 2008). This clearly shows that the mechanism underlying these cleavage events is still not well understood. Then again, further evidence for the role of the caspase signalling pathway in HD neurodegeneration comes from the application of a caspase inhibitor in R6/2 mice (Chen *et al.* 2000) and from the use of caspase inhibitors as therapeutic treatment in HD patients, which delay degeneration and ameliorate symptoms in the patient (Bonelli *et al.* 2004).

Some evidence has also suggested a role for autophagy in the HD disease process. Autophagy involves sequestration of cellular components within autophagosomes, which fuse with lysosomes where their content is degraded (Mizushima *et al.* 2002). Pronounced autophagic vacuoles have been observed in

HD lymphoblasts, and a positive correlation was found between the number of vacuoles and the length of the polyglutamine expansion (Nagata *et al.* 2004). It has also been suggested that the expression of mutant huntingtin induces lysosomal activity (Kegel *et al.* 2000). Furthermore, it was hypothesised that aggregated proteins may not be able to access the proteasome (section 1.7.6), and therefore rely on autophagy for degradation. This would imply that impaired autophagy can contribute to HD pathology. In this context it was shown that autophagosome-lysosome fusion can be impaired by a decreased function of dynein, a molecular motor which transports cellular components along the microtubules to the perinucleus. In this way dynein mutations may be linked to impaired clearance of aggregates, which could be toxic to neurons (Ravikumar *et al.* 2005).

1.7.5 Loss of trophic support

A deficiency in neurotrophic support for the degenerating cells of the striatum has also been singled out as a mechanism perhaps reinforcing HD pathology. The main mediator under investigation in this is brain-derived neurotrophic factor (BDNF), the transport and transcription of which is partly regulated by wild-type huntingtin (section 1.6.3). The loss of BDNF upregulation by wild-type huntingtin in HD, and the reduction in cortical BDNF messenger as a result (Zuccato *et al.* 2001), correlated with the progression of the disease in transgenic R6/2 mice (Zucker *et al.* 2005) and points towards the involvement of trophic factors in HD pathology (Zuccato & Cattaneo 2007). Expression profiling based on striatal gene expression data supported the hypothesis that reduced trophic support is a major pathway contributing to striatal degeneration in HD. As

striatal BDNF is synthesised mainly in the cortex, the data also imply that cortical dysfunction contributes to striatal pathology in HD (Strand *et al.* 2007).

1.7.6 Impaired ubiquitin-proteasome system

It has been proposed that the ubiquitin proteasome system (UPS) is impaired in HD and that this contributes to HD pathology. The UPS is a major protein degradation pathway in cells, degrading short-lived and damaged proteins. Through this, the proteasome impacts on many cellular pathways, and impairment of the UPS might have considerable consequences on normal cellular functions.

It has been suggested that the UPS is impaired in HD through the sequestration of ubiquitin and proteasome subunits in polyglutamine aggregates (Bence *et al.* 2001; Bennett *et al.* 2005). Another hypothesis proposes that expanded polyglutamine containing proteins are not easily degraded by the proteasome. As a result, they block the proteasome and prevent proteasomal degradation of other substrates (Holmberg *et al.* 2004).

In HD, however, the impairment of the UPS is controversial. Some studies report decreased proteasome activity (Bence *et al.* 2001; Seo *et al.* 2004; Bennett *et al.* 2005), some see no change (Ding *et al.* 2002), and others even show increases in proteasome subunits and proteasome activity (Diaz-Hernandez *et al.* 2003; Bett *et al.* 2006). It is clear that further study is required to resolve the conflict involving UPS participation in HD pathogenesis.

1.7.7 Transcriptional dysregulation

The detection of accumulated cleaved mutant huntingtin fragments in the nucleus (section 1.6.4) fuelled the idea that mutant huntingtin might interfere with transcription. Moreover, the presence of a polyglutamine stretch in wild-type huntingtin had already suggested a possible role in transcription (Perutz *et al.* 1994), and the way in which wild-type huntingtin could perform this transcriptional regulatory function has been described in section 1.6.3.

Recent gene expression studies have confirmed the association of strong transcriptional dysregulation and the presence of mutated huntingtin in HD (Luthi-Carter *et al.* 2000; Chan *et al.* 2002; Fossale *et al.* 2002; Kita *et al.* 2002; Luthi-Carter *et al.* 2002a; Luthi-Carter *et al.* 2002b; Zucker *et al.* 2005; Desplats *et al.* 2006; Hodges *et al.* 2006; Kuhn *et al.* 2007; Woodman *et al.* 2007; Hodges *et al.* 2008). Various hypotheses to explain the way in which the mutation in huntingtin could have this dysregulatory effect have been put forward. One model suggests that the intranuclear aggregates of mutant huntingtin fragments sequester soluble proteins essential for transcription (Luthi-Carter & Cha 2003). Another theory, discussed in section 1.6.3, involves the interference of mutant huntingtin with histone modification, possibly through its interaction with histone acetyltransferase (Sadri-Vakili & Cha 2006a; Sadri-Vakili & Cha 2006b; Anderson *et al.* 2008). Mutant huntingtin can also interfere with transcription and affect changes by interacting directly with soluble transcriptional regulators, perhaps through an altered affinity for certain proteins (Dunah *et al.* 2002). One example of this is the repression of the transcriptional coactivator PGC-1α by mutant huntingtin (section 1.7.2), which may be through direct binding of mutant huntingtin to PGC-1α (Weydt *et al.* 2006), or by the downregulation of PGC-1α transcription through

association of mutant huntingtin with the CREB/TAF4 complex on the PGC-1α promoter (Cui *et al.* 2006), or a combination of the two. The ineffective binding of mutant huntingtin with the transcriptional repressor REST/NRSF is another illustration of the direct interference of mutant huntingtin with transcriptional regulators. Normal huntingtin binds REST/NRSF and allows transcription of proteins regulated by this repressor, one of which is BDNF. The polyglutamine expansion in mutant huntingtin is thought to reduce this affinity and allow repression of these proteins (Zuccato *et al.* 2003).

Aside from the mechanisms of transcriptional dysregulation in HD, it is also not at all certain what functional effect a change in mRNA level would have. Some of these effects have been discussed earlier. Altered levels of neurotransmitters can bring about excitotoxicity, changes in OXPHOS subunits can result in mitochondrial dysfunction, impaired energy metabolism and oxidative stress, and a reduction in BDNF might cause a deficiency in neurotrophic support. However, the assumed impact of transcriptional dysregulation in the cell, and on the organism as a whole, is based on the assumption that a change in mRNA is translated to a change at the protein level, which is not at all certain.

Furthermore, it is likely that some of the changes in mRNA levels are not a direct consequence of mutant huntingtin interactions with transcription, but may correspond to secondary effects of disease progression, almost certainly involving a large number of compensatory responses.

1.8 Animal models of Huntington's disease

Animal models of human diseases are important in order to study all stages of disease development, and to investigate possible therapies before they are translated into human clinical trials. Chemical models of HD, that mimicked some of the known phenotypes in HD brain, were originally used, but the identification of the HD gene (Huntington's Disease Collaborative Research Group 1993) allowed the development of genetically accurate HD models in which the pathophysiology and aetiology of the disease caused by the expanded CAG repeat could be examined. The development of animal models recapitulating aspects of the human HD phenotype opened new lines of investigation, particularly in the study of the presymptomatic and early stages of the disorder, and offered the possibility of testing therapeutic interventions.

The disease has been modelled in mouse and rat (Yamamoto *et al.* 2000; Regulier *et al.* 2003; von Horsten *et al.* 2003), in fish (Lumsden *et al.* 2007), in invertebrates such as the fruitfly *Drosophila melanogaster* (Jackson *et al.* 1998; Steffan *et al.* 2001; Lee *et al.* 2004) and the nematode *Caenorhabditis elegans* (Faber *et al.* 1999; Parker *et al.* 2001; Brignull *et al.* 2006), and in yeast (Krobitsch & Lindquist 2000). The development of a non-human primate HD model is still in progress (Yang *et al.* 2008).

Animal models of HD have been generated by the administration of toxins and by genetic means. Until the identification of the genetic mutation responsible for HD in 1993 (Huntington's Disease Collaborative Research Group 1993), only toxin induced models were available. These models are typically generated either by the administration of an excitotoxic agent, which induces excitotoxic cell death,

or by the disruption of the mitochondrial machinery by a mitochondrial toxin. The main excitotoxic agents used in rodent models are kainic acid (KA) (Coyle & Schwarcz 1976), ibotenic acid (IA) (Isacson *et al.* 1985), quinolinic acid (QA) (Schwarcz *et al.* 1983) and homocysteic acid (L-HCA) (Beal *et al.* 1990). The main mitochondrial toxin is 3-nitropropionic acid (3-NP), which brings about cell death in striatal neurons through the irreversible inhibition of succinate dehydrogenase (complex II) of the electron transport chain, and as such mimics mitochondrial impairment seen in human HD brain (Beal *et al.* 1993). Although toxin induced animal models have certainly been of great help in HD research, they have limitations. The principal problem lies in the way they are generated, and they are therefore a representation of only a particular stage in the disease process, dissociated from the genetic cause of HD. While the pathology in HD develops gradually, toxin induced models present only the stage after which cell death has already occurred. Therefore, they cannot provide any information on the mechanism and importance of mutant huntingtin misfolding, the development of aggregates and inclusions, or the progressive nature of the disease to the point of severe pathology. They are also inefficient for studying the development of cognitive, motor and behavioural disturbances and their relationship to neuronal pathology.

Sequencing *Hdh*, the murine homologue of the HD gene, revealed a high degree of conservation between the mouse and the human HD gene, with 86% nucleotide sequence identity and 90% amino acid sequence identity. However, the CAG repeat length differed, with only 7 repeats in mice (Lin *et al.* 1994). This homology presented the opportunity to create genetic mouse models recapitulating aspects of human HD. The first genetic technique used, knocking

out the *Hdh* locus, did not create a model of the disease, although it did explain some aspects of normal huntingtin (Duyao *et al.* 1995; Nasir *et al.* 1995; Zeitlin *et al.* 1995). The majority of HD genetic mouse models have been developed by either the transgenic or the knock-in genetic method. The transgenic approach involves the random insertion of genomic or cDNA transgenes, expressing truncated or full-length human huntingtin, into the mouse genome. The knock-in technique involves the insertion of the mutation into the mouse HD gene. Some conditional models were also developed using the tetracycline-regulatable system. A summary of the HD genetic mouse models can be found in Table 1.1.

1.8.1 Knock-out mouse models of HD

Knock-out mice were generated by three groups (Duyao *et al.* 1995; Nasir *et al.* 1995; Zeitlin *et al.* 1995) and all nullizygous embryos showed abnormal development during gastrulation and died around day 8 of gestation. This demonstrated that huntingtin is vital during embryonic development, but it did not contribute further to the understanding of the normal function of the protein or of its role in HD pathology.

Table 1.1 Mouse models of Huntington's disease.

Mouse model line	Promoter	Construct	Models + number CAG repeats	Reference
Transgenic R6 lines	Human HD	Human exon 1	R6/1 (116 CAG), R6/0 (142 CAG), R6/2 (144 CAG), R6/5 (128-156 CAG)	Mangiarini et al., 1996
Transgenic N171 lines	Mouse prion	Human HD first 171 aas	N171-18Q, N171-44Q, N171-82Q	Shilling et al., 1999
Transgenic HD lines	Rat neuron specific enolase	Human HD ± first 1000 aas	CT18, HD46, HD100	Laforet et al., 2001
Transgenic cDNA lines	CMV	Human full-length cDNA	HD16, HD48, HD89	Reddy et al., 1998
Transgenic YAC lines	Human HD	Human full-length genomic	YAC18, YAC46, YAC72	Hodgson et al., 1999
			YAC128	Slow et al., 2003
Transgenic BAC line	Human HD	Human full-length genomic	BACHD (97 CAG)	Gray et al., 2008
Knock-in	Mouse HD	Mouse full length genomic exon 1 replaced with human exon 1 + expanded repeat	*Hdh*^{Q92}, *Hdh*^{Q111}	Wheeler et al., 1999 and 2000
Knock-in	Mouse HD	Mouse full length genomic + expanded repeat	*Hdh*$^{(CAG)80}$, *Hdh*$^{(CAG)150}$	Lin et al., 2001
Knock-in	Mouse HD	Human full-length genomic	*Hdh4/Q80, Hdh6/Q72*	Shelbourne et al., 1999
			CAG71, CAG94	Levine et al., 1999
			CAG140	Menalled et al., 2003

Mouse models used in this project are in red. CMV = cytomegalovirus.

1.8.2 Transgenic mouse models with a truncated human HD gene

The R6 transgenic mouse models

The R6 lines were the first transgenic models generated by the microinjection of a 1.9 kb genomic fragment containing the human promoter sequences and exon 1 of the human HD gene with approximately 130 CAGs. One male founder (R6) was obtained and backcrossed to CBAxC57BL/6 females. Integration of the fragment into five different regions of the founder's genome gave rise to five mouse lines. R6/T had a single highly truncated copy with no CAG repeats. R6/0 had a single copy with 142 repeats, integrated adjacent to a repetitive genomic structure which probably caused the suppression of the transgene expression. These two lines were rejected for obvious reasons. Lines R6/1 with 116 repeats, R6/2 with 144 repeats and R6/5 with 5 copies integrated ranging from 128 to 156 repeats, were established. All three lines showed a phenotype similar to the human one, with components of the motor disorder, weight loss and characteristic vocalisations. Although brains of transgenic animals were smaller than those of controls, there was no apparent neurodegeneration and it was suggested that localised atrophy might not be the prime cause of the clinical symptoms in HD. R6/1 mice developed disease symptoms between 15-21 weeks and died at 32-40 weeks. In R6/2 mice, age of onset was observed as early as 4 weeks and death followed at about 10-13 weeks. For reasons that are unclear, the phenotype in the R6/5 homozygotes was a great deal milder than in the R6/1 and R6/2 lines and did not develop before 9 months of age. R6/5 heterozygotes showed no phenotype (Mangiarini *et al.* 1996).

Subsequent neurological profiling of the R6 lines identified nuclear localisation of the transgene protein. While normal huntingtin was detected only in

the neuronal cytoplasm, dendrites and axons in control animals, the transgene protein was also identified within the neuronal nucleus. These neuronal intranuclear inclusions (NIIs) were present in all the R6 lines exhibiting a disease phenotype, but absent in the ones that were not symptomatic. The largest inclusions were found in the cerebral cortex, striatum and cerebellum. In striatal neurons, the appearance of inclusions was followed by increased nuclear abnormalities and it was suggested that this may be the result of a neuronal response of the striatum to axonal injury (Davies *et al.* 1997). Further to the original study by Mangiarini (1996), comprehensive characterisation of the R6/1 and R6/2 lines was carried out to evaluate them as a model for HD.

In the R6/1 line, although overt behavioural changes were not apparent before 4 months of age (Mangiarini *et al.* 1996; Hansson *et al.* 1999; Clifford *et al.* 2002; Naver *et al.* 2003; Hodges *et al.* 2008), sensitive tests recorded the development of motor deficits in R6/1 transgenic mice from 7 weeks (van Dellen *et al.* 2000; Hansson *et al.* 2001b; van Dellen *et al.* 2008), and differences in exploratory behaviour were observed as early as 4 weeks (Bolivar *et al.* 2004). On the other hand, gait abnormalities were not registered before 38 weeks (Clifford *et al.* 2002). Immunocytochemical analysis identified NIIs of the transgene and associated nuclear changes, including invaginations of the nuclear membrane and increased nuclear pore density, in symptomatic R6/1 mice (Davies *et al.* 1997; Iannicola *et al.* 2000; Turmaine *et al.* 2000). These neuronal inclusions were subsequently detected in a small percentage of brain cells from as early as 8 weeks and were widespread in the brain by the 16th week (Hansson *et al.* 2001b; Naver *et al.* 2003). NIIs were also found in skeletal muscle in conjunction with ultrastructural changes in muscle in 15 month old R6/1 (Sathasivam *et al.* 1999).

Abnormal nuclear morphology (Davies *et al.* 1997; Turmaine *et al.* 2000) and neurodegeneration, including neuronal condensation and shrinkage, in transgenic R6/1 striatum, hippocampus, cortex and cerebellum (Iannicola *et al.* 2000; Turmaine *et al.* 2000; Spires *et al.* 2004a; Lazic *et al.* 2007) were observed in animals at 5 months. It was also noted that the survival of neural precursor cells in the dentate gyrus, the part of the hippocampus which undergoes a relatively high rate of neurogenesis under normal circumstances, was compromised in transgenic R6/1 animals (Lazic *et al.* 2006). On the other hand, changes in the physiology of transgenic R6/1 striatal neurons offered some measure of resistance to striatal cell death induced by either quinolinic acid or malonate at 18 weeks of age. This was not observed in 6 week old animals, implying it could be an age dependent protective mechanism (Hansson *et al.* 1999; Hansson *et al.* 2001a). Histological examination demonstrated weight reduction of the whole brain as well as reduced striatal volume in 15 week old transgenic R6/1 (Hansson *et al.* 1999; Lazic *et al.* 2007).

Altered brain gene expression was detected in 18 and 22 week transgenic R6/1 (Iannicola *et al.* 2000; Kuhn *et al.* 2007; Hodges *et al.* 2008) and one study showed that 81% of a set of genes, selected for predominant expression in the striatum, were downregulated by the time the animals were 6 months old (Desplats *et al.* 2006). Several proteins were also found to be differentially expressed, some from as early as 8 weeks. R6/1 animals also showed a loss in dopamine receptors in the striatum at 43 weeks (Clifford *et al.* 2002) and a reduction of BDNF protein in the striatum and the hippocampus as well as a downregulation of the dopamine regulator DARPP-32 in the striatum at 5 months (Spires *et al.* 2004b). Alterations in the release of striatal neurotransmitters

(Nicniocaill *et al.* 2001; Smith *et al.* 2006) and the reduction of the synaptic vesicle protein rabphilin 3A in the cerebral cortex and the striatum were detected by 16 weeks (Smith *et al.* 2006). The earliest protein change observed was the downregulation of the cannabinoid receptor 1 at 8 weeks (Naver *et al.* 2003). A summary of the disease characteristics of transgenic R6/1 mice, with the earliest timepoints at which these present, is shown in Figure 1.3 and Table 1.2.

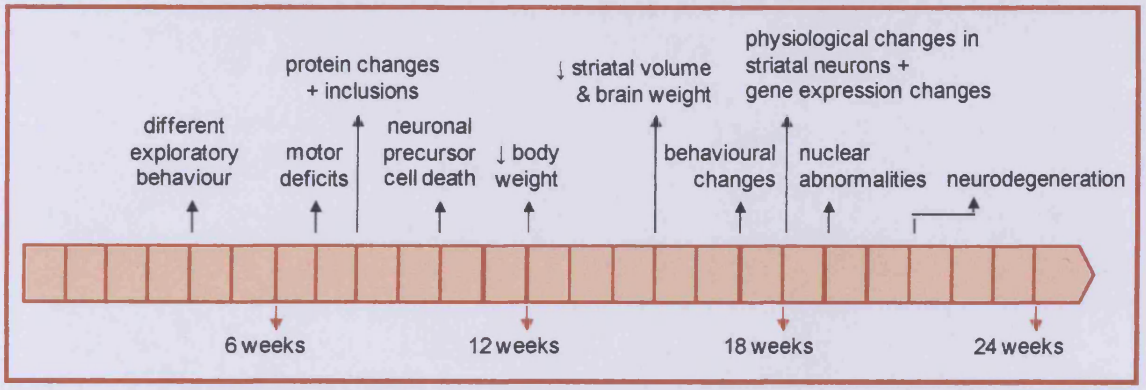

Figure 1.3 Timeline of disease development in the R6/1 HD mouse model. The diagram shows the earliest timepoints at which different aspects of the behavioural, molecular and neuropathological phenotypes have been detected.

Table 1.2 Summary of disease development in the R6/1 HD mouse model.

BEHAVIOURAL PHENOTYPE	Earliest timepoint	References
differences in exploratory behaviour	4 weeks	Bolivar *et al.*, 2004
motor deficits	7 weeks	Van Dellen *et al.*, 2000 and 2008; Hansson *et al.*, 2001b; Hodges *et al.*, 2008
loss of body weight	12 weeks	Van Dellen *et al.*, 2000; Clifford *et al.*, 2002; Naver *et al.*, 2003
behavioural changes	4 months	Mangiarini *et al.*, 1996; Hansson *et al.*, 1999; Clifford *et al.*, 2002; Naver *et al.*, 2003; Hodges *et al.*, 2008
gait abnormalities	38 weeks	Clifford *et al.*, 2002
MOLECULAR PHENOTYPE		
protein changes (striatal neurotransmitters)	8 weeks	NicNiocaill *et al.*, 2001; Clifford *et al.*, 2002; Naver *et al.*, 2003; Spires *et al.*, 2004b; Smith *et al.*, 2006
NIIs	8 weeks	Davies *et al.*, 1997; Iannicola *et al.*, 2000; Turmaine *et al.*, 2000; Hansson et al., 2001b; Naver et al., 2003
changes in physiology of striatal neurons	18 weeks	Hansson *et al.*, 1999 and 2001a
differences in gene expression	18 weeks	Iannicola *et al.*, 2000; Hodges *et al.*, 2008
nuclear abnormalities	4.5 months	Davies *et al.*, 1997; Turmaine *et al.*, 2000
NIIs in skeletal muscle + ultrastructural changes in muscle	12-15 months	Sathasivam *et al.*, 1999
NEUROPATHOLOGY		
compromised survival neural precursor cells	10 weeks	Lazic *et al.*, 2006
reduced striatal volume	15 weeks	Hansson et al., 1999; Lazic *et al.*, 2007
reduced brain weight	15 weeks	Lazic *et al.*, 2007
neurodegeneration	5 months	Iannicola *et al.*, 2000; Turmaine *et al.*, 2000; Spires *et al.*, 2004a; Lazic *et al.*, 2007

The table lists the earliest timepoints at which different aspects of the behavioural, molecular and neuropathological phenotypes have been detected.

Other transgenic mouse models with a truncated HD gene

The N171 lines express a cDNA encoding an N-terminal fragment of 171 amino acids of the human HD gene with 18, 44 or 82 CAG repeats. Only the transgenic N171-82Q presented behavioural and neuropathological abnormalities, with NIIs and neuritic aggregates (Schilling *et al.* 1999).

The HD lines express the first 3 kb of the human HD gene with 18, 46 and 100 CAG repeats. The HD48 and HD100 lines showed neuropathological changes, such as cortical and striatal NIIs, nuclear localisation of huntingtin and dysmorphic cortical dendrites. Striatal electrophysiological abnormalities were marked in HD100 mice, even preceding the onset of a phenotype (Laforet *et al.* 2001).

1.8.3 Transgenic mouse models with a full length human HD gene

cDNA of the human HD gene was used to create transgenic mouse model with 16, 48 or 89 CAG repeats. HD48 and HD89 showed behavioural and motor dysfunction and a neuropathology similar to that in human HD patients, but only a relatively small number of NIIs. This model also displayed a marked difference between heterozygote and homozygote transgenic mice (Reddy *et al.* 1998).

The first animal model expressing the full length human HD gene under the control of its own promoter was generated by means of yeast artificial chromosomes (YACs) with 18, 46 and 72 CAG repeats. YAC72 mice exhibited a progressive behavioural and neuropathological phenotype, with translocation of N-terminal fragments of huntingtin into the nucleus and significant striatal atrophy by 12 months (Hodgson *et al.* 1999). Although a YAC model with 128 CAG repeats developed early cognitive and motor deficits, striatal atrophy was evident only much later, reflecting the condition in human patients, where cognitive and motor deficits precede the onset of neurodegeneration (Slow *et al.* 2003; Van Raamsdonk *et al.* 2005).

A new model with human full length genomic huntingtin with 97 mixed CAA- CAG repeats has recently been generated using the bacterial artificial

chromosome (BAC) transgenic approach. The BACHD model was designed with two *LoxP* sites to allow for Cre-mediated excision of exon 1 of mutant huntingtin, and as such it can be used as a conditional inactivation model. The BACHD mice exhibit progressive motor deficits and selective late-onset neuropathology. There is no somatic polyglutamine repeat instability in these mice due to the interruptions of the CAG repeat (Gray *et al.* 2008).

1.8.4 Knock-in mouse models of HD

Knock-in mouse models are considered a better genetic representation of the human disease than the transgenic models because the mutation is framed in a homologous genomic context to that in humans. On the other hand, the presence of a mild, or the total absence of an overt phenotype has initially severely reduced their value in research, but closer examination and the development of more sensitive tests have revealed an early though subtle phenotype.

The introduction of 72 and 80 CAG repeats into the murine *Hdh* gene generated two HD mouse models which, apart from increased male aggression, developed no overt phenotype during their lifetime. However, analysis of the mutation showed significant germline instability (Shelbourne *et al.* 1999).

The Hdh^{Q92} knock-in mouse model

To investigate this length-dependent inter-generational instability of the HD gene, single CAG tracts of 18, 48, 90 and 111 repeats were inserted in exon 1 of the *Hdh* gene, creating four new mouse lines. The increasing number of repeats correlated with an increase in repeat instability. Although none of these animals

displayed a clear behavioural phenotype (Wheeler *et al.* 1999), the *Hdh*^{Q92} and *Hdh*^{Q111} mice presented with progressive nuclear relocation of the expanded huntingtin protein in MSN in the striatum, starting at 1.5 months in *Hdh*^{Q111} and at 2.5 months in *Hdh*^{Q92} transgenic mice. Subsequent aggregation of mutant huntingtin took place around 10 months in *Hdh*^{Q111} and around 12 months in *Hdh*^{Q92} mice (Wheeler *et al.* 2000). Further study, however, detected inclusions as early as 5 months in *Hdh*^{Q111} mice (Wheeler *et al.* 2002). A similar course of events was observed in the *Hdh*^{Q92} colony used in the present study (Bayram-Weston, unpublished results).

Further to the original studies by Wheeler *et al.* (1999, 2000, 2002), additional characterisation of these mouse models was carried out to assess their value as a model for HD. In the light of this study, only the emerging picture of the *Hdh*^{Q92} will be detailed. Tests with increased sensitivity revealed a mild behavioural phenotype without the conventional motor deficit, but with an implicit learning deficit at 4 months and an impairment in response selection from 5 months of age (Trueman *et al.* 2007; Trueman *et al.* 2008). Molecular and neuropathological changes were detected from as early as 5 months. *Hdh*$^{Q92/Q92}$ demonstrated a time-specific change in striatal physiology, in the form of a supersensitivity to Ca^{2+}, at the age of 5 months, but this had disappeared by the time the animals were a year old (Brustovetsky *et al.* 2005). Long-term potentiation was impaired in the hippocampus at 6 months (Lynch *et al.* 2007). Gene expression studies revealed an increase in *Rrs1* mRNA, encoding a ribosomal protein, in 8.5 month *Hdh*^{Q92} (Fossale *et al.* 2002) and significant gene expression changes in the striatum at 18 months, but not at 3 months (Kuhn *et al.*

2007). A summary of the disease characteristics of transgenic *Hdh*^{Q92}, with the earliest timepoints at which these present, is shown in Figure 1.4 and Table 1.3.

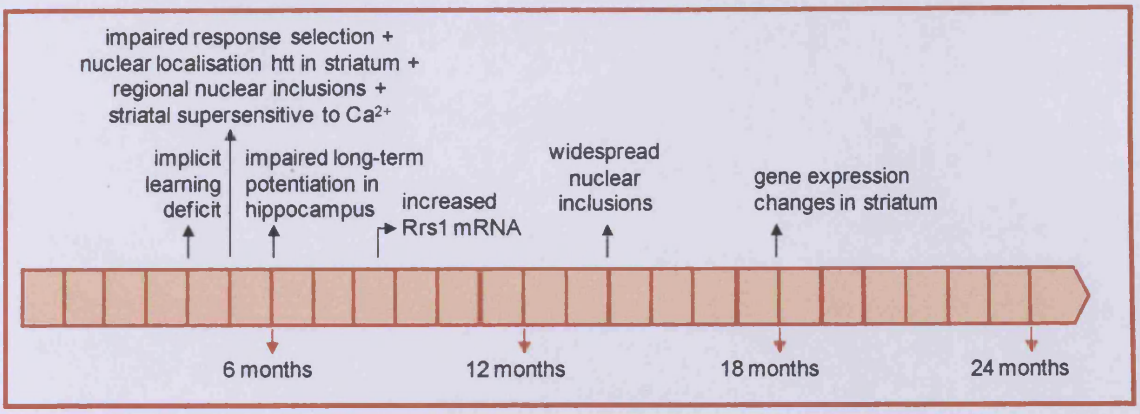

Figure 1.4 Timeline of disease development in the *Hdh*^{Q92} mouse model. The diagram shows the earliest timepoints at which different aspects of the behavioural, molecular and neuropathological phenotypes have been detected.

Table 1.3 Summary of disease development in the *Hdh*^{Q92} mouse model.

BEHAVIOURAL PHENOTYPE	Earliest timepoint	References
no behavioural phenotype		Wheeler *et al.*, 1999 and 2000
sensitive tests show implicit learning deficit	4 months	Trueman *et al.*, 2007
impairment in response selection	5 months	Trueman *et al.*, 2008
MOLECULAR PHENOTYPE		
gametic instability		Wheeler *et al.*, 1999
nuclear localisation of mutant huntingtin in medium spiny neurons in striatum	5 months	Wheeler *et al.*, 2000
NIIs, initially in dorsal caudate and olfactory tubercle	5 months	Wheeler *et al.*, 2000; Trueman *et al.*, 2008; Bayram-Weston, unpublished
long-term potentiation impaired in hippocampus	6 months	Lynch *et al.*, 2007
increased Rrs1 mRNA	8.5 months	Fossale *et al.*, 2002
significant gene expression changes in striatum	18 months	Kuhn *et al.*, 2007
NEUROPATHOLOGY		
striatal supersensitivity to calcium	5 months	Brustovetsky *et al.*, 2005

The table lists the earliest timepoints at which different aspects of the behavioural, molecular and neuropathological phenotypes have been detected.

The Hdh^{Q150} knock-in mouse model

In order to create a mouse model that displayed a disease phenotype without overexpressing the mutant HD gene, the short murine CAG repeat was replaced by 80 and 150 CAG repeats. $Hdh^{Q80/+}$ mice showed no behavioural phenotype. $Hdh^{Q150/+}$ developed the symptoms of late-onset HD, such as motor deficits, gait abnormalities and decreased activity by 40 weeks of age, while $Hdh^{Q150/Q150}$ displayed this phenotype as early as 15 weeks. $Hdh^{Q150/+}$ were susceptible to seizures and suffered weight loss from 25 weeks. No major cell death was observed, but 40 week old $Hdh^{Q150/+}$ presented with reactive gliosis in the striatum and NIIs in some brain regions (Lin *et al.* 2001).

The behavioural phenotype described in knock-in Hdh^{Q150} by Lin *et al.* (2001) proved difficult to substantiate in subsequent studies. Except for a decreased grip strength at 10 months, no phenotype could be detected before 12 months of age, only some behavioural changes by 15 months, and motor deficit no earlier than 18 months (Woodman *et al.* 2007). Another study confirmed the difference between $Hdh^{Q150/+}$ and $Hdh^{Q150/Q150}$. While $Hdh^{Q150/Q150}$ showed reduced activity, hindleg clasping and weight loss at 16 months and resting tremor, unsteady movements, gait abnormalities and motor impairment by 23 months, $Hdh^{Q150/+}$ displayed very little phenotype (Heng *et al.* 2007). $Hdh^{Q150/Q150}$ even displayed cognitive and memory deficits as early as six months (Brooks *et al.* 2006). The relatively early presentation of aggregates was confirmed in subsequent studies, with nuclear localisation of mutant huntingtin and aggregates as early as 6 months in the striatum and later in other brain regions (Tallaksen-Greene *et al.* 2005; Woodman *et al.* 2007).

Gene expression changes were detected in the striatum and cerebellum from the age of 22 months, but not at 15 months, and in the cortex by 22 months (Kuhn *et al.* 2007; Woodman *et al.* 2007). In skeletal muscle of $Hdh^{Q150/Q150}$, gene expression was already dysregulated by 6 months (Strand *et al.* 2005). The distinction between $Hdh^{Q150/Q150}$ and $Hdh^{Q150/+}$ was again demonstrated when alterations in D_1 and D_2 receptor binding was found in $Hdh^{Q150/Q150}$ at 16 months, but not before 23 months in $Hdh^{Q150/+}$ (Heng *et al.* 2007).

A neuropathological phenotype with reactive gliosis and degenerating neurons was observed from 14 months of age and a substantial reduction in the number of striatal neurons and in striatal volume by 23 months (Yu *et al.* 2003; Heng *et al.* 2007). Impaired mitochondrial trafficking through association with N-terminal mutant huntingtin was first observed at three months (Orr *et al.* 2008). A summary of the disease characteristics of knock-in Hdh^{Q150} mice, with the earliest timepoints at which these present, is shown in Figure 1.5 and Table 1.4.

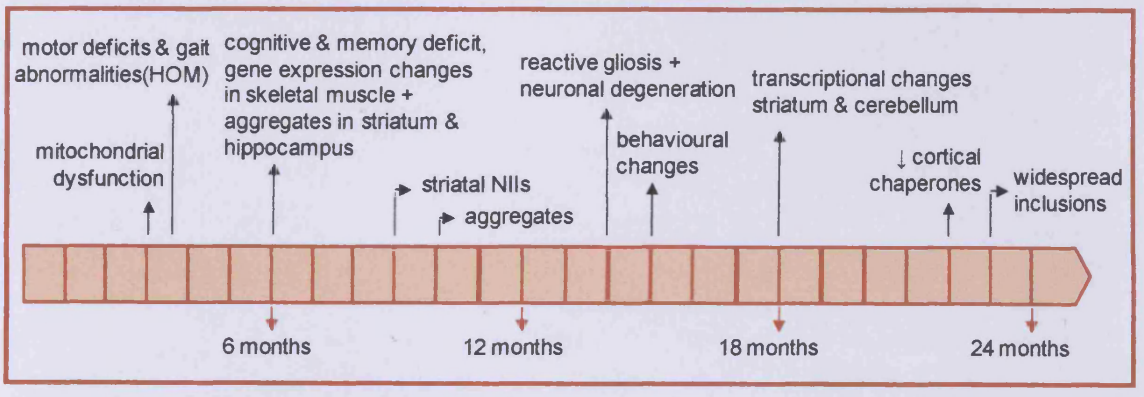

Figure 1.5 Timeline of disease development in the Hdh^{Q150} mouse model. The diagram shows the earliest timepoints at which different aspects of the behavioural, molecular and neuropathological phenotypes have been detected.

Table 1.4 Summary of disease development in the *Hdh*^{Q150} mouse model.

BEHAVIOURAL PHENOTYPE	Earliest timepoint	References
diabetes in homozygotes	3 months	Strand *et al.*, 2005
motor deficits in homozygotes	15 weeks	Lin *et al.*, 2001; Woodman *et al.*, 2007; Heng *et al.*, 2007
gait abnormalities in homozygotes	15 weeks	Lin *et al.*, 2001; Heng *et al.*, 2007
seizure susceptibility	25 weeks	Lin *et al.*, 2001
weight loss	25 weeks	Lin *et al.*, 2001; Woodman et al, 2007; Heng *et al.*, 2007
cognitive deficit	6 months	Brooks *et al.*, 2006
memory deficit	6 months	Brooks *et al.*, 2006
behavioural changes	15 months	Woodman *et al.*, 2007; Heng *et al.*, 2007
MOLECULAR PHENOTYPE		
N-terminal mutant huntingtin associates with mitochondria, impairing mitochondrial trafficking	3 months	Orr *et al.*, 2008
gene expression changes in skeletal muscle in homozygotes	6 months	Strand *et al.*, 2005
aggregates in striatum and hippocampus	6 months	Woodman *et al.*, 2007
aggregates in most brain regions	10 months	Woodman *et al.*, 2007
NIIs striatum, earlier in homozygotes	40 weeks	Lin *et al.*, 2001; Yu *et al.*, 2003; Tallaksen-Greene *et al.*, 2005
NIIs in some layers of the cortex	75 weeks	Tallaksen-Greene *et al.*, 2005
gene expression changes in striatum and cerebellum	18 months	Woodman *et al.*, 2007; Kuhn *et al.*, 2007
widespread NIIs	100 weeks	Tallaksen-Greene *et al.*, 2005
chaperones decreased in cortex	22 months	Woodman *et al.*, 2007
NEUROPATHOLOGY		
reactive gliosis	14 months	Lin *et al.*, 2001; Yu *et al.*, 2003
neuronal degeneration	14 months	Yu *et al.*, 2003; Heng *et al.*, 2007
reduced striatal neuron numbers	100 weeks	Heng *et al.*, 2007
reduced striatal volume	100 weeks	Heng *et al.*, 2007

The table lists the earliest timepoints at which different aspects of the behavioural, molecular and neuropathological phenotypes have been detected.

Other knock-in mouse models

Two knock-in mouse models have been established by exchanging the mouse HD exon 1 by a mouse/human chimeric exon 1 with an expanded repeat. The first contained 94 CAG repeats (Levine *et al.* 1999) and developed a biphasic behavioural phenotype some time before aggregates and NIIs were detected (Menalled *et al.* 2002). The second model with 140 CAG repeats displayed a

similar biphasic behavioural phenotype as the *Hdh*^{Q94}, but with an earlier onset. Again, neuropathological features followed behavioural symptoms by several months (Menalled *et al.* 2003).

1.8.5 A conditional mouse model of HD

A conditional mouse model was developed using the tetracycline-regulatable system, with the bidirectional tetracycline responsive promoter flanked by a chimeric mouse/human exon 1 with 94 CAG repeats in one direction, and the β-galactosidase reporter in the other. Continuous expression of mutant huntingtin showed an early behavioural phenotype, followed by neuropathological changes. Shutting off expression of the transgene halted and even reversed the pathology (Yamamoto *et al.* 2000).

1.8.6 Advantages and disadvantages of genetic HD mouse models

The development of an animal model is not straightforward. The ultimate HD model should recapitulate the symptoms and the neuropathology of the human disease, as well as the genetic and molecular mechanisms that underlie the degenerative processes involved. For practical reasons, onset of the phenotype in this model should be early, with a measurable disease progression in a reasonable time frame. None of the mouse models available today fulfils all these requirements.

In transgenic mouse models (section 5.5.2 – 5.5.3), the full-length or truncated human mutant huntingtin gene is inserted randomly into the mouse genome, so three copies of the huntingtin gene, two mouse endogenous and one

human mutant copy, are expressed. Because of this, transgenic mice are not considered an accurate representation of human HD in genetic terms. In addition, the expression of the mutant huntingtin gene in these animals is driven by various exogenous promoters, so expression may be significantly different from what it would be under the control of the endogenous mouse promoter, or of the human promoter in a human background. Moreover, it is uncertain what the consequence is of the integration of the mutant gene sequence in an indiscriminate part of the mouse genome, or whether this brings about a degree of pathology unrelated to HD. An additional issue with transgenic mouse models generated with truncated mutant huntingtin is that these fragments are synthetic and therefore may have different properties from the full length endogenous gene (Hersch & Ferrante 2004). All transgenic mice develop some phenotypes relevant to the human disease, but none is a perfect match with the human pathology.

In knock-in mouse models (section 1.8.4), part of the mouse huntingtin gene is replaced by the mutant human copy with an expanded CAG region or an expanded CAG has been inserted into the mouse HD gene. This approach eliminates some of the concerns raised about the transgenic models, as the knock-in mice have only two copies of the huntingtin gene, the expression of which is driven by the endogenous mouse huntingtin promoter. For that reason, knock-in mouse models are considered the more accurate genetic model for HD. On the other hand, the lack of a strong phenotype, and the time the disease takes to develop in these animals, make these models less practical to use in research and in therapy driven studies.

1.9 Aims of this study

While widespread changes in brain gene expression in both human HD brain and mouse models of HD have been described, there have been fewer studies of the equivalent changes in the brain proteome. The proteome in the brains of mouse models of HD was examined to complement ongoing studies of gene expression changes.

The specific aims were:-

1. To determine whether the patterns of protein expression in the brains of HD mice were altered in a concerted and specific fashion in comparison with their wild-type littermates, by means of two complementary proteomic techniques:
    - Surface-Enhanced Laser Desorption Ionization - Time Of Flight (SELDI-TOF);
    - 2-D fluorescence Difference Gel Electrophoresis (DIGE).
2. To identify the changes observed with SELDI-TOF and DIGE by MALDI TOF/TOF ananlysis.
3. To confirm the changes observed with SELDI-TOF and DIGE, for some of the proteins identified by MALDI TOF/TOF, by western blot analysis.
4. To compare the changes in protein levels observed with changes in gene expression known to occur in human HD and genetic mouse models of HD.

Chapter 2. Materials and methods

2.1 Materials

2.1.1 Chemicals

CHAPS, HCl and KCl were supplied by BDH Biochemical Laboratories, Poole, UK. Glycerol, Glycine, Acetic acid, Ethanol, Methanol, Tris base, Na_2HPO_4, NaCl and Trifluoroacetic acid were supplied by Fisher Scientific UK Ltd., Loughborough, UK. Tween 20, Antifoam A, Ammonium acetate, CAPS, Lysine and DTT were supplied by Sigma-Aldrich, Gillingham, UK. Triton-x-100, Bromophenol blue, SDS, Tris-HCl, Agarose, Iodoacetamide, Acrylamide, Bisacrylamide, Temed and APS were supplied by GE Healthcare, Giles, UK. Chemicals not listed will be specified elsewhere.

Sinapinic acid

Sinapinic acid (SPA) (Ciphergen Biosystems, Guildford, UK) was made up to a total volume of 400 µl of 50% acetonitrile (Acrõs Organics through Fisher, UK) and 0.5% trifluoroacetic acid (TFA), vortexed for 5 min and left to settle for 5 min.

2.1.2 Buffers

PBS and PBS-T

Phosphate Buffered Saline (PBS) was made up with 8.18 g/l NaCl, 0.2 g/l KCl, 1.43 g/l Na_2HPO_4 and 0.24 g/l KH_2PO_4 (Fisons Scientific Equipment,

Loughborough, UK). Phosphate Buffered Saline – Tween (PBS-T) was PBS with 0.1% Tween 20.

Urea-thiourea lysis buffer

Urea-thiourea lysis buffer was made up with 7M Urea-Ultra Pure (MP Biomedicals, Cambridge, UK), 2M Thiourea-AnalaR (VWR International Llc., Lutterworth, UK), 2% w/v CHAPS and 4% v/v complete EDTA-free protease inhibitor cocktail (Roche Diagnostics Ltd., Burgess Hill, UK).

2.1.3 Gels for DIGE

Six 10% polyacrylamide gels of 1 mm were prepared simultaneously in the Ettan DALT six Gel Caster (GE Healthcare) between low fluorescing LF glass sets (GE Healthcare), with 150 ml 30% Acrylamide/0.8% Bisacrylamide, 113 ml 1.5 M Tris pH 8.8, 4.5 ml 10% SDS, 4.5 ml 10% APS and 77 µl TEMED in a total volume of 450 ml. They were covered with 0.1% SDS solution and left to set for 5 h.

2.1.4 Animals

All the animals used in this study were bred in-house. The R6/1 colony is routinely maintained by outbreeding male R6/1 from the colony with B6CBA F1 (isolator breed: offspring of a cross between C57BL/6JOlaHsd inbred female and the CBA/CaOlaHsd inbred male) from Harlan, Bicester, UK. In the experiments, 18 week old littermates, all male, were used. The Hdh^{Q92} colony was derived from $Hdh^{Q92/Q92}$ mice on a mixed 129SvEv/CD1 background strain (founders from JAX, Maine, USA), crossed in-house onto C57BL/6J for four generations. From these,

Hdh$^{Q92/+}$ were mated and the *Hdh*$^{Q92/Q92}$ and their *Hdh*$^{+/+}$ littermates used in the experiments. The 12 and 10 month old animals used in the experiments were all females. The 18 month old animals used in the experiments were a combination of five female and one male wild types against three female and three male homozygotes. The *Hdh*^{Q150} mice were bred in-house on the original C57BL/6J x 129 background (Lin *et al.* 2001), and again *Hdh*$^{Q150/+}$ were mated and the *Hdh*$^{Q150/Q150}$ and their *Hdh*$^{+/+}$ littermates used in the experiments. The 15 and 10 month old animals used in the experiments were all female, the 3 and 4 month old animals were all male and the 18 month old animals used in the experiments were a combination of three female and six male wild types against five female and four male homozygotes in the SELDI experiment and two female and four male wild types against three female and three male homozygotes in the DIGE experiment.

All animals were housed with three or four per cage, on sawdust flooring and enriched with a cardboard tube. Animals had access to food and water *ad libitum*.

At the chosen timepoints, animals were killed by cervical dislocation. Subsequent procedures were different between cohorts. For some, the brain was snap frozen in liquid nitrogen and stored at -80 °C before being defrosted for either micro-dissection or protein extraction. For others, micro-dissection was performed immediately, followed by protein extraction, or brain regions were snap frozen in liquid nitrogen and stored at -80 °C before being defrosted for protein extraction. The exact course of action for the different cohorts is listed in table 2.1. Micro-dissection was carried out by Dr. S. Brooks, School of Biological Sciences, Cardiff University. All procedures were carried out in accordance with the requirements of the United Kingdom Animals Scientific Procedures Act 1986.

Table 2.1 Successive steps from brain to protein sample.

Mouse model	Timepoint	successive steps from brain to protein sample				
		snap frozen	micro-dissection	snap frozen	protein extraction	frozen -80°C
R6/1	18 weeks					
Hdh ^{Q92}	18 months					
	12 months					
	10 months					
Hdh ^{Q150}	18 months					
	15 months					
	10 months					
	3+4 months					

Snap freezing whole and microdissected brain tissue was done in liquid nitrogen. Gray fill indicates that a particular step was performed.

2.1.5 Antibodies

Primary antibody Mouse monoclonal anti-COX (cytochrome c oxidase) VIb (A21366) and Rabbit anti-Calmodulin (61-8500) were purchased from Invitrogen, Paisley, UK. Primary antibody Rabbit polyclonal anti-Myelin Basic Protein (MBP) (AB980) was purchased from Chemicon-Millipore, Watford, UK. All other commercial primary antibodies were purchased from Abcam, Cambridge, UK: Rabbit polyclonal to Cnp 10 (ab53106), Rabbit polyclonal to Calcineurin A (ab3673), Rabbit polyclonal to Creatine Kinase BB (ab38211), Rabbit polyclonal to Glutamine Synthetase (ab49873), Mouse monoclonal [2A1] to Superoxide Dismutase 2 (ab16956), Rabbit monoclonal [EP1374Y] to Apolipoprotein E (ab52607) and Rabbit polyclonal to Hsp60 (ab46798). Primary antibody against α-tubulin was produced in-house from the I2G10 hybridoma (Iowa Hybridoma Cell Bank, Iowa, USA) following standard procedures. Secondary antibody raised against mouse IR Dye 800 anti-mouse was purchased from Lorne Laboratories, Reading, UK. Secondary antibody raised against rabbit Alexa Fluora 680 goat anti-rabbit IgG was purchased from Invitrogen.

2.2 Methods

2.2.1 Sample homogenisation and quantitation

Homogenate of half cerebra

Cerebral halves were divided into three parts, weighing 60-100 mg each. Each part was homogenised in 1 ml of ice cold Urea-Thiourea Lysis Buffer with 1 µl of Antifoam-A in a pre-chilled Lysing Matrix D tube (Q-BIOgene, Cambridge, UK). The tubes were shaken in a Thermo Savant FastPrep (Thermo Scientific, Basingstoke, UK) for 15 sec at speed-setting 4.0 and then centrifuged in a Fresco Biofuge (Kendro Laboratories Products Plc., Bishops Stortford, UK) at 2,000 rpm for 1 min at 4 °C. The homogenate of all tubes was combined and split in 1.5 ml Eppendorf tubes (≈ 750 µl/tube).These were centrifuged in the Fresco Biofuge at 13,000 rpm for 1 h at 4 °C. Homogenate was frozen in 50 µl aliquots at -80 °C.

Homogenate of microdissected brain regions

The complete microdissected brain tissue was put in 300 µl of ice cold Urea-Thiourea Lysis Buffer and 1 µl of Antifoam-A in a pre-chilled 0.5 ml microtube (Bioquote Ltd., York, UK) filled with 0.5 g of Lysing Matrix D (Q-BIOgene). The tube was shaken in the FastPrep machine for 15 sec at speed-setting 4.0 and centrifuged in the Fresco Biofuge at 2,000 rpm for 1 min at 4 °C. The homogenate was transferred to a clean 1.5 ml Eppendorf tube and centrifuged in the Fresco Biofuge at 13,000 rpm for 1 h at 4 °C. The homogenate was frozen in 50 µl aliquots at -80 °C.

Quantitation of protein homogenate

Protein concentration was assayed with the Bradford assay (Bradford 1976).

2.2.2 All-in-1 Protein Standard II Calibration Chip

2 µl of reconstituted All-in-1 Protein Standard II (Ciphergen Biosystems) was mixed with 8 µl of sinapinic acid (SPA) (Ciphergen Biosystems). Each spot of an NP20 protein chip (Ciphergen Biosystems) was washed with 3 µl of dH_2O and blotted dry without touching the spots. 1 µl of the SPA/All-in-1 mix was placed on each spot and air dried.

2.2.3 2-D Clean-up

The 2-D Clean-Up Kit from GE Healthcare was used following the manufacturer's instructions. The protocol has Enhanced Procedure A for sample volumes of 1-100 µl containing 1-100 µg of protein, and Enhanced Procedure B for larger samples with more than 100 µg of protein. Both procedures were used.

2.2.4 Protein fractionation

Protein samples were fractionated in SC1000 SigmaPrep spin columns (Sigma) with polymeric reversed phase media PLRP-S (Polymer Laboratories Ltd., Church Stretton, UK). 50 µl of sample (250-500 µg protein) was made up to 200 µl of 10% ACN and 0.5% TFA. The initial volume could vary when starting with a pellet from 2-D clean-up, but was always made up to a final volume of 200

µl. 100 µl of polymeric reversed phase beads were suspended in 300 µl of 50% ACN. The spin column was washed with 300 µl of 50% ACN and spun at 2,000 rpm for 15 sec to remove the wash. The suspended beads were added to the spin column, mixed on the rotator for 1 min, and spun at 2,000 rpm for 15 sec. The flow-through was discarded. The spin column containing the beads was washed a number of times for 1 min on the rotator, followed by a 15 sec spin at 2,000 rpm: two washes with 300 µl of 50% ACN, four washes with 300 µl of 10% ACN and two washes with 300 µl of 10% ACN+0.1% TFA. Finally 100 µl of 10% ACN+0.1% TFA was added and the column vortexed at setting 1000 for 1 min. The 200 µl of prepared sample was now added to the spin column containing the beads, mixed on the rotator for 30 min and centrifuged at 2,000 rpm for 15 sec. The fractions obtained were the flow-through, followed by fractions obtained by increasing concentrations of ACN in 300 µl (10%, 20%, 30%, 40%, 50%, 60% and 80%), each mixed on the rotator for 10 min and centrifuged at 2,000 rpm for 15 sec. The fractions were kept at -20 °C for short-term storage and at -80 °C for long-term storage.

2.2.5 Isoelectric focusing of proteins

Isoelectric focusing of proteins for 2-DE using NuPage mini-gels

A 7 cm 3-10NL IPG strip (GE Healthcare) was rehydrated overnight in 125 µl rehydration buffer (7 M Urea, 2 M Thiourea, 2% w/v CHAPS, 0.008% w/v Bromophenol blue, 1.6% strip specific IPG buffer (GE Healthcare) and 50 mM DTT), covered with 0.5 ml of DryStrip Cover Fluid (GE Healthcare). Isoelectric focusing (IEF) was performed on the Ettan IPGPhor3 platform (GE Healthcare). Samples were loaded on the rehydrated focusing strips by means of loading cups

and focused overnight at 20 °C under the conditions listed in table 2.2. The following morning the IEF strips were equilibrated, first with 5 ml of reducing solution (10% of 10X NuPAGE Sample Reducing agent and 90% of 1X NuPAGE LDS Sample Buffer, both from Invitrogen) and next with 5ml of alkylating solution (2.32% w/v iodoacetamide in 1X NuPAGE LDS Sample Buffer). Both equilibration steps were performed for 15 min whilst gently rocking.

Table 2.2 Isoelectric focusing conditions.

50 μA per strip		
	Voltage (V)	Time (h)
1. Step and hold	500	1
2. Gradient	1,000	2
4. Step and hold	1,000	1
5. Gradient	8,000	2
6. Step and hold	8,000	8

Samples were focused overnight on 7 cm 3-10NL IPG strips on the IPGphor platform.

Isoelectric focusing of proteins for 2-DE using large gels

A 24 cm 3-10NL IPG strip (GE Healthcare) was rehydrated overnight in 450 μl rehydration buffer (7 M Urea, 2 M Thiourea, 4% w/v CHAPS, 0.005% w/v Bromophenol blue, 0.5% strip specific IPG buffer and 20 mM DTT), covered with 4 ml of DryStrip Cover Fluid. Isoelectric focusing (IEF) was performed on the Ettan IPGPhor3 platform. Samples were loaded on the rehydrated focusing strips by means of loading cups and focused overnight under the conditions listed in table 2.3. The next morning, the IEF trips were equilibrated, first with 15 ml of DTT equilibration buffer (50 mM Tris-HCl pH 8.8, 6 M Urea, 2% w/v SDS, 30% v/v Glycerol, 0.002% w/v Bromophenol blue and 1% w/v DTT) and next with 15 ml of IAA equilibration buffer (50 mM Tris-HCl pH 8.8, 6 M Urea, 2% w/v SDS, 30% v/v

Glycerol, 0.002% w/v Bromophenol blue and 2.5% w/v IAA). Both equilibration steps were performed for 15 min whilst gently rocking. Focusing of protein samples for DIGE analysis was performed in the dark.

Table 2.3 Isoelectric focusing conditions.

	Voltage (V)	Time (h)	kVh
1. Step and hold	500	1	0.5
2. Gradient	1,000	7	5.2
3. Gradient	10,000	3	16.5
4. Step and hold	10,000	4	40
5. Gradient	500	1	5.2
6. Step and hold	500	6	30

Samples were focused overnight on 24 cm 3-10NL IPG strips on the IPGphor platform.

2.2.6 SDS-PAGE

SDS-PAGE of protein fractions on NuPage mini-gels

Protein fractions were dried in the Speedvac, on manual setting at 43 °C for 40 min initially. Then they were checked every 10 min and the Eppendorf tube closed when a fraction was dry. The fractions were separated on polyacrylamide mini-gels with the XCell *SureLock* Mini-Cell system (Invitrogen). The pellets were resuspended in 20 µl 2xLDS sample buffer, provided with Invitrogen's gel system, and heated on the Thermomixer Comfort (Eppendorf UK, Cambridge, UK) at 80 °C for 10 min. The fractions were loaded onto a 12% Bis-Tris NuPage gel with 10 µl of Seeblue Plus-2 Pre-Stained Standard (Invitrogen) in the outer lane. SDS-PAGE was carried out in MES running buffer (Invitrogen) under non-reducing conditions at 200 V until the 4 kDa marker reached a point $^4/_5$ down the gel.

SDS-PAGE of proteins on NuPage mini-gels for western blotting

SDS-PAGE was performed with the XCell *SureLock* Mini-Cell system. Unless otherwise specified, all pre-cast gels, buffers and chemicals were provided by Invitrogen. Depending on the size of the protein, samples were run on 10% or 12% Bis-Tris NuPage gels. Samples were prepared with 20-50 μg of protein to a total concentration of 25% LDS Sample Buffer (x4) and 10% Sample Reducing Agent (x10). Samples were vortexed and heated to 70 °C for 10 min. SDS-PAGE on 10% gels was carried out in MES running buffer and in MOPS running buffer for 12% gels, with 500 μl of anti-oxidant, at 150V until the dye front reached the bottom of the gel.

SDS-PAGE of proteins in the second dimension of 2DE on mini-gels

SDS-PAGE was carried out with the XCell *SureLock* Mini-Cell system. All gels and buffers were provided by Invitrogen. The focused IEF strip (section 2.2.5) was applied to a 1 mm NuPAGE 4-12% Bis-Tris Zoom Gel and SDS-PAGE was carried out in 1X MOPS running buffer at 200V for approximately 50 min, until the dye front reached the bottom of the gel.

SDS-PAGE of proteins in the second dimension of 2DE on large gels

The focused IEF strip (section 2.2.5) was applied to the gel (section 2.1.3) and sealed with 200 μl agarose sealing solution (250 mM Tris, 1.92 M Glycine, 1% w/v SDS and 0.5% Agarose). SDS-PAGE was carried out with up to six gels simultaneously in the Ettan DALT six electrophoresis unit (GE Healthcare), in chilled anodic 1 x SDS electrophoresis buffer (250 mM Tris, 1.92 M Glycine and 1% w/v SDS) in the lower chamber and cathodic 2 x SDS electrophoresis buffer in

the upper chamber. The run was carried out overnight at 12 °C, 10 mA/gel and 80 V for 1 h, followed by 14-16 h at 12 mA/gel and 150 V until the dye front reached the bottom of the gel. SDS-PAGE of DIGE gels was carried out in the dark.

2.2.7 Staining gels

Staining NuPage mini-gels with Colloidal Blue

NuPage gels were stained in a glass dish which had been cleaned with detergent, ethanol and methanol, and air dried. The Colloidal Blue Staining Kit from Invitrogen was used, following the manufacturer's instructions.

Silver staining of proteins on NuPage mini-gels

NuPage mini-gels were stained in a glass dish which had been cleaned with detergent, ethanol and methanol, and air dried. The SilverQuest Silver Staining Kit from Invitrogen was used, as this is compatible with mass spectrometry, following the manufacturer's instructions.

Silver staining of proteins on large 2DE gels

Silver staining of proteins on large 2DE gels was automated in the Processor Plus with the PlusOne Protein Staining Kit, both from GE Healthcare. The gel was placed in 250 ml of fixative (10% v/v acetic acid and 40% v/v ethanol) for 30 min, then in 250 ml of sensitizer (30% v/v ethanol, 4% v/v Na-thiosulphate 5% w/v stock and 6.8% w/v Na-acetate) for 30 min, followed by three washes in 250 ml dH_2O for 5 min each. The gel was stained in 250 ml silver stain (10% v/v silver nitrate 2.5% w/v stock) for 20 min, followed by two washes in 250 ml dH_2O for 1 min each. The gel was then placed in 250 ml developer (2.5% w/v Na-

carbonate and 0.4% v/v formaldehyde 37% w/v stock) for up to 10 min. When the gel was sufficiently stained, the staining process was stopped with 250 ml of stop solution (1.46% w/v EDTA) for 10 min, followed by three washes in 250 ml dH_2O for 5 min each. The gel was preserved in 1% acetic acid.

2.2.8 Collecting gel plugs from gels

Gel plugs were collected from NuPage mini-gels and DIGE gels using a spot picker 1.5 mm diameter One Touch Plus, with spot picker tips One Touch Plus 1.5 mm, both from Web Scientific Ltd., Crewe, UK. To avoid contamination, a glass screen was placed between the gel and the operator.

2.2.9 Western blotting

Blotting paper (Schleicher and Schuell, London, UK) and sponge pads (Invitrogen) were soaked in transfer buffer (Invitrogen), made up to a final concentration of 10% methanol. The PVDF Immobilon-P membrane (Millipore, Watford, UK) was first soaked in methanol for 15 sec, washed in dH_2O for 2 min and left in transfer buffer until used. Protein transfer was achieved by applying 30 V for 1 h.

Blots were dismantled and membranes blocked with 200 ml of 5% milk (Marvel) in PBS-T for 1 h. Next, membranes were incubated in primary antibody in 10 ml PBS-T + 5% milk in 50 ml Falcon tubes (Greiner Bio-One, Stonehouse, UK) on the spiramix (Thermo Electron Corporation, Rugby, UK) for 1 h. Primary antibody raised against α-tubulin was added to each incubation at a 1/50,000 dilution, as previously optimised in the lab. Membranes were rinsed twice in the

Falcon tubes with PBS-T, followed by one 15 min and two 5 min washes in 200 ml PBS-T. Membranes were then incubated in a 1/5,000 dilution of IR Dye 800 anti-mouse secondary antibody (Lorne Laboratories) for primary antibodies raised in mouse, and in a 1/5,000 dilution of Alexa Fluora 680 goat anti-rabbit IgG secondary antibody (Invitrogen) for primary antibodies raised in rabbit. This incubation was performed in 10 ml PBS-T + 5% milk in 50 ml Falcon tubes on the spiramix for 30 min in the dark. Membranes were rinsed twice in the Falcon tubes with PBS-T, followed by a 15 min and a 5 min wash in 200 ml PBS-T and a final 5 min wash in 200 ml PBS in the dark.

Chapter 3. Comparison of the proteome in brain tissue of HD mouse models using surface-enhanced laser desorption ionisation – time of flight (SELDI-TOF) mass spectrometry

3.1 Introduction to SELDI-TOF

Surface-Enhanced Laser Desorption Ionisation – Time Of Flight (SELDI-TOF) mass spectrometry, the Ciphergen ProteinChip system, was first described 15 years ago (Hutchens & Yip 1993), and has since been used successfully in a variety of research projects: for protein expression profiling in schizophrenia (Mei *et al.* 2006), in the search for biomarkers in Alzheimer's disease (Carrette *et al.* 2003; Davidsson & Sjögren 2006), and in a large number of cancer research projects (Petricoin *et al.* 2002; Engwegen *et al.* 2006; Lee *et al.* 2006).

SELDI-TOF simplifies protein mixtures by separating them according to their chemical properties, before analysing them quantitatively using mass spectrometry. While the technique is able to detect proteins that are hard to visualise by other proteomic methods, such as 2D-gel electrophoresis, the detection limits of the system restrict the analysis to proteins of a molecular weight between 5-20 kDa, as it cannot detect the bulk of higher molecular weight cellular proteins. The SELDI system produces a linear chromatogram that is used to measure and compare the relative quantities of proteins over multiple samples.

In the present study, SELDI-TOF analysis was used to determine whether the patterns of protein expression in the brains of transgenic mice were altered in a concerted and specific fashion in comparison with their wild-type littermates. The brain proteomes of three genetic mouse models of HD were analysed: the

R6/1 line, (Mangiarini *et al.* 1996 and section 1.8.2), the Hdh^{Q92} line, (Wheeler *et al.* 1999 and section 1.8.4) and the Hdh^{Q150} line (Lin *et al.*, 2001 and section 1.8.4). This comparison therefore included one line with a human exon 1 transgene (R6/1), one with a human exon 1 knocked into the mouse *Hdh* locus replacing mouse exon 1 (Hdh^{Q92}), and one line with the full mouse *Hdh* gene with 150 CAG repeats (Hdh^{Q150}) replacing the normal mouse seven CAG repeats at this locus. The pathology in the R6/1 mouse is widespread throughout the brain (section 1.8.2), and in this line half cerebra were used to generate samples for experimentation. The effect of the more specific pathology in the two knock-in lines was examined by using microdissected brain areas for analysis: caudate-putamen was used in both lines as this is known to be affected early and specifically in both these mouse lines (section 1.8.4) and in human brain (section 1.4). In addition, a comparison was made with other brain areas in the Hdh^{Q92} model to see if the more restricted pathology in these regions was reflected in a more restricted pattern of proteome changes.

Protein peaks found to be differentially expressed by SELDI-TOF analysis were identified using Matrix Assisted Laser Desorption Ionisation Time-Of-Flight tandem (MALDI TOF/TOF) mass spectrometry.

3.2 Identification of differentially expressed proteins in HD mouse brain using SELDI-TOF

3.2.1 The SELDI-TOF procedure

An overview of the workflow for identifying differentially expressed proteins by SELDI-TOF is shown in Figure 3.1. SELDI-TOF works by simplifying protein

mixtures using the intrinsic properties of the proteins, such as charge, size, hydrophobicity, metal affinity or specific biological affinities. Mixed protein samples are applied to spots on a ProteinChip array with a specific chromatographic surface, to selectively bind proteins in a protein mixture, based on the properties of the proteins. The coupling surface chemistry can be chemical (anionic, cationic, immobilized metal affinity, hydrophobic, normal phase) or biological (pre-activated, antibody-antigen, receptor-ligand, DNA-protein). Energy Absorbing Molecules (EAM) are applied to each spot as well. EAM have a high molar absorptivity at laser wavelength and are responsible for converting laser energy to thermal energy, which facilitates desorption and ionisation of proteins in the sample. Commonly used EAM are CHCA (α-cyano-4-hydroxycinnamic acid), SPA (sinapinic acid) and EAM-1 (Ciphergen's in house EAM). The EAM used in this study were SPA, as advised by Ciphergen, as it is suitable for matrix ions with a mass both higher and lower than 15 kDa. The EAM solubilise a large proportion of the proteins on the chip surface, which then co-crystallise with the EAM as the solution dries.

The ProteinChip arrays are read in the ProteinChip SELDI reader, which consists of a vacuum chamber in which the samples on the ProteinChip are eluted by laser desorption and ionisation. The EAM-protein crystals absorb the laser energy and instigate desorption and ionisation. A short electrical pulse sends the ions down the TOF-MS tube towards the detector. Protein measurement is based on the mass-to-charge ratio (m/z). The signal is processed by a converter and translated into a spectrum. The peak intensity on the y-axis indicates the relative abundance of the detected protein, while the m/z ratio, calculated by the time taken for the ions to reach the detector, is read on the x-axis.

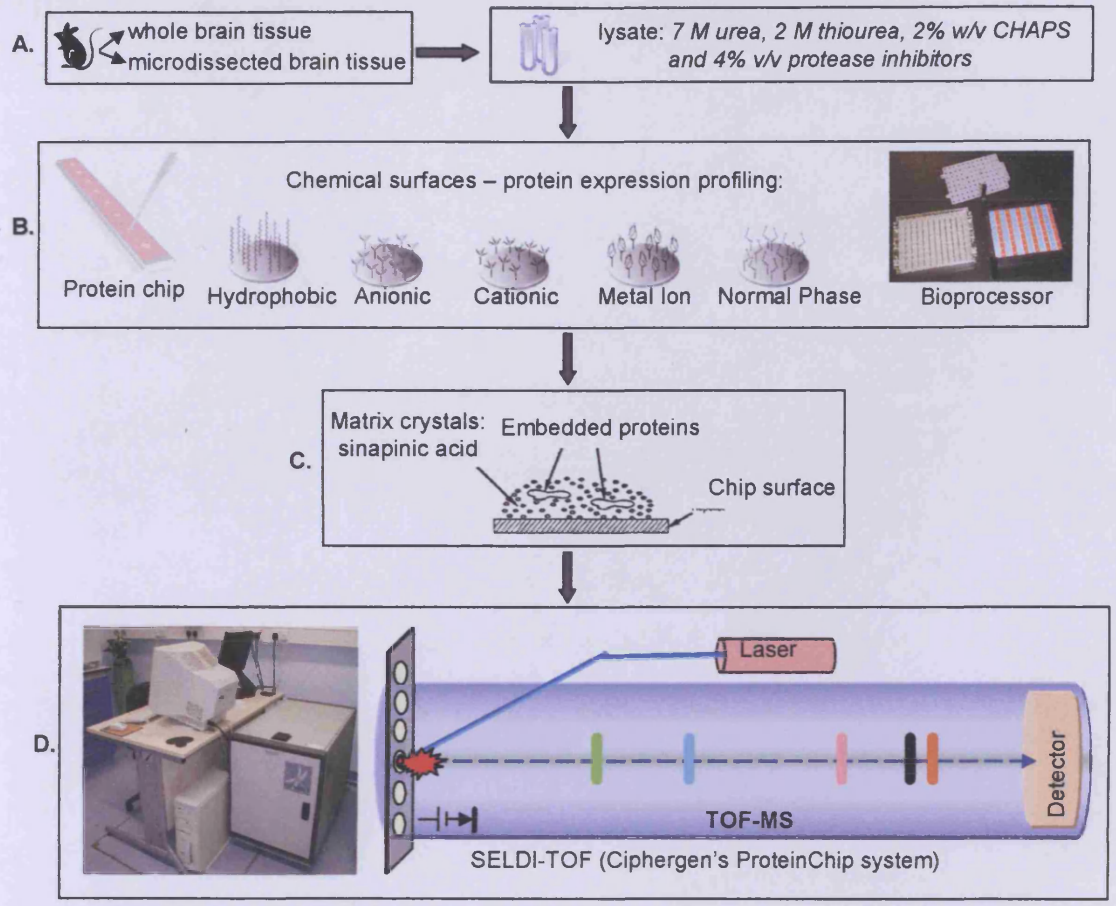

Figure 3.1 Workflow of the SELDI-TOF ProteinChip system.
A. Whole or microdissected mouse brain lysate was prepared in urea-thiourea lysis buffer.
B. Samples were applied to spots on a ProteinChip array, each with a specific chromatographic surface to bind selected proteins from the mixture, based on the intrinsic properties of the proteins. Up to 12 chips could be processed simultaneously in a bioprocessor.
C. Energy Absorbing Molecules (EAM) were applied to each spot. EAM convert laser energy to thermal energy, thus facilitating the desorption and ionisation of the proteins.
D. The ProteinChip is fed into the SELDI-TOF mass spectrometer, which consists of a vacuum chamber in which the samples are hit with a laser, causing desorption and ionisation of the proteins. The ions are projected down the TOF MS tube towards the detector. Protein mass is determined based on their mass-to-charge ratio (m/z). Reproduced from General Ciphergen seminar Microsoft PowerPoint presentation.

See next page

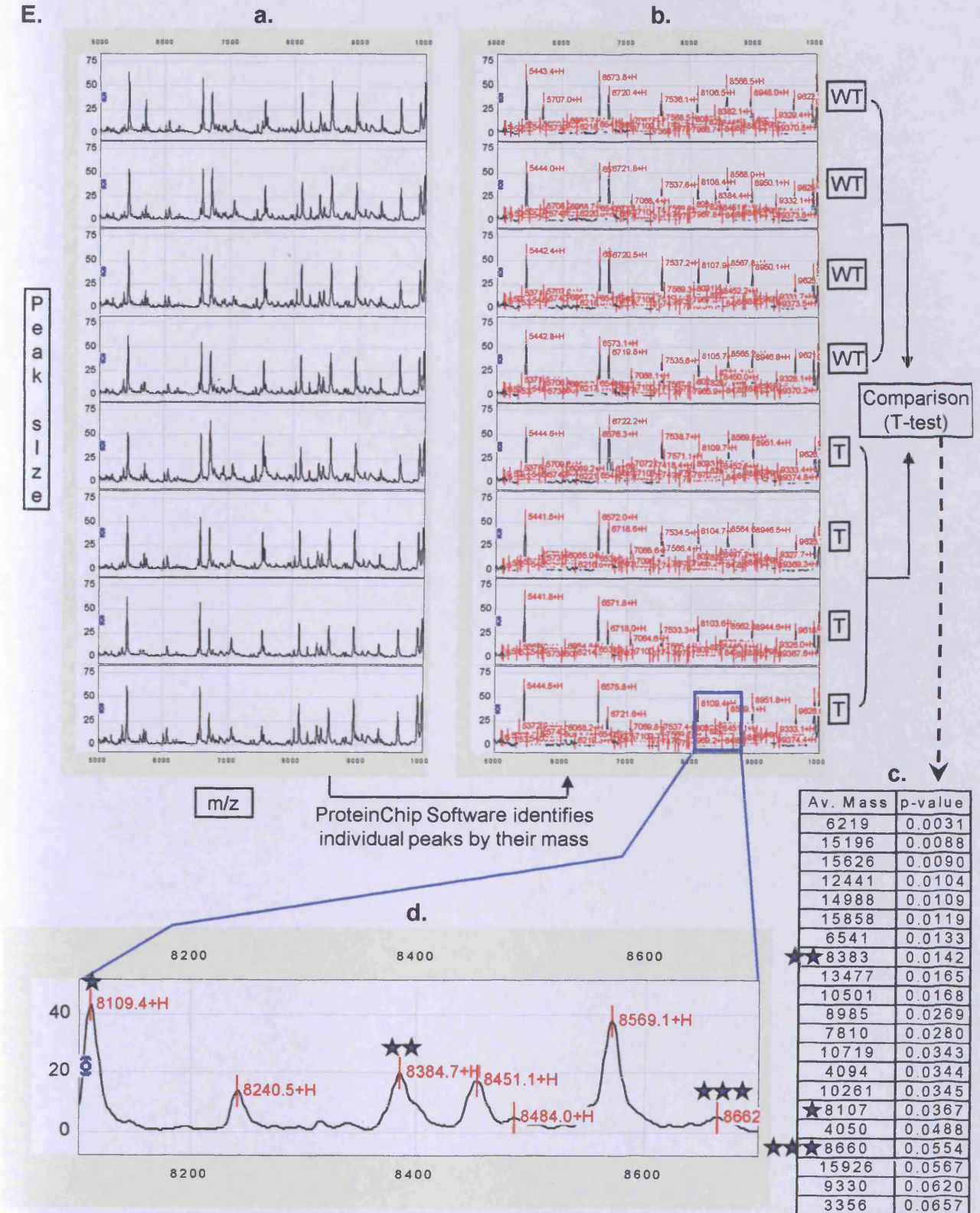

Av. Mass	p-value
6219	0.0031
15196	0.0088
15626	0.0090
12441	0.0104
14988	0.0109
15858	0.0119
6541	0.0133
★★8383	0.0142
13477	0.0165
10501	0.0168
8985	0.0269
7810	0.0280
10719	0.0343
4094	0.0344
10261	0.0345
★8107	0.0367
4050	0.0488
★★★8660	0.0554
15926	0.0567
9330	0.0620
3356	0.0657
10375	0.0661
7494	0.0705
6927	0.0719
9623	0.0757
6825	0.0842
5651	0.0854
15292	0.0864
4897	0.0949
5443	0.0952
7569	0.0961

E. a. The signal received from the detector is translated into a spectrum, showing relative abundance against m/z of the detected proteins. **b.** Individual peaks are identified and their relative abundance compared with that of the corresponding peaks on the other spectra. **c.** Statistical analysis by Student's t-test gives a list of proteins which show a significant difference between the sample groups. **d.** Part of a spectrum zoomed in on masses 8100-8700. The stars indicate the peaks with $p < 0.01$. WT = wild type; T = transgenic.

3.2.2 Mouse brain samples

Each experiment used the maximum number of biological replicates available and two technical replicates of each sample. All the samples were randomly distributed over the ProteinChip arrays, based on a randomised set-up generated by Microsoft Excel, as demonstrated in Tables 3.1A and B.

The samples were homogenates from either half cerebra or micro-dissected brain regions of HD mice and their wild type littermates. The mouse models studied were R6/1 (Mangiarini *et al.* 1996), Hdh^{Q92} (Wheeler *et al.* 1999) and Hdh^{Q150} (Lin *et al.* 2001). For the Hdh^{Q92} and Hdh^{Q150}, only homozygous animals were used to compare with their wild type littermates. An overview of the experimental design can be found in Table 3.2.

Table 3.1 Random distribution of samples in an experiment.

Sample	Model	Genotype	Age
CA-CP	Hdh^{Q92}	WT	18 months
CB-CP	Hdh^{Q92}	WT	18 months
CC-CP	Hdh^{Q92}	HOM	18 months
CD-CP	Hdh^{Q92}	HOM	18 months
CE-CP	Hdh^{Q92}	HOM	18 months
CF-CP	Hdh^{Q92}	HOM	18 months
CG-CP	Hdh^{Q92}	HOM	18 months
CH-CP	Hdh^{Q92}	HOM	18 months
CI-CP	Hdh^{Q92}	WT	18 months
CJ-CP	Hdh^{Q92}	WT	18 months
CK-CP	Hdh^{Q92}	WT	18 months
CL-CP	Hdh^{Q92}	WT	18 months

Table A

spot	Chip 1	Chip 2	Chip 3
A	CD-CP(2)	CC-CP(2)	CI-CP(2)
B	CH-CP(1)	CI-CP(1)	CA-CP(2)
C	CB-CP(2)	CA-CP(1)	CK-CP(1)
D	CJ-CP(2)	CK-CP(2)	CJ-CP(1)
E	CL-CP(2)	CF-CP(1)	CF-CP(2)
F	CD-CP(1)	CH-CP(2)	CE-CP(2)
G	CB-CP(1)	CG-CP(2)	CL-CP(1)
H	CG-CP(1)	CE-CP(1)	CC-CP(1)

Table B

Table A lists the samples (CA-L refers to the individual; CP=caudate-putamen), the mouse model, genotype and age. Table B shows the random distribution of the samples in duplicate over three chips.

Table 3.2 Experimental design of the ProteinChip experiments.

mouse model	age	brain tissue	number samples	gender samples	ProteinChip type
R6/1	18 weeks	whole brain	3 WT x 3 T	M	CM10; Q10; IMAC-Cu
Hdh^{Q92}	18 months	caudate-putamen	6 WT x 6 HOM	WT: 5 F + 1 M HOM : 3 F + 3 M	CM10; Q10
		hippocampus	6 WT x 6 HOM	WT: 5 F + 1 M HOM : 3 F + 3 M	CM10
		cerebellum	6 WT x 5 HOM	WT: 5 F + 1 M HOM : 3 F + 2 M	CM10
		motor + prefrontal cortex	6 WT x 6 HOM	WT: 5 F + 1 M HOM : 3 F + 3 M	CM10
	12 months	caudate-putamen	5 WT x 5 HOM	F	CM10
	10 months	caudate-putamen	3 WT x 6 HOM	F	CM10
Hdh^{Q150}	18 months	caudate-putamen	9 WT x 9 HOM	WT: 3 F + 6 M HOM : 5 F + 4 M	CM10
	15 months	caudate-putamen	3 WT x 5 HOM	F	CM10

The different mouse models are listed with the ages and brain tissues used, the number of transgenic (T) / homozygous (HOM) samples that were compared with their wild type (WT) littermates, indicating the gender of the samples (F=female; M=male), on the different ProteinChip arrays.

3.2.3 ProteinChip arrays

Table 3.2 gives an overview of the ProteinChip arrays used in the different experiments. The ProteinChip CM10 array incorporates a negatively charged carboxylate chemistry and acts as a weak cation exchanger. The surface of the ProteinChip binds proteins through positively charged residues, such as lysine, arginine and histidine, under low pH and low salt conditions.

The ProteinChip Q10 array incorporates a positively charged quaternary amine chemistry and acts as a strong anion exchanger. The surface of the ProteinChip binds proteins through negatively charged residues, such as aspartic acid and glutamic acid residues, under high pH and low salt conditions.

The ProteinChip IMAC-Cu array incorporates a nitrilotriacetic acid surface which chelates metal ions, in this case copper sulphate. The charged ProteinChip surface binds phosphorylated proteins and proteins with histidine, tryptophan and cysteine residues under high salt conditions and a pH 6.0-8.0.

The ProteinChip NP20 array incorporates a silicon dioxide surface that binds proteins by hydrogen bonds through hydrophilic and charged residues on the protein surface. The binding conditions are determined by the buffer.

3.2.4 Preparation of ProteinChip arrays and samples for SELDI-TOF

All the ProteinChips used in one experiment were prepared in a bioprocessor, which can hold up to 12 ProteinChips in a 96-well format, as shown in Figure 3.2. The bioprocessor was washed in 1% Triton-x100 in PBS for 1-24 h. Protein samples were diluted to 2 mg/ml by adding appropriate volumes of urea-thiourea lysis buffer. The required number of CM10, Q10 or IMAC-Cu ProteinChips were placed in the bioprocessor.

Prior to equilibration, IMAC-Cu ProteinChip arrays were charged with 50 µl of 100 mM copper sulphate and incubated on the Micromix (Euro/DPC Ltd, Caernarfon, UK) (form 20; amplitude 5) for 5 min. Each well was rinsed with 150 µl dH_2O and incubated with 50 µl of 50 mM sodium acetate (pH 4.0) on the Micromix for 5 min to remove unbound copper. Each well was rinsed with 150 µl dH_2O before the equilibration step with the binding buffer was performed.

The spots were equilibrated with 150 µl each of the appropriate binding buffer, an overview of which can be found in Table 3.3. The ProteinChips were incubated on the Micromix for 5 min. The buffer was removed and the equilibration step repeated. The samples were diluted 1/5.5 in the appropriate binding buffer to a total volume of 55 µl and applied to the spot. The wells were sealed with tape and incubated on the Micromix for 40 min at room temperature. To eliminate sample noise, non-specific binding proteins and buffer contaminants were washed away during three wash steps with 150 µl of appropriate wash buffer

for 5 min each on the Micromix. A final wash was performed with 150 µl of 1 mM HEPES (pH 7.0), for 1 min on the Micromix. The bioprocessor was dismantled and the ProteinChips air dried. 1 µl of SPA solution was applied to the spots twice, each with an air dry time of 20 min.

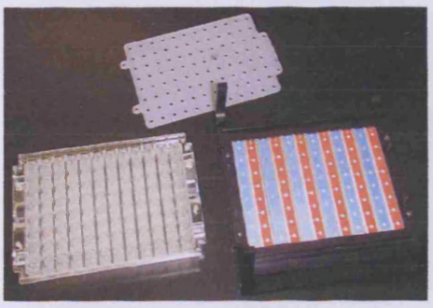

Figure 3.2 Bioprocessor with up to 12 ProteinChip arrays in a 96-well format.

Table 3.3 ProteinChip arrays used in the present study.

Protein Chip	Chromatographic Surface	Protein Selection	Binding Conditions	Binding & Wash Buffer	Buffer pH
CM10	anionic surface	cationic exchanger	-low pH (pH<pI-1) -low salt	50mM ammonium acetate	pH 4.0
Q10	cationic surface	anionic exchanger	-high pH (pH>pI+1) -low salt	50mM CAPS	pH 10.0
IMAC-Cu	nitrilotriacetic acid + 100mM copper sulphate	immobilized metal affinity capture	-pH 6-8 -high salt	PBS	pH 7.2
NP20	SiO2 surface	normal phase chip	buffer conditions	dH_2O	

3.2.5 Reading ProteinChip arrays

The ProteinChip data are time-of-flight measurements converted to mass measurements by the calibration equation. Before each experiment, the machine was re-calibrated with the All-in-1 Protein Standard II calibration ProteinChip (section 2.2.2).

Every new experiment needs an updated spot and chip protocol. Spot protocols hold the instructions for automatic data collection from a single spot, as shown in Figure 3.3. Most parameters, such as the optimised mass range, the acquisition settings and the detector sensitivity, were held constant for all the experiments. The laser intensity and warming positions varied between experiments, and were determined before data collection by manually reading chosen points on each spot of the ProteinChip. The laser intensity that generated the clearest spectra, with the highest peak no higher than 100 and the majority of the peaks ideally between 50-75, was chosen for automatic data collection. The warming position was always set at laser intensity +5, as advised by the supplier. Figure 3.4 shows an example of a ProteinChip protocol, which contains the instructions for automatic data collection from a series of spots on an array.

LOW MW SPOT PROTOCOL
1: Set high mass to 50000 Daltons, optimised from 3000 Daltons to 50000 Daltons.
2: Set starting laser intensity to 230.
3: Set starting detector sensitivity to 10.
4: Focus mass at 15000 Daltons.
5: Set data acquisition method to Seldi Quantitation
6: Set Seldi acquisition parameters 20. delta to 4. transients per to 10 ending position to 82.
7: Set warming positions with 2 shots at intensity 235 and Don't include warming shots.
8: Process sample.

Figure 3.3 Spot protocol for automatic data collection from a single spot. Instructions indicated in red were held constant for all experiments. Laser intensity (2) varied and was determined by manually reading chosen points on each spot of a new ProteinChip before automatic data collection. Warming positions (7) were always set at laser intensity +5. The data from the warming shots were not included in the resulting spectra.

Spot	Spectrum Tag	Spot Protocol
A	Q150-EA-CP-unb	Low MW
B	Q150-EA-CP-10%	Low MW
C	Q150-EA-CP-20%	Low MW
D	Q150-EA-CP-30%	Low MW
E	Q150-EA-CP-40%	Low MW
F	Q150-EA-CP-50%	Low MW
G	Q150-EA-CP-60%	Low MW
H	Q150-EA-CP-80%	Low MW

Figure 3.4 Chip protocol for automatic data collection from all spots on a ProteinChip. For each spot (A-H), the sample and the spot protocol are listed.

3.2.6 Analysis by ProteinChip software: detecting peaks

The data collected by the ProteinChip reader for each spot is translated into a spectrum. An eight-spot ProteinChip gives eight spectra, one spectrum for each spot. To compensate for variations in sample loading, the spectra are normalised using the Total Ion Current method. This method calculates the average intensity for each spectrum by dividing the total ion current by the number of data points on that spectrum. The mean of all average intensities of all spectra gives the normalisation coefficient. For each spectrum, the normalisation coefficient is divided by the average intensity for that spectrum, which gives the normalisation factor. Finally, the intensity of each data point in a given spectrum is multiplied by the normalisation factor for that spectrum.

The m/z range used for normalisation in these experiments was 3,000-50,000 Da, which means that average intensities were calculated only within this range. The normalisation range of 3,000-50,000 Da was chosen because the initial goal was to screen for proteins within this band. However, the results of the early experiments demonstrated that only peaks under 20,000 Da were sufficiently consistent for comparison over multiple samples. Determining the size

of peaks over 20,000 Da became increasingly inaccurate, so that it was often not feasible to identify the same peak in different spectra with sufficient certainty. In addition, the shapes of the peaks in this higher molecular weight range became somewhat amorphous and they eventually disappeared into the background noise. However, to standardise all the SELDI experiments, the original normalisation range of 3,000-50,000 Da was used throughout, although only peaks with a molecular weight less than 20,000 Da were taken into account.

ProteinChip Software 3.1, from Ciphergen Biosystems Inc., was used to detect the individual peaks, with the default settings. All the detected peaks were manually checked for accuracy and presence in all the spectra. When a peak was not present in some of the spectra, it was manually selected. However, when a peak appeared in less than 30% of the spectra, it was rejected for further analysis and manually de-selected.

3.2.7 Statistical analysis of detected peaks

The details of the aligned peaks of a selected spectrum can be found in the 'List substances' window in the ProteinChip Software, shown in Figure 3.5. The mass and intensity data for all the peaks in each spectrum were used for statistical analysis in Microsoft Excel. The mass refers to the predicted masses of the proteins corresponding to the peaks and the intensity relates to the amount of that protein present in the sample.

The mass of each peak was averaged over all the spectra in an experiment. The intensities of the two technical replicates of each sample were also averaged. For each peak, a two-tailed student's t-test with unequal variance was performed on the intensities of the biological replicates, testing the null

hypothesis that there was no difference between HD and WT animals. As it was planned to confirm results by western blot analysis, the threshold chosen for exploratory significance was $p < 0.1$. For each peak with $p < 0.1$, the $\log_2$ fold change was calculated on the averaged intensities of HD and WT samples.

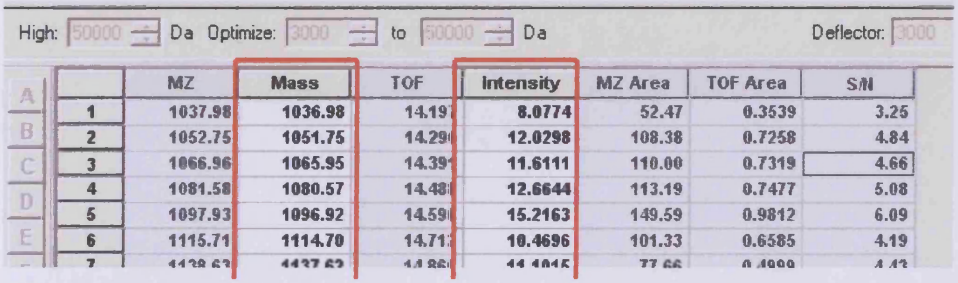

	MZ	Mass	TOF	Intensity	MZ Area	TOF Area	S/N
1	1037.98	1036.98	14.19	8.0774	52.47	0.3539	3.25
2	1052.75	1051.75	14.29	12.0298	108.38	0.7258	4.84
3	1066.96	1065.95	14.39	11.6111	110.00	0.7319	4.66
4	1081.58	1080.57	14.48	12.6644	113.19	0.7477	5.08
5	1097.93	1096.92	14.59	15.2163	149.59	0.9812	6.09
6	1115.71	1114.70	14.71	10.4696	101.33	0.6585	4.19
7	1139.63	1137.62	14.86	11.1015	77.66	0.4999	4.43

Figure 3.5 'List substances' window in the ProteinChip Software. Details are given on all peaks of a selected spectrum. The red boxes indicate the data (Mass and Intensity) that was used for statistical analysis in Microsoft Excel.

3.3 Optimisation of SELDI-TOF for mouse brain samples

3.3.1 Protein concentration

To determine the optimal protein concentration of mouse brain homogenate to use in experiments, a concentration range of an *Hdh*$^{Q92/+}$ half cerebra homogenate was run on a Q10 ProteinChip array. Figure 3.6 shows that, while a concentration of 2 mg/ml presented more peaks than the lower concentrations of 1 or 0.5 mg/ml, using the higher concentration of 4 mg/ml produced no more peaks and they were less well defined. It was concluded that 2 mg/ml was the optimal protein concentration.

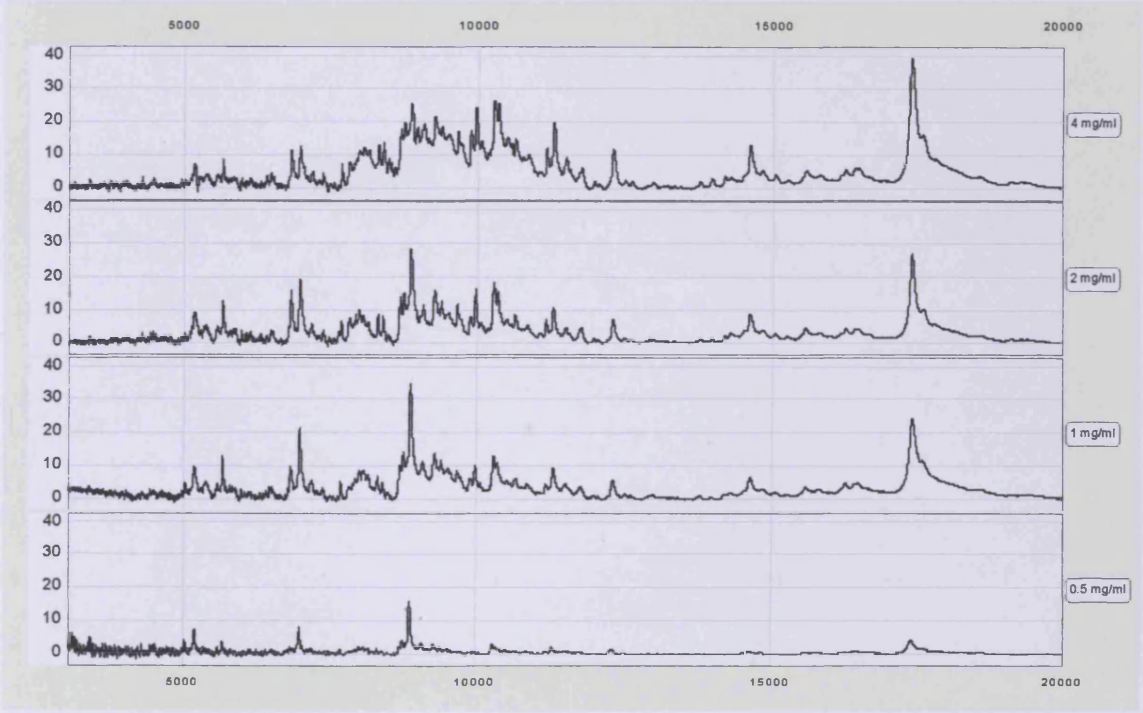

Figure 3.6 Spectra of four spots on a Q10 ProteinChip array in a protein concentration optimisation experiment. *Hdh*$^{Q92/+}$ half cerebra homogenate was used, at four different protein concentrations (4 mg/ml, 2 mg/ml, 1 mg/ml and 0.5 mg/ml).

3.3.2 Homogenate volume

To determine the effect of different volumes of homogenate applied to the spots, three optimisation experiments were carried out. The first two used All-in-1 Protein Standard II, provided by Ciphergen. All-in-1 Protein Standard II is a mixture of 7 proteins, used to calibrate the ProteinChip reader. The mixture consists of hirudin BHVK (6,964 Da), bovine cytochrome C (12,230 Da), equine myoglobin (16,951 Da), bovine carbonic anhydrase (29,023 Da), yeast enolase (46,671 Da), bovine albumin (66,433 Da) and bovine IgG (147,300 Da). Figure 3.7 shows a representative spectrum of this standard.

Figure 3.8 shows the spectra of three spots on the first ProteinChip, with a 1/50 and a 1/200 dilution of All-in-1 Protein Standard II in 50 μl of 50 mM CAPS buffer. EAM/All-in-1 Protein Standard II mixture was used as a control. The spectra showed that a dilution factor of 1/50 or more was too high.

Figure 3.9 shows the spectra of five spots on the second ProteinChip, with a selection of different concentrations of All-in-1 Protein Standard II in different volumes of 50 mM CAPS buffer: 1/2.5 in 5 μl, 1/5 in 10 μl, 1/10 in 20 μl and 1/15 in 30 μl. EAM/All-in-1 Protein Standard II mixture was used as a control. The spectra showed that the sample dilution and the total volume have an effect on the reading and that a 1/5 dilution produced the highest and best defined peaks.

Figure 3.10 shows the spectra of three spots on the third ProteinChip, with a 1/10 dilution of Chicken Lysozyme in 50 μl, 100 μl and 200 μl of 50 mM CAPS buffer. The spectrum clearly showed that the total volume had an impact on the size and the shape of the peaks. Although increasing the volume gave stronger peaks, the shapes of the peaks became less defined. In combination with the

previous experiments, it was decided that a total volume of 50 µl with a lower dilution factor of 1/5 would present the best defined spectra.

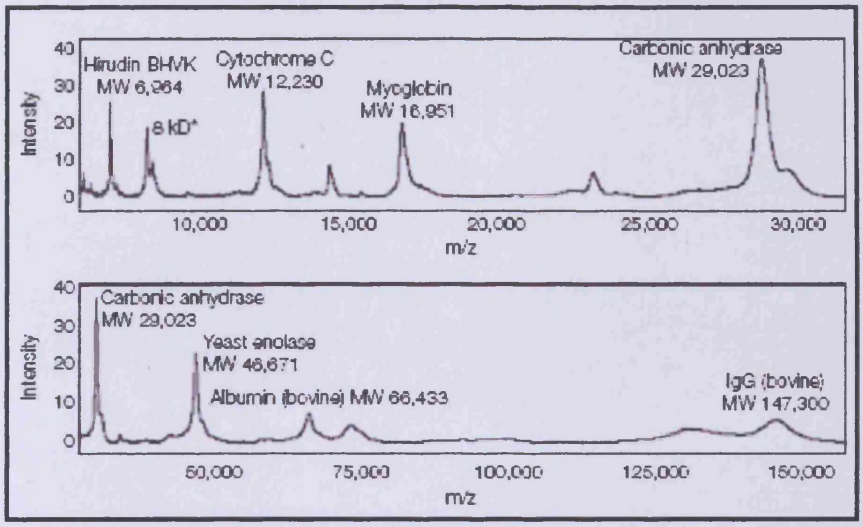

Figure 3.7 Representative spectra for ProteinChip All-in-1 Protein Standard II.

Figure 3.8 Spectra of three spots on a Q10 ProteinChip array in a sample volume optimisation experiment using different dilutions.

1. the spectrum of 1 µl of EAM/All-in-1 Protein Standard II mix, used as control, shows the expected peaks;
2. the spectrum of 50 µl of 1/50 All-in-1 Protein Standard II in 50 mM CAPS buffer shows no peaks over the noise level.
3. the spectrum of 50 µl of 1/200 All-in-1 Protein Standard II in 50 mM CAPS buffer shows no peaks over the noise level.

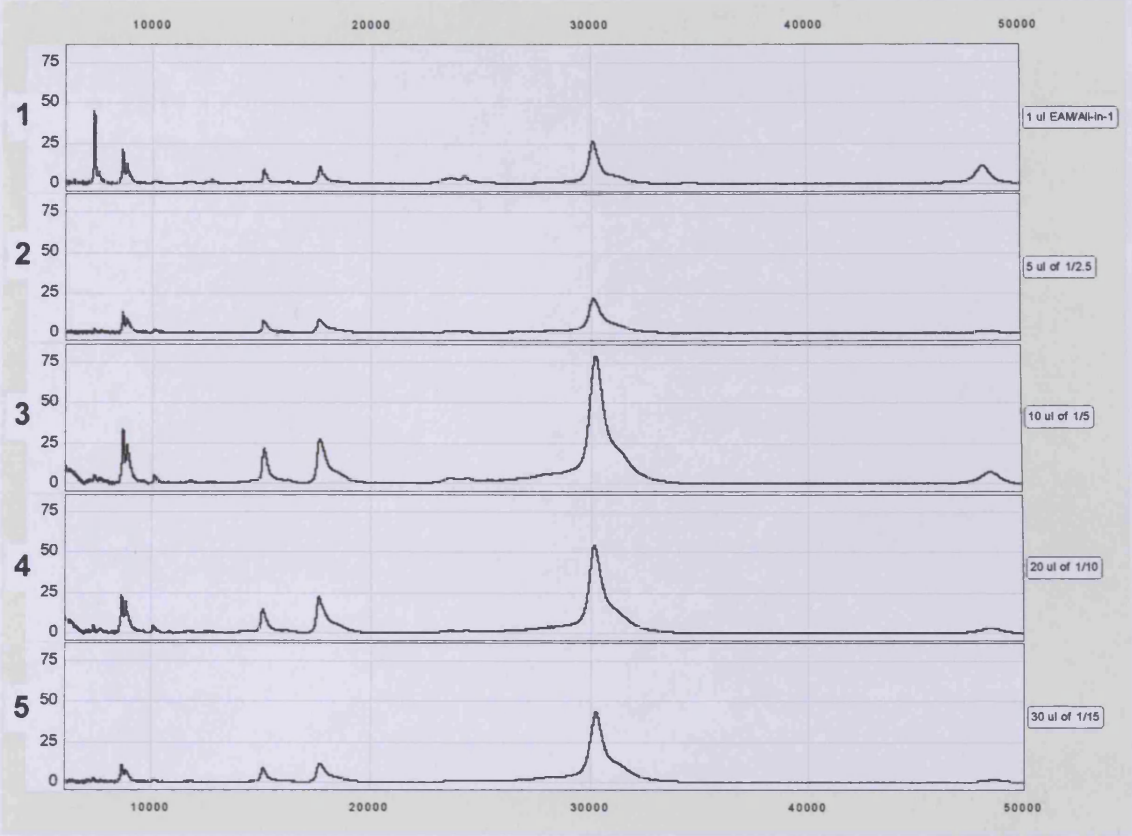

Figure 3.9 Spectra of five spots on a Q10 ProteinChip array in a sample volume optimisation experiment using different dilutions in different total volumes. On each spot, a different dilution of All-in-1 Protein Standard II in a different volume of 50 mM CAPS buffer was applied:

1. the spectrum of 1 µl of EAM/All-in-1 Protein Standard II mix, used as control, shows the expected peaks;
2. spectrum of 5 µl of 1/2.5 All-in-1 Protein Standard II;
3. spectrum of 10 µl of 1/5 All-in-1 Protein Standard II;
4. spectrum of 20 µl of 1/10 All-in-1 Protein Standard II;
5. spectrum of 30 µl of 1/15 All-in-1 Protein Standard II.

Figure 3.10 Spectra of three spots on a Q10 ProteinChip array in a sample volume optimisation experiment using the same dilution in different total volumes. A 1/10 dilution of Chicken Lysozyme in different volumes of 50 mM CAPS buffer was applied:

1. spectrum of 50 μl of 1/10 Chicken Lysozyme;
2. spectrum of 100 μl of 1/10 Chicken Lysozyme;
3. spectrum of 200 μl of 1/10 Chicken Lysozyme.

3.3.3 Binding and washing pH

To investigate the effect of pH on Q10 and CM10 ProteinChip arrays, *Hdh*$^{Q92/+}$ half cerebra homogenate was applied to both ProteinChips, each spot pre-treated with a different buffer with different pH: 50 mM Ammonium Acetate (pH 4.0), 50 mM Tris/HCl (pH 6.0), 50 mM Tris (pH 8.0) and 50 mM CAPS (pH 10.0). The spectra in Figure 3.11 show the importance of the pH for optimal protein binding on the different ProteinChips arrays. Protein binding was significantly increased on the anionic exchange Q10 ProteinChip under alkaline conditions (pH 10.0) (Figure 3.11A), while the cationic exchange CM10 ProteinChip needed acidic conditions (pH 4.0) for optimal protein binding (Figure 3.11B). Both sets of spectra put together illustrate the divergence between the two, demonstrating the different subset of proteins they select for. The strongest

signal is generated under alkaline conditions on the Q10 ProteinChip and under acidic conditions on the CM10 ProteinChip, as expected.

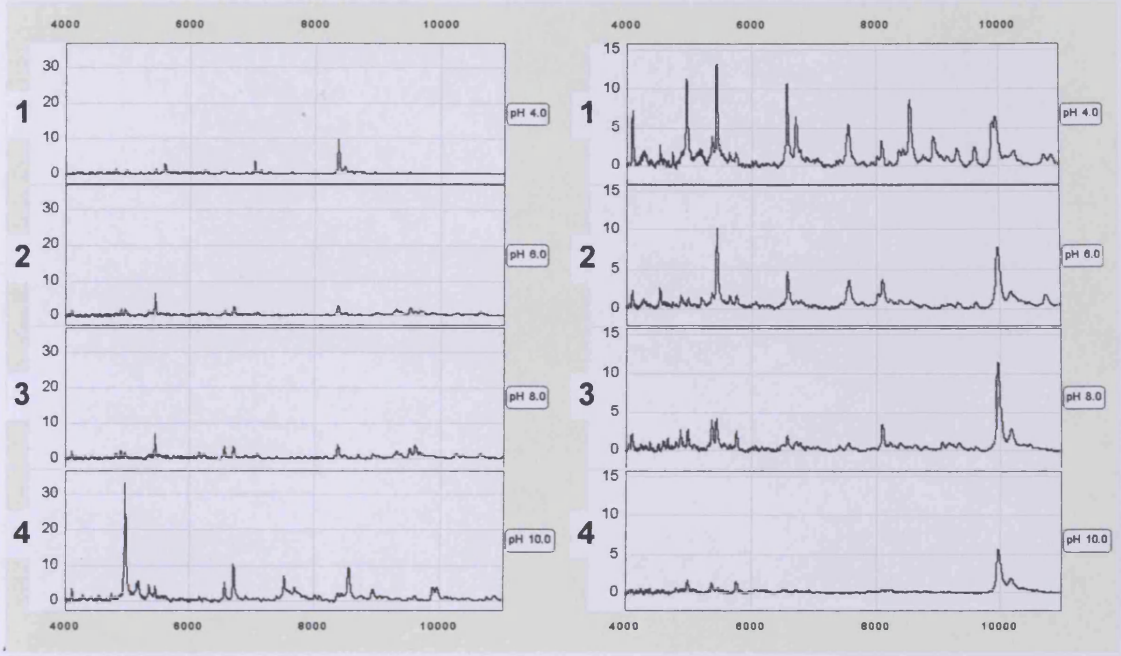

Figure 3.11 Spectra of four spots on a Q10 **(A)** and CM10 ProteinChip **(B),** each spot pre-treated with a different buffer.

1. 50 mM Ammonium Acetate (pH 4.0);
2. 50 mM Tris/HCl (pH 6.0);
3. 50 mM Tris (pH 8.0);
4. and 50 mM CAPS (pH 10.0).

3.3.4 Technical and biological replicates

The number of biological replicates was determined by the number of animals available. To assess the need for multiple technical replicates, eight technical replicates of an R6/1 half cerebra homogenate were assayed on a CM10 ProteinChip array. From the spectra, 25 consecutive peaks with masses within the range of interest for this project were analysed for lot to lot reproducibility of peak intensity. The chart in Figure 3.12 shows the peak masses

and the means of peak intensities, with the coefficient of variance ranging between 9-27%. As the aim of the project was to compare biological replicates, two technical replicates of each were considered adequate. This would allow samples with technical artifacts to be removed from the analysis, while limiting the cost and saving sample, which was already in short supply.

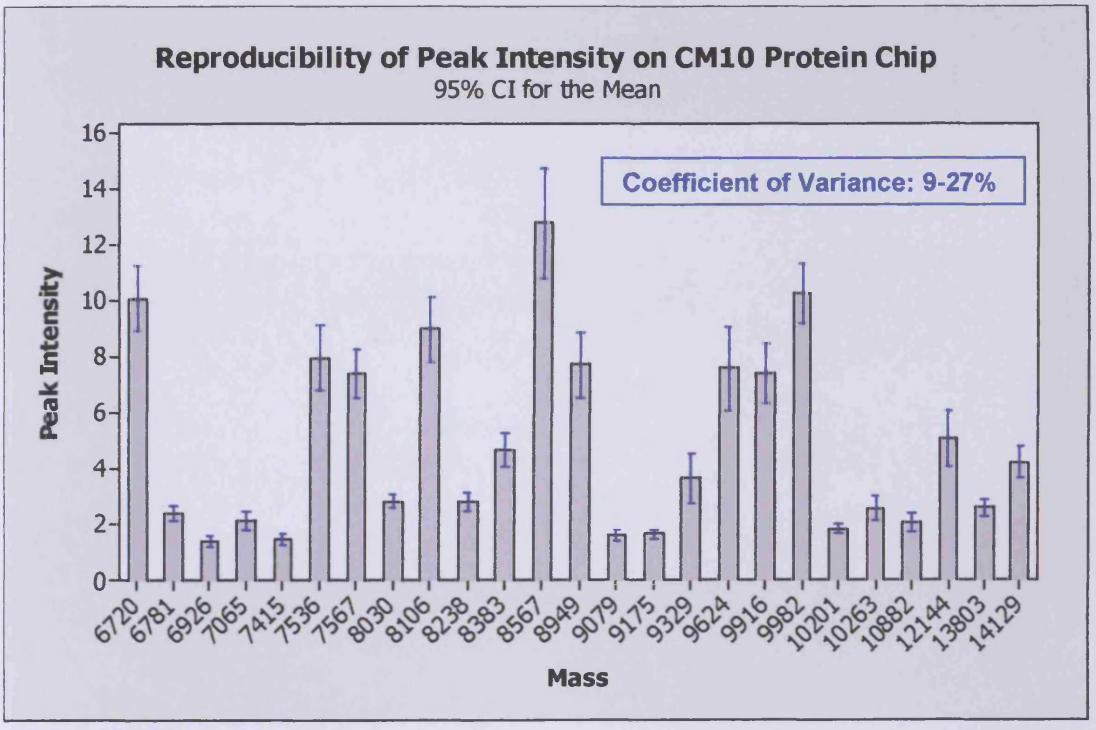

Figure 3.12 The reproducibility of peak intensity on a CM10 ProteinChip array. For 25 consecutive peak, the mean of peak intensity of eight technical replicates of an R6/1 half cerebra homogenate on a CM10 ProteinChip was calculated. Blue error bars indicate the coefficient of variance for each of the means, ranging between 9-27%.

3.4 Comparison of R6/1 and wild type mouse brain proteome

Homogenates of half cerebra of 18 week old R6/1 were examined using CM10, Q10 and IMAC-Cu ProteinChip arrays. Table 3.4 lists the peaks which were significantly different between transgenic and WT animals ($p < 0.1$).

The CM10 ProteinChips identified five peaks which were significantly different, corresponding to 11% of the total number of peaks detected. Three of these were increased and two decreased in transgenic R6/1 brain compared with wild type. The magnitude of the changes ranged between 19-81%.

The Q10 ProteinChips showed fewer differences, with three of 46 (=7%) peaks significantly different, all of which were decreased in transgenic animals compared with wild type. The magnitude of the changes ranged between 27-64%, similar to the ones on the CM10 ProteinChips. Two of the three peaks were also detected and significant on the CM10 ProteinChips.

The IMAC-Cu ProteinChips showed only one peak out of 20 with a significant difference. However, the total number of peaks detected on these chips was very low and less than half of the number on the CM10 and Q10 ProteinChips. It was also clear that the total number of peaks detected on any of the ProteinChips was well below that expected, based on previous experiments with similar samples (B. Hoogendoorn; personal communication).

Table 3.4 Protein peaks shown to be changed in intensity in 18 month R6/1 mouse brain compared with controls.

mouse model	R6/1								
age	18 weeks								
brain tissue	half cerebra			half cerebra			half cerebra		
ProteinChip	CM10			Q10			IMAC-CU		
total nr peaks	46			46			20		
	Av. Mass	p-value	log_2 FC	Av. Mass	p-value	log_2 FC	Av. Mass	p-value	log_2 FC
	6781	0.0159	-0.35	6919	0.0291	-0.53	5465	0.0362	-0.30
	8567	0.0355	0.20	6717	0.0921	-0.64			
	6720	0.0375	-0.81	7648	0.0987	-0.27			
	6926	0.0756	-0.55						
	9079	0.0846	0.19						

Protein peaks with a significant ($p < 0.1$) difference, detected by SELDI-TOF on CM10, Q10 and IMAC-Cu ProteinChip arrays. The lists show the average mass of the peaks with corresponding p-value, the log_2 fold change (negative=decrease; positive=increase) and the total number of peaks detected. The red entries are the peaks found to be significant on more than one ProteinChip array.

3.5 Comparison of *Hdh*$^{Q92/Q92}$ and *Hdh*$^{+/+}$ brain proteome

The *Hdh*$^{Q92/Q92}$ and *Hdh*$^{+/+}$ animals compared were 18, 12 and 10 months old. The microdissected brain regions used were caudate-putamen (CP), hippocampus (HC), cerebellum (CB) and a combination of motor and prefrontal cortex (MC+PFC). The motor and prefrontal cortex were jointly homogenised because the prefrontal cortex alone gave a homogenate with a protein concentration below 2 mg/ml, the minimum needed to load the ProteinChips.

Initially, 18 month *Hdh*$^{Q92/Q92}$ and *Hdh*$^{+/+}$ were analysed on both CM10 and Q10 ProteinChip arrays. However, the results (Table 3.5) showed the same trend as in the R6/1 experiment, with more peaks detected and more significant results with CM10 than with Q10 arrays. Because of the cost of the ProteinChips, it was decided to use only CM10 chips in future, and screen more brain regions as well as a different mouse model (*Hdh*^{Q150}). On the CM10 ProteinChips, a substantial

proportion of the protein peaks showed a significant difference in the caudate-putamen of the 18 month animals: 17 of 94 peaks (=18%), eight increased and nine decreased. The magnitude of the changes ranged between 21-114%, with some slightly larger changes than in the R6/1 experiments.

Caudate-putamen of 18, 12 and 10 month $Hdh^{Q92/Q92}$ and $Hdh^{+/+}$ was compared on CM10 ProteinChips. A substantial proportion of the peaks were significantly different at all ages, this only being marginally lower in the younger animals: 18% of peaks differed at 18 months, 14% at 12 months and 13% at 10 months (Table 3.6). At 10 months, half of these peaks were increased and half decreased. At 12 months, all peaks apart from one were decreased. The magnitude of the changes was larger in the older animals, with a maximum change of 114% at 18 months, 77% at 12 months and 60% at 10 months.

Peaks in different spectra are considered to correspond when their m/z ratios lie close together and when, upon comparison of the spectra, the shapes of the peaks and of the areas around the peaks are similar. Of the 17 significant peaks at 18 months, seven were likely to be the same as those significant at one of the previous timepoints, all but one showing the same directional change. The trace view of this seemingly ambiguous peak indicated however that this was indeed likely to be the same peak at both timepoints. None of the peaks appeared to be significant at all three timepoints.

Table 3.7 shows the results of a comparison between different brain regions in 18 month $Hdh^{Q92/Q92}$ and $Hdh^{+/+}$ on CM10 ProteinChip arrays. The high level of differences in the caudate-putamen (18%) was not observed in the other regions. The hippocampus and cortex showed a few differences, respectively four (5%) and three (4%), while there was only one change in the cerebellum. The

magnitude of the changes in these regions was considerably smaller than in the caudate-putamen, with a maximum change of 38% in the cortex, 26% in the hippocampus and 23% in the cerebellum against 114 % in the caudate-putamen. Only one peak appeared to be different in more than one region, showing a change in the same direction but larger in the caudate-putamen (57%) than in the cortex (38%).

Table 3.5 Evaluation of the CM10 and Q10 ProteinChip arrays for comparing the caudate-putamen proteome of 18 month $Hdh^{Q92/Q92}$ and $Hdh^{+/+}$.

mouse model	***Hdh*^{Q92}**					
age	**18 months**					
brain tissue	**caudate-putamen**			**caudate-putamen**		
ProteinChip	**CM10**			**Q10**		
total nr peaks	**94**			**71**		
	Av. Mass	p-value	log_2 FC	Av. Mass	p-value	log_2 FC
	10604	0.0020	0.52	3215	0.0044	0.39
	5372	0.0076	0.65	8446	0.0186	-0.32
	6066	0.0104	-0.34	4961	0.0365	0.25
	7662	0.0266	0.57	5397	0.0366	0.80
	7490	0.0316	-0.73	7647	0.0719	-0.18
	5103	0.0407	0.21	13773	0.0871	0.24
	13991	0.0450	0.33	15442	0.0966	-0.28
	3555	0.0465	0.50			
	10872	0.0656	-0.23			
	7366	0.0689	0.45			
	7805	0.0740	-1.14			
	15835	0.0775	-0.29			
	5490	0.0787	0.35			
	15180	0.0831	-0.37			
	15274	0.0886	-0.28			
	14971	0.0950	-0.50			
	15608	0.0978	-0.86			

Protein peaks with a significant ($p < 0.1$) difference, showing average mass with corresponding p-value, log_2 fold change (negative=decrease; positive=increase) and total number of peaks.

Table 3.6 Comparison of changes in the caudate-putamen of *Hdh*$^{Q92/Q92}$ at 18, 12 and 10 months.

mouse model	*Hdh* ^{Q92}								
age	18 months			12 months			10 months		
brain tissue	caudate-putamen			caudate-putamen			caudate-putamen		
ProteinChip	CM10			CM10			CM10		
total nr peaks	94			91			82		
	Av. Mass	p-value	log_2 FC	Av. Mass	p-value	log_2 FC	Av. Mass	p-value	log_2 FC
	10604	0.0020	0.52	4899	0.0016	-0.77	8770	0.0019	0.30
	5372	0.0076	0.65	11351	0.0022	0.49	14987	0.0102	-0.48
	6066	0.0104	-0.34	13478	0.0088	-0.42	8563	0.0149	0.20
	7662	0.0266	0.57	6784	0.0139	-0.34	11083	0.0172	0.22
	7490	0.0316	-0.73	5103	0.0160	-0.37	15716	0.0341	-0.60
	5103	0.0407	0.21	15624	0.0185	-0.64	15198	0.0431	-0.38
	13991	0.0450	0.33	9624	0.0236	-0.46	5196	0.0479	0.52
	3555	0.0465	0.50	6828	0.0367	-0.47	4271	0.0589	0.30
	10872	0.0656	-0.23	10719	0.0642	-0.54	8026	0.0775	0.21
	7366	0.0689	0.45	9331	0.0727	-0.30	14126	0.0838	-0.33
	7805	0.0740	-1.14	7812	0.0764	-0.46	7489	0.0851	-0.33
	15835	0.0775	-0.29	15854	0.0958	-0.32			
	5490	0.0787	0.35	11797	0.0981	-0.72			
	15180	0.0831	-0.37						
	15274	0.0886	-0.28						
	14971	0.0950	-0.50						
	15608	0.0978	-0.86						

Protein peaks with a significant ($p < 0.1$) difference between *Hdh*$^{Q92/Q92}$ and *Hdh*$^{+/+}$ caudate-putamen at 18, 12 and 10 months on CM10 ProteinChip arrays are listed with their average mass, p-value, log_2 fold change (negative=decrease; positive=increase) and total number of peaks. The red entries are the peaks found to be significant on more than one ProteinChip array.

Table 3.7 Comparison of changes in different brain regions of 18 month $Hdh^{Q92/Q92}$.

mouse model	Hdh^{Q92}											
age	18 months			18 months			18 months			18 months		
brain tissue	hippocampus			cerebellum			motor+prefrontal cortex			caudate-putamen		
ProteinChip	CM10			CM10			CM10			CM10		
total nr peaks	76			74			84			94		
	Av. Mass	p-value	log_2 FC	Av. Mass	p-value	log_2 FC	Av. Mass	p-value	log_2 FC	Av. Mass	p-value	log_2 FC
	10209	0.0070	0.16	8391	0.0821	0.23	18454	0.0289	-0.25	10604	0.0020	0.52
	7005	0.0091	-0.13				7663	0.0453	0.38	5372	0.0076	0.65
	10127	0.0128	0.26				7066	0.0994	-0.30	6066	0.0104	-0.34
	9919	0.0297	0.20							7662	0.0266	0.57
										7490	0.0316	-0.73
										5103	0.0407	0.21
										13991	0.0450	0.33
										3555	0.0465	0.50
										10872	0.0656	-0.23
										7366	0.0689	0.45
										7805	0.0740	-1.14
										15835	0.0775	-0.29
										5490	0.0787	0.35
										15180	0.0831	-0.37
										15274	0.0886	-0.28
										14971	0.0950	-0.50
										15608	0.0978	-0.86

Protein peaks with a significant ($p < 0.1$) difference in the hippocampus, cerebellum, motor+prefrontal cortex and caudate-putamen of 18 month $Hdh^{Q92/Q92}$ compared to $Hdh^{+/+}$ on CM10 ProteinChip arrays are listed with their average mass, p-value, log_2 fold change (negative=decrease; positive=increase) and total number of peaks detected. The red entry is the only peak found to be significant in more than one brain region.

3.6 Comparison of *Hdh*$^{Q150/Q150}$ and *Hdh*$^{+/+}$ caudate-putamen proteome

A comparison was carried out between *Hdh*$^{Q150/Q150}$ and *Hdh*$^{+/+}$ caudate-putamen of 18 and 15 month animals on CM10 ProteinChip arrays. There were also animals of 10 months of age and a combination of 3 and 4 months old, but these samples became available after the ProteinChip analysis was finished and were used only in western blot analysis. A substantial proportion of the protein peaks in the 18 month samples were significantly different: 31 out of 97 peaks (=32%), nearly all of which were increased in *Hdh*$^{Q150/Q150}$ (Table 3.8). The magnitude of the changes ranged between 12-92%, similar to the changes seen in the R6/1. There were considerably fewer differences in the 15 month *Hdh*$^{Q150/Q150}$: seven out of 85 peaks (=8%), half increased and half decreased. The magnitude of the changes was noticeably smaller in the younger animals: a maximum change of 43% at 15 months compared with 92% at 18 months. Only two of the significant peaks at 18 months appeared to be significant at 15 months.

Table 3.8 Comparison of *Hdh*$^{Q150/Q150}$ and *Hdh*$^{+/+}$ caudate-putamen proteome.

mouse model	*Hdh*^{Q150}					
age	18 months			15 months		
brain tissue	caudate-putamen			caudate-putamen		
ProteinChip	CM10			CM10		
total nr peaks	97			85		
	Av. Mass	p-value	log_2 FC	Av. Mass	p-value	log_2 FC
	6219	0.0031	0.37	6775	0.0052	-0.19
	15196	0.0088	0.37	8025	0.0102	0.22
	15626	0.0090	0.68	8979	0.0181	0.43
	12441	0.0104	0.37	7931	0.0229	0.42
	14988	0.0109	0.55	6568	0.0281	-0.26
	15858	0.0119	0.30	9325	0.0722	-0.23
	6541	0.0133	0.46	8788	0.0763	0.20
	8383	0.0142	0.47			
	13477	0.0165	0.34			
	10501	0.0168	0.26			
	8985	0.0269	0.23			
	7810	0.0280	0.67			
	10719	0.0343	0.30			
	4094	0.0344	0.92			
	10261	0.0345	0.25			
	8107	0.0367	0.23			
	4050	0.0488	0.27			
	8660	0.0554	0.27			
	15926	0.0567	0.27			
	9330	0.0620	0.32			
	3356	0.0657	-0.65			
	10375	0.0661	0.20			
	7494	0.0705	0.47			
	6927	0.0719	-0.58			
	9623	0.0757	0.21			
	6825	0.0842	0.26			
	5651	0.0854	0.26			
	15292	0.0864	0.25			
	4897	0.0949	0.23			
	5443	0.0952	0.12			
	7569	0.0961	-0.43			

Protein peaks with a significant ($p < 0.1$) difference at 18 and 15 months on CM10 ProteinChip arrays with their average mass, p-value, log_2 fold change (negative= decrease; positive=increase) and total number of peaks detected. Red entries are peaks significant at both timepoints.

3.7 Similarities and differences in the brain proteome of the HD genetic mouse models

The total number of peaks with a significant difference in all experiments with the three HD mouse models was 103. More than half were significant in more than one experiment. These peaks are listed in Table 3.9. Out of these, 83% were significant not only in multiple experiments, but also in different mouse models.

Figure 3.13 shows the total number of peaks detected in all experiments, the number of peaks that was found in multiple experiments, and the number that was unique to one experiment. Figures 3.13 A-B illustrate the expected overlap between CM10 and Q10 ProteinChip arrays. Figures 3.13 C-D demonstrate that the majority of the peaks detected at different ages in the same mouse model are the same. Figure 3.13 E shows that about half of the proteins detected are present in all brain regions examined and that the caudate-putamen and the cerebellum have the highest number of proteins detected only in these regions.

Table 3.9 Peaks with $p < 0.1$ in more than one experiment.

av. mass	p-value	log2 FC	model	age	ProteinChip	brain tissue
4897	0.0949	0.23	Q150	18 months	CM10	caudate-putamen
4899	0.0016	-0.77	Q92	12 months	CM10	caudate-putamen
5103	0.0407	0.21	Q92	18 months	CM10	caudate-putamen
5103	0.0160	-0.37	Q92	12 months	CM10	caudate-putamen
6717	0.0921	-0.64	R6/1	18 weeks	Q10	half cerebra
6720	0.0375	-0.81	R6/1	18 weeks	CM10	half cerebra
6775	0.0052	-0.19	Q150	15 months	CM10	caudate-putamen
6781	0.0159	-0.35	R6/1	18 weeks	CM10	half cerebra
6784	0.0139	-0.34	Q92	12 months	CM10	caudate-putamen
6825	0.0842	0.26	Q150	18 months	CM10	caudate-putamen
6828	0.0367	-0.47	Q92	12 months	CM10	caudate-putamen
6919	0.0291	-0.53	R6/1	18 weeks	Q10	half cerebra
6926	0.0756	-0.55	R6/1	18 weeks	CM10	half cerebra
6927	0.0719	-0.58	Q150	18 months	CM10	caudate-putamen
7489	0.0851	-0.33	Q92	10 months	CM10	caudate-putamen
7490	0.0316	-0.73	Q92	18 months	CM10	caudate-putamen
7494	0.0705	0.47	Q150	18 months	CM10	caudate-putamen
7647	0.0719	-0.18	Q92	18 months	Q10	caudate-putamen
7648	0.0987	-0.27	R6/1	18 weeks	Q10	half cerebra
7662	0.0266	0.57	Q92	18 months	CM10	caudate-putamen
7663	0.0453	0.38	Q92	18 months	CM10	motor+prefrontal cortex
7805	0.0740	-1.14	Q92	18 months	CM10	caudate-putamen
7810	0.0280	0.67	Q150	18 months	CM10	caudate-putamen
7812	0.0764	-0.46	Q92	12 months	CM10	caudate-putamen
8025	0.0102	0.22	Q150	15 months	CM10	caudate-putamen
8026	0.0775	0.21	Q92	10 months	CM10	caudate-putamen
8383	0.0142	0.47	Q150	18 months	CM10	caudate-putamen
8391	0.0821	0.23	Q92	18 months	CM10	cerebellum
8563	0.0149	0.20	Q92	10 months	CM10	caudate-putamen
8567	0.0355	0.20	R6/1	18 weeks	CM10	half cerebra
8770	0.0019	0.30	Q92	10 months	CM10	caudate-putamen
8788	0.0763	0.20	Q150	15 months	CM10	caudate-putamen
8979	0.0181	0.43	Q150	15 months	CM10	caudate-putamen
8985	0.0269	0.23	Q150	18 months	CM10	caudate-putamen
9325	0.0722	-0.23	Q150	15 months	CM10	caudate-putamen
9330	0.0620	0.32	Q150	18 months	CM10	caudate-putamen
9331	0.0727	-0.30	Q92	12 months	CM10	caudate-putamen
9623	0.0757	0.21	Q150	18 months	CM10	caudate-putamen
9624	0.0236	-0.46	Q92	12 months	CM10	caudate-putamen
10719	0.0343	0.30	Q150	18 months	CM10	caudate-putamen
10719	0.0642	-0.54	Q92	12 months	CM10	caudate-putamen
13477	0.0165	0.34	Q150	18 months	CM10	caudate-putamen
13478	0.0088	-0.42	Q92	12 months	CM10	caudate-putamen
14971	0.0950	-0.50	Q92	18 months	CM10	caudate-putamen
14987	0.0102	-0.48	Q92	10 months	CM10	caudate-putamen
14988	0.0109	0.55	Q150	18 months	CM10	caudate-putamen
15180	0.0831	-0.37	Q92	18 months	CM10	caudate-putamen
15196	0.0088	0.37	Q150	18 months	CM10	caudate-putamen
15198	0.0431	-0.38	Q92	10 months	CM10	caudate-putamen
15274	0.0886	-0.28	Q92	18 months	CM10	caudate-putamen
15292	0.0864	0.25	Q150	18 months	CM10	caudate-putamen
15624	0.0185	-0.64	Q92	12 months	CM10	caudate-putamen
15626	0.0090	0.68	Q150	18 months	CM10	caudate-putamen
15835	0.0775	-0.29	Q92	18 months	CM10	caudate-putamen
15854	0.0958	-0.32	Q92	12 months	CM10	caudate-putamen
15858	0.0119	0.30	Q150	18 months	CM10	caudate-putamen

Each block contains the peaks which, in all probability, represent the same protein. Q92 refers to Hdh^{Q92} and Q150 refers to Hdh^{Q150}.

A.

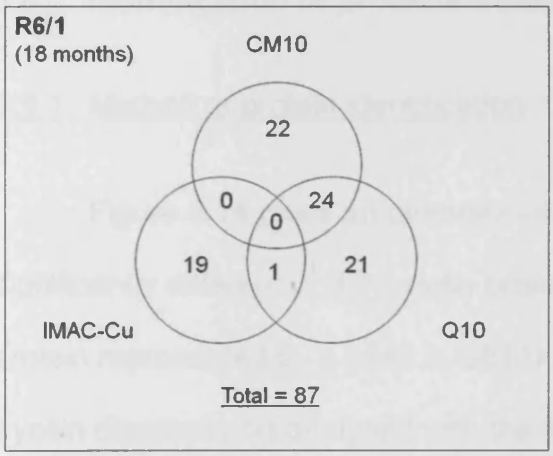

B.

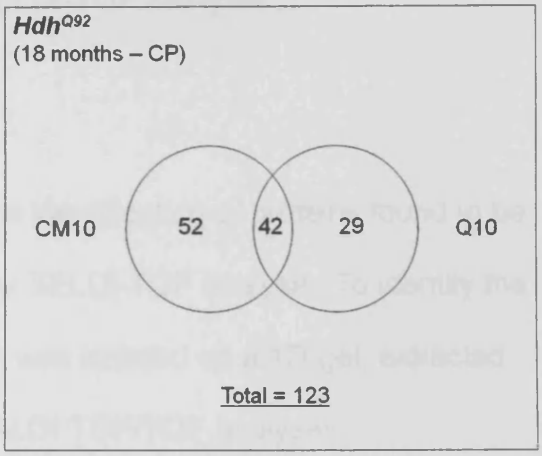

C.

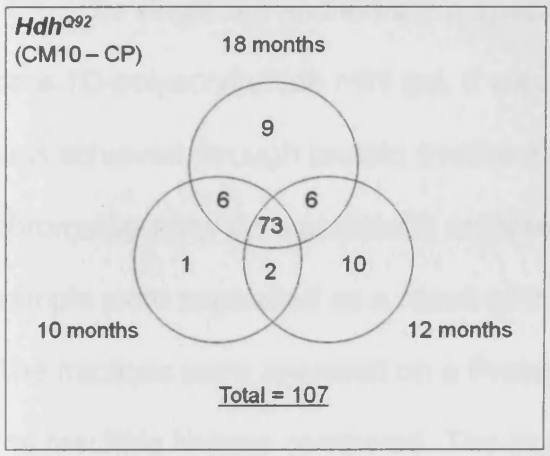

D.

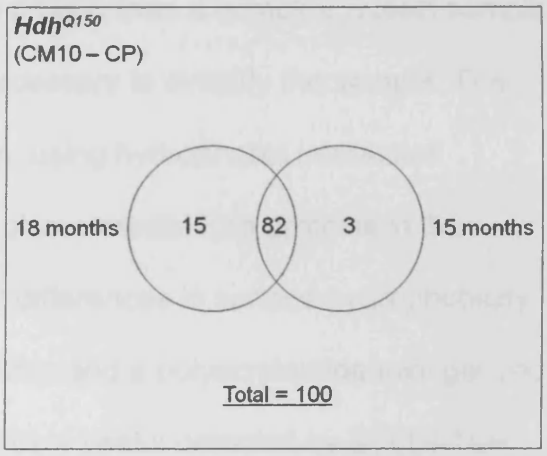

E.

brain regions	CP	HC	MC+PFC	CB	MC+PFC CB	HC CB	HC MC+PFC	HC MC+PFC CB
CP	13	0	7	2	3	1	15	53
HC	0	2	1	0	4			
MC+PFC	7	1	0	1		4		
CB	2	0	1	10			4	
Total = 112								

Figure 3.13 Total number of peaks detected in all experiments and overlap between experiments.

- **A.** R6/1: 18 month samples on CM10, Q10 and IMAC-Cu ProteinChip arrays.
- **B.** *Hdh*^{Q92}: 18 month caudate-putamen (CP) samples on CM10 and Q10 ProteinChip arrays.
- **C.** *Hdh*^{Q92}: 18, 12 and 10 month CP samples on CM10 ProteinChip arrays.
- **D.** *Hdh*^{Q150}: 18 and 15 month CP samples on CM10 ProteinChip arrays.
- **E.** *Hdh*^{Q92}: 18 month CP, cerebellum (CB), motor cortex (MC) + prefrontal cortex (PFC) and hippocampus (HC) samples on CM10 ProteinChip arrays.

The Venn diagrams in A-D and the Table in E show the number of peaks detected in multiple experiments and the number unique to one experiment. The light grey fills in E denote combinations that have already been entered and the dark grey fills are non-existent combinations.

3.8 Identification of proteins from SELDI-TOF analysis

3.8.1 Method of protein identification

Figure 3.14 gives an overview of the identification of proteins found to be significantly different in HD mouse brain by SELDI-TOF analysis. To identify the protein represented by a peak in SELDI, it was isolated on a 1D-gel, extracted, trypsin digested and analysed with the MALDI TOF/TOF analyzer.

To single out and extract a specific protein from a complex protein sample on a 1D-polyacrylamide mini gel, it was necessary to simplify the sample. This was achieved through protein fractionation, using hydrophobic interaction chromatography on a polymeric reversed phase media. The proteins in the sample were separated as a result of their differences in surface hydrophobicity. The fractions were analysed on a ProteinChip and a polyacrylamide mini gel and the resulting images compared. The significant peaks detected by SELDI-TOF were first identified on the ProteinChip spectrum. To assist in relating the ProteinChip reading with the image obtained by running the same fractions on a gel, the ProteinChip software offers the facility to view the spectrum as a gel image. When the relevant bands on the gel were identified, a single gel plug was removed, trypsin digested, analysed in the MALDI TOF/TOF analyzer and the ensuing data compared with online protein databases SWISS-PROT and NCBI for protein identification.

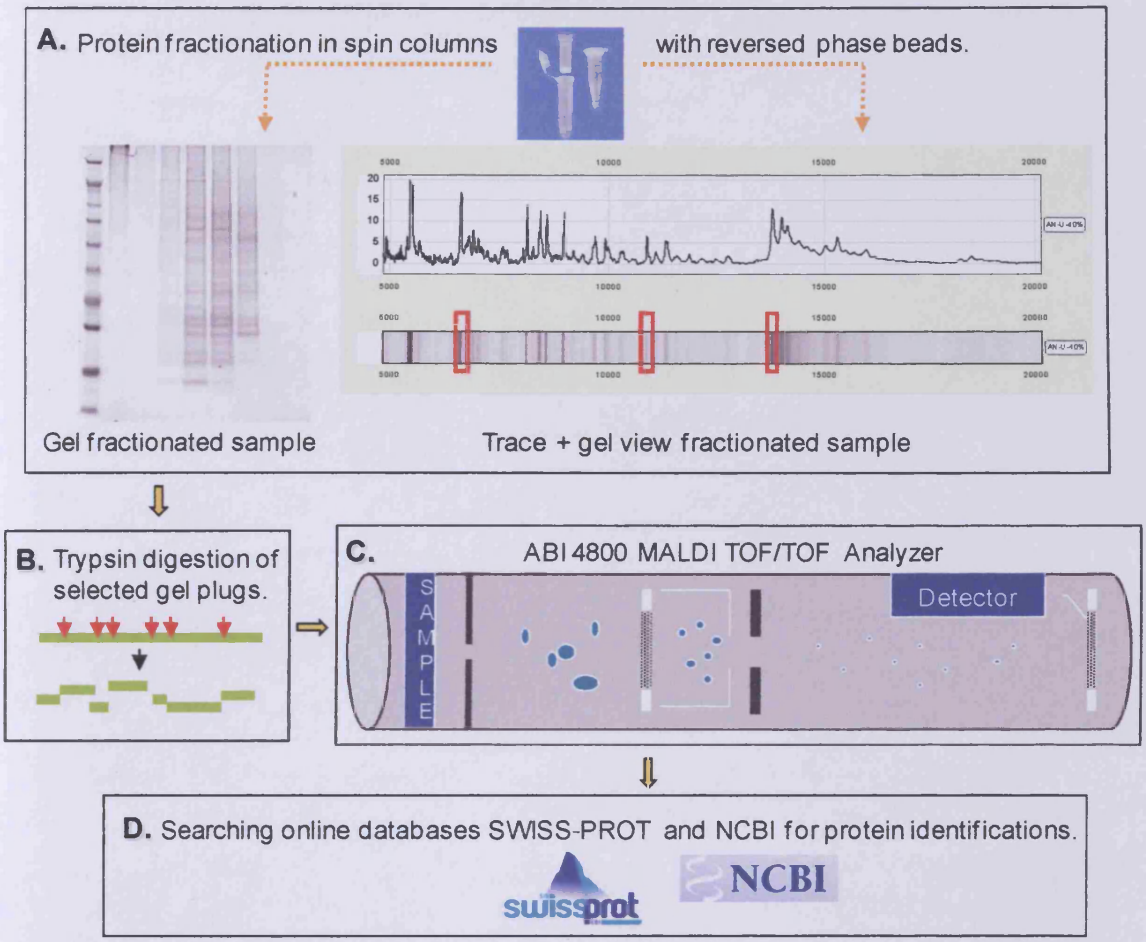

Figure 3.14 Work flow for isolating, analysing and identifying proteins found to be differentially expressed by SELDI-TOF analysis.
A. Protein samples are fractionated by hydrophobic character in spin columns with reversed phase beads. The fractions are run on a polyacrylamide gel, which is stained with colloidal coomassie to visualise the protein bands. The same fractions are analysed on normal phase ProteinChip arrays in the SELDI-TOF mass spectrometer. The gel view of the spectra is compared with the stained polyacrylamide gel to identify the appropriate bands.
B. Gel plugs are collected from the bands identified on the gel and trypsin digested.
C. The digests are analysed in the ABI 4800 MALDI TOF/TOF analyzer. The sample is spotted onto a metal plate and excited with laser light. The ionised peptides are sparated on the basis of their molecular weight. During the second TOF analysis, individual peptides are selected and fragmented in a collision chamber, generating the ions which produce the fragmentation spectra.
D. The SWISS-PROT and NCBI online databases are searched to identify the proteins.

3.8.2 Optimisation of fractionation

Protein samples were fractionated (section 2.2.4) and fractions analysed on normal phase (NP20) ProteinChip arrays. As some of the protein is already lost during fractionation, NP20 arrays were chosen to avoid further reduction in protein of the sample. The spots were prepared with 3 µl of dH_2O and air dried, after which 3 µl of the fractions were applied and air dried, followed by 1 µl of SPA solution twice, each with an air dry time of 20 min. The ProteinChips were read and analysed as in section 3.2.1.

Some optimisation experiments were performed to determine the optimal number of fractions, method and materials. A repetitive signal was seen on these spectra and attempts were made to identify its source and eliminate the signal.

Number of fractions

A homogenate of half cerebra of an 18 week WT R6/1 was fractionated into flow-through and fractions eluted with 10%, 15%, 20%, 23%, 26%, 29%, 32%, 35%, 38%, 41%, 44%, 47%, 50%, 53%, 56% and 80% acetonitrile (ACN). The spectra in Figure 3.15 show there was no need for fractions between 20-29%, as very little sample was eluted. The same was the case for fractions > 47% ACN. Although there were more peaks in the 32-47% fractions, many of these were present in more than one fraction. The low intensity of the peaks indicated that the protein concentration in these fractions was low, which suggested that too many fractions between 30-50% diluted the proteins, making it difficult to visualise them on a gel. It was decided that a 10%, 20%, 30%, 40%, 50%, 60% and 80% ACN fraction would be adequate. The additional benefit of this was that all eight fractions could be analysed on one ProteinChip.

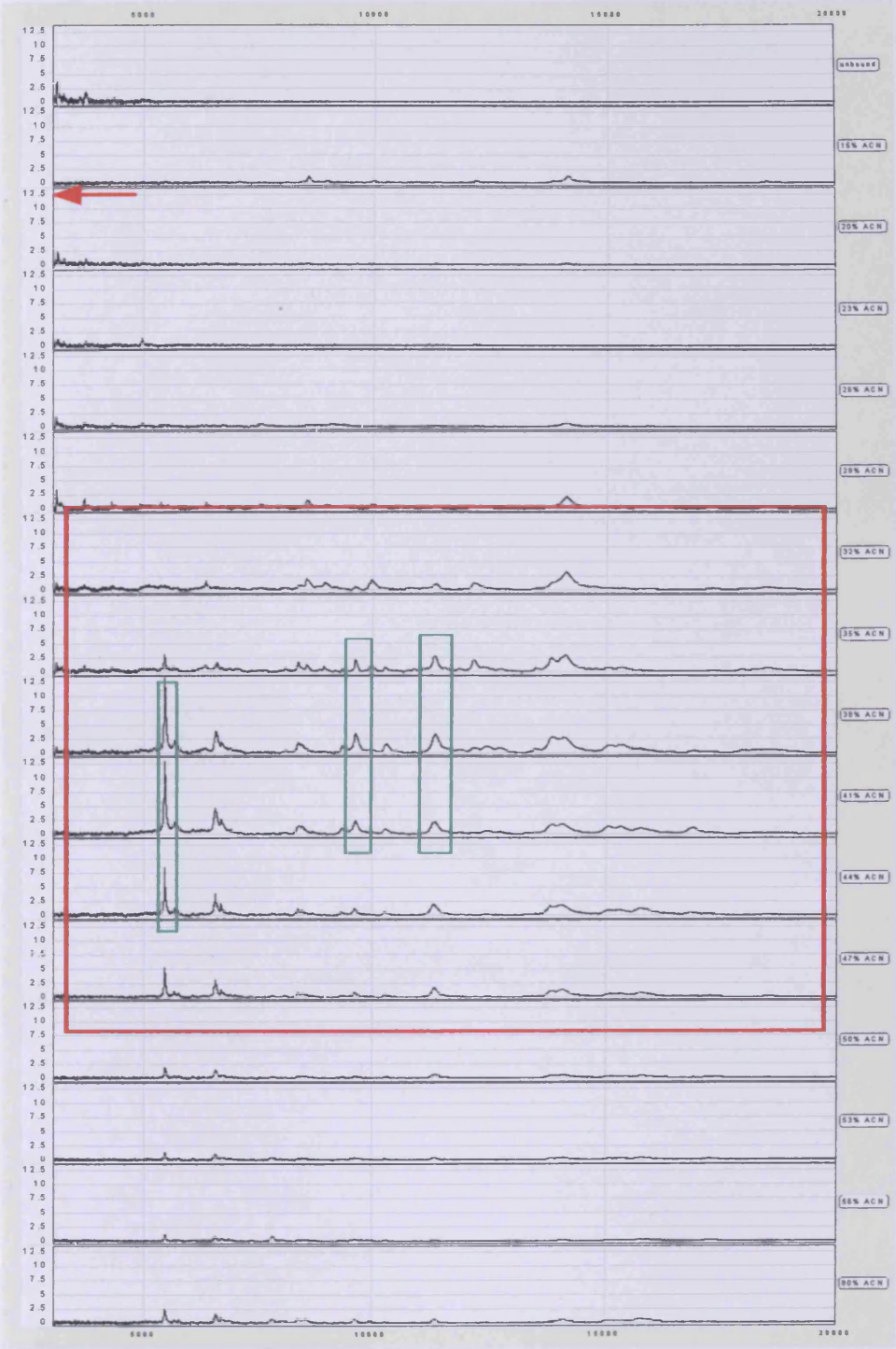

Figure 3.15 Spectra of 16 spots on two NP20 ProteinChips with fractions of 18 week old WT R6/1 half cerebra. From top to bottom are the flow-through and 10%, 15%, 20%, 23%, 26%, 29%, 32%, 35%, 38%, 41%, 44%, 47%, 50%, 53%, 56% and 80% ACN fractions. The red box indicates the 32-47% fractions, in which most of the protein was eluted. The green boxes show a few examples of peaks that were present in more than one fraction. The red arrow points out the low intensity of the peaks.

Method of fractionation

To determine the best method and materials for fractionation, four reversed phase chromatography approaches were compared:

- method 1: use of Sigma spin columns with PLRP-S beads (section 2.2.4); each fraction eluted in one step with 300 µl of the appropriate concentration of ACN.
- method 2: use of Sigma spin columns with PLRP-S beads; each fraction eluted in three steps with three times 100 µl of the appropriate concentration, combining the flow-through.
- method 3: use of 1.5 ml Eppendorf tubes with PLRP-S beads; each fraction eluted in one step with 300 µl of the appropriate concentration of ACN.
- method 4: use of Methyl Ceramic HyperD F Spin Columns (reversed phase column from Ciphergen Biosystems), following the company's instructions; fractions obtained by a decreasing concentration of ammonium sulphate.

For the first three methods, a homogenate of half cerebra of 10 week transgenic R6/1 was fractionated in flow-through and 10%, 20%, 30%, 40%, 50%, 60% and 80% fractions. For method four, the same homogenate was fractionated in flow-through and 2M, 1.6M, 1.2M, 0.8M, 0.4M and 0M fractions. All fractions were analysed on NP20 ProteinChip arrays. The four ProteinChips were processed and read in one batch. The spectra in Figure 3.16 show that method 1, fractionation in Sigma spin columns in one step by adding 300 µl of the appropriate concentration of ACN, produced an adequate separation as well as more and better defined peaks. This protocol was used for further fractionation.

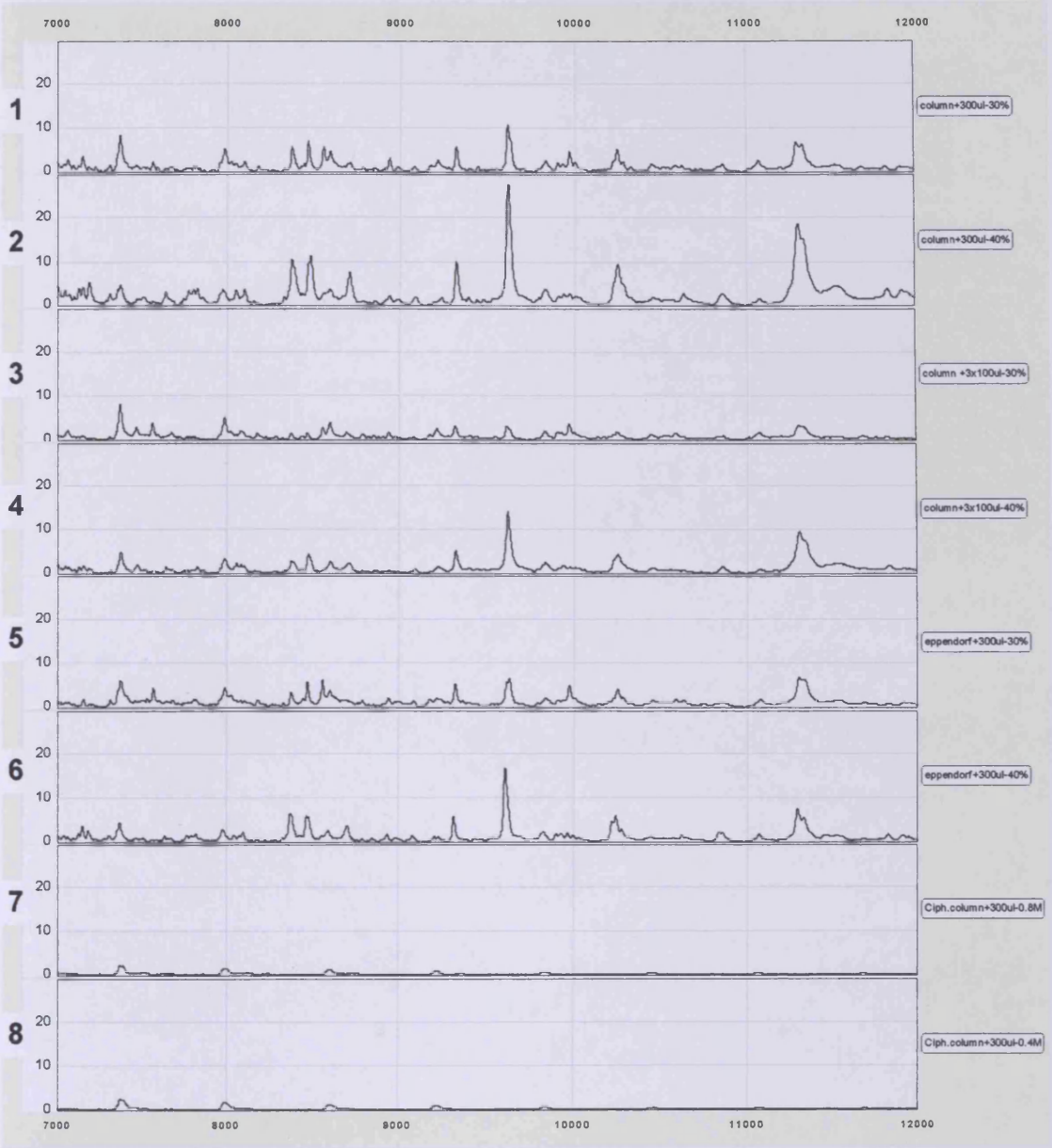

Figure 3.16 Spectra of eight spots comparing four method of reversed phase chromatography fractionation. The spectra were selected from a 31 spot experiment on NP20 ProteinChip arrays. Homogenate of half cerebra of 10 week transgenic R6/1 was fractionated in eight fractions by the first three methods (spectra 1-6) and in seven fractions by the fourth method (spectra 7-8). The spectra chosen correspond to two fractions from each method:

1. fraction eluted with 300 μl of 30% ACN in Sigma spin column;
2. fraction eluted with 300 μl of 40% ACN in Sigma spin column;
3. fraction eluted in three steps with 3 x 100 μl of 30% ACN in Sigma spin column;
4. fraction eluted in three steps with 3 x 100 μl of 40% ACN in Sigma spin column;
5. fraction eluted with 300 μl of 30% ACN in Eppendorf tube;
6. fraction eluted with 300 μl of 40% ACN in Eppendorf tube;
7. 0.8M ammonium sulphate fraction in Methyl Ceramic HyperD F spin column;
8. 0.4M ammonium sulphate fraction in Methyl Ceramic HyperD F spin column.

Troubleshooting a repetitive signal

The spectra of the fractionation optimisation experiments showed a repetitive signal below 6,000 Da that could not be explained. This was likely to interfere with the signal from proteins being fractionated, so attempts were made to remove it.

Figure 3.17 shows the signal, made up of two distinct peaks of different intensities and repeated roughly every 600 Da. The intensity of the repeats dropped with increasing mass. The repetitive nature of the signal and its even spacing suggested it was, in all probability, generated by a chemical breakdown product of one of the reagents, formed during fractionation. Tests were run to determine the cause of the signal and to find a way of removing it.

(A) 2-D CLEAN-UP

2-D clean-up was performed on homogenate of half cerebra of 10 week transgenic R6/1 with 98 μg of protein (procedure A, section 2.2.3). The pellet was resuspended in 10 μl of urea-thiourea lysis buffer and fractionated (section 2.2.4). The fractions were analysed on an NP20 ProteinChip. The spectra in Figure 3.18 show that, although the intensity of the repeat was lower, the 30% fraction still showed as many repeats as it did without the 2D-clean up. In the other fractions, the repeat had nearly disappeared. However, as the 30% fraction contained most of the proteins, further investigation was needed.

(B) UREA-THIOUREA LYSIS BUFFER

To test whether the urea-thiourea lysis buffer was causing the signal repeat, three different fractionations were compared: (1) 50 μl homogenate of half cerebra of 10 week transgenic R6/1 in HEPES lysis buffer in a total volume of 200

μl of 10% ACN and 0.5% TFA; (2) 200 μl of 10% ACN and 0.5% TFA without sample; (3) 50 μl of urea-thiourea lysis buffer without protein in a total volume of 200 μl of 10% ACN and 0.5% TFA. Figure 3.19 shows the spectra of the fractions analysed on an NP20 ProteinChip. The spectra generated by fractions from methods (1) and (2) showed no repeat signal, while those from method (3) showed the repeat signal. These results suggested that the signal repeat was produced by the breakdown product of one of the constituents of the urea-thiourea lysis buffer.

(C) THIOUREA

To test if the thiourea was causing the signal repeat, fractions of a homogenate of half cerebra of 10 week transgenic R6/1 were analysed on an NP20 ProteinChip without thiourea present. Because all samples were homogenated in urea-thiourea lysis buffer, a 2D-clean-up with 50 μg of protein was performed (procedure A, section 2.2.3) to remove the thiourea. The pellet was resuspended in 50 μl of 9 M urea + 2% CHAPS and fractionated. Figure 3.20 shows that the signal repeat was present in all fractions, indicating it was not the thiourea causing the problem. The spectra also showed very few protein peaks, suggesting that the clean-up procedure removes some of the protein and that 50 μg of protein is insufficient to withstand the protein loss caused by 2D-clean-up.

(D) CHAPS

To test whether the CHAPS was causing the signal repeat, fractions of a homogenate of half cerebra of 10 week transgenic R6/1 with only 10% of the CHAPS were analysed on an NP20 ProteinChip. To remove the CHAPS from the

homogenate, a 2D-clean-up with 98 μg of protein was performed (procedure A, section 2.2.3). The pellet was resuspended in 20 μl of 9 M urea + 0.5% CHAPS and fractionated. Figure 3.21 shows that the repeat was still there, but its intensity was considerably reduced.

Next, the CHAPS concentration was reduced to 5%. 2D-clean-up was performed on a homogenate of half cerebra of 10 week transgenic R6/1 with 130 μg of protein (procedure B, section 2.2.3). The pellet was resuspended in 20 μl of 9 M urea + 0.25% CHAPS and fractionated in Methyl Ceramic HyperD F Spin Columns (Ciphergen) to find out whether this new combination would eliminate the signal repeat. The fractions were analysed on an NP20 ProteinChip. Figure 3.22 shows that the intensity of the repeat was again greatly reduced. However, there was very little protein in the fractions, although more protein had been used to start with. Part of the problem may be that the CHAPS was used at a concentration too low to resuspend the pellet adequately from the 2D-clean-up. In fact, it was no longer possible to resuspend the pellet when the concentration of CHAPS was lowered any further.

The CHAPS was subsequently replaced with ASB-C8Φ (Calbiochem-Merck Chemicals, Beeston, UK), an alternative zwitterionic detergent. 2D-clean-up was carried out on a homogenate half cerebra of 10 week old transgenic R6/1with 96 μg of protein (procedure A, section 2.2.3). The pellet was resuspended in 50 μl of 7 M urea + 2 M thiourea + 2% ASB-C8Φ and fractionated. The fractions were analysed on an NP20 ProteinChip. Figure 3.23 shows a very clear and intense repeat in most fractions. However, the pattern of the repeat is different from that in the spectra with CHAPS. The repeat generated by ASB-C8Φ had two distinctive peaks, changing to one peak over 5,000 Da. There were more

repeats, closer together and they continued further down the spectrum to about 10,000 Da. These differences suggest that the detergent is broken down during fractionation, with different detergents generating different breakdown products.

The CHAPS experiments also showed there was a trade-off between the amount of detergent used and the number and concentration of proteins obtained: reducing the level of detergent gave a weaker signal with fewer peaks. In addition, the 2D-clean-up removed a substantial amount of protein. Taking into consideration that this procedure did not eliminate the signal repeat, it was decided not to use 2D-clean-up. As the signal repeat was present only below 6,000 Da, any peaks lower than this would be disregarded.

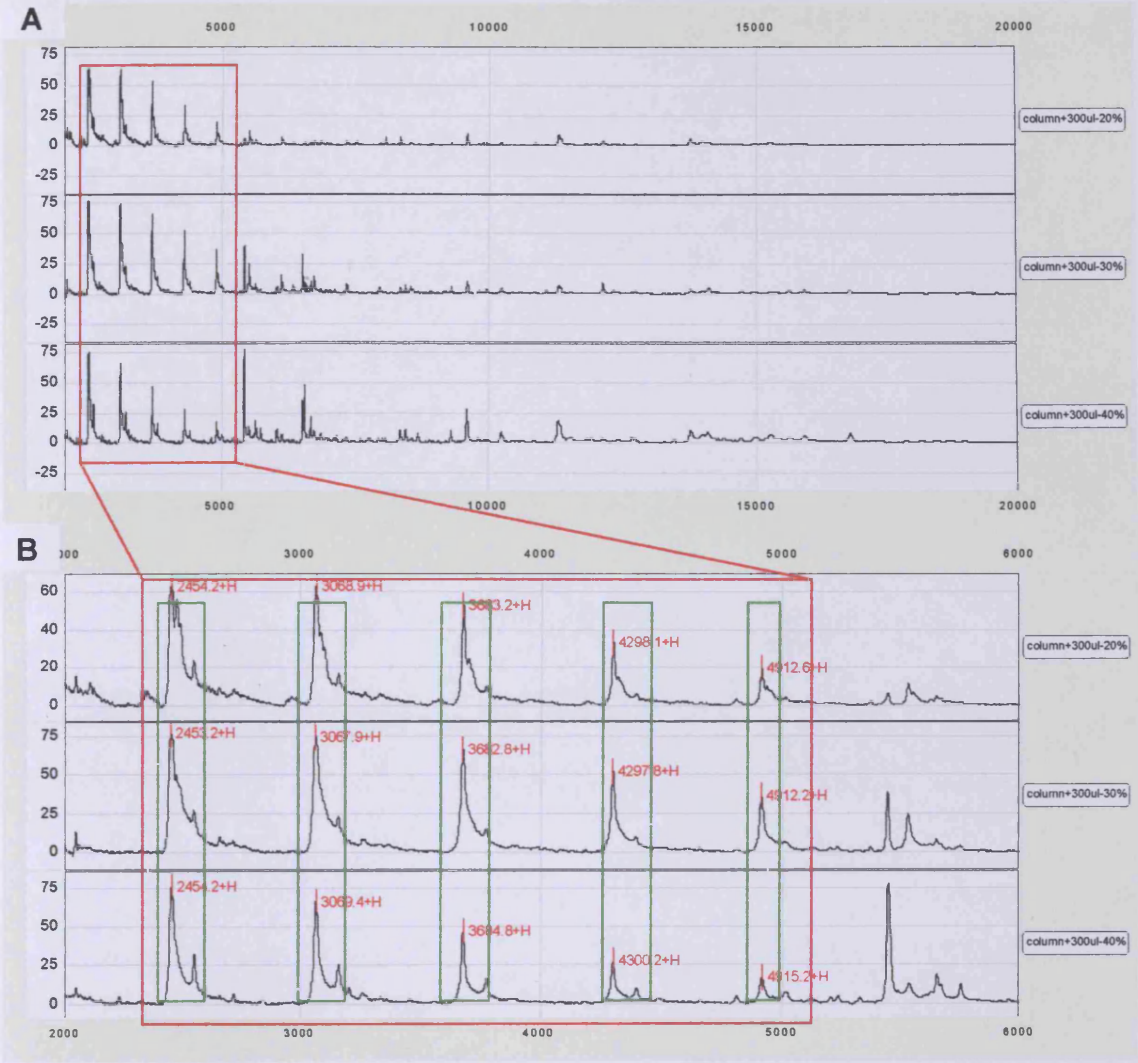

Figure 3.17 Spectra of three spots showing a repetitive signal. The spots were selected from the experiment described in Figure 3.16. The spectra correspond to three fractions obtained in Sigma spin columns with 300 µl of 20%, 30% and 40% ACN. The three spectra are shown twice, with a different zoom range. The window in **(A)** is zoomed in on the masses between 2,000-20,000 Da. The red box indicates the area with the repetitive signal. The window in **(B)** is zoomed in on the masses between 2,000-6,000 Da. The red box indicates the same area as in (A). The green boxes show the individual copies of the repeat, illustrating its repetitive nature. It is also clear that the intensity of the peaks falls with an increase in mass. The mass of the main peak of each of the repeats is indicated in red next to it. The repeats are evenly spaced, with an interval of roughly 600 Da.

Figure 3.18 Spectra of three spots after 2-D clean-up. The spectra correspond to the 20%, 30% and 40% fractions of a homogenate of half cerebra of 10 week transgenic R6/1, on which 2-D clean-up was performed on an NP20 ProteinChip. The repeat signal is still present, but at a considerably lower intensity in the 20% and 40% fractions and even somewhat lower in the 30% fraction.

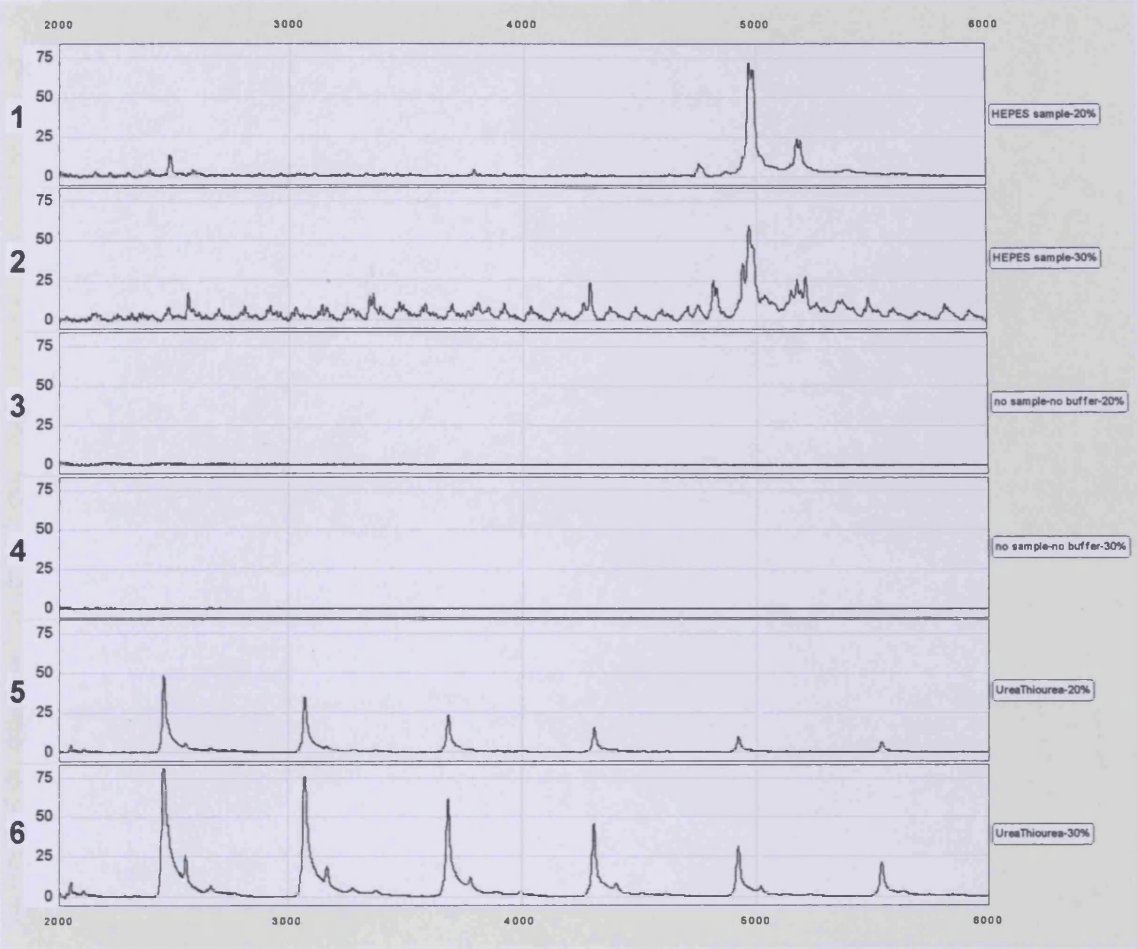

Figure 3.19 Spectra of six spots testing if the urea-thiourea lysis buffer was causing the signal repeat. The spectra correspond to three fractionations on an NP20 ProteinChip:

1-2 20% and 30% fraction of 50 μl homogenate of half cerebra of 10 week old transgenic R6/1 in HEPES lysis buffer in a total volume of 200 μl of 10% ACN and 0.5% TFA;

3-4 20% and 30% fraction of 200 μl of 10% ACN and 0.5% TFA without sample;

5-6 20% and 30% fraction of 50 μl urea-thiourea lysis buffer without protein in a total volume of 200 μl of 10% ACN and 0.5% TFA.

Only spectra 5 and 6 show the signal repeat.

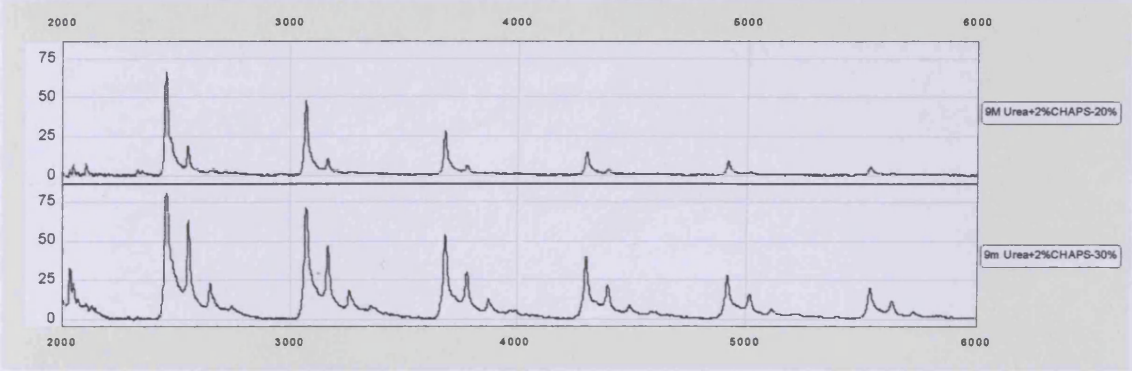

Figure 3.20 Spectra of two spots testing if the thiourea in the lysis buffer was causing the signal repeat. The spectra correspond to the 20% and 30% fractions of homogenate of half cerebra of 10 week transgenic R6/1 without thiourea on an NP20 ProteinChip. 2-D clean-up removed the thiourea from the sample. The pellet was resuspended in 50 μl of 9 M urea + 2% CHAPS and fractionated. The signal repeat is present in all fractions.

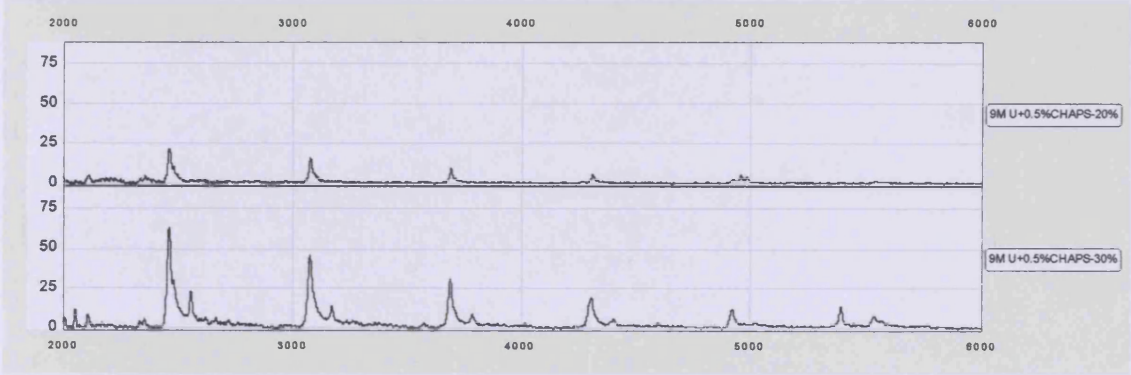

Figure 3.21 Spectra of two spots testing if the CHAPS in the lysis buffer was causing the signal repeat. The spectra correspond to the 20% and 30% fractions of homogenate of half cerebra of 10 week transgenic R6/1 with only 10% of the original amount of CHAPS on an NP20 ProteinChip. 2-D clean-up removed the CHAPS from the sample. The pellet was resuspended in 20 μl of 9 M urea + 0.5% CHAPS and fractionated. The signal repeat is present in all the spectra, but at a much lower intensity.

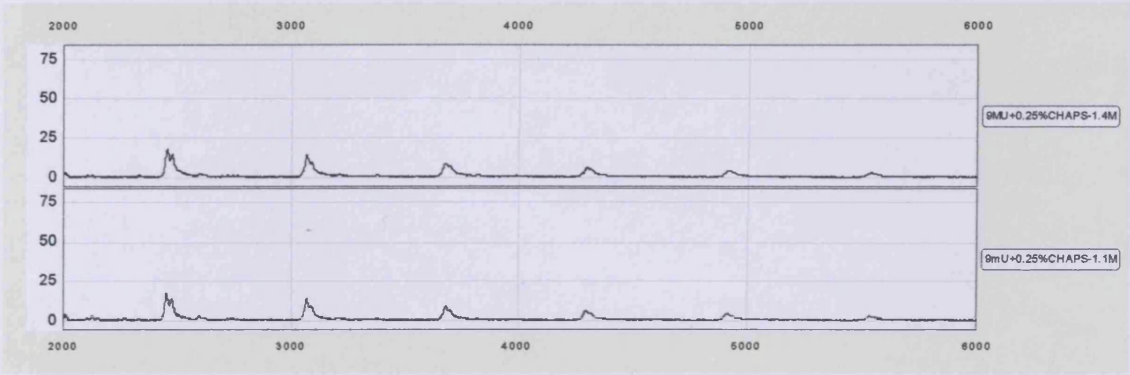

Figure 3.22 Spectra of two spots with further reduction of CHAPS. The spectra correspond to fractions eluted with 1.4M and 1.1M ammonium sulphate in Methyl Ceramic HyperD F spin columns on an NP20 ProteinChip. Homogenate of half cerebra of 10 week transgenic R6/1 was fractionated with only 5% of the original amount of CHAPS present. Prior to fractionation, 2-D clean-up removed the CHAPS from the sample. The pellet was resuspended in 20 μl of 9 M urea + 0.25% CHAPS. The signal repeat is strongly reduced in all the spectra.

Figure 3.23 (1) Spectra of three spots with CHAPS replaced by ASB-C8Φ. The spectra correspond to the 30%, 40% and 50% fractions of homogenate of half cerebra of 10 week transgenic R6/1 after replacing CHAPS with ASB-C8Φ on an NP20 ProteinChip. 2-D clean-up removed the CHAPS from the sample. The pellet was resuspended in 50 μl of 7 M urea + 2 M thiourea + 2% ASB-C8Φ and fractionated. The spectra show a strong repetitive signal, indicated by the green boxes. The pattern of this repeat is different from that in the spectra with CHAPS (2): the ASB-C8Φ spectra show more repeats that are closer together. The repeats have two distinct peaks, with one of the peaks disappearing over 5,000 Da.

3.8.3 Isolation of protein bands using 1D-gel electrophoresis

After 3 μl of each fraction of a sample was analysed on an NP20 ProteinChip, the remainder of the fractions were separated on a 12% Bis-Tris NuPage gel (section 2.2.6). The gel was stained with colloidal blue (section 2.2.7). Figure 3.24 shows how the gel was compared with the spectra and how peaks from the spectra were identified as bands on the gel. Both the trace view and the gel view of the spectra were used. First, bands between 5,000-20,000 Da were identified on both gel and spectra for landmarking. Then, bands in that area on the gel were matched to peaks on the spectra. A single gel plug of each band identified as a protein of interest was removed for trypsin digestion and MALDI TOF/TOF analysis. Table 3.10 lists the bands that were isolated.

Fractions of four Hdh^{Q92} samples were analysed. The first were 18 month $Hdh^{+/+}$ caudate-putamen fractions. Five bands were isolated. The second were 12 month $Hdh^{+/+}$ caudate-putamen fractions. Two more bands were found. The last two were 10 month $Hdh^{Q92/Q92}$ caudate-putamen fractions and 18 month $Hdh^{+/+}$ hippocampus fractions. No bands were isolated on either. Fractions of two Hdh^{Q150} samples were analysed. The first were 18 month $Hdh^{+/+}$ caudate-putamen fractions. Five bands were isolated. The second were 15 month $Hdh^{Q150/Q150}$ caudate-putamen fractions. Two more bands were found. For the R6/1, several fractionated samples were separated on gels, but no relevant peaks could be isolated.

Figure 3.24 Identifying peaks from SELDI-TOF spectra on a 1D-gel.
(A) Image of a fractionated caudate-putamen homogenate of an 18 month *Hdh*$^{+/+}$, separated on a 12% Bis-Tris NuPage gel, stained with colloidal blue.
(B) Gel view of the SELDI-TOF spectra of the same fractions analysed on an NP20 ProteinChip. The window is zoomed in between 5,000-17,000 Da. The green arrows illustrate two of the bands that were identified on the spectra for landmarking. The red arrows indicate the five bands that were identified as some of the significant peaks for the *Hdh*^{Q92} model.
(C) The same gel view as in (B), but with the relevant bands identified.
(D) Trace view of the 30%, 40% and 50% fractions of the spectra in (B) and (C). The same peaks have been identified.

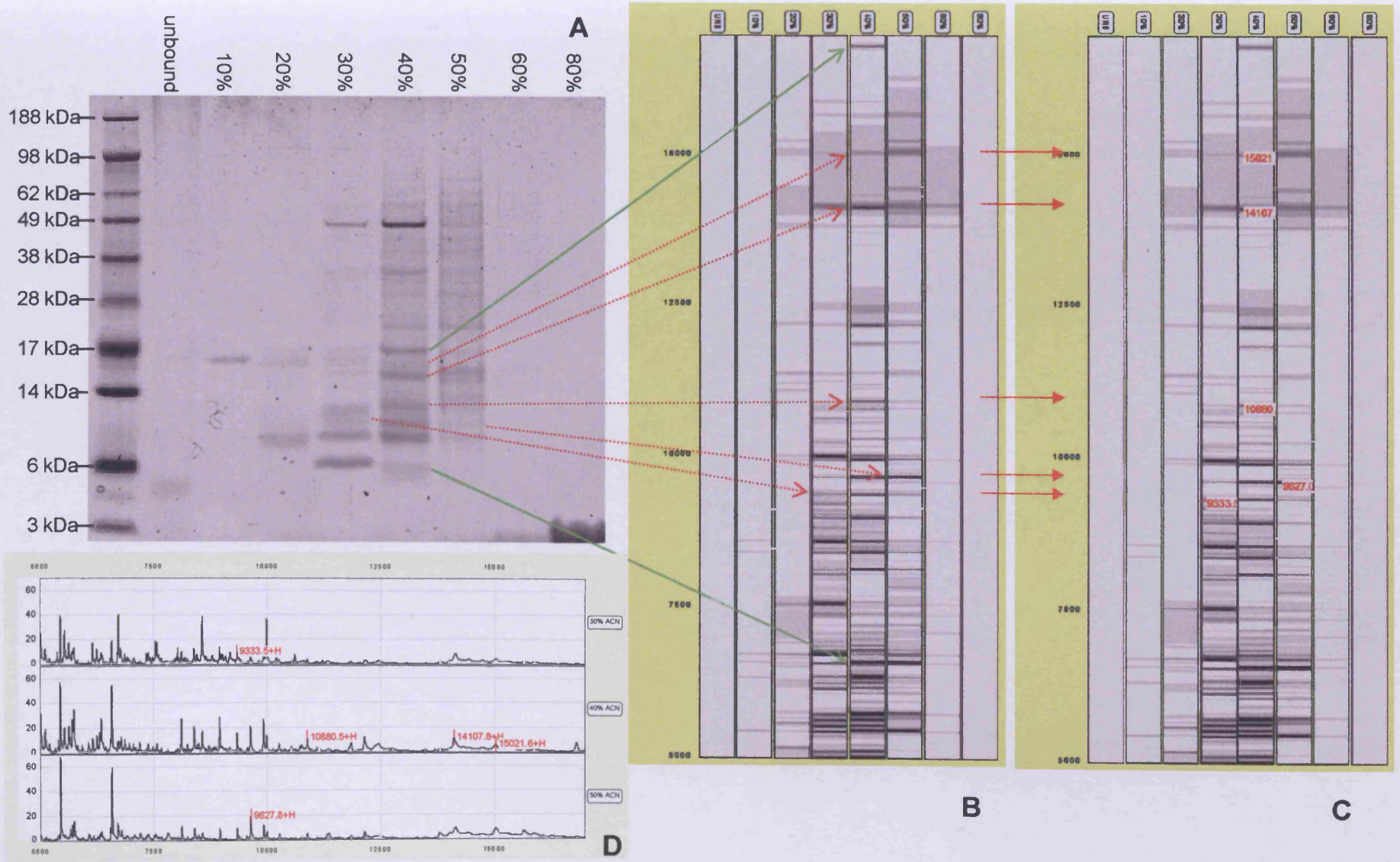
A
unbound
10%
20%
30%
40%
50%
60%
80%
188 kDa
98 kDa
62 kDa
49 kDa
38 kDa
28 kDa
17 kDa
14 kDa
6 kDa
3 kDa
B
C
D
30% ACN
40% ACN
50% ACN
9333.5+H
10880.5+H
14107.8+H
15021.6+H
9627.8+H

Table 3.10 SELDI-TOF peaks identified as bands on a gel with fractionated samples.

Fractionated sample				Fraction	Mass	SELDI-TOF results				
Model	Age	Genotype	Tissue			Age	Tissue	Chip	p-value	Log2FC
HdhQ92	18 months	WT	CP	30%	9333	12 months	CP	CM10	0.0727	-0.30
HdhQ92	18 months	WT	CP	40%	10883	18 months	CP	CM10	0.0656	-0.23
HdhQ92	18 months	WT	CP	40%	14107	10 months	CP	CM10	0.0838	-0.33
HdhQ92	18 months	WT	CP	40%	15021	18 months	CP	CM10	0.0950	-0.50
						10 months	CP	CM10	0.0102	-0.48
HdhQ92	18 months	WT	CP	50%	9627	12 months	CP	CM10	0.0236	-0.46
HdhQ92	12 months	WT	CP	60%	11340	12 months	CP	CM10	0.0022	0.49
HdhQ92	12 months	WT	CP	60%	13806	18 months	CP	Q10	0.0871	0.24
HdhQ150	18 months	WT	CP	40%	8955	15 months	CP	CM10	0.0181	0.43
						18 months	CP	CM10	0.0269	0.23
HdhQ150	18 months	WT	CP	40%	9630	18 months	CP	CM10	0.0757	0.21
HdhQ150	18 months	WT	CP	40%	12449	18 months	CP	CM10	0.0104	0.37
HdhQ150	18 months	WT	CP	40%	15025	18 months	CP	CM10	0.0109	0.55
HdhQ150	18 months	WT	CP	40%	6579	15 months	CP	CM10	0.0281	-0.26
HdhQ150	15 months	HOM	CP	30%	9338	18 months	CP	CM10	0.0620	0.32
						15 months	CP	CM10	0.0722	-0.23
HdhQ150	15 months	HOM	CP	30%	15644	18 months	CP	CM10	0.0090	0.68

The first four columns give details on the fractionated samples separated on a 12% Bis-Tris NuPage gel. The next two columns record the masses of the bands isolated and the fraction they were found in. The last five columns give the SELDI-TOF results on the equivalent peaks. A total of 14 bands were found, seven each for Hdh^{Q92} and Hdh^{Q150}.

3.8.4 MALDI TOF/TOF analysis and results

Trypsin digestion was carried out by Mrs S.H.V. Nixon and MALDI TOF/TOF analysis by Dr. I. Brewis at the Proteomics Unit of the Central Biotechnology Services at Cardiff University. All 14 gel plugs provided protein identification, detailed in Table 3.11. The criteria for identification take into account the expectation (E) value, both for the final identification and for the peptide matches. The expectation value is the probability that the match is a chance event. There are four MALDI TOF/TOF identification categories:

- Category 1: Conclusive identification with excellent tandem MS data for two or more peptides, each peptide with $E < 0.05$.
- Category 2: Conclusive identification with good tandem MS data for one peptide with $E < 0.0001$.
- Category 3: Probable/possible identification with tandem MS data for one or more peptides with overall $0.05 < E < 0.0001$.
- Category 4: Probable/possible identification with MS (not tandem MS) with $E < 0.01$.

However, category 1 and 2 identifications are a great deal more significant than category 3 identifications and a category 4 identification would generally only be accepted if there are additional factors supporting the identification.

Seven identifications were category 1. Two proteins were identified in both the Hdh^{Q92} and the Hdh^{Q150} model: Cytochrome c oxidase subunit VIb and Calmodulin.

Table 3.11 MALDI TOF/TOF identifications of proteins found to be changed in the *Hdh*^{Q92} and *Hdh*^{Q150} mouse models by SELDI-TOF analysis.

The left section of the table gives the SELDI-TOF results for the relevant peaks, the right section shows the MALDI TOF/TOF identifications, with the protein match and name, the gene name and the amino acid code for each peptide match. The identification criteria uses the expectation value (E.), both for the overall identification and for the peptide matches. The four MALDI TOF/TOF identification categories are: (Cat.1) Conclusive identification with excellent tandem MS data for two or more peptides, each peptide with $E < 0.05$; (Cat.2) Conclusive identification with good tandem MS data for one peptide with $E < 0.0001$; (Cat.3) Probable/possible identification with tandem MS data for one or more peptides with overall $0.05 < E < 0.0001$; (Cat.4) Probable/possible identification with MS (not tandem MS) with $E < 0.01$.

Model	SELDI-TOF results			MALDI TOF/TOF identification						
	Age	p-value	Log2FC	Match	Protein	Gene name	Cat.	E. overall	Peptide match	E. peptide
HdhQ92	12 months	0.0727	-0.30	CX6B1_MOUSE	Cytochrome c oxidase subunit VIb isoform 1	*Cox6b1*	1	7.60E-11	TAPFDSRFPNQNQTK	1.20E-04
									FPNQNQTK	1.10E-02
	18 months	0.0656	-0.23	QCR7_MOUSE	Cytochrome b-c1 complex subunit 7	*Uqcrb*	3	1.40E-03	RLPEDLYNDR	2.20E-02
	10 months	0.0838	-0.33	HBA_MOUSE	Hemoglobin subunit alpha	*Hba*	2	6.00E-08	IGGHGAEYGAEALER	1.00E-09
	18 months	0.0950	-0.50	CALM_MOUSE	Calmodulin	*Calm1, Calm2 and Calm3*	1	1.90E-21	DTDSEEEIREAFR	1.90E-07
	10 months	0.0102	-0.48						VFDKDGNGYISAAELR	1.30E-11
	12 months	0.0236	-0.46	FKB1A_MOUSE	FK506-binding protein 1A	*Fkbp1a*	3	1.20E-06	GVQVETISPGDGR	6.40E-04
									GWEEGVAQMSVGQR	1.90E-01
	12 months	0.0022	0.49	MBP_MOUSE	Myelin basic protein, 14 kDa	*Mbp*	2	3.80E-12	TQDENPVVHFFK	1.50E-05
									FFSGDRGAPK	1.50E-01
	18 months	0.0871	0.24	HBA_MOUSE	Hemoglobin subunit alpha	*Hba*	1	9.60E-31	IGGHGAEYGAEALER	7.00E-15
									TYFPHFDVSHGSAQVK	1.00E-12
HdhQ150	15 months	0.0181	0.43	CH10_MOUSE	10kDa heat shock protein, mitochondrial	*Hspe1*	1	1.10E-21	VVLDDKDYFLFR	1.20E-09
	18 months	0.0269	0.23						KFLPLFDR	5.20E-04
									FLPLFDR	3.50E-03
	18 months	0.0757	0.21	CX6B1_MOUSE	Cytochrome c oxidase subunit VIb isoform 1	*Cox6b1*	1	3.80E-08	TAPFDSRFPNQNQTK	1.30E-03
									FPNQNQTK	2.80E-03
	18 months	0.0104	0.37	CYC_BOVIN	Cytochrome c	*Cycs*	3	1.20E-02	TGPNLHGLFGR	1.90E-04
	18 months	0.0109	0.55	CALM_MOUSE	Calmodulin	*Calm1, Calm2 and Calm3*	2	4.80E-12	VFDKDGNGYISAAELR	2.90E-13
	15 months	0.0281	-0.26	UBIQ_MOUSE	Ubiquitin	*Rps27a, Uba52, Ubb and Ubc*	1	6.00E-26	TITLEVEPSDTIENVK	1.70E-08
									IQDKEGIPPDQQR	8.90E-10
									EGIPPDQQR	4.00E-02
	18 months	0.0620	0.32	CX6B1_MOUSE	Cytochrome c oxidase subunit VIb isoform 1	*Cox6b1*	1	1.20E-24	GGDVSVCEWYR	1.50E-07
									FPNQNQTK	2.20E-04
	15 months	0.0722	-0.23						TAPFDSRFPNQNQTK	5.60E-04
									IAEGTFPGKI	2.20E-03
	18 months	0.0090	0.68	STMN1_MOUSE	Stathmin	*Stmn1*	2	3.70E-05	ASGQAFELILSPR	3.40E-07

3.9 Discussion

The work reported in this chapter was carried out using a relatively new proteomics technique, SELDI-TOF, to investigate the brain proteomes of three genetic mouse models of Huntington's Disease. SELDI-TOF has been successfully used in biological and medical research (section 3.1), particularly to screen for serum-based biomarkers and for the development of diagnostic tests for a variety of cancers (section 3.1). Although the majority of these projects used serum samples, most of the issues identified in these studies apply to the experiments with brain samples in the present study. One of the advantages of SELDI-TOF is that the technique is particularly well suited for investigating low molecular weight proteins, which are a subset of the proteome that is difficult to access with other methods, such as 2D-electrophoresis.

One of the main problems in proteomic research is the vast number of proteins involved. Proteomic techniques, even powerful ones such as protein arrays which can select thousands of proteins simultaneously, can identify only the most abundant proteins in a sample. This presents a challenge particularly in neuroscientific research, as a wide variety of proteins are expressed in the brain and many proteins of interest are expressed at relatively low levels (Freeman & Hemby 2004). By focusing on the fraction of the proteome below 20 kDa, SELDI-TOF probes a much reduced number of proteins and can detect proteins that might not be found by techniques such as 2-DE and DIGE. The use of different ProteinChip coupling surfaces simplifies the protein sample, again making lower abundance proteins more accessible. In spite of this, even when the full battery of

available ProteinChip arrays is used, an experiment can detect only a few hundred proteins, a fraction of the proteome.

To maximise the number of proteins captured in this project, samples were analysed on three different ProteinChip arrays: the weak ionic exchange CM10 ProteinChip array, the strong anionic exchange Q10 ProteinChip array and the immobilized metal affinity capture IMAC-Cu ProteinChip array. However, the initial experiments indicated that the CM10 ProteinChip array detected more proteins and presented more significant results than the Q10 and IMAC-Cu ProteinChip arrays. The additional findings obtained by running the samples on Q10 and IMAC-Cu ProteinChips after processing them on CM10 ProteinChips did not weigh up against the substantial additional cost in both money and time. It was therefore decided to analyse further samples on CM10 ProteinChip arrays only.

Many studies, particularly in the field of cancer research, have used SELDI-TOF to identify protein fingerprints that are indicative of pathology, without trying to identify the proteins involved (Veenstra *et al.* 2004). These projects have sidestepped what is probably SELDI's main drawback, which lies in the considerable difficulty in identifying the proteins represented by peaks in the spectra. The need to identify protein peaks as protein bands on a 1D-gel proved to be a major bottleneck. One complication is the variation introduced by the differences in methodology for analysing the samples on ProteinChips and on gels. In addition, lining up gel images with spectra is not at all straightforward. Although the ProteinChip software provides the option to show the spectra in gel view, the SELDI image still deviates a great deal from the 1D-gel image. This is partly due to the higher sensitivity of the ProteinChip system compared with the gel technique. In addition the gel view of the spectra is linear, while a 1D-gel

image is not. Of the 70 protein peaks found to be significantly different with SELDI, only 14 (20%) could be isolated on a 1D-gel. Thanks to excellent MALDI-TOF results, all of those that could be isolated were identified.

A complication specific to neuroproteomics is the requirement for often large amounts of sample for experiments, which is invariably limited with brain tissue from mouse. In addition, the temptation to turn out larger amounts of sample by using whole brain must be weighed against the wish for regional specificity. This was certainly the case with the *Hdh*^{Q92} and *Hdh*^{Q150} mouse models in this study. The decision to analyse microdissected caudate-putamen made the issue of total protein available in each sample even more pressing. Here, SELDI had an advantage by using only 20 μg of protein per sample, which is considerably less than other gel-based techniques.

The choice of timepoints for the different mouse models in this study was based on previous research conducted in these models by other methods. The R6/1 was the first model screened with SELDI-TOF. To maximize the chance of detecting differences in the brain proteomes of transgenic R6/1 compared with wild type littermates, the timepoint was selected after the age of onset of overt phenotypic changes in these animals. In transgenic R6/1, explicit behavioural changes were detected only from about 4 months of age (Mangiarini *et al.* 1996; Hansson *et al.* 1999; Clifford *et al.* 2002; Naver *et al.* 2003; Hodges *et al.* 2008). Research into the neuropathology of transgenic R6/1 confirmed this overall age of onset: neuronal intranuclear inclusions of the transgene, abnormal nuclear morphology and neurodegeneration were observed in transgenic R6/1 from 5 months (Davies *et al.* 1997; Iannicola *et al.* 2000; Turmaine *et al.* 2000; Spires *et al.* 2004a; Lazic *et al.* 2007). Changes in the physiology of striatal neurons were

present in transgenic mice of 18 weeks, but not in younger animals (Hansson *et al.* 1999; Hansson *et al.* 2001a). Histological examination demonstrated weight reduction of the whole brain as well as reduced striatal volume in 15 week old transgenic R6/1 (Hansson *et al.* 1999; Lazic *et al.* 2007) and RNA microarray analysis revealed alterations in brain gene expression from 18 weeks (Iannicola *et al.* 2000; Desplats *et al.* 2006; Hodges *et al.* 2008). All these studies substantiated an age of onset of 4 months. Some studies, however, reported changes in the transgenic mice a good deal earlier than 4 months, indicating the development of a mild disease phenotype at a much younger age: more sensitive tests recorded motor deficits from 7 weeks (Van Dellen *et al.* 2000; Hansson *et al.* 2001b; Van Dellen *et al.* 2008), the survival of neural precursor cells in the dentate gyrus was found to be compromised by the age of 10 weeks (Lazic *et al.* 2006) and, although neuronal inclusions were present in the majority of cells only by the 16th week, a small fraction of brain cells were found to contain them already at 8 weeks (Hansson *et al.* 2001b; Naver *et al.* 2003). One experiment even found differences in exploratory behaviour as early as 4 weeks (Bolivar *et al.* 2004).

Previous proteomic research identified several dysregulated proteins in transgenic R6/1: a loss in dopamine receptors in the striatum at 43 weeks (Clifford *et al.* 2002), a reduction of BDNF protein in the striatum and the hippocampus as well as a downregulation of DARPP-32 in the striatum at 5 months (Spires *et al.* 2004b), alterations in the release of striatal amino acid neurotransmitters at 16 weeks (NicNiocaill *et al.* 2001) and the reduction of the synaptic vesicle protein rabphilin 3A in the cerebral cortex and the striatum from 16 weeks (Smith *et al.* 2006). The Smith study also investigated the level of rabphilin 3A in 4 and 9 week old R6/1 and found no change, suggesting that protein changes coincide with

other phenotypic changes, and that the majority of changes probably take place after the 16th week in these animals. But again an earlier change was detected in 8 week transgenic R6/1 with the downregulation of the cannabinoid receptor 1 (Naver *et al.* 2003), clearly showing the beginning of alteration several months before other changes were noted. Based on all these findings, 18 week old animals were chosen for SELDI-TOF analysis, a timepoint at which they were expected to present with significant differences, but before the animals became so ill that the alterations might no longer be HD specific but rather the effect of a more widespread deterioration.

As this was the first model investigated and previous research suggested a widespread pathology in the R6 mouse models (Li *et al.* 1999), homogenate of half cerebra was used, keeping in mind that only the largest changes in expression would be observed, and that less significant changes or alterations in specific brain regions or in subpopulations of neurons would not be found. On the CM10 ProteinChip array, 11% of the peaks were significantly different, with 60% of the changes increased and 40% decreased. These results were consistent with the brain gene expression data previously obtained with 18 week R6/1 half cerebra (Hodges *et al.* 2008), where 15% of the probesets were dysregulated, with 60% upregulated and 40% downregulated.

Choosing the timepoint to analyse the *Hdh*^{Q92} brain proteome was less easy than it was with the R6/1, as there was no evidence of an overt behavioural phenotype in these animals at the time of the experiments (Wheeler *et al.* 1999). However, the existence of nuclear inclusions by the age of 14 months (Wheeler *et al.* 2000) and even as early as 5 months in the caudate and the olfactory tubercle in the colony used in this study (Bayman-Weston, unpublished), indicated that

changes consistent with HD pathology were certainly taking place in the older animals. As this model was considered a more accurate representation of the adult onset form of the human disease (Menalled 2005) and these animals were living a normal lifespan, an 18 month timepoint was expected to present with many differentially expressed proteins. Subsequent studies endorsed this choice: although there were no overt motor deficits, a mild behavioural phenotype was detected from as early as 4 months (Trueman *et al.* 2007; Trueman *et al.* 2008), molecular and neuropathological changes from 5 months (Brustovetsky *et al.* 2005; Lynch *et al.* 2007) and gene expression changes in the striatum at 18 months (Kuhn *et al.* 2007). In contrast to the initial experiments with the R6/1 model where half cerebra was used, the more specific pathology in the Hdh^{Q92} model (Wheeler *et al.* 2000; Trueman *et al.* 2007; Trueman *et al.* and 2008) was investigated using microdissected brain regions. At the outset, the caudate-putamen was examined as this is known to be the earliest and most affected brain region in HD, both in this mouse model (Wheeler *et al.* 2000; Brustovetsky *et al.* 2005; Kuhn *et al.* 2007; Trueman *et al.* 2008) and others (Laforet *et al.* 2001; Kennedy *et al.* 2003; Menalled *et al.* 2003; Slow *et al.* 2003, Freeman *et al.* 2004; Van Raamsdonk *et al.* 2005), as well as in humans (Vonsattel *et al.* 1985; Myers *et al.* 1988; Heinsen *et al.* 1994; Kennedy *et al.* 2003; Hodges *et al.* 2006). However, various degrees of pathology have been shown in other brain areas in the Hdh^{Q92} (Lynch *et al.* 2007; Trueman *et al.* 2008) and other mouse models (Reddy *et al.* 1998; Slow *et al.* 2003; Van Raamsdonk *et al.* 2005), and in humans (Spargo *et al.* 1993; Heinsen *et al.* 1994; Macdonald *et al.* 1997; Halliday *et al.* 1998). To assess whether this more limited pathology in the other regions was reflected in fewer protein changes in these areas, a comparison was made

between the caudate-putamen, the hippocampus, the cerebellum and the prefrontal and motor cortex combined, all taken from 18 month old littermates. The analysis on the CM10 ProteinChip arrays detected a relatively high proportion of differentially expressed proteins in the caudate-putamen of *Hdh*$^{Q92/Q92}$. This high level of differential expression was not observed in the other regions, with few changes in the hippocampus and the cortex and almost none in the cerebellum. These results agree with the picture of HD as a disease affecting predominantly the caudate, to a lesser degree the cortex (Sotrel *et al.* 1991; Ruocco *et al.* 2008 and section 1.4) and the hippocampus (Spargo *et al.* 1993; Jech *et al.* 2007 and section 1.4) and with very little pathology in the cerebellum (Gutekunst *et al.* 2002 and section 1.4). Moreover, the large fold changes in the caudate-putamen were not found in the other regions. Our results also correspond with the findings obtained by mRNA microarray analysis on human tissue, which showed changes in 21% of the probe sets in the caudate, 3% in the BA4 motor cortex and only 1% in the cerebellum. This gene expression study also observed that the magnitude of the changes was smaller in the cerebellum than in the caudate (Hodges *et al.* 2006).

Earlier studies both in humans (Weeks *et al.* 1996; Augood *et al.* 1997) and in mouse models (Cha *et al.* 1998; Cha *et al.* 1999; Denovan-Wright & Robertson 2000; Luthi-Carter *et al.* 2000) have shown alterations in gene expression as an early event in the disease process, often prior to the development of other behavioural or molecular phenotypes. To investigate whether animals representing stages of minimal deterioration would show alterations in their proteomes, the caudate-putamen of 10 and 12 month *Hdh*$^{Q92/Q92}$ were analysed and compared with *Hdh*$^{+/+}$ littermates. Surprisingly, the younger animals showed

only marginally fewer differences than the 18 month old ones, but the magnitude of the changes was significantly smaller. Seven significant peaks at 18 months were also significant at either 12 or 10 months. Although some changes were expected in the younger animals, this relatively high level of differential expression was unexpected. On the other hand, the behavioural study performed on littermates of these animals showed an early impairment at 4 months, which was present through to 14 months without being progressive, not even with the appearance of neuronal nuclear inclusions during this period (Trueman *et al.* 2008). This would seem to indicate that widespread molecular changes take place early on without developing a severe phenotype and that, as the disease progresses, some of these changes might be compensated for, some might increase in magnitude to intensify the disease characteristics, whilst new alterations develop and cause further damage. A high level of differential expression early on might also be evidence of compensatory mechanisms at work which keep the disorder temporarily under control, despite the early expression of the genetic mutation.

Even though the CAG repeat in the Hdh^{Q150} mouse model is about 60% longer than in the Hdh^{Q92} model, both lines have a normal lifespan and there is some parallel in the development of the disorder in these mice (section 1.8.4). Hence, the first time point chosen for investigation in the Hdh^{Q150} was 18 months, as with the Hdh^{Q92}, to allow comparison between the models. $Hdh^{Q150/Q150}$ brain was expected to present with many differentially expressed proteins at this age, given that previous studies reported a succession of behavioural, molecular, neuropathological and transcriptional changes prior to this (Lin *et al.* 2001; Yu *et al.* 2003; Strand *et al.* 2005; Tallaksen-Greene *et al.* 2005; Brooks *et al.* 2006;

Woodman *et al.* 2007; Heng *et al.* 2007; Kuhn *et al.* 2007). As with the Hdh^{Q92}, microdissected caudate-putamen was examined, as this brain region presented an earlier neuropathology, with nuclear inclusions, reactive gliosis and neuronal death, than the rest of the brain in this mouse model (Lin *et al.* 2001; Yu *et al.* 2003; Heng *et al.* 2007; Woodman *et al.* 2007; Kuhn *et al.* 2007). The SELDI-TOF results were largely consistent with these reports. The 18 month $Hdh^{Q150/Q150}$ showed a substantial proportion of differentially expressed proteins and nearly twice as many as were found in the 18 month $Hdh^{Q92/Q92}$. The magnitude of the changes was somewhat lower in the $Hdh^{Q150/Q150}$ though, with only a third showing a change > 40%, compared with more than half in the $Hdh^{Q92/Q92}$.

Because $Hdh^{Q150/Q150}$ developed various disease characteristics a good deal earlier than 18 months, caudate-putamen of 15 month $Hdh^{Q150/Q150}$ was screened as well. There were significantly fewer differences at 15 than at 18 months and the magnitude of the changes was considerably smaller in the younger animals. These results agree with earlier gene expression results, which showed an increasing number of gene expression changes with mounting severity of the disease phenotype (Woodman *et al.* 2007; Kuhn *et al.* 2007).

Several studies have explored the differences and similarities of the HD genetic mouse models (Luthi-Carter *et al.* 2000; Chan *et al.* 2002; Menalled 2005; Woodman *et al.* 2007; Kuhn *et al.* 2007). In the present study, nearly half of the differentially expressed proteins were changed in more than one of the mouse models tested. The majority of these were found in the two knock-in models. This might be due partly to the fact that the assays in these models were performed on microdissected tissue, while half cerebra were used for the R6/1. It might also point towards a stronger similarity between the Hdh^{Q92} and Hdh^{Q150} mouse

models, which would not be surprising bearing in mind that they were generated following similar strategies, even though they have different constructs inserted in their *Hdh* gene (section 1.8.4). One unexpected outcome however, was that more than half of the changes detected in both Hdh^{Q92} and Hdh^{Q150} displayed a change in the opposite direction. This could indicate that, despite being of the same age, the animals were in another phase of the disease, and the discrepancy in the direction of the changes could be the outcome of compensatory mechanisms at work at different stages of the disease process. However, it is also possible that some of these discrepancies are due to technical artifacts.

By and large, the results obtained with SELDI-TOF correlated with the individual behavioural phenotypes of the different mouse models as well as with the findings of the majority of previous research. SELDI-TOF certainly has a number of advantages over other proteomic techniques, but some key disadvantages too. Several reports have also questioned the reproducibility of the system (Diamandis 2004b; Diamandis 2004a; Veenstra *et al.* 2004; Bons *et al.* 2006; De Boer *et al.* 2006; Harezlak *et al.* 2007), an issue that was highlighted when a group of prostate cancer studies using SELDI failed to reproduce previous results (Adam *et al.* 2002; Qu *et al.* 2002; Semmes *et al.* 2005; McLerran *et al.* 2008a; McLerran *et al.* 2008b).

To complement the results obtained by SELDI-TOF, DIGE was used for further investigation of the caudate-putamen proteome of the Hdh^{Q150} mouse model. The biological significance in HD of the proteins already identified will be discussed in Chapter 6.

Chapter 4. Comparison of the proteome in the caudate-putamen of the *Hdh*^{Q150} mouse model using 2-D Fluorescence Difference Gel Electrophoresis (DIGE)

4.1 Introduction to DIGE

The SELDI approach, reported in chapter 3, has some shortcomings. To complement the SELDI findings, it was decided to investigate further one of the mouse models using a different technique. As the SELDI results showed that the caudate-putamen of 18 month *Hdh*$^{Q150/Q150}$ (Lin *et al.* 2001 and section 1.8.4) displayed the most protein changes, this model, brain region and timepoint were chosen for analysis with 2-D fluorescence difference gel electrophoresis (DIGE), the Ettan DIGE system of GE Healthcare. The caudate-putamen proteome of 18 month *Hdh*$^{Q150/Q150}$ was compared with that of their littermates. Protein spots found to be differentially expressed by DIGE were identified using matrix assisted laser desorption ionisation time-of-flight tandem (MALDI TOF/TOF) mass spectrometry.

4.2 Identification of differentially expressed proteins in the *Hdh*$^{Q150/Q150}$ caudate-putamen using DIGE

4.2.1 The DIGE procedure

2-D electrophoresis (Klose 1975; O'Farrell 1975) is a widely used method for separating proteins on a polyacrylamide gel. Proteins are first separated according to their isoelectric point (pI) during isoelectric focusing. Isoelectric

focusing is a technique for separating proteins by their electric charge. The total electric charge of a protein will change with the pH of its environment: a protein in a solution with a pH lower or higher than its pI will have a positive or negative charge respectively. During isoelectric focusing, protein samples are applied to the anode end of a gel strip with an immobilised pH gradient. An electric current is passed through the gel and proteins will migrate towards the cathode until they reach the pH at which the total electric charge of the protein is zero, the pI. This procedure concentrates the proteins into well-defined bands, at a point in the pH gradient corresponding to the pI of the proteins. To resolve the second dimension, the focused gel strip is placed at the top of a polyacrylamide gel and the proteins are separated with SDS-PAGE according to their molecular weight, at an angle of 90° to the first dimension separation.

The DIGE system is a modification of traditional 2-DE (Unlu *et al.* 1997) that has been commercialised by GE Healthcare. It has been successfully used in protein profiling (Gade *et al.* 2003; Apraiz *et al.* 2006), to screen for biomarkers (Huang *et al.* 2006; Hye *et al.* 2006; Wu *et al.* 2007) and to study various types of cancer (Somiari *et al.* 2003; Liang *et al.* 2005; Yu *et al.* 2005; Nishimori *et al.* 2006) and other diseases, such as schizophrenia (Swatton *et al.* 2004) and severe acute respiratory syndrome (Wan *et al.* 2006).

DIGE is an improvement of 2-DE because it allows multiplexing of up to three samples on a single 2-D gel by labelling the samples prior to 2-DE with one of three spectrally resolvable fluorescent cyanine dyes (Cy2, Cy3 and Cy5). The dyes attach to the ε-amino groups of lysine side-chains and are designed to match in terms of charge and molecular weight (~450 Da), so that proteins will keep the same mobility in the gel. Initial experiments showed, however, that

adding too much label could cause precipitation of the proteins due to the hydrophobicity of the dyes. Minimal labelling, a protocol in which only 3% of the lysine side-chains are labelled, was found to be optimal, as there was still sufficient dye present for detection, but it no longer had an effect on the solubility of the proteins. As a rule, only one dye molecule attaches per protein in this approach. The few proteins with more than one dye molecule attached would be in such small numbers that they would not be visible.

Multiplexing with DIGE limits the number of gels used and allows for direct comparison between the samples on a single gel. However, the most powerful tool in this approach is the option to use one of the dyes for labelling a standard. When comparing numerous samples on multiple gels, two samples, one test sample and one control, are usually labelled with Cy3 and Cy5 and separated on the same gel. The third dye, Cy2, is used to label an internal standard, made up of an equal amount of all the samples to be compared in the experiment. An aliquot of this standard is applied to each of the gels. Instead of comparing the Cy3 and Cy5 samples directly, a ratio is calculated between the measurements of the samples and those of the standard. Figure 4.1 shows how these ratios are normalised across all the gels involved, based on the Cy2 signal for each gel. The option of using an internal standard is one of the key benefits of DIGE. The pooled internal standard should also ensure that every protein in each sample appears on all the gels. All the experimental samples are then quantified against the same standard. This method compensates for gel to gel variation, assists in inter-gel matching and significantly increases the accuracy of spot comparison and statistics (Alban *et al.* 2003).

The 2D-gels are scanned on the Typhoon Trio Variable Mode Imager from GE Healthcare. A coloured image is obtained with a different false colour overlay for each of the Cy dyes. This is for illustrative purposes only, as quantitative measurements are obtained with greyscale pixel intensities. The ensuing images are analysed with the DeCyder 2D Software, Version 6.5, from GE Healthcare.

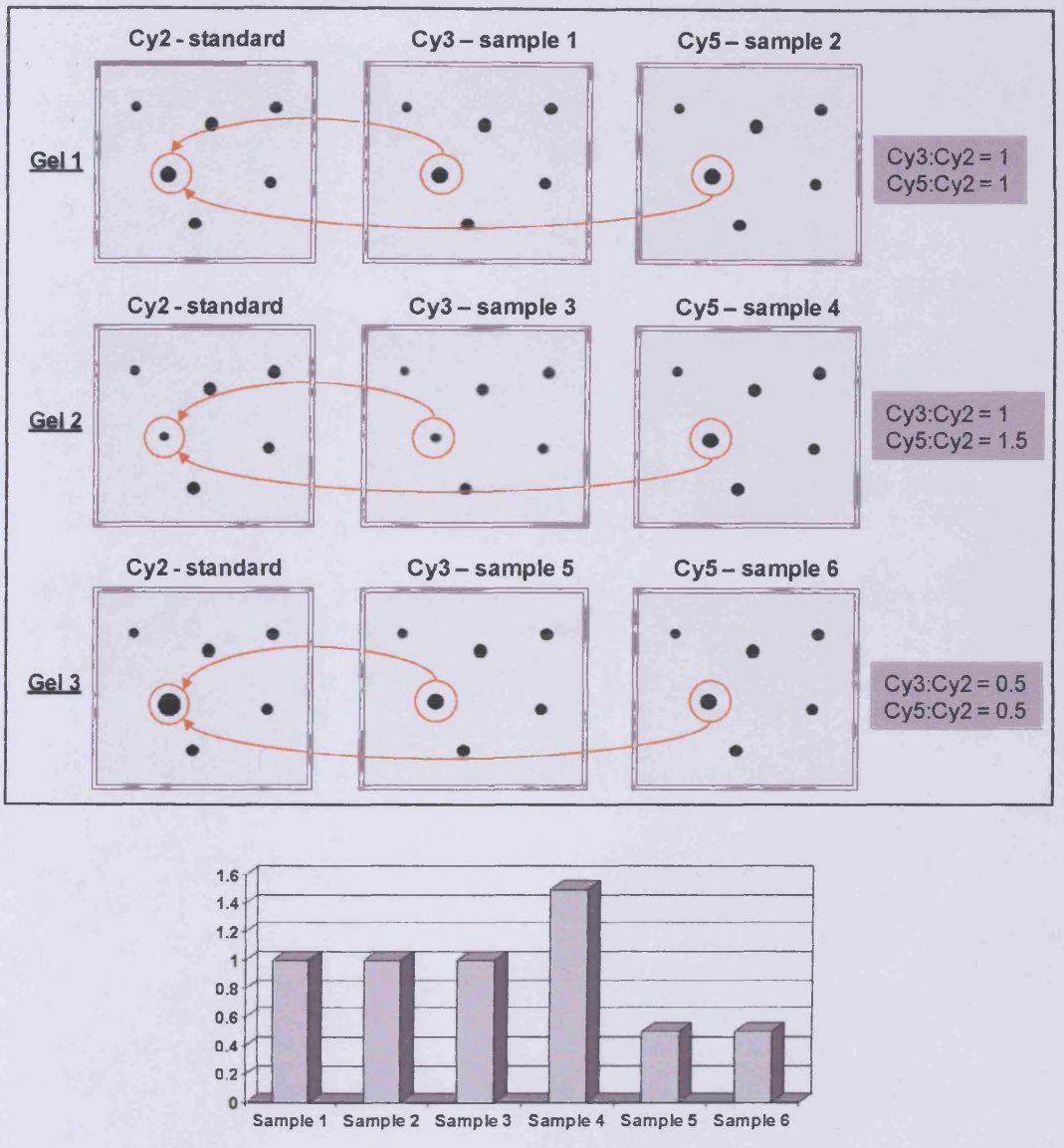

Figure 4.1 Multi-gel DIGE experiment using an internal standard. When comparing the spots circled in orange in samples 1-6 visually, the conclusion would be that only the protein in sample 3 is differentially expressed and decreased. The measurements normalised with the Cy2 signal are listed in the grey boxes next to the gels and assembled in the graph below. It shows that, contrary to the first conclusion, sample 3 is not differentially expressed but samples 4-6 are, with sample 4 increased and samples 5-6 decreased.

4.2.2 Mouse brain samples

The experiment compared the caudate-putamen of six 18 month *Hdh*$^{Q150/Q150}$ (Lin *et al.* 2001), two female and four male, with six *Hdh*$^{+/+}$, three female and three male, on six gels. All were littermates from the same colony. Each gel ran one test and one control sample. The distribution of the samples over the six gels was random, based on a randomised set-up generated by Microsoft Excel.

4.2.3 Preparation of samples for DIGE

Sample homogenates in 1.5 ml Eppendorf tubes at the recommended protein concentration of 5 mg/ml in a total volume of 10 μl of urea-thiourea lysis buffer were labelled with 400 pmol dye (Cy3 or Cy5), according to the manufacturer's instructions. Dilute solutions (< 1 mg/ml) do not label efficiently and high protein concentrations (> 10 mg/ml) may cause streaking in the gel due to aggregation and precipitation of the proteins (Gorg *et al.* 2000). Protein sample and dye were mixed thoroughly by pipetting and vortexing. The solution was microcentrifuged briefly and left on ice for 30 min in the dark. Processing the labelled samples and DIGE gels must be carried out in the dark as far as possible, to avoid photobleaching of the fluorescent dyes upon exposure to light. The reaction was stopped with 1 μl of 10 mM lysine. The solution was mixed and spun briefly again and left on ice in the dark for 10-15 min. To compensate for possible differences brought about by the dyes, three of the test samples and three controls were labelled with Cy3, while the remaining six were labelled with Cy5.

Parallel to labelling the samples, the internal standard was made up and labelled. For this six-gel experiment with 12 samples, the standard was made up of a 5 μl aliquot of each caudate-putamen homogenate containing 25 μg of protein in urea-thiourea lysis buffer. The 60 μl total volume of standard was labelled with 2.4 nmol Cy2 dye following the protocol described earlier. Before loading the samples on to the focusing strips, one Cy3 sample, one Cy5 sample and 10 μl of the Cy2 standard were combined in a 1.5 ml Eppendorf tube and mixed. An equal volume of 2 x sample buffer (7 M Urea, 2 M Thiourea, 4% w/v CHAPS, 0.01 w/v Bromophenol blue, 1% strip specific IPG buffer and 40 mM DTT) was added to the mix and incubated on ice in the dark for 15 min. The combined samples were subjected to isoelectric focusing (section 2.2.5) and separated on polyacrylamide gels (section 2.1.3) by SDS-PAGE (section 2.2.6).

4.2.4 Analysis on the Typhoon Imager: scanning gels

The DIGE gels were scanned on the Typhoon Trio Variable Mode Imager while still held between the glass casting plates. This approach is an improvement from traditional 2-DE. One of the difficulties in identifying protein spots on, and computing matches between, several 2-DE images arises from various degrees of distortion of the 2-DE gels during fixing and staining. With DIGE, the gels are kept between the casting plates for scanning, which avoids gel distortion and thus prevents the introduction of further technical variation.

The three different Cy dyes on a single gel were scanned successively, producing three different images, with the default setup specifications. Cy3 was scanned with a 532 nm laser and a 580 band pass (BP) 30 emission filter, Cy5

with a 633 nm laser and a 670 BP 30 emission filter and Cy2 with a 488 nm laser and a 580 BP 30 emission filter.

4.2.5 Image analysis by the DeCyder software: identifying spots

The DeCyder 2D Software, Version 6.5, is a fully automated approach for analysing DIGE images obtained with the Typhoon scanner. The software detects, matches and quantitates the protein spots and performs statistical analysis on the measurements.

Figure 4.2 shows the software start-up screen with the different modules and workflow. The Typhoon images are imported into the software by the Image Loader module and stored in an Oracle database. There are two possible pathways for further analysis. The first uses the Differential In-gel Analysis (DIA), followed by the Biological Variation Analysis (BVA) for multiple gels. The second uses the Batch Processor.

Differential In-gel Analysis (DIA)

The DIA module analyses up to three images from a single gel, performing automated spot detection, background subtraction, quantitation, normalisation and within-gel matching. The internal standard is specified as the primary image, while the samples to be compared are the secondary and tertiary images. A merged image is created from the three individual ones, integrating all the spot details in one image. Spot detection and boundary designation are carried out based on the pixel data from the individual images in combination with the merged image. The sensitivity of the spot detection process is determined by manually specifying the total number of spots to be detected. The number recommended in the GE

Healthcare software manual is 2,500. This should include practically all the protein spots present on most 2D gels. Specifying a higher number of spots for detection will give more spots, although the majority of the additional spots usually prove to be artifacts. An exclusion filter, applied after spot detection, eliminates artifacts from the final analysis, by removing spots corresponding to a set of chosen parameters from the final spot list. The parameters used in these experiments were suggested by the company: maximum slope > 1.1, area < 100, maximum volume < 10,000 and maximum peak < 80 and > 65,000. These were somewhat lenient and failed to take out all the artifacts, but more rigorous settings risked removing real spots as well. The resulting spot map is superimposed on the three separate images. As explained in section 4.2.1, protein abundance for the secondary and tertiary image is expressed as a ratio of the corresponding spots on the primary image. Information on all the protein spots on a gel is saved as an XML file, which can be used for inter-gel analysis in other DeCyder modules. Figure 4.3 shows the DIA user interface, which offers four types of display: the gel image, a three dimensional view of a selected spot, a histogram of all the spots in that gel image and a table with information on all these spots.

Biological Variation Analysis (BVA)

The BVA module carries out inter-gel statistical analysis using the information held on the XML files. All spot maps are matched to a master image, which is generally the one with the highest number of spots. Spot matching is done through pattern recognition based on the neighbouring spots. Similar to the DIA, the BVA user interface, shown in Figure 4.4, links the gel image, the three dimensional view of selected spots and the spot table, but the histogram is

replaced by a dot plot showing the selected spot in all the samples clustered in sample groups. The BVA also has the option to display the gel view of up to 48 images at once as shown in Figure 4.5, making it easier to verify that a spot has been identified correctly in the different images.

Batch Processor

The Batch Processor module links the DIA and BVA module in an automated process, which allows analysis of multiple gels without manual intervention. Subsequent manual verification of the results is done in the BVA module.

The twelve sample experiment of Hdh^{Q150} on six gels was analysed with the Batch Processor. All the spots identified as significantly different between the two sample groups were manually checked in the BVA module and corrected where the matching was found deficient.

4.2.6 Statistical analysis of identified spots

The BVA module offers different statistical tests, but this project only used the average ratio calculation and the Student's t-test. The average ratio specifies the fold change: a value of 1.0 represents an unchanged spot, 2.0 indicates a two-fold increase and -2.0 a two-fold decrease. The Student's t-test was performed between the sample groups $Hdh^{Q150/Q150}$ and $Hdh^{+/+}$. The threshold for statistical significance was set at 0.05. Only spots with $p < 0.05$ and an average ratio >1.20 or <-1.20 were followed up.

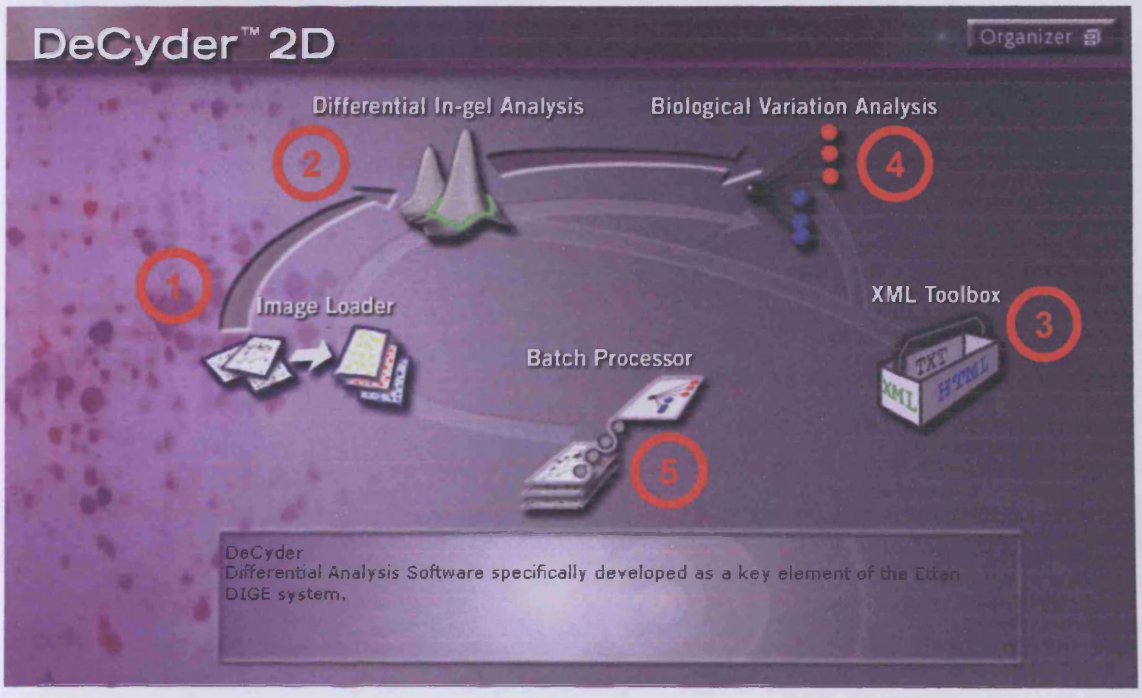

Figure 4.2 Decyder 2D software start-up screen showing the different modules and workflow. **(1)** Images are imported into the software by the Image Loader module. **(2)** The individual images are analysed in the Differential In-gel Analysis (DIA) module and **(3)** the data obtained is stored as an XML file in the XML Toolbox. **(4)** Multiple gels analysed by the DIA can be matched and compared in the Biological Variation Analysis (BVA) module. **(5)** An alternative approach is the automated analysis performed by the Batch Processor, which integrates the DIA and the BVA for the analysis of multiple gels without manual intervention.

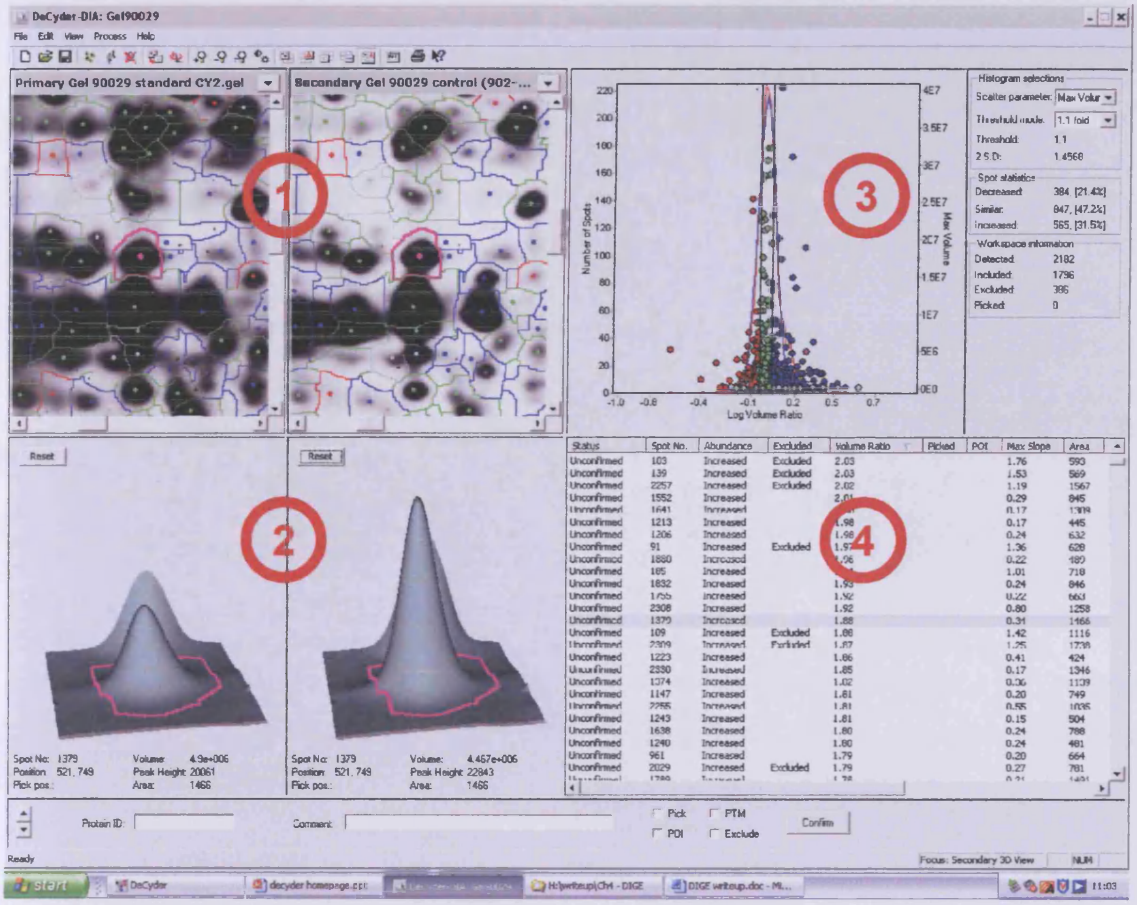

Figure 4.3 DIA user interface, presenting four types of display linked together. **(1)** Gel image with the internal control on the primary gel on the left being compared with one of the samples on the secondary or tertiary gel on the right. **(2)** Three dimensional view of a selected spot. **(3)** Histogram of all the spots on the secondary or tertiary gel image. **(4)** Table with information on all the spots.

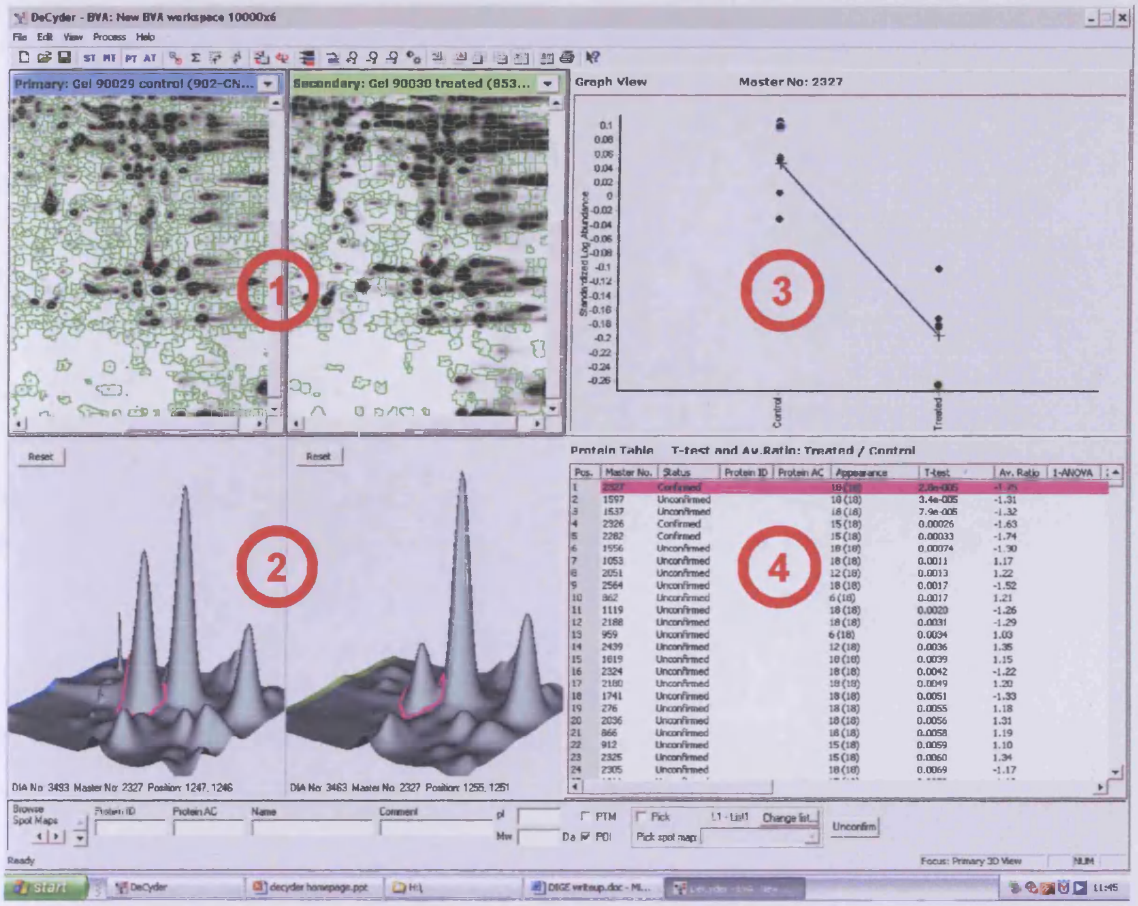

Figure 4.4 BVA user interface, presenting four types of display linked together. **(1)** Gel image with the master gel on the left compared to another gel image on the right. **(2)** Three dimensional view of selected spots. **(3)** Dot plot of the selected spot in all the samples clustered in sample groups. **(4)** Spot table.

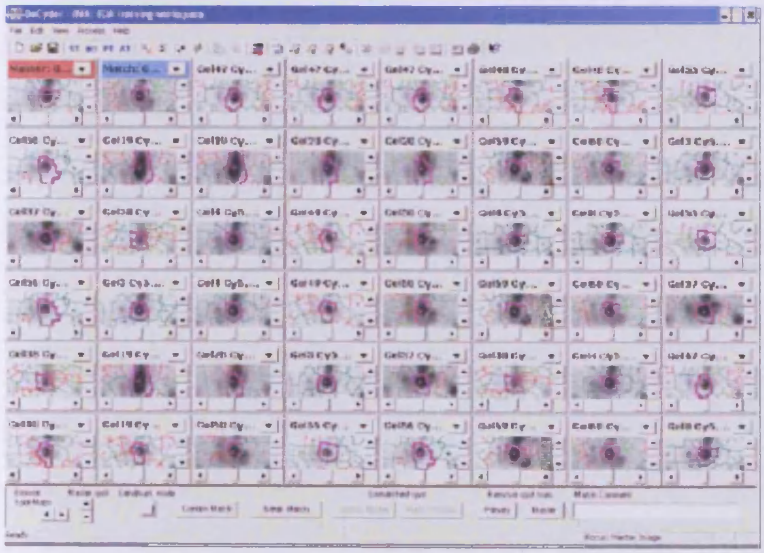

Figure 4.5 Gel view of up to 48 images simultaneously in the BVA module.

4.3 Optimisation of DIGE technique for mouse brain samples

4.3.1 Sample quality and amount of protein on mini gels

To check the quality of the samples and the optimal amount of protein for gel loading, two 2DE experiments were performed with 18 month *Hdh*$^{Q150/Q150}$ caudate-putamen on NuPAGE 4-12% Bis-Tris Zoom mini gels. Focusing was carried out on 7 cm 3-10NL IPG strips (section 2.2.5), followed by SDS-PAGE (section 2.2.6). On the first gel 5 μg of protein in 5 μl of homogenate was separated and 10 μg of protein in 10 μl of homogenate on the second gel. Both gels were silver stained (section 2.2.7). The two scanned gels in Figure 4.6 show a clean image with numerous distinct spots and only a small amount of streaking. It was decided that the samples were clean enough to be run without 2D-clean up. This prevented the introduction of further technical variation into the sample groups during the 2D-clean up step. The gel with 10 μg of protein presented not only with more pronounced spots, but also with spots that were hardly or not at all visible when using only 5 μg of protein.

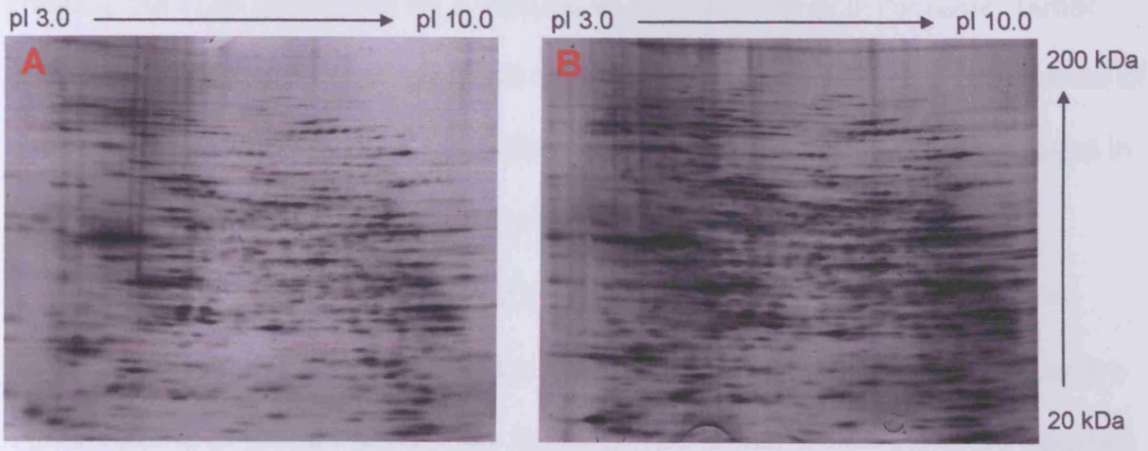

Figure 4.6 2DE separation of 18 month *Hdh*$^{Q150/Q150}$ caudate-putamen homogenate on NuPAGE 4-12% Bis-Tris Zoom mini gels. Both gels were silver stained. Gel **A** separated 5 μg of protein in 5 μl of homogenate. Gel **B** separated 10 μg of protein in 10 μl of homogenate.

4.3.2 Amount of protein on large gel format

To determine the optimal amount of protein on large format gels, two 2DE experiments were performed with 18 month *Hdh*$^{Q150/+}$ caudate-putamen homogenate on in-house large format gels (section 2.1.3). Focusing was carried out on 24 cm 3-10NL IPG strips (section 2.2.5) and SDS-PAGE was performed as a batch (section 2.2.6). On the first gel 35 μg of protein in 25 μl of homogenate was separated. On the second gel 50 μg of protein in 25 μl of homogenate was separated. A third gel separated 75 μg of protein in 25 μl of homogenate, but this was carried out in a separate batch on a different day. All gels were silver stained (section 2.2.7).

Figure 4.7 shows the scanned images of the silver stained gels. While the gels with 35 μg (A) and 50 μg of protein (B) presented a clear image with little streaking, the gel with 75 μg of protein (C) had an area with distinct tear formation. However, this was believed to be caused not by the higher amount of protein

present, but in all probability by a leak between the lower and the upper buffer chamber during electrophoresis. This notion was corroborated by the presence of a matching region on a DIGE gel, pictured in Figure 4.8, which was processed in the same electrophoresis batch as gel C.

Although the gel with 35 μg of protein presented a clear image with a reasonable number of well defined spots, many of the spots were weak. Using a higher volume of protein gave more and stronger spots. It was therefore decided to use 50 μg of protein per sample in future DIGE experiments.

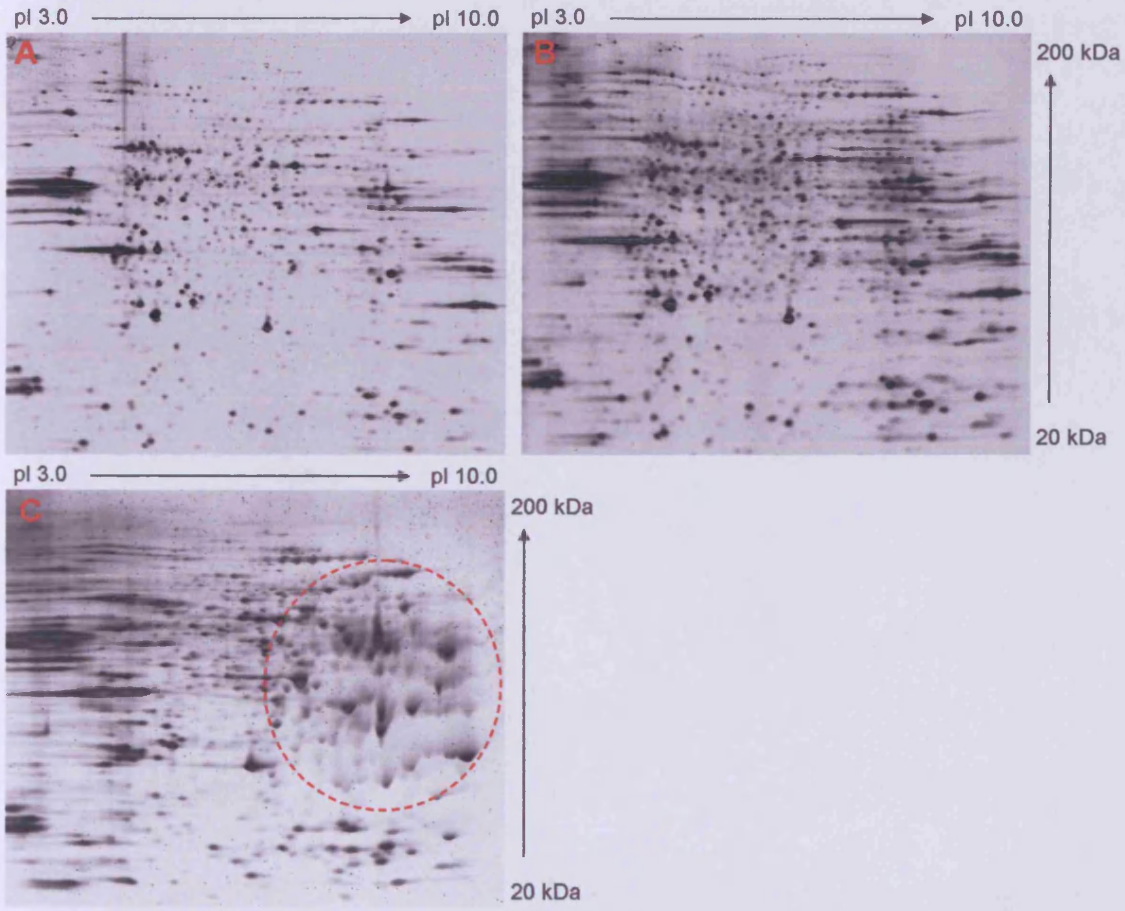

Figure 4.7 Silver stained 2D-gels of 18 month *Hdh*$^{Q150/+}$ caudate-putamen homogenate. Gel **A** separated 35 μg of protein, gel **B** 50 μg of protein and gel **C** 75 μg of protein. SDS-PAGE was performed on gel A and B in the same batch, while gel C was processed separately. While A and B present a clear image with little streaking and well defined spots, gel C has an area, highlighted by the red circle, with distinct tear formation, possibly due to a leak between the lower and the upper buffer chamber.

4.3.3 DIGE trials

A DIGE experiment was performed with 18 month *Hdh*$^{+/+}$ and *Hdh*$^{Q150/Q150}$ caudate-putamen homogenate on an in-house large format gel (section 2.1.3) with 50 μg of protein for each sample. The *Hdh*$^{Q150/Q150}$ sample was labelled with Cy5 and the *Hdh*$^{+/+}$ sample with Cy3 (section 4.2.3). Focusing was carried out on 24 cm 3-10NL IPG strips (section 2.2.5), followed by SDS-PAGE (section 2.2.6) and silver staining (section 2.2.7). Figure 4.8 shows the coloured overlaid DIGE image and the silver stained image. SDS-PAGE was performed in the same batch as gel C in Figure 4.7. Both gels have a corresponding distorted area, highlighted by the red circle, which is in all probability due to a leak between the lower and the upper buffer chamber. The region is on opposite sides of the gels because they were inserted back to back in the electrophoresis unit.

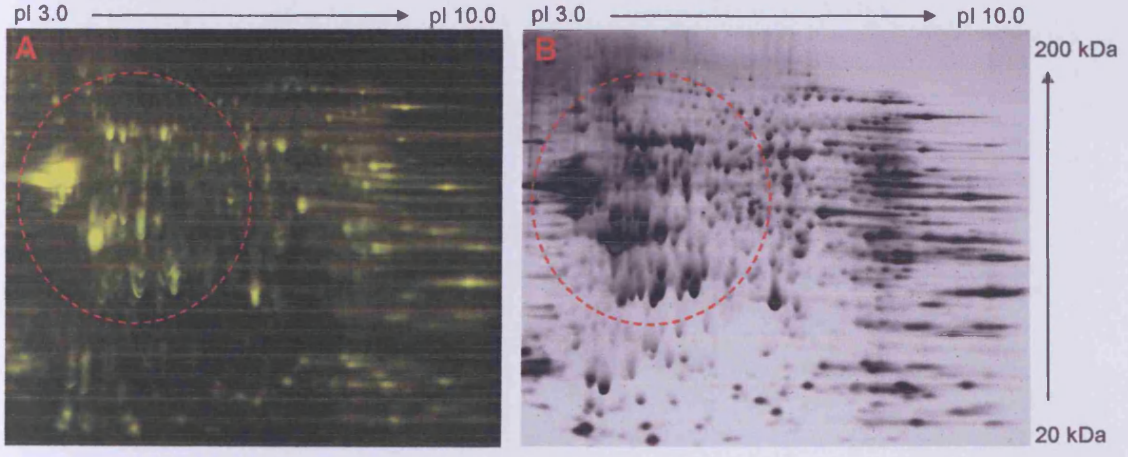

Figure 4.8 DIGE gel of 18 month *Hdh*$^{+/+}$ and *Hdh*$^{Q150/Q150}$ caudate-putamen homogenate. The gel separated 50 μg of protein of each sample. The *Hdh*$^{+/+}$ sample was labelled with Cy3 and the *Hdh*$^{Q150/Q150}$ sample with Cy5. **A** shows the coloured image obtained with false overlays for each of the Cy dyes. Green spots represent Cy3 and red spots Cy5 labelled proteins and yellow spots are proteins that are present in both samples. **B** shows the silver stained gel. The red circle highlights a distorted area, probably caused by a leak between the lower and the upper buffer chamber.

A different DIGE experiment was performed with the same samples and protocols as in the previous trial. Figure 4.9 shows the silver stained gel and the coloured DIGE images. The gel presented a clear image with a large number of well defined spots and little streaking, indicating that both the Cy dye labelling and the 2DE had worked well. The gel was analysed with the DeCyder DIA module. The number of spots to be detected was set at 2,500. An exclusion filter was applied with the parameters set out in section 4.2.5. After automated spot detection, background subtraction, quantitation, normalisation, artifact exclusion and within gel matching, the volume ratio of $Hdh^{Q150/Q150}$ over $Hdh^{+/+}$ was calculated. All the spots which showed a fold change > 1.5, indicating a 50% increase or decrease, were manually checked for accuracy and corrected where matching was found to be inadequate. A total of 2084 spots were detected. The exclusion filter removed 362 (=17%) of these. Of the 1722 spots left, 62 (=4%) were decreased > 1.5-fold and 53 (=3%) were increased > 1.5-fold. When selecting only changes > 2-fold, these numbers dropped to 18 (=1%) decreased and 20 (=1%) increased spots.

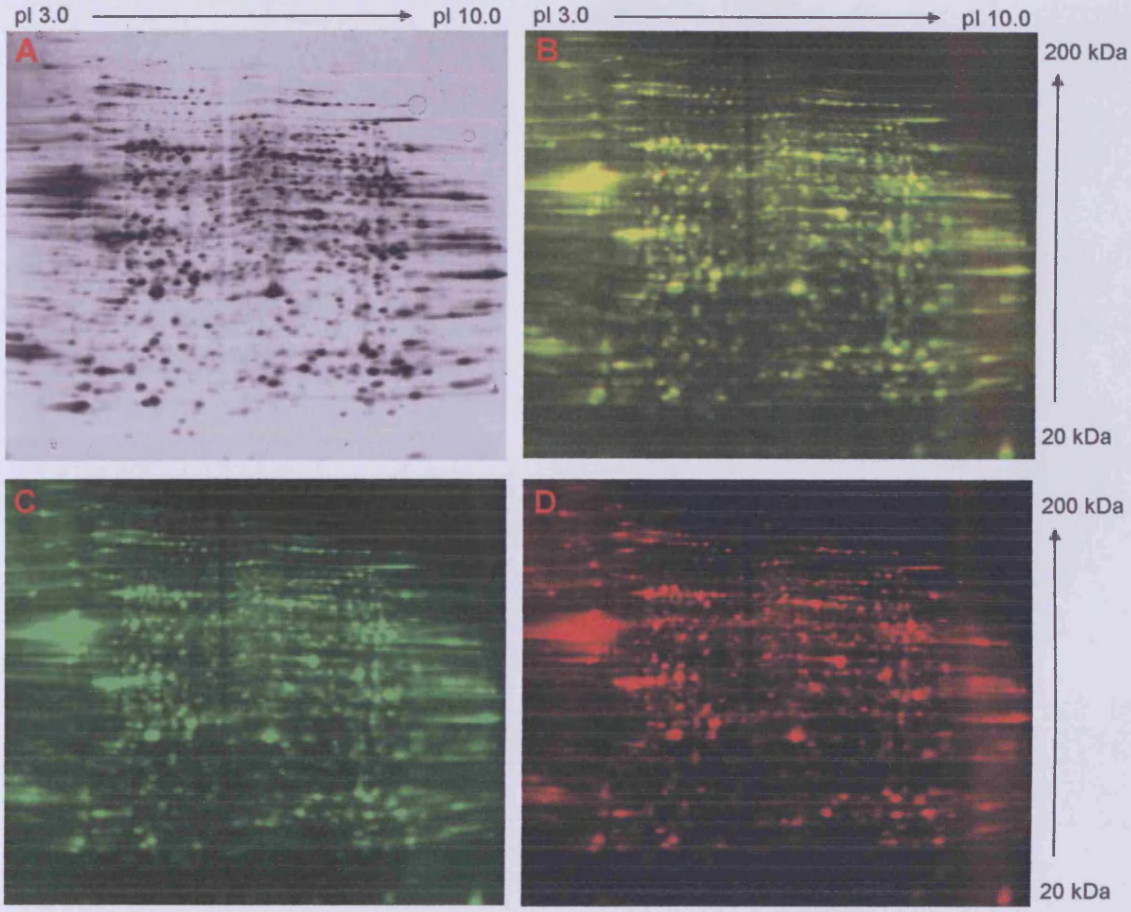

Figure 4.9 DIGE gel of 18 month $Hdh^{+/+}$ and $Hdh^{Q150/Q150}$ caudate-putamen homogenate. The gel separated 50 μg of protein of each sample. **A** shows the silver stained gel. **B** is the coloured image obtained with false overlays for each of the Cy dyes. Green spots represent Cy3 and red spots Cy5 labelled proteins. Yellow spots are proteins that are present in both samples. **C** is the individual coloured image of the Cy3 labelled $Hdh^{+/+}$ sample and **D** of the Cy5 labelled $Hdh^{Q150/Q150}$ sample.

4.4 Comparison of *Hdh*$^{Q150/Q150}$ and *Hdh*$^{+/+}$ caudate-putamen proteome

The caudate-putamen proteome of six 18 month *Hdh*$^{Q150/Q150}$ was compared with six *Hdh*$^{+/+}$ littermates using DIGE. The samples were run on six gels, each with a *Hdh*$^{Q150/Q150}$ and a *Hdh*$^{+/+}$ sample and an internal standard. The internal standard was labelled with Cy2, while Cy3 and Cy5 were alternated between the sample groups. Table 4.1 gives an overview of the experimental design. After the gels were scanned on the Typhoon Imager, they were removed from the glass plates and silver stained to visualise the spots for picking. Spots cannot be picked directly from the fluor labelled proteins on the gels because the Cy dyes increase the molecular weight of the proteins, which causes a shift between the minimal amount of labelled protein and the bulk of still unlabelled protein. Because of this shift, the fluorescent spots do not correspond to the peak of unlabelled protein, which is essential to maximise identification. Figure 4.10 shows the scanned images of the six silver stained gels.

The six gels were analysed in the DeCyder batch module. Gel matching was manually checked and corrected where necessary. Table 4.2 shows the number of spots included in the analysis after applying the exclusion filter for each of the gels in Figure 4.10, and the number of these that were matched to the master gel. Because gel 1 had the highest number of spots, it was designated the master gel. Table 4.3 shows what proportion of the spots was present on various numbers of gels. Although only 23% of the spots were matched over all the gels, almost half of the spots were matched on at least five gels and 82% of them on three gels or more. The Student's t-test took only the results of the gels on which

a particular spot was detected into the analysis. Gels where the spot was absent were excluded for that particular spot.

Of the 2760 spots on the master gel, 47 were differentially expressed with an average ratio > 1.20 or < -1.20 and $p < 0.05$. All 47 spots were checked manually for accurate matching and rematched where needed, with a new average ratio and p-value calculated for the modified spots. On two occasions, this rematching altered the statistical results for a spot so it was no longer significantly different. Of the 45 spots left, 10 were gel artifacts and 14 were not considered real peaks. Figure 4.11 shows a comparison between a real peak and spots which are rejected. A further three spots were too difficult to identify on the silver stained gels. This left 18 spots, of which 15 were decreased and 3 increased. These spots were picked and analysed by MALDI TOF for protein identification.

To ensure that no significant spots were missed, all the spots with a p-value between 0.05-0.1, 100 in total, were manually checked, rematched where necessary and the p-value and average ratio recalculated. For two of the spots, this approach moved $p < 0.05$. These were also picked and analysed by MALDI TOF.

Table 4.4 shows the details of the 47 spots with $p < 0.05$ that were checked and the two with initially $0.05 < p < 0.1$, which were added after rematching. Although not all gel plugs were taken from the same gel, the gel plug numbers given in Table 4.4 are all marked on the image of gel 6 in Figure 4.12 for easier presentation.

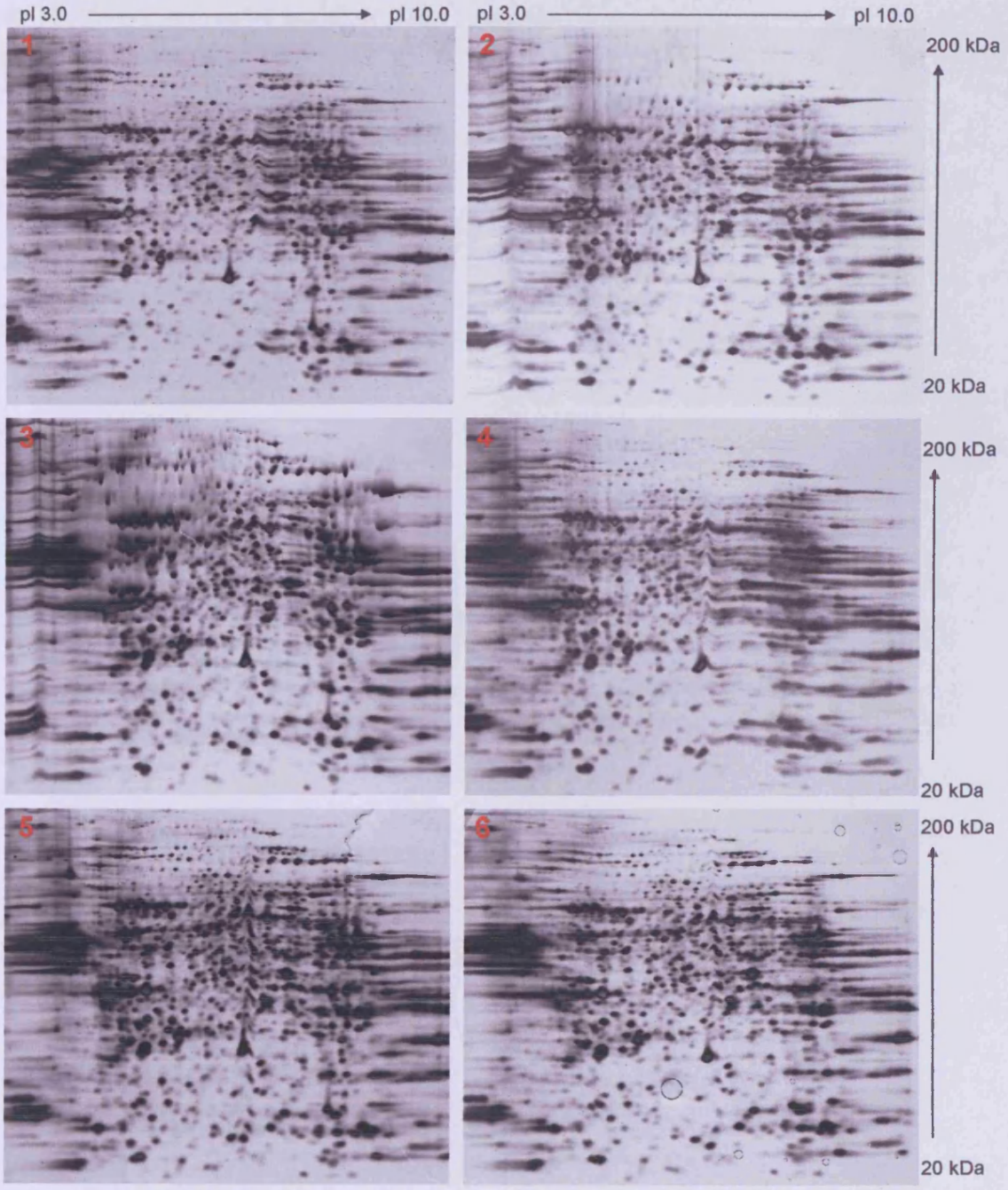

Figure 4.10 Six silver stained DIGE gels, comparing the caudate-putamen proteome of six 18 month *Hdh*$^{Q150/Q150}$ with six *Hdh*$^{+/+}$ littermates. On each gel there was one *Hdh*$^{Q150/Q150}$ sample, one *Hdh*$^{+/+}$ sample and an internal standard. The internal standard was labelled with Cy2, while Cy3 and Cy5 were alternated between the sample groups (ref. Table 4.1). The circles in the top right hand corner and in the lower half of gel 6 are air bubbles trapped under the gel during scanning of the silver stain image.

Table 4.1 Experimental design of a six gel DIGE experiment comparing the caudate-putamen proteome of six 18 month *Hdh*$^{Q150/Q150}$ with six *Hdh*$^{+/+}$ littermates.

Gel	Cy2	Cy3	Cy5
1	Standard	*Hdh* $^{+/+}$ sample 1	*Hdh* $^{Q150/Q150}$ sample 1
2	Standard	*Hdh* $^{+/+}$ sample 2	*Hdh* $^{Q150/Q150}$ sample 2
3	Standard	*Hdh* $^{+/+}$ sample 3	*Hdh* $^{Q150/Q150}$ sample 3
4	Standard	*Hdh* $^{Q150/Q150}$ sample 4	*Hdh* $^{+/+}$ sample 4
5	Standard	*Hdh* $^{Q150/Q150}$ sample 5	*Hdh* $^{+/+}$ sample 5
6	Standard	*Hdh* $^{Q150/Q150}$ sample 6	*Hdh* $^{+/+}$ sample 6

Table 4.2 Number of spots on six DIGE gels comparing the caudate-putamen proteome of six 18 month *Hdh*$^{Q150/Q150}$ with six *Hdh*$^{+/+}$ littermates.

Number of spots for all gels		
gel	**spots included**	**spots matched to master gel**
gel 1	2760 = master	2760
gel 2	2741	1821
gel 3	2479	1659
gel 4	2474	1775
gel 5	2528	1811
gel 6	2334	1641

The first column lists the number of spots included after applying the exclusion filter and the second column shows the number of spots in each gel that were matched to the master gel, in this case gel 1. Gel 1 served as master gel because it generated the highest number of spots.

Table 4.3 Number and proportion of spots matched on six DIGE gels comparing the caudate-putamen proteome of six 18 month $Hdh^{Q150/Q150}$ with six $Hdh^{+/+}$ littermates.

Number and % of spots matched over number of gels			
number gels	number spots	% of total number	accumulated %
6/6 gels	644	23	23
5/6 gels	664	24	47
4/6 gels	561	20	68
3/6 gels	406	15	82
2/6 gels	331	12	94
1/6 gels	154	6	100

The first column shows the number of gels. Columns two and three give the number of spots matched and the proportion of the total number of spots. The last column gives the accumulated percentage of the spots matched.

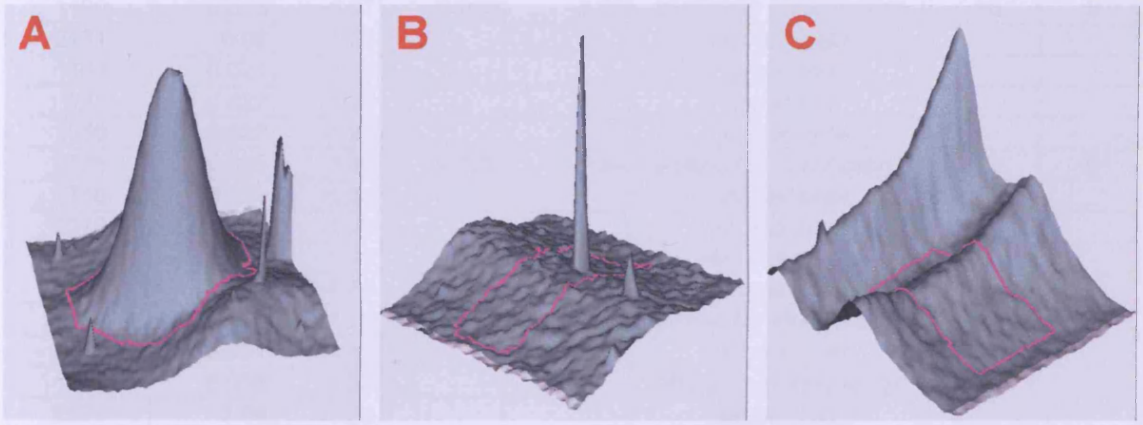

Figure 4.11 Difference between a real peak and a spot not considered a real peak. **A** shows a real peak. **B** shows a peak caused by a dust particle on the gel. Although the pattern in **C** is generated by proteins present in the gel, they fail to present as individual peaks, which makes them impossible to isolate.

Table 4.4 Spots with a significant difference in the caudate-putamen of *Hdh*$^{Q150/Q150}$ compared with *Hdh*$^{+/+}$ littermates.

The caudate-putamen proteomes of six 18 month *Hdh*$^{Q150/Q150}$ were compared with six *Hdh*$^{+/+}$ littermates on six DIGE gels. The spots listed have an average ratio > 1.20 or < -1.20 and $p < 0.05$. The spot number was allocated by the DeCyder software for the spots on the master gel. The initial p-value and average ratio are listed, as well as the new p-value and average ratio for spots that were rematched. The comments indicate which spots were picked for MALDI/TOF identification and the reason why others were not. The plug numbers can be cross-referenced with the numbers on Figure 4.12 and the gel numbers are the reference given to the gels in Figure 4.10. The last two rows show the spots which initially had $0.05 < p < 0.1$ but acquired $p < 0.05$ after rematching.

spot number on master gel	p-value	average ratio	p-value after rematch	average ratio after rematch	comment	plug number (*)	gel for picking (**)
2327	2.80E-05	-1.75			picked for identification	1	5
1597	3.40E-05	-1.31			picked for identification	2	6
1537	8.90E-05	-1.32	7.90E-05	-1.32	picked for identification	3	5
2326	0.00026	-1.63			picked for identification	4	2
2282	0.00033	-1.74			not real peak		
1556	0.0004	-1.29	0.00074	-1.30	picked for identification	5	1
2051	0.0013	1.22			gel artifact		
862	0.0017	1.21			gel artifact		
1119	0.002	-1.26			picked for identification	6	1
2188	0.0031	-1.29			picked for identification	7	4
2439	0.0036	1.35			not real peak		
2324	0.0042	-1.22			picked for identification	8	5
2180	0.0049	1.20			picked for identification	9	4
1741	0.0051	-1.33			picked for identification	10	1
2302	0.0055	-1.20	0.039	-1.32	picked for identification	11	6
2760	0.0057	-1.21	0.0089	-1.21	picked for identification	12	1
2050	0.008	1.24			not real peak		
2380	0.0086	1.58			not real peak		
2036	0.0096	1.35	0.0056	1.31	picked for identification	13	5
2564	0.011	-1.43	0.0017	-1.52	picked for identification	14	1
1116	0.011	1.21			gel artifact		
2062	0.014	1.63			gel artifact		
1120	0.015	-1.27	0.016	-1.23	picked for identification	15	5
2171	0.02	1.22			not real peak		
1109	0.021	1.25			gel artifact		
700	0.022	-1.25			gel artifact		
1050	0.022	-1.20			not real peak		
2325	0.025	1.35	0.006	1.34	picked for identification	16	4
2718	0.029	-1.61			not real peak		
2279	0.032	-1.29			not real peak		
846	0.032	1.22	0.026	1.19	rematched out		
2177	0.034	-1.36			not real peak		
1581	0.034	-1.23	0.046	-1.23	picked for identification	17	1
2502	0.037	1.41			not real peak		
1108	0.038	1.27			difficult to identify on gel		
2228	0.04	-1.28			not real peak		
1803	0.04	1.27	0.05	1.20	rematched out		
53	0.042	-1.50			not real peak		
2170	0.042	-1.31			not real peak		
61	0.042	-1.20			gel artifact		
216	0.043	1.23			gel artifact		
937	0.047	-1.40			not real peak		
1857	0.047	-1.27	0.043	-1.21	picked for identification	18	4
1577	0.047	-1.20			difficult to identify on gel		
2501	0.048	1.23			gel artifact		
763	0.049	-1.54			difficult to identify on gel		
1111	0.049	1.39			gel artifact		
Spots with initial p-value between 0.05-0.1 but rematched to < 0.05							
1082	0.061	-1.29	0.021	-1.29	picked for identification	19	4
1570	0.061	-1.16	0.016	-1.22	picked for identification	20	5

(*) number of spot plug picked can be found on Figure 4.12

(**) gel number refers to the numbers given in Figure 4.10

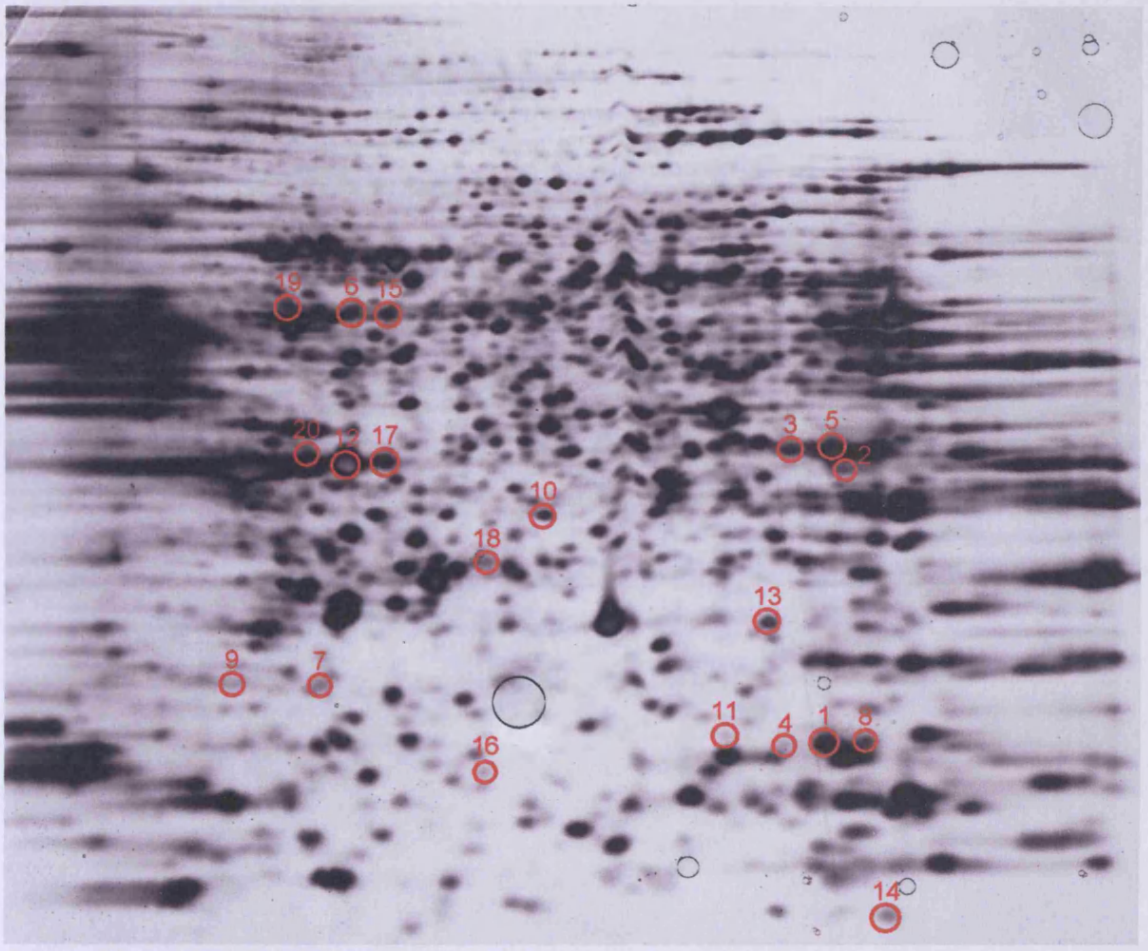

Figure 4.12 Spots picked for MALDI TOF/TOF analysis. Gel 6 shows the spots circled in red. The numbers of the spots refer to the plug numbers in Table 4.4.

4.5 Identification of proteins from DIGE by MALDI TOF/TOF

Trypsin digestion was carried out by Mrs S.H.V. Nixon and MALDI TOF/TOF analysis by Dr. I. Brewis at the Proteomics Unit of the Central Biotechnology Services at Cardiff University. Of the 20 spots picked, 11 were identified, detailed in Table 4.5. The MALDI TOF/TOF identification categories are listed in section 3.8.4.

Of the 11 identifications, five were a category 1 and six a category 3. Because some proteins were identified from several spots, only six different proteins were isolated in total: serine/threonine protein phosphatase 2B (generally known as calcineurin) α-isoform (CaN-A) and creatine kinase B chain (CKB) were both identified from three spots each, glutamine synthetase (GS) was isolated from two different spots and carbonic anhydrase II (CA2), superoxide dismutase (SODM) and apolipoprotein E precursor (APOE) were found in single spots. Figure 4.13 shows the identified spots with the protein match. The proteins that were isolated from multiple spots were in most cases a category 1 identification. Interestingly, the magnitudes of the changes for the different spots of one particular protein were nearly identical. The protein showing the largest change was CA2, with an average ratio of -1.75.

Table 4.5 MALDI TOF/TOF identifications of DIGE spots.

The left section of the table gives the DIGE result for the 20 gel plugs picked fo
identification. The right section shows the MALDI TOF/TOF identifications, with
protein match and name, the gene name and the amino acid code for each pep
match. The criteria for identification use the expectation value (E.), both for the
identification and for the peptide matches. The four MALDI TOF/TOF identificat
categories are: (Cat.1) Conclusive identification with excellent tandem MS data
more peptides, each peptide with E < 0.05; (Cat.2) Conclusive identification wit
tandem MS data for one peptide with E < 0.0001; (Cat.3) Probable/possible ide
with tandem MS data for one or more peptides with 0.05 < overall E < 0.05-0.0
(Cat.4) Probable/possible identification with MS (not tandem MS) with E < 0.01

DIGE RESULTS			MALDI TOF/TOF identification						
Plug	p-value	Ratio	Match	Protein	Gene name	Cat.	E. overall	Peptide match	E. peptide
1	2.80E-05	-1.75	CAH2_MOUSE	Carbonic anhydrase II	*Ca2*	3	2.30E-13	DFPIANGDR GGPLSDSYR	1.80E-01 9.30E-03
2	3.40E-05	-1.31	GLNA_MOUSE	Glutamine synthetase	*Glul*	3	5.10E-04	DIVEAHYR	2.90E-02
3	7.90E-05	-1.32	no match						
4	0.00026	-1.63	no match						
5	0.00074	-1.3	GLNA_MOUSE	Glutamine synthetase	*Glul*	1	7.20E-44	VQAMYIWVDGTGEGLR DIVEAHYR MGDHLWIAR LTGFHETSNINDFSAGVANR RPSANCDPYAVTEAIVR HQYHIR	1.30E-03 1.30E-03 4.80E-02 8.50E-02 1.20E-01 1.30E-01
6	0.002	-1.26	PP2BA_MOUSE	Serine/threonine protein phosphatase 2B, catalytic subunit,alpha isoform (Calcineurin A)	*Ppp3ca*	4	1.80E-05	AVPFPPSHR YLFLGDYVDR	3.20E-01 5.00E-01
7	0.0031	-1.29	APOE_MOUSE	Apolipoprotein E precursor	*Apoe*	3	6.00E-05	LQAEIFQAR	2.60E-02
8	0.0042	-1.22	no match						
9	0.0049	1.2	no match						
10	0.0051	-1.33	no match						
11	0.039	-1.32	no match						
12	0.0089	-1.21	KCRB_MOUSE	Creatine kinase, B chain	*Ckb*	1	8.60E-79	GTGGVDTAAVGGVFDVSNADR DLFDPIIEER VLTPELYAELR GFCLPPHCSR TFLVWINEEDHLR LAVEALSSLDGDLSGR LLIEMEQR LLIEMEQR	9.10E-13 3.50E-06 3.70E-06 4.50E-06 8.00E-05 9.20E-04 1.20E-03 3.50E-02
13	0.0056	1.31	no match						
14	0.0017	-1.52	SODM_MOUSE	Superoxide dismutase (Mn) - mitochondrial precursor	*Sod2*	3	2.30E-08	GDVTTQVALQPALK GELLEAIKR NVRPDYLK	1.40E-01 2.90E-01 5.20E-01
15	0.016	-1.23	PP2BA_MOUSE	Serine/threonine protein phosphatase 2B, catalytic subunit,alpha isoform (Calcineurin A)	*Ppp3ca*	1	9.10E-16	LFEVGGSPANTR YLFLGDYVDR	4.40E-05 2.00E-03
16	0.006	1.34	no match						
17	0.046	-1.23	KCRB_MOUSE	Creatine kinase, B chain	*Ckb*	3	7.60E-05	VLTPELYAELR	5.20E-04
18	0.043	-1.21	no match						
19	0.021	-1.29	PP2BA_MOUSE	Serine/threonine protein phosphatase 2B, catalytic subunit,alpha isoform (Calcineurin A)	*Ppp3ca*	1	9.10E-11	LFEVGGSPANTR EVFDNDGKPR	2.70E-03 4.70E-02
20	0.016	-1.22	KCRB_MOUSE	Creatine kinase, B chain	*Ckb*	1	4.30E-13	GTGGVDTAAVGGVFDVSNADR VLTPELYAELR DLFDPIIEER	8.50E-05 6.50E-03 1.40E-02

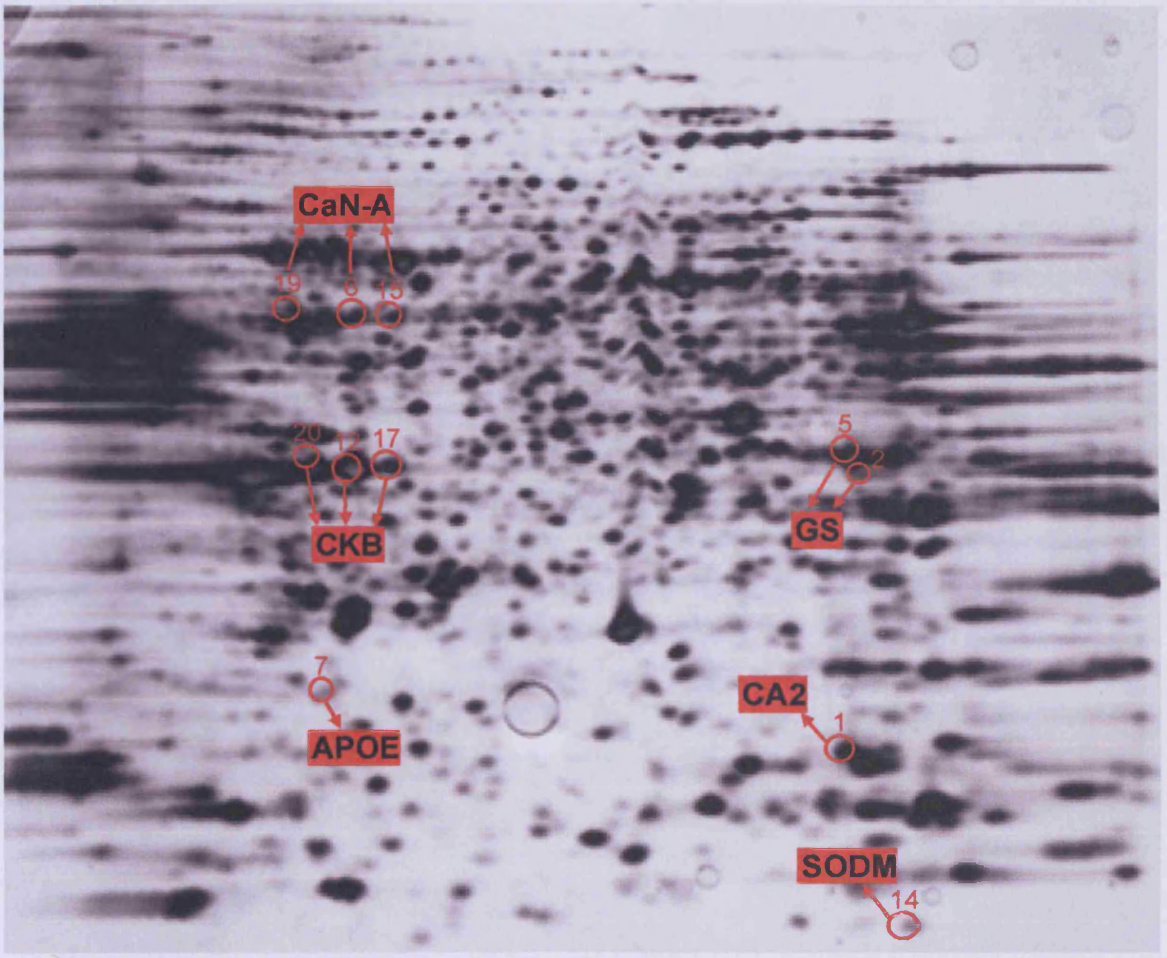

Figure 4.13 Spots with identifications. The spots that were identified are circled in red and the corresponding protein matches are specified. The numbers of the spots and details of the protein matches can be found in Table 4.5.

4.6 Discussion

The work reported in this chapter was carried out using DIGE, a variation of two-dimensional gel electrophoresis, which allows multiplexing of samples on the same gel by using fluorescent dyes. This technique was chosen to complement the SELDI analysis since some of the limitations of SELDI are not an issue or are less of an issue with DIGE. While the molecular weight range available to SELDI is limited to proteins below 20 kDa, the 2-DE approach with DIGE can theoretically visualise proteins of any size, although in actual fact high and low molecular weight proteins are still difficult to detect (Corthals *et al.* 2000; Oh-Ishi *et al.* 2000). This was obvious in the present study where the sizes of the identified proteins were all between 25-59 kDa even though the corresponding spots were distributed over the larger part of the gels, from high to low molecular weight. This demonstrated that the main separation happened between approximately 20-100 kDa and that few proteins were detected outside this molecular weight range.

2-DE has other limitations which restrict the number of proteins within reach. Very acidic and very basic proteins are difficult to detect (Bae *et al.* 2003). This was evident on the experimental gels, where the extreme left (low pI) and extreme right (high pI) of the gels showed a substantial amount of streaking, with few clearly defined individual spots. The proteins that were identified ranged between pI 5.3-8.8 and the areas to the left and to the right of these became increasingly streaky and indistinct. Due to poor solubilisation, membrane bound proteins also prove hard to capture on a gel (Molloy 2000; Santoni *et al.* 2000a;

Santoni *et al.* 2000b) and lower abundance proteins are notoriously difficult to isolate (Fountoulakis *et al.* 1999a; Fountoulakis *et al.* 1999b; Gygi *et al.* 2000a).

Another concern with DIGE is the numerous steps in the protocol which can introduce a substantial degree of technical variation, perhaps limiting the value of the quantitative outcome. Therefore, being able to avoid the 2D-clean up certainly limited the degree of error in this study. The cost of the dyes used in DIGE can definitely be a restricting factor for any large scale experiments too.

Despite a number of limitations, DIGE does have some key advantages over SELDI. One discussed earlier is the wider molecular weight range accessible with DIGE. Another is the number of proteins resolved simultaneously. Although one study reported 10,000 proteins on a single large format 2-DE gel (Klose 1999), gels routinely resolve around 2,000 spots (Ong & Pandey 2001), a number which was exceeded in this study. This is about twenty times as many proteins as with SELDI, even though it is still only a fraction of the mouse brain proteome. The 2DE approach of DIGE also provides some basic information on the captured proteins, such as their approximate molecular weight and isoelectric point, and it allows the study of protein isoforms and post-translational modifications. Still, the main advantage of DIGE over SELDI is undoubtedly the straightforward access to the proteins of interest for isolation and identification. With DIGE, only 6% of the significantly different spots were not picked because they were too difficult to identify on the gels. This is in stark contrast to SELDI, where 80% of the significantly altered proteins could not be isolated. This direct way of processing also compensates for the larger amount of sample 2-DE requires.

The SELDI analysis of the R6/1, Hdh^{Q92} and Hdh^{Q150} mouse models established 18 month Hdh^{Q150} caudate-putamen as the model, brain region and time point with the highest number of differentially expressed proteins. As this was the first time the DIGE technique was used to screen and compare a large number of samples within one experiment in this laboratory, the 18 month Hdh^{Q150} caudate-putamen samples were chosen as they were expected to show a substantial number of differences. Since the DIGE equipment can process only six gels simultaneously, six $Hdh^{Q150/Q150}$ were compared with six $Hdh^{+/+}$. All six gels were of sufficient quality to be included in the analysis and more than 80% of the spots were matched on at least half of the gels, which was a high rate of matching (Freeman & Hemby 2004). The $Hdh^{Q150/Q150}$ displayed a little less than 5% differentially expressed proteins, about half increased and half decreased. This measure of change was significantly lower than that detected by SELDI, which found 18% differentially expressed proteins, when only changes with $p < 0.05$ are considered. The magnitude of the changes detected with SELDI and DIGE was comparable. The discrepancy in the levels of dysregulation between the two techniques may be a technical difference introduced by the individual procedures. On the other hand, it may correspond to a true variation, with a higher proportion of small proteins being dysregulated.

MALDI-TOF analysis identified only 11 of the 20 spots picked. It was recognised that five of the spots without identification were weak spots (Figure 4.12: spots number 4, 9, 11, 16 and 18), which most likely did not contain enough protein for the analysis. A way to avoid this obstacle in future would be to use a preparative spot picking gel with a higher protein load of the sample mix, thus maximising the amount of protein extracted from each spot. This gel would be

matched to the data obtained from the analytical gels so that spots of interest could be accurately picked. The failure to identify the remaining four spots could be due to some technical shortcoming of the MALDI process, possibly caused by co-migrating proteins, which MALDI may not be able to distinguish. It is also possible that the proteins in the samples have not yet been entered in the reference databases.

Three of the six proteins identified were isolated from more than one spot on the gel. Because of this, the category 4 identification for plug number 6 was accepted as a true identification. Different spots for one protein on a gel could correspond to different isoforms of this protein or may represent post-translational modifications such as phosphorylation, glycosylation or proteolytic cleavage. All these alterations could adjust the molecular weight of the protein or its charge, and therefore the isoelectric point, or both, and affect how the protein travels in the gel. This behaviour has been noted repeatedly in the past (Gygi *et al.* 2000b; Johnston-Wilson *et al.* 2000; Zabel *et al.* 2002; Welin *et al.* 2004; Brigulla *et al.* 2006; McDonald *et al.* 2006; Selicharova *et al.* 2007).

Previous studies have reported behavioural, molecular, neurological and transcriptional changes by 18 months in Hdh^{Q150}, with many changes happening earlier in the striatum than in the other brain regions (section 1.8.4 and Lin *et al.* 2001; Yu *et al.* 2003; Strand *et al.* 2005; Tallaksen-Greene *et al.* 2005; Brooks *et al.* 2006; Woodman *et al.* 2007; Heng *et al.* 2007; Kuhn *et al.* 2007). Therefore, $Hdh^{Q150/Q150}$ caudate-putamen was expected to show a significant number of differentially expressed proteins by this age. Although DIGE did not identify as high a proportion of changes as SELDI did, the outcome was still consistent with previous results.

DIGE certainly offers some clear advantages over SELDI and other proteomic techniques, despite certain limitations. One of these shortcomings is the difficulty in capturing certain groups of proteins. This can, to some degree, be matched by enriching samples for certain proteins, either by pre-fractionation or by separation through multiple narrow-range isoelectric focusing steps (Gorg *et al.* 2000). The DIGE approach can also be complemented by peptide-based shotgun proteomics, which identifies proteins in complex mixtures using a combination of high performance liquid chromatography combined with mass spectrometry (Hu *et al.* 2007). This method is no longer limited by the molecular weight or isoelectric point of proteins.

As with many high throughput biological research tools, the statistical and experimental management of research projects is paramount. This is also the case with DIGE and has been examined by various groups (Fodor *et al.* 2005; Karp & Lilley 2005; Karp *et al.* 2007). Despite some drawbacks, DIGE certainly has potential in biological and medical research, although thorough experimental design and the right statistical analysis are essential.

To confirm the results obtained by SELDI-TOF and DIGE and to investigate further the proteins identified, western blot analysis was performed on several of the proteins. The biological significance of the proteins discovered will be discussed in Chapter 6.

Chapter 5. Confirmation of SELDI-TOF and DIGE results by western blot analysis

5.1 Introduction to western blot

Some of the proteins identified by MALDI TOF/TOF from the SELDI-TOF and DIGE results were further investigated by western blot analysis. The quantities of these proteins in brain samples of *Hdh*$^{Q92/Q92}$ and *Hdh*$^{Q150/Q150}$ were compared with those of their wild type littermates. The samples matched the mouse models, ages and brain regions in which the differential expression of these proteins was detected by SELDI-TOF and DIGE. To complete the picture, some western blot analysis was performed on samples in which no significant difference had been detected by SELDI-TOF or DIGE previously. Samples were probed with antibodies against Cytochrome c oxidase polypeptide VIb (COX-VIb), 10 kDa heat shock protein (HSP10), 60 kDa heat shock protein (HSP60), Myelin Basic Protein (MBP), Calcineurin A (CaN-A), Creatine Kinase BB (CKB), Glutamine Synthetase (GS) and Superoxide Dismutase (SODM).

5.2 Optimisation of antibodies

All antibody optimisation experiments were performed with 10 month *Hdh*$^{Q92/+}$ homogenate of half cerebra on 10% and 12% Bis-Tris NuPage gels, testing two or three primary antibody dilutions for each, based on the recommendations of the suppliers (section 2.2.9). The primary antibodies chosen for optimisation were raised against COX-VIb, HSP10, MBP, CaN-A, CKB, GS,

SODM, Calmodulin (CaM) and Apolipoprotein (APOE). The primary antibodies against HSP60 and α-tubulin and the secondary antibodies had previously been optimised in this laboratory. Only one dilution was tried for CKB to avoid using too much of the antibody. The blots were scanned on the LiCor Odyssey infrared detection system (LI-COR Biosciences).

The antibodies against COX-VIb, HSP10, CaN-A, CKB, GS and SODM presented a clear discrete band of the expected size. The antibody against MBP was expected to detect the four isoforms of MBP (14 kDa, 17.2 kDa, 18.5 kDa and 21.5 kDa), which was the case. The antibodies against CaM and APOE failed to produce bands and were not used for further screening. Table 5.1 summarises the optimisation particulars, with images of the bands and the antibody dilutions used for further screening.

Table 5.1 Antibody optimisation experiments.

Antibody	Gel	Sample	Protein/ lane	Results	Dilution for screening
Mouse monoclonal anti-COX (cytochrome c oxidase) VIb (COX-VIb)	12% Bis-Tris	*Hdh*$^{Q92/+}$ 10 months ½ cerebra	50 µg	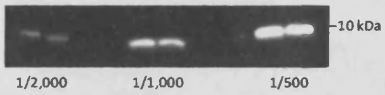	1/1,000
Rabbit polyclonal anti-Cnp10 (HSP10)	12% Bis-Tris	*Hdh*$^{Q92/+}$ 10 months ½ cerebra	50 µg	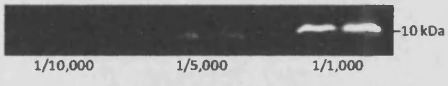	1/1,000
Rabbit polyclonal anti-Myelin Basic Protein (MBP)	12% Bis-Tris	*Hdh*$^{Q92/+}$ 10 months ½ cerebra	50 µg		1/2,000
Rabbit polyclonal anti-Calmodulin (CaM)	12% Bis-Tris	*Hdh*$^{Q92/+}$ 10 months ½ cerebra	20 µg 50 µg 100 µg	[1] 20 µg protein in 1/2,000 - 1/1,000 - 1/500 → no bands [2] 100 µg protein in 1/500 and 50 µg in 1/500 - 1/100 → no bands [3] 50 µg protein in 1/1,000 - 1/500 - 1/100 (no tween) → no bands [4] 50 µg protein in 1/1,000 - 1/200 (overnight) → no bands	not used for screening
Rabbit polyclonal anti-Calcineurin A (CaN-A)	10% Bis-Tris	*Hdh*$^{Q92/+}$ 10 months ½ cerebra	20 µg	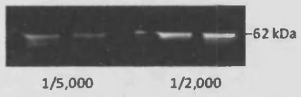	1/2,000
Rabbit polyclonal anti-Creatine Kinase BB (CKB)	12% Bis-Tris	*Hdh*$^{Q92/+}$ 10 months ½ cerebra	50 µg	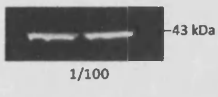	1/200
Rabbit polyclonal anti-Glutamine Synthetase (GS)	10% Bis-Tris	*Hdh*$^{Q92/+}$ 10 months ½ cerebra	20 µg	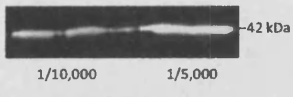	1/10,000
Mouse monoclonal [2A1] anti-Superoxide Dismutase 2 (SODM)	10% Bis-Tris	*Hdh*$^{Q92/+}$ 10 months ½ cerebra	20 µg	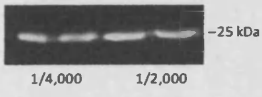	1/2,000
Rabbit monoclonal [EP1374Y] anti-Apolipoprotein E (APOE)	10% Bis-Tris	*Hdh*$^{Q92/+}$ 10 months ½ cerebra	50 µg	1/50,000 - 1/20,000→ no bands	not used for screening

Summary of the optimisation of antibodies against proteins found to be differentially expressed in *Hdh*$^{Q92/Q92}$ and *Hdh*$^{Q150/Q150}$ by SELDI-TOF and DIGE. The protein abbreviation between brackets under the name of the antibody in the first column will be used henceforth.

5.3 Western blot procedure

Western blot analysis was carried out on 10% or 12% Bis-Tris NuPage gels, following procedures in sections 2.2.6 and 2.2.9. The blots were scanned and quantitated on the LiCor Odyssey infrared detection system, which can read multiple proteins on a single membrane. Primary antibodies raised in mouse were probed with secondary IR Dye 800 anti-mouse and scanned at wavelength 800 nm, generating green bands. Primary antibodies raised in rabbit were probed with secondary Alexa Fluora 680 goat anti-rabbit IgG and scanned at wavelength 700 nm, generating red bands. This made it possible to probe for two proteins on a single blot, even if these proteins were similar in size, provided that the primary antibodies were raised in different species. Every blot was at the same time probed with an antibody against α-tubulin, to control for variation in loading. Student's T-test analysis was performed on the normalised fluorescence intensity values, generated by the LiCor Odyssey system. Table 5.2 gives a summary of the antibodies used for comparing $Hdh^{Q92/Q92}$ and $Hdh^{Q150/Q150}$ caudate-putamen with WT littermates.

Table 5.2 Antibodies for comparing *Hdh*$^{Q92/Q92}$ and *Hdh*$^{Q150/Q150}$ caudate-putamen with WT littermates.

Protein	Company	Cat. No.	Production	Dilution	Secondary antibody
COX-VIb	Invitrogen	A21366	mouse mono	1/1,000	IR Dye 800 anti-mouse
MBP	Chemicon	AB980	rabbit poly	1/1,000	Alexa Fluora 680 goat anti-rabbit IgG
HSP10	Abcam	ab53106	rabbit poly	1/2,000	Alexa Fluora 680 goat anti-rabbit IgG
CaN-A	Abcam	ab3673	rabbit poly	1/2,000	Alexa Fluora 680 goat anti-rabbit IgG
CKB	Abcam	ab38211	rabbit poly	1/200	Alexa Fluora 680 goat anti-rabbit IgG
GS	Abcam	ab49873	rabbit poly	1/10,000	Alexa Fluora 680 goat anti-rabbit IgG
SODM	Abcam	ab16956	mouse mono	1/2,000	IR Dye 800 anti-mouse
HSP60	Abcam	ab46798	rabbit poly	1/20,000	Alexa Fluora 680 goat anti-rabbit IgG
α-tubulin	in-house		mouse mono	1/50,000	IR Dye 800 anti-mouse

Summary of antibodies used in western blot analysis (section 5.4). All secondary antibodies are used at a 1/5,000 dilution. (Cat. No. = company catalogue number; mono = monoclonal; poly = polyclonal).

5.4 Comparison of *Hdh*$^{Q92/Q92}$ and *Hdh*$^{Q150/Q150}$ caudate-putamen with their WT littermates by western blot analysis

COX-VIb was identified as differentially expressed in 12 month *Hdh*$^{Q92/Q92}$ and 15 and 18 month *Hdh*$^{Q150/Q150}$ by SELDI -TOF. Western blot analysis confirmed these results in 12 month *Hdh*$^{Q92/Q92}$ and 18 month *Hdh*$^{Q150/Q150}$ with $p < 0.05$ (Figure 5.1 and Table 5.3).

The 14 kDa isoform of MPB was identified as differentially expressed in 12 and 18 month *Hdh*$^{Q92/Q92}$ by SELDI -TOF. Western blot analysis confirmed these results in 12 month *Hdh*$^{Q92/Q92}$, but only with a band of $p < 0.1$. To investigate whether a change in 14 kDa MPB could be detected in younger animals, western blot analysis was performed with 10 month *Hdh*$^{Q92/Q92}$. The result was not significant. To examine whether a change in 14 kDa MPB could be detected in

Hdh$^{Q150/Q150}$, western blot analysis was performed with 18 month *Hdh*$^{Q150/Q150}$; the result was not significant (Figure 5.2 and Table 5.3). Since the antibody against MPB also detects the 17.2, 18.5 and 21.5 kDa isoforms, quantitation was performed on these bands as well. None of these isoforms was significantly different in *Hdh*$^{Q92/Q92}$ and *Hdh*$^{Q150/Q150}$ (Table 5.4).

HSP10 was identified as differentially expressed in 15 and 18 month *Hdh*$^{Q150/Q150}$ by SELDI-TOF. Western blot analysis showed the same directional change in the 18 month animals, although only with a band of $p < 0.1$. To investigate whether a change in HSP10 could be detected in younger animals, western blot analysis was performed with 10 month old *Hdh*$^{Q150/Q150}$ and a combination of 3 and 4 month old *Hdh*$^{Q150/Q150}$. There was a decrease in the 10 month *Hdh*$^{Q150/Q150}$, but as there were only two samples of each genotype available, no statistical comparison was performed. The result in the 3 and 4 month animals showed no significant difference. To investigate whether the changes of HSP10 shown in *Hdh*$^{Q150/Q150}$ could also be detected in *Hdh*$^{Q92/Q92}$, western blot analysis was performed with 18 month *Hdh*$^{Q92/Q92}$. The result was highly significant and showed a substantial decrease in *Hdh*$^{Q92/Q92}$ (Figure 5.3 and Table 5.3).

Although HSP60 was not one of the proteins identified by SELDI-TOF or DIGE, its association with HSP10 (section 6.2) made it a candidate for further examination. Unfortunately the protein bands visualised by the antibody were too weak for accurate statistical analysis. Increasing the antibody concentration or using more protein did not improve the intensity of the bands.

Using DIGE, a 23%-29% decrease of CaN-A was observed in 18 month *Hdh*$^{Q150/Q150}$. Although the western blot result was not significant, it showed the

same directional change of near identical magnitude. *Hdh*$^{Q150/Q150}$ of 15 months showed a larger decrease with $p < 0.1$ (Figure 5.4 and Table 5.3).

A decrease of around 22% for CKB in 18 month *Hdh*$^{Q150/Q150}$ was observed using DIGE. Western blot analysis showed a significant and more substantial decrease in the 18 month animals. This was also the case for 15 month *Hdh*$^{Q150/Q150}$ with $p < 0.1$. *Hdh*$^{Q150/Q150}$ of 10 months showed a substantial increase (Figure 5.5 and Table 5.3).

For GS, DIGE analysis showed a highly significant decrease of around 31% in 18 month *Hdh*$^{Q150/Q150}$. Western blot analysis confirmed this result. *Hdh*$^{Q150/Q150}$ of 15 months showed a more substantial decrease with $p < 0.1$. The results in 18 month *Hdh*$^{Q92/Q92}$ were significant and showed a slight increase (Figure 5.6 and Table 5.3).

One of the highest expression differences detected by DIGE was a 52% decrease of SODM. However, western blot analysis was not significant (Figure 5.7 and Table 5.3).

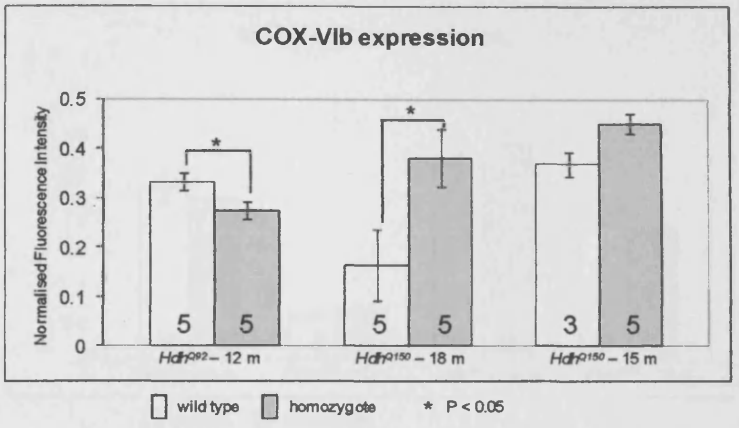

Figure 5.1 Differential expression of COX-VIb in mouse caudate-putamen.
A. Bar chart showing the results of western blot analysis of caudate-putamen of

- 12 month $Hdh^{Q92/Q92}$ compared with $Hdh^{Q+/+}$;
- 18 month $Hdh^{Q150/Q150}$ compared with $Hdh^{Q+/+}$;
- 15 month $Hdh^{Q150/Q150}$ compared with $Hdh^{Q+/+}$.

A significant difference in COX-VIb expression is shown in 12 month $Hdh^{Q92/Q92}$ and 18 month $Hdh^{Q150/Q150}$ caudate-putamen compared with $Hdh^{Q+/+}$ caudate-putamen. The number of samples in the wild type and homozygote sample groups are indicated inside the bars. Error bars indicate standard error of the mean. For details on antibodies and western blot procedures see section 5.3 and Table 5.2. Representative images are shown in Figure 5.1.B.

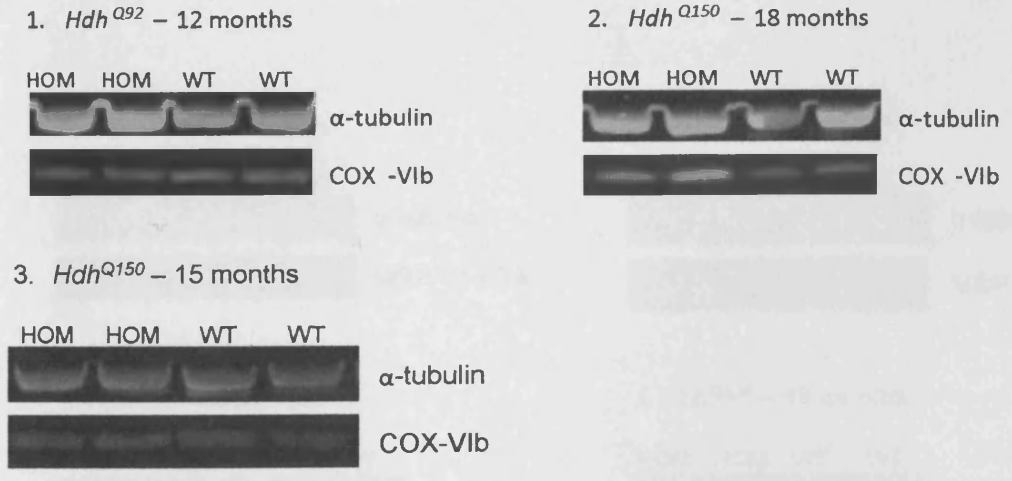

B. Representative greyscale images of western blot analysis presented in Figure 5.1.A: (1) 12 month Hdh^{Q92}; (2) 18 month Hdh^{Q150}; (3) 15 month Hdh^{Q150}. (HOM = homozygote; WT = wild type)

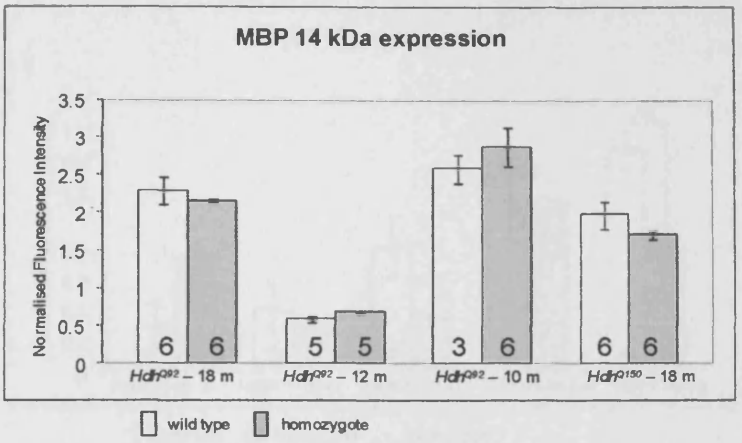

Figure 5.2 Differential expression of the 14 kDa isoform of MBP in mouse caudate-putamen.

A. Bar chart showing the results of western blot analysis of caudate putamen of

- 18 month $Hdh^{Q92/Q92}$ compared with $Hdh^{Q+/+}$;
- 12 month $Hdh^{Q92/Q92}$ compared with $Hdh^{Q+/+}$;
- 10 month $Hdh^{Q92/Q92}$ compared with $Hdh^{Q+/+}$;
- 18 month $Hdh^{Q150/Q150}$ compared with $Hdh^{Q+/+}$.

The lack of difference in the expression of the 14 kDa isoform of MBP is shown in $Hdh^{Q92/Q92}$ and $Hdh^{Q150/Q150}$ caudate-putamen compared with $Hdh^{Q+/+}$ caudate-putamen. The number of samples in the wild type and homozygote sample groups are indicated inside the bars. Error bars indicate standard error of the mean. For details on antibodies and western blot procedures see section 5.3 and Table 5.2. Representative images are shown in Figure 5.2.B.

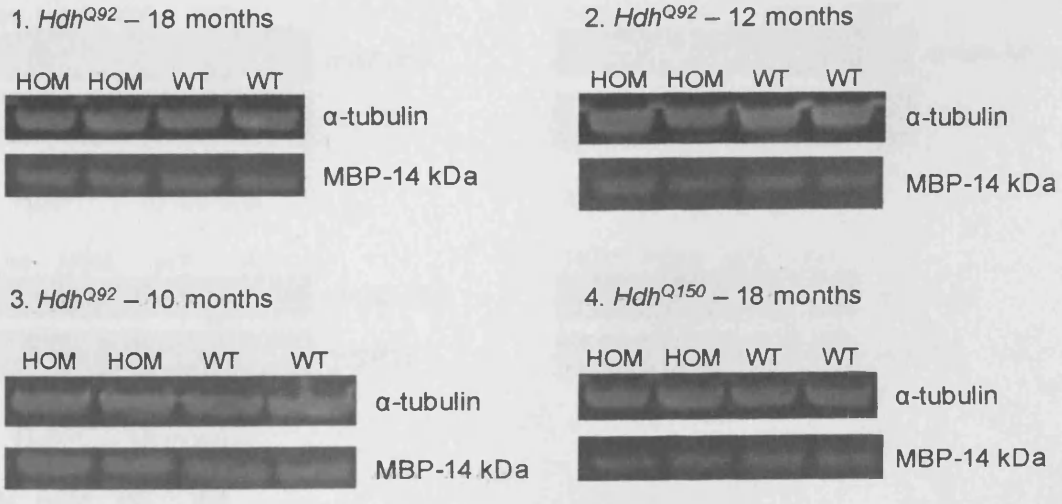

B. Representative greyscale images of western blot analysis presented in Figure 5.2.A: (1) 18 month Hdh^{Q92}; (2) 12 month Hdh^{Q92}; (3) 10 month Hdh^{Q92}; (4) 18 month Hdh^{Q150}. (HOM = homozygote; WT = wild type)

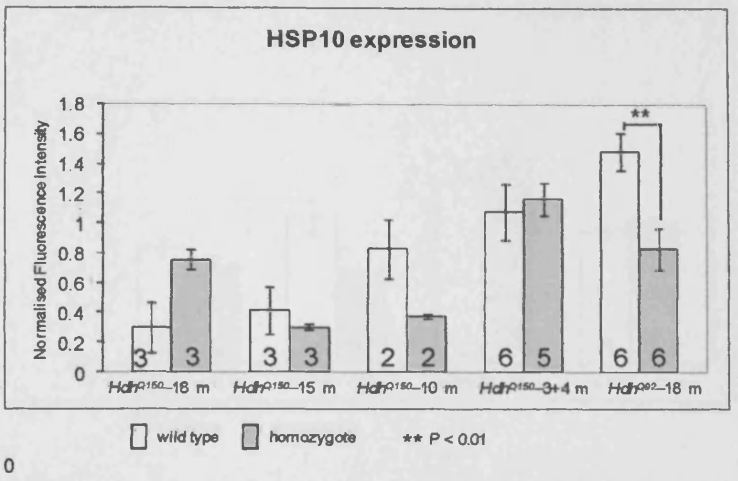

0

Figure 5.3 Differential expression of HSP10 in mouse caudate-putamen.
A. Bar chart showing the results of western blot analysis of caudate-putamen of

- 18 month $Hdh^{Q150/Q150}$ compared with $Hdh^{Q+/+}$;
- 15 month $Hdh^{Q150/Q150}$ compared with $Hdh^{Q+/+}$;
- 10 month $Hdh^{Q150/Q150}$ compared with $Hdh^{Q+/+}$;
- 3+4 month $Hdh^{Q150/Q150}$ compared with $Hdh^{Q+/+}$;
- 18 month $Hdh^{Q92/Q92}$ compared with $Hdh^{Q+/+}$.

A significant difference in HSP10 expression is shown in $Hdh^{Q92/Q92}$ caudate-putamen, a difference in 10 month $Hdh^{Q150/Q150}$ caudate-putamen and the lack of difference in 18 and 15 month $Hdh^{Q150/Q150}$ caudate-putamen compared with $Hdh^{Q+/+}$ caudate-putamen. The number of samples in the wild type and homozygote sample groups are indicated inside the bars. Error bars indicate standard error of the mean. For details on antibodies and western blot procedures see section 5.3 and Table 5.2. Representative images are shown in Figure 5.3.B.

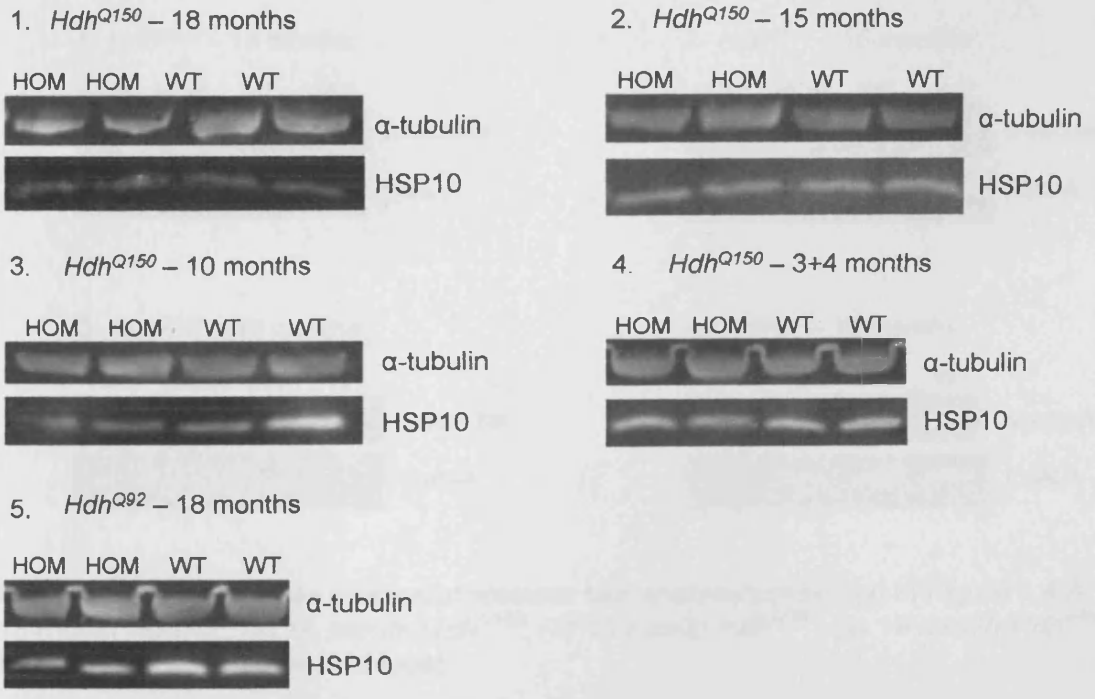

B. Representative greyscale images of western blot analysis presented in Figure 5.3.A: (1) 18 month Hdh^{Q150}; (2) 15 month Hdh^{Q150}; (3) 10 month Hdh^{Q150}; (4) 3+4 month Hdh^{Q150}; (5) 18 month Hdh^{Q92}. (HOM = homozygote; WT = wild type)

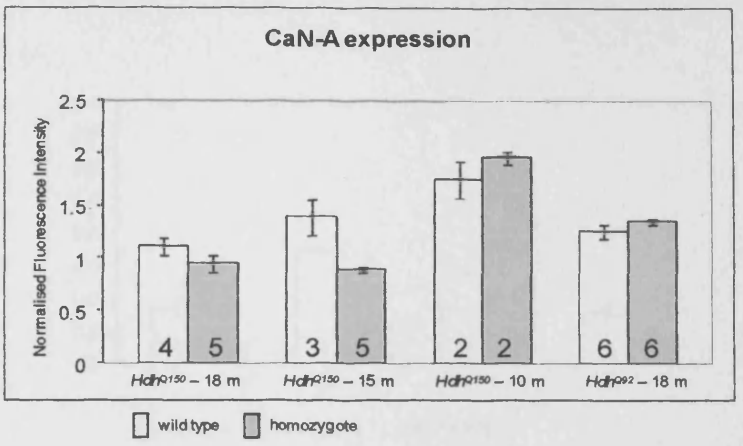

Figure 5.4 Differential expression of CaN-A in mouse caudate-putamen.
A. Bar chart showing the results of western blot analysis of caudate-putamen of

- 18 month $Hdh^{Q150/Q150}$ compared with $Hdh^{Q+/+}$;
- 15 month $Hdh^{Q150/Q150}$ compared with $Hdh^{Q+/+}$;
- 10 month $Hdh^{Q150/Q150}$ compared with $Hdh^{Q+/+}$;
- 18 month $Hdh^{Q92/Q92}$ compared with $Hdh^{Q+/+}$.

The lack of difference in the expression of CaN-A is shown in $Hdh^{Q150/Q150}$ and $Hdh^{Q92/Q92}$ caudate-putamen compared with $Hdh^{Q+/+}$ caudate-putamen. The number of samples in the wild type and homozygote sample groups are indicated inside the bars. Error bars indicate standard error of the mean. For details on antibodies and western blot procedures see section 5.3 and Table 5.2. Representative images are shown in Figure 5.4.B.

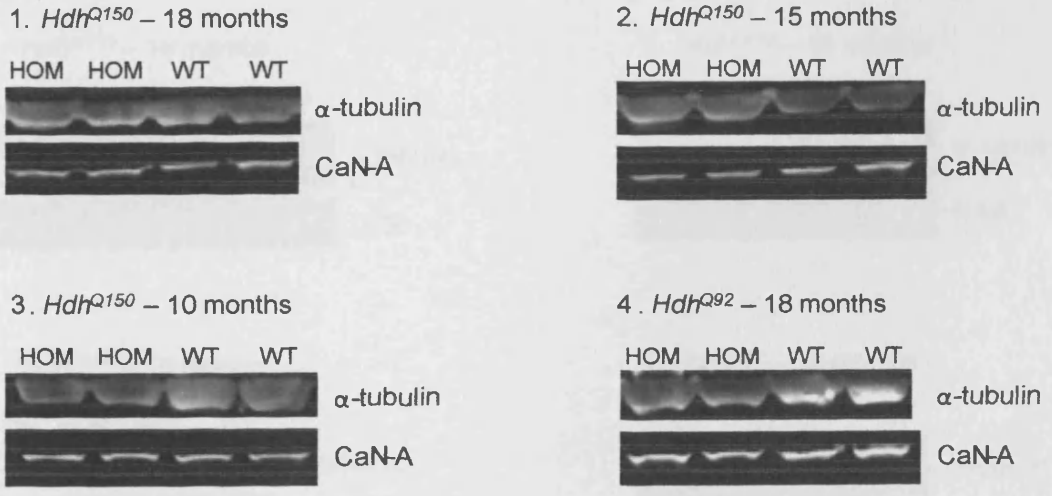

B. Representative greyscale images of western blot analysis presented in Figure 5.4.A: (1) 18 month Hdh^{Q150}; (2) 15 month Hdh^{Q150}; (3) 10 month Hdh^{Q150}; (4) 18 month Hdh^{Q92}. (HOM = homozygote; WT = wild type)

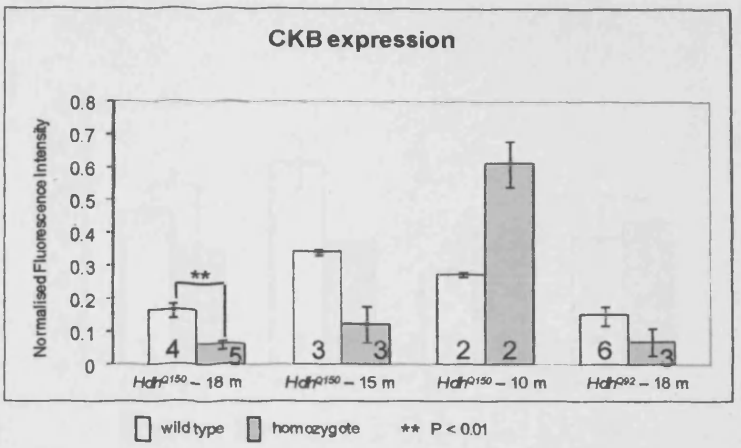

Figure 5.5 Differential expression of CKB in mouse caudate-putamen.
A. Bar chart showing the results of western blot analysis of caudate-putamen of

- 18 month $Hdh^{Q150/Q150}$ compared with $Hdh^{Q+/+}$;
- 15 month $Hdh^{Q150/Q150}$ compared with $Hdh^{Q+/+}$;
- 10 month $Hdh^{Q150/Q150}$ compared with $Hdh^{Q+/+}$;
- 18 month $Hdh^{Q92/Q92}$ compared with $Hdh^{Q+/+}$.

A significant difference in CKB expression is shown in 18 month $Hdh^{Q150/Q150}$ caudate-putamen, a difference in 15 and 10 month $Hdh^{Q150/Q150}$ caudate-putamen, and the lack of difference in $Hdh^{Q92/Q92}$ caudate-putamen compared with $Hdh^{Q+/+}$ caudate-putamen. The number of samples in the wild type and homozygote sample groups are indicated inside the bars. Error bars indicate standard error of the mean. For details on antibodies and western blot procedures see section 5.3 and Table 5.2. Representative images are shown in Figure 5.5.B.

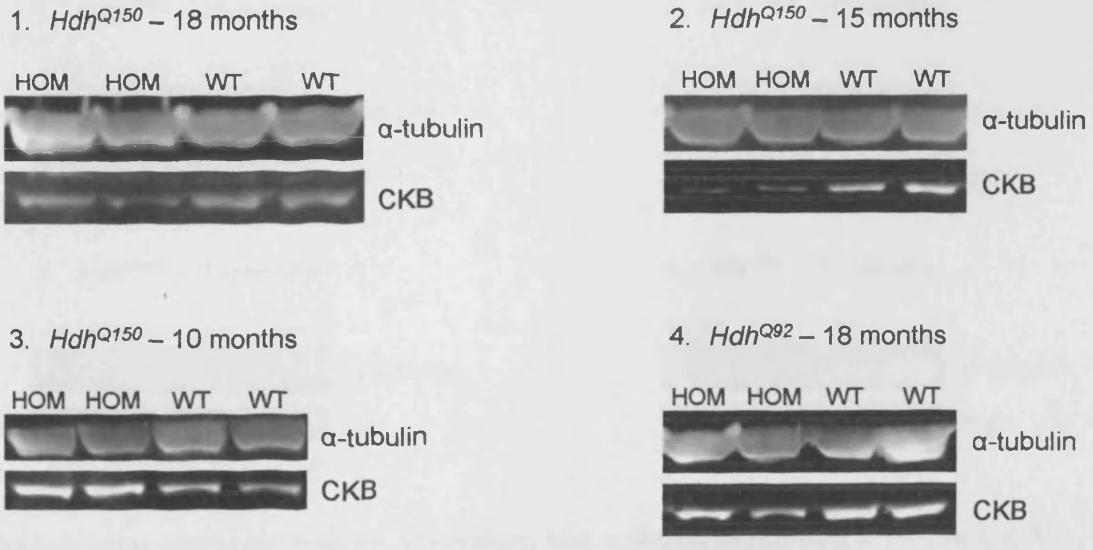

B. Representative greyscale images of western blot analysis presented in Figure 5.5.A: (1) 18 month Hdh^{Q150}; (2) 15 month Hdh^{Q150}; (3) 10 month Hdh^{Q150}; (4) 18 month Hdh^{Q92}. (HOM = homozygote; WT = wild type)

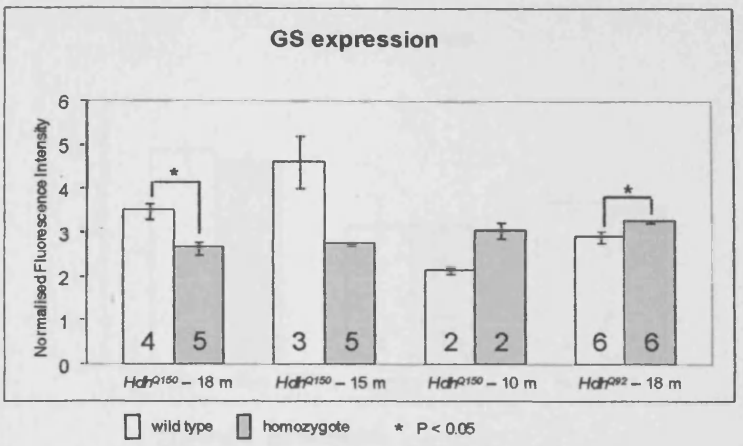

Figure 5.6 Differential expression of GS in mouse caudate-putamen.
A. Bar chart showing the results of western blot analysis of caudate-putamen of

- 18 month $Hdh^{Q150/Q150}$ compared with $Hdh^{Q+/+}$;
- 15 month $Hdh^{Q150/Q150}$ compared with $Hdh^{Q+/+}$;
- 10 month $Hdh^{Q150/Q150}$ compared with $Hdh^{Q+/+}$;
- 18 month $Hdh^{Q92/Q92}$ compared with $Hdh^{Q+/+}$.

A significant difference in GS expression is shown in 18 month $Hdh^{Q150/Q150}$ caudate-putamen and 18 month $Hdh^{Q92/Q92}$ caudate-putamen and a difference in 15 and 10 month $Hdh^{Q150/Q150}$ caudate-putamen compared with $Hdh^{Q+/+}$ caudate-putamen. The number of samples in the wild type and homozygote sample groups are indicated inside the bars. Error bars indicate standard error of the mean. For details on antibodies and western blot procedures see section 5.3 and Table 5.2. Representative images are shown in Figure 5.6.B.

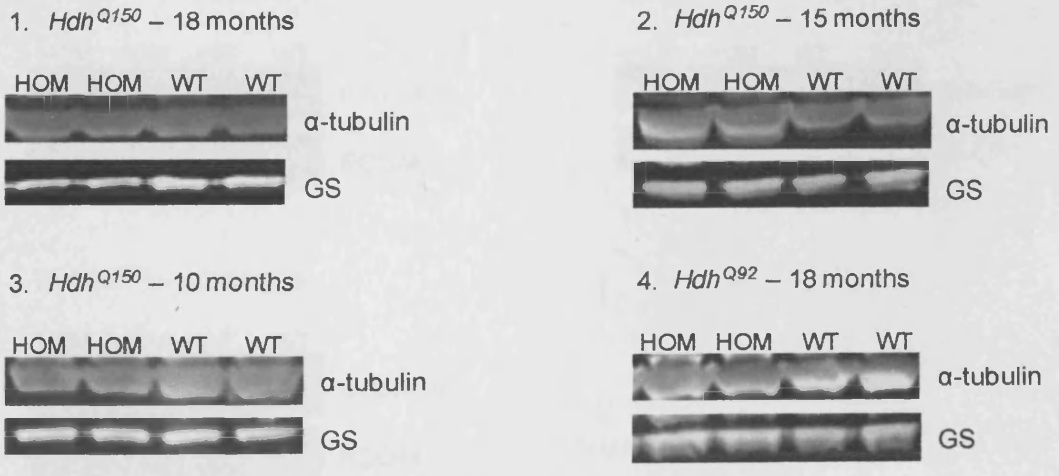

B. Representative greyscale images of western blot analysis presented in Figure 5.6.A: (1) 18 month Hdh^{Q150}; (2) 15 month Hdh^{Q150}; (3) 10 month Hdh^{Q150}; (4) 18 month Hdh^{Q92}. (HOM = homozygote; WT = wild type)

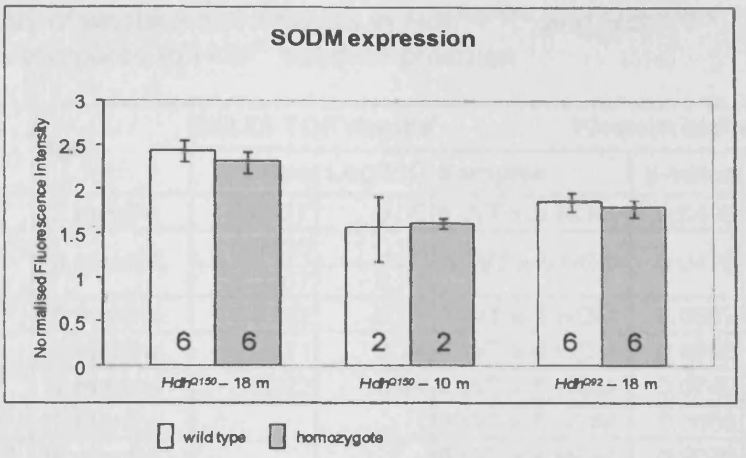

Figure 5.7 Differential expression of SODM in mouse caudate-putamen.
A. Representative greyscale images of western blot analysis of

- 18 month $Hdh^{Q150/Q150}$ compared with $Hdh^{Q+/+}$;
- 10 month $Hdh^{Q150/Q150}$ compared with $Hdh^{Q+/+}$;
- 18 month $Hdh^{Q92/Q92}$ compared with $Hdh^{Q+/+}$.

The lack of difference in the expression of SODM is shown in $Hdh^{Q150/Q150}$ and $Hdh^{Q92/Q92}$ caudate-putamen compared with $Hdh^{Q+/+}$ caudate-putamen. The number of samples in the wild type and homozygote sample groups are indicated inside the bars. Error bars indicate standard error of the mean. For details on antibodies and western blot procedures see section 5.3 and Table 5.2. Representative images are shown in Figure 5.7.B.

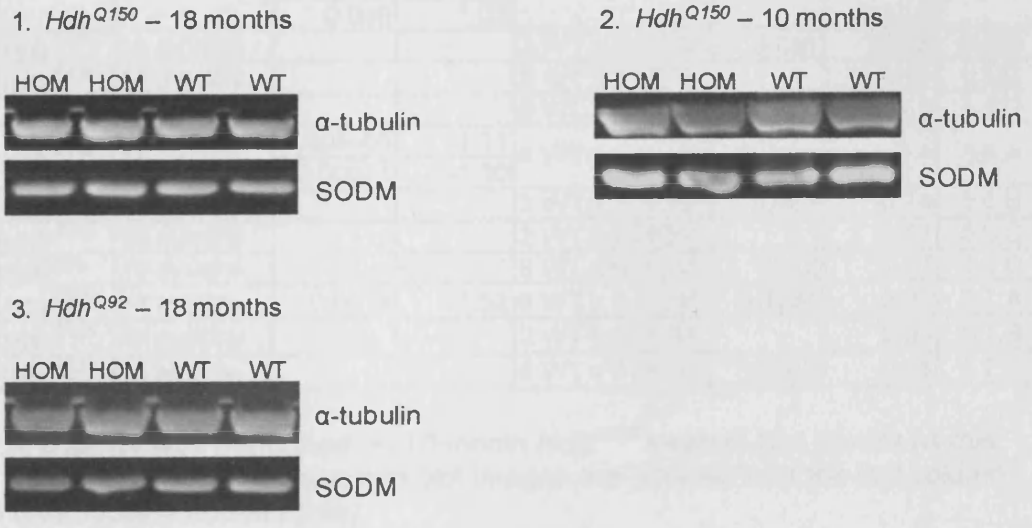

B. Representative greyscale images of western blot analysis presented in Figure 5.7.A: (1) 18 month Hdh^{Q150}; (2) 10 month Hdh^{Q150}; (3) 18 month Hdh^{Q92}. (HOM = homozygote; WT = wild type)

Table 5.3 Summary of western blot analysis in *Hdh*$^{Q92/Q92}$ and *Hdh*$^{Q150/Q150}$ mouse caudate-putamen compared to *Hdh*$^{+/+}$ caudate-putamen.

Protein	Mouse model	Age	SELDI-TOF results		Western blot results			
			p-value	Log2FC	Samples	p-value	Log2FC	Figure
COX-VIb	*Hdh*^{Q92}	12 months	0.0727	-0.30	5 WT x 5 HOM	0.0498	-0.28	5.1.A
	Hdh^{Q150}	18 months	0.0620	0.32	5 WT x 5 HOM	0.0475	1.22	5.1.B
			0.0757	0.21				
	Hdh^{Q150}	15 months	0.0722	-0.23	3 WT x 5 HOM	0.0569	0.29	5.1.C
MBP - 14 kDa	*Hdh*^{Q92}	18 months	0.0871	0.24	6 WT x 6 HOM	0.4908	-0.08	5.2.A
	Hdh^{Q92}	12 months	0.0022	0.49	5 WT x 5 HOM	0.0749	0.21	5.2.B
	Hdh^{Q92}	10 months			3 WT x 6 HOM	0.3836	0.16	5.2.C
	Hdh^{Q150}	18 months			6 WT x 6 HOM	0.2046	-0.21	5.2.D
HSP10	*Hdh*^{Q150}	18 months	0.0270	0.23	3 WT x 3 HOM	0.0948	1.35	5.3.A
	Hdh^{Q150}	15 months	0.0181	0.43	3 WT x 3 HOM	0.5618	-0.45	5.3.B
	Hdh^{Q150}	10 months			2 WT x 2 HOM		-1.14	5.3.C
	Hdh^{Q150}	3+4 months			6 WT x 5 HOM	0.6961	0.11	5.3.D
	Hdh^{Q92}	18 months			6 WT x 6 HOM	0.0065	-0.84	5.3.E
			DIGE results					
			p-value	Ratio				
CaN-B	*Hdh*^{Q150}	18 months	0.002	-1.26	4 WT x 5 HOM	0.1985	-0.22	5.4.A
			0.016	-1.23				
			0.021	-1.29				
	Hdh^{Q150}	15 months			3 WT x 5 HOM	0.0963	-0.64	5.4.B
	Hdh^{Q150}	10 months			2 WT x 2 HOM		0.17	5.4.C
	Hdh^{Q92}	18 months			6 WT x 6 HOM	0.2171	0.11	5.4.D
CKB	*Hdh*^{Q150}	18 months	0.0089	-1.21	4 WT x 5 HOM	0.0079	-1.42	5.5.A
			0.016	-1.22				
			0.046	-1.23				
	Hdh^{Q150}	15 months			3 WT x 3 HOM	0.051	-1.48	5.5.B
	Hdh^{Q150}	10 months			2 WT x 2 HOM		1.15	5.5.C
	Hdh^{Q92}	18 months			6 WT x 3 HOM	0.188	-1.1	5.5.D
GS	*Hdh*^{Q150}	18 months	3.40E-05	-1.31	4 WT x 5 HOM	0.0101	-0.4	5.6.A
			0.00074	-1.30				
	Hdh^{Q150}	15 months			3 WT x 5 HOM	0.084	-0.74	5.6.B
	Hdh^{Q150}	10 months			2 WT x 2 HOM		0.51	5.6.C
	Hdh^{Q92}	18 months			6 WT x 6 HOM	0.042	0.17	5.6.D
SODM	*Hdh*^{Q150}	18 months	0.0017	-1.52	6 WT x 6 HOM	0.4934	-0.08	5.7.A
	Hdh^{Q150}	10 months			2 WT x 2 HOM		0.05	5.7.B
	Hdh^{Q92}	18 months			6 WT x 6 HOM	0.6262	-0.06	5.7.C

No statistical analysis was performed on 10 month *Hdh*^{Q150} western blot results as this was a 2x2 analysis. The relevant western blot images are referred to in the last column. (WT = wild type; HOM = homozygote)

Table 5.4 Analysis of the differential expression of the 17.2 kDa, 18.5 kDa and 21.5 kDa isoforms of MBP in *Hdh*$^{Q92/Q92}$ and *Hdh*$^{Q150/Q150}$ mouse caudate-putamen compared to *Hdh*$^{+/+}$ caudate-putamen.

Model	Age	Samples	17.2 kDa		18.5 kDa		21.5 kDa	
			p-value	Log2FC	p-value	Log2FC	p-value	Log2FC
Hdh^{Q92}	18 months	6 WT x 6 HOM	0.5756	0.07	0.5022	-0.09	0.8263	-0.04
Hdh^{Q92}	12 months	5 WT x 5 HOM	0.3871	0.12	0.2904	0.15	0.4499	0.15
Hdh^{Q92}	10 months	3 WT x 6 HOM	0.3373	0.24	0.4840	0.12	0.7085	-0.08
Hdh^{Q150}	18 months	6 WT x 6 HOM	0.9789	0.00	0.4712	-0.15	0.3994	0.18

(WT = wild type; HOM = homozygote)

5.5 Discussion

Western blotting is a critical tool in protein detection and analysis. The technique makes it possible to identify a protein in a complex protein mixture and to provide information on the protein size. Enhanced chemiluminescence, the use of an enzyme-conjugated antibody to cleave a chemiluminescent substrate, is probably the dominant technique for detecting proteins in western blot format today (Patton 2000). However, as this approach detects single proteins only, comparative studies generally involve stripping and re-probing of blots, which can introduce a degree of technical variation; stripping can result in uneven protein loss across the membrane and incomplete stripping of antibodies can give rise to interfering bands when the blot is re-probed (Kaufmann *et al.* 1987). Other western blot methods have attempted to avoid these problems by multiplexing, using direct fluorescence in the visible light region, but the reliability of quantitation with these techniques has been questioned, as membranes have a degree of autofluorescence that can affect the signal. This drawback is largely avoided by using fluorophores in the longer wavelength region of the spectrum, where

membranes have a much lower autofluorescence (Sowell *et al.* 2002). The main advantage of near-infrared (NIR) fluorescence technology, however, is that the fluorescent signal provides a linear response to the amount of protein present over a much wider range than is the case with non-fluorescent methods (Picariello *et al.* 2006). The NIR detection system also simplifies the protocol as there is no longer need for the use of substrate or a dark room. In addition, the fluorescent blots are stable for months and can be re-scanned any number of times without a significant loss of signal. Despite all of this, western blot analysis is still a semi-quantitative methodology.

To minimize variation, all the samples that were compared in one experiment in this study were analysed on a single blot. Seven of the proteins identified as differentially expressed in $Hdh^{Q92/92}$ and $Hdh^{Q150/150}$ caudate-putamen compared with $Hdh^{Q+/+}$ caudate-putamen by SELDI-TOF or DIGE analysis were further examined by western blot analysis. The SELDI/DIGE results for three of these proteins (COX-VIb, CKB and GS) were confirmed by western blot analysis with $p < 0.05$. Two more proteins (14 kDa MBP and HSP10) showed a change in the same direction, but only with $p < 0.1$. Western blot results for two of the proteins (SODM and CaN-A) were not significant, although a comparable change was detected ($p < 0.1$) for CaN-A at an earlier timepoint in the same mouse model. The lack of confirmation by western blot analysis of some of the significant SELDI-TOF and DIGE results could be a technical artifact owing to the variation between 1D-gel and 2D-gel systems, the difference in sensitivity of the detection systems, inadequate specificity of the antibodies used in western blot analysis or the number of samples, which could have been too low to give sufficient power to detect any differences. Bearing in mind that all experiments were performed on

biological replicates, the variation between the individuals within the same sample groups could have an effect on the outcome as well. Although the western blot analysis was performed on the same brain region, age and mouse model used in the SELDI-TOF and DIGE experiments, the samples were not always obtained from the same individuals. Further investigation into the expression of these proteins in HD transgenic mouse brain with different antibodies and more samples might give a better insight. Subsequent analysis of brain sections by immunohistochemistry could provide more detailed information on the localisation of specific changes. All the proteins identified in this study by SELDI-TOF and DIGE were detected in caudate-putamen samples, and it would be most interesting to see whether these changes can also be seen in other brain regions.

Chapter 6. General discussion

The two complementary proteomic techniques used in this study, SELDI-TOF and DIGE, identified a total of 16 proteins that were differentially expressed in the caudate-putamen of *Hdh*^{Q92} and *Hdh*^{Q150} mouse models of Huntington's disease. As SELDI-TOF and DIGE select for proteins in different molecular weight ranges, the lack of overlap between the two sets of identifications was to be expected. Figure 6.1 gives a summary of the proteins with the molecular pathways they play a role in.

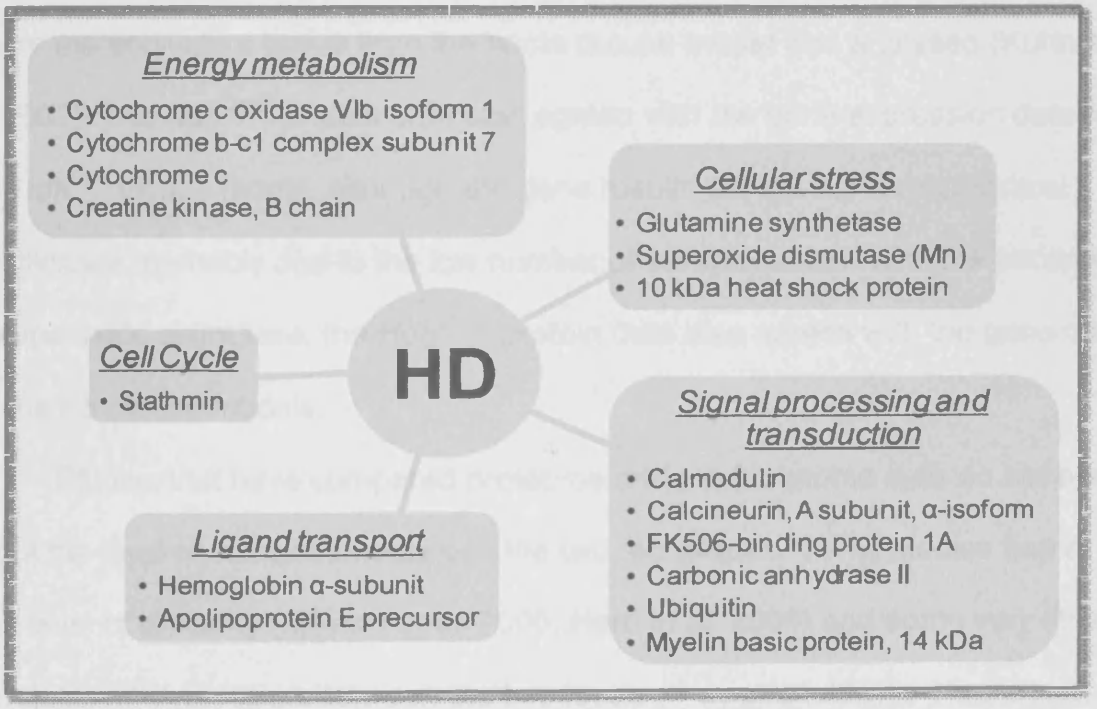

Figure 6.1 Proteins identified by SELDI-TOF or DIGE analysis to be differentially expressed in HD mouse brain, and the molecular pathways they are part of.

6.1 The correlation between proteome and global gene expression studies in HD

Of the 16 proteins found to be changed in HD mouse brain in this study, 13 were also significant in gene expression studies (Luthi-Carter *et al.* 2000; Morton *et al.* 2005; Hodges *et al.* 2006; Kuhn *et al.* 2007; Hodges *et al.* 2008). Table 6.1 gives a summary of the proteins identified in this study, which were also significant in gene expression studies of HD mouse brain and human HD brain. In general, the protein and the gene expression data are consistent. Both data sets show a higher number of proteins/genes decreased rather than increased in expression. Particularly significant is the agreement between the protein and the gene data for the 18 month Hdh^{Q150}, which provides the only direct comparison where the equivalent tissue from the same mouse model was analysed (Kuhn *et al.* 2007). The Hdh^{Q150} protein data also agrees with the gene expression data for the Hdh^{Q92} mouse model, although the gene results did not achieve statistical significance, probably due to the low number of samples used. With the exception of superoxide dismutase, the Hdh^{Q150} protein data also agrees with the gene data for the R6 mouse models.

Studies that have compared proteome and transcriptome data do not agree about the level of correlation between the two techniques. Some studies find a high level of similarity (Mijalski *et al.* 2005; Hartl *et al.* 2008) and some very little correlation in expression between the two levels (Frey *et al.* 2007). Hartl et al. (2008) examined the mouse brain transcriptome and proteome during embryonic development and found 60-70% concordance between the two techniques. As a large part of the control of embryonic development is known to be at the transcriptional level it may be that the concordance is less in adult mouse brain,

but the data reported here do show a level of concordance that is consistent with that reported by Hartl et al. (2008).

The fact that the human gene expression data are less consistent with the mouse model proteomic data than the gene expression in the mouse models can be attributed to several factors. Most fundamentally, the effects of the HD gene may be different in human and in mouse brain: an example of this is the alteration in the 14kDa isoform of MBP, which does not exist in humans, that is seen in mouse (section 6.2 and Boggs 2006). The human HD brain samples in Hodges et al. (2006) had shorter CAG repeats and much longer courses of disease than those seen in the animal models. The human brains were nearly all from clinically diagnosed HD cases and all will have had some level of neurodegeneration with cell loss. Most of these mouse models have no frank neurodegeneration at the times at which they were examined (sections 1.8.2 and 1.8.4). Finally, the fact that neurodegeneration is more advanced means that in the human brain, especially in the caudate, most of the effects on transcription are likely to be secondary, and some will be a result of retrograde or anterograde signalling from other degenerating brain areas. Nevertheless some of the proteomic changes seen in the mouse model striatum are also seen in human caudate.

Table 6.1 Summary of proteins changed in mouse HD brain, which were also changed in gene expression studies in mouse and human HD brain.

Proteins	Gene	Protein expression		Gene expression				
		Hdh ^{Q92}	*Hdh* ^{Q150}	*Hdh* ^{Q92} (1)	*Hdh* ^{Q150} (2)	R6/1 (3)	R6/2	Human HD caudate (4)
Cytochrome b-c1 complex	*Uqcrb*							
Cytochrome c	*Cycs*						(6)	
Creatine kinase, B chain	*Ckb*						(5), (6)	
Superoxide dismutase (Mn)	*Sod2*							
Glutamine synthetase	*Glul*							
10kDa heat shock protein	*Hspe1*						(6)	
Calmodulin	*Calm1,2,3*						(6)	
Calcineurin-A, α-isoform	*Ppp3ca*				β-isoform		B subunit (5)	
FK506-binding protein	*Fkbp1a*						(7)	
Carbonic anhydrase II	*Ca2*						(5), (6)	CA XI
Myelin basic protein	*Mbp*	14 kDa					(6)	
Apolipoprotein E precursor	*Apoe*						(5), (6)	cortex
Stathmin	*Stmn1*							

significant decrease
result not significant, but negative trend
significant increase
result not significant, but positive trend
increased/decreased in different samples/experiments
not detected or result not significant

(1) Kuhn *et al.*, 2007
(2) Luthi-Carter *et al.*, unpublished findings
(3) Hodges *et al.*, 2008
(4) Hodges *et al.*, 2006
(5) Luthi-Carter *et al.*, 2000
(6) Morton *et al.*, 2005
(7) increased (Luthi-Carter *et al.*, 2000); decreased (Morton *et al.*, 2005)

Where the results refer to a different subunit, isoform or brain region, it is indicated in the table.

6.2 The functional implications of the observed proteome changes

Some of the proteins identified in this study have been implicated in HD pathogenesis, and others are parts of molecular pathways previously recognised to play a role in the disorder. Five cellular pathways can be picked out from the data: cytochrome c oxidase, cytochrome b-c1, cytochrome c and creatine kinase B all contribute to cellular energy metabolism; glutamine synthetase, superoxide dismutase and the 10 kDa heat shock protein are associated with cellular stress; calmodulin, calcineurin-A, FK506-binding protein, carbonic anhydrase II, ubiquitin and myelin basic protein play a role in signal processing and transduction; haemoglobin and apolipoprotein E are ligand transporters, and stathmin plays a part in the cell cycle.

6.2.1 Proteins involved in energy metabolism changed in HD mouse brain

Mitochondrial dysfunction, energy deficiency and the generation of free radicals have been recognised as early events in HD pathology (section 1.7.2). Four of the proteins identified in this study are key players in the energy production pathway, and their dysregulation may cause some degree of disruption to this process.

Cytochrome c oxidase, cytochrome b-c1 and cytochrome c are members of the electron transport chain located in the inner mitochondrial membrane (Figure 6.2). The electron transport chain is the mechanism by which energy, in the form of adenosine triphosphate (ATP), is extracted from redox reactions by the transport of electrons through the chain. Significant changes have been found in

the activity of the electron transport chain complexes in human HD brain (section 1.7.2).

Cytochrome bc1 complex is the third complex in the electron transport chain. Mutations in complex III are known to cause exercise intolerance as well as multisystem disorders (Bouzidi *et al.* 1993). Subunit 7 of this complex was found to be decreased in the 18 month $Hdh^{Q92/Q92}$. Changes in complex III have been detected in HD earlier (section 1.7.2). It was also demonstrated that it is possible to curb metabolic energy insufficiency in HD by promoting complex III, through the administration of coenzyme Q10 supplements in HD patients (Koroshetz *et al.* 1997; Andrich *et al.* 2004), in rats (Kasparova *et al.* 2005) and in R6/2 mice (section 1.7.2 and Smith *et al.* 2006; Stack *et al.* 2006).

Cytochrome c oxidase (COX), or complex IV, is the last enzyme in the electron transport chain and has been identified as a marker of neuronal metabolic activity (Wong-Riley 1989). Subunit VIb of COX was decreased in 12 month $Hdh^{Q92/Q92}$ and in 15 month $Hdh^{Q150/Q150}$, but then increased in 18 month $Hdh^{Q150/Q150}$. Previous studies found COX activity significantly decreased in human HD caudate (Brennan *et al.* 1985; Browne *et al.* 1997; Gourfinkel-An *et al.* 2002), and in the striatum, cortex and muscle mitochondria of transgenic R6/2 mice (Tabrizi *et al.* 2000; Gizatullina *et al.* 2006). These reports are in agreement with our results in the younger animals, which show a decrease of COX VIb, which may correspond to a deficiency in energy metabolism. Although the increase in the 18 month $Hdh^{Q150/Q150}$ might seem inconsistent, a similar outcome was found in a QA rat model of HD (Maksimovic *et al.* 2001).

The reduction of subunits of complexes III and IV in the *Hdh*$^{Q92/Q92}$ and the 15 month *Hdh*$^{Q150/Q150}$ could be indicative of reduced levels of oxidative phosphorylation (OXPHOS) and metabolic energy deficiency. Transcriptional dysregulation has been suggested as the basis of mitochondrial dysfunction in HD, through the interference of mutant huntingtin with transcription factors involved with mitochondrial biogenesis and function, such as p53 (Bae *et al.* 2005 and section 1.7.2) and the transcriptional coactivator PGC-1α (Cui *et al.* 2006; Weydt *et al.* 2006 and section 1.7.2), or through direct interaction of mutant huntingtin with mitochondria (Panov *et al.* 2002; Choo *et al.* 2004; Orr *et al.* 2008 and section 1.7.2). It should be noted that the changes identified in complex III and IV relate to only one subunit of each of the complexes, and it is uncertain how critical an alteration in these would be for the complex as a whole. The increase in subunit VIb of complex IV in 18 month *Hdh*$^{Q150/Q150}$ could be the result of compensatory mechanisms at work trying to rescue a failing mitochondrial system.

Cytochrome c (cyt c) is not one of the four electron transport complexes, but a free floating small heme protein, associated with the mitochondrial membrane, that transfers electrons between complex III and complex IV of the chain. Cyt c was increased in 18 month *Hdh*$^{Q150/Q150}$. Cyt c was also found to be increased in *Hdh*^{Q111} mice, following the interaction of mutant huntingtin with the mitochondrial membrane (Choo *et al.* 2004 and section 1.7.2). The disintegration of the OXPHOS system may lead to increased levels of cyt c as a compensatory mechanism to keep OXPHOS running, which in turn could induce apoptosis through caspase activation (section 1.7.4). The increase in cyt c in the older *Hdh*$^{Q150/Q150}$ could be the result of advanced mitochondrial dysfunction. In support

of this, increased cyt c, in conjunction with elevated caspase 1 and caspase 3 activity, eventually leading to neuronal dysfunction and cell death, has been observed in both mouse and human brain (section 1.7.4).

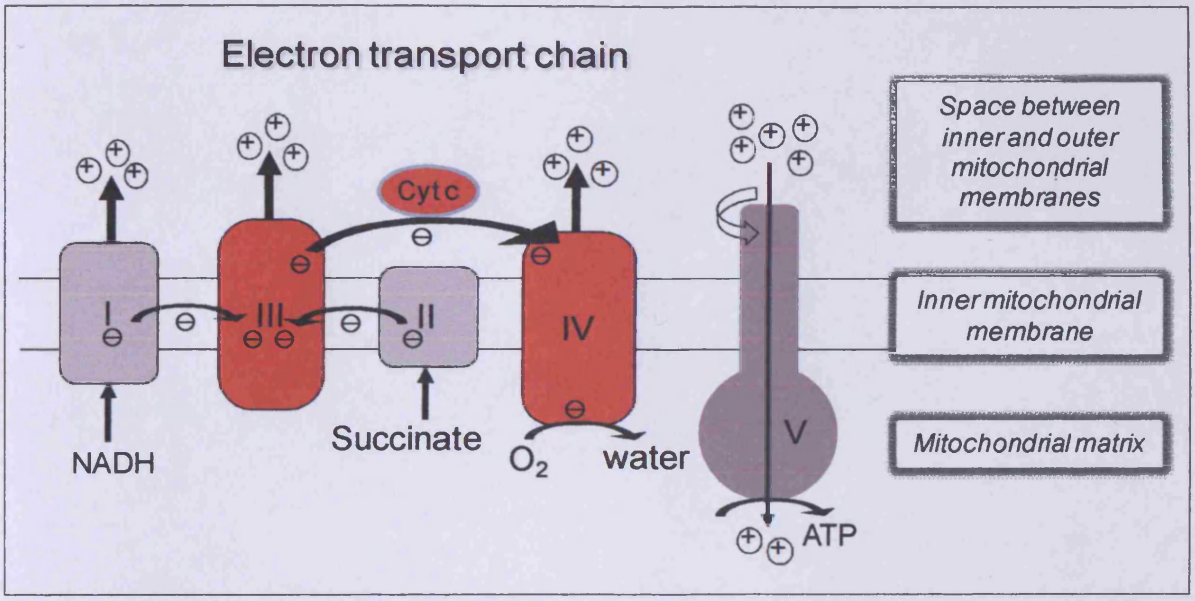

Figure 6.2 The electron transport chain. Schematic of the different complexes in the electron transport chain and the production of ATP. NADH carries protons (+) and electrons (-) to the electron transport chain located in the inner mitochondrial membrane. The transfer of electrons along the chain provides the energy to transport protons across the membrane, which generates an electrochemical gradient. The accumulating protons follow the electrochemical gradient back across the membrane through an ATP synthase complex, thus providing the energy to synthetase ATP. The components identified in this study are shown in red: III = the cytochrome b-c1 complex; IV = the cytochrome c oxidase complex; Cyt c = cytochrome c.

Creatine kinase (CK) is an enzyme which also plays a part in the energy housekeeping of the cell by catalysing the conversion of creatine and ATP to phosphocreatine and adenosine diphosphate (ADP). This reaction is reversible and phosphocreatine, in turn, serves as an energy reservoir for the regeneration of ATP, especially in tissues with rapid ATP consumption, such as skeletal muscle, smooth muscle and brain. The presence of this energy buffer system

keeps the ATP/ADP ratio high at subcellular locations where ATP is needed, and the breakdown of this system could bring about cellular dysfunction. CK consists of two subunits, a muscle (CKM) and a brain (CKB) type. The CKB form was found to be decreased in the 18 month $Hdh^{Q150/Q150}$. In HD, it was demonstrated that a decrease in the phosphocreatine ratio (Koroshetz *et al.* 1997; Lodi *et al.* 2000) and a reduction in creatine levels (Sanchez-Pernaute *et al.* 1999) can result in general energy deficiency. Phosphocreatine levels were decreased in human HD muscle, reducing the rate of mitochondrial ATP production in symptomatic HD patients, and only marginally less so in presymptomatic carriers. Reduced levels of creatine in HD patients, and to a lesser degree in presymptomatic carriers, correlated with motor and cognitive performance. Creatine supplements are widely used to enhance athletic performance and have also been shown to enhance brain performance (Rae *et al.* 2003). In R6/2 mice too, dietary creatine supplements were found to exert a neuroprotective effect by increasing phosphocreatine levels (Ferrante *et al.* 2000).

6.2.2 Proteins involved in cellular stress changed in HD mouse brain

Excitotoxicity and oxidative stress have been strongly implicated as mechanisms leading to cell death in HD (section 1.7.1 and 1.7.3). Excitotoxicity is initiated by pathologically high levels of neurotransmitters, such as glutamate, in the brain. A possible contributor to this process is glutamine synthetase (GS). GS is an enzyme that is essential in the metabolism of nitrogen by catalysing the condensation of glutamate and ammonia to form glutamine. A consequence of this process is that GS has an impact on the level of glutamate in the cell and a reduction of GS can allow glutamate to accumulate to potentially toxic levels. GS

was decreased in three samples of 18 month $Hdh^{Q150/Q150}$. GS activity was also reduced in post-mortem brain from patients with HD and it has been suggested that a reduction in its activity may well contribute to HD neuronal pathology (Carter 1982; Butterworth 1986). In transgenic R6/1 and R6/2 mice, mRNA levels of GS were decreased, prior to any evidence of neurodegeneration (Lievens *et al.* 2001; Behrens *et al.* 2002).

A protein involved in restricting oxidative stress in the cell is mitochondrial superoxide dismutase (SODM). SODM, or SOD2, serves a key antioxidant role by binding to the superoxide by-products of the electron transport chain and converting them to oxygen and hydrogen peroxide. SODM is one of the three forms of superoxide dismutase in humans, each with a different cellular location. Mice lacking SODM die shortly after birth, displaying massive oxidative stress, which illustrates its vital function (Li *et al.* 1995). SOD has been investigated extensively in HD, not always with consistent results. SOD1 and SOD2 were found to be expressed at only low levels in MSN, which could explain their selective vulnerability in HD to some extent (Medina *et al.* 1996). Striatal SOD1, but not SOD2, was found to be increased in young and decreased in older transgenic R6/1 mice. It is possible that this is the result of an early compensatory mechanism at work to protect cells from free radical-induced damage, followed by a failure of the system in the older animals. In a 3-NP rat model of HD, both SOD1 and SOD2 were reduced (Santamaria *et al.* 2001). In HD patients, neither form of SOD showed a significant difference in enzymatic activity in skin fibroblast cultures (del Hoyo *et al.* 2006), but SOD2 activity was reduced in peripheral blood (Chen *et al.* 2007). Overexpression of SOD1 reversed the HD phenotype in cells expressing mutant huntingtin (Goswami *et al.* 2006). In this study, SODM was

found decreased in 18 month *Hdh*$^{Q150/Q150}$. Although there is little conclusive evidence from previous studies with respect to the role of SODM in HD, the analogy with its family member SOD1 suggests that a decreased SODM in HD brain may add to oxidative damage and accelerate neuronal death.

Another group of proteins involved in cell stress and stress responses are heat shock proteins (HSPs), or molecular chaperones. When cells are exposed to elevated temperatures or other forms of cellular stress, the expression of HSPs is increased. HSPs help to establish proper protein conformation, to stabilise partially unfolded proteins and to break down old or malfunctioning proteins. In our study, the 10 kDa heat shock protein (HSP10) was increased in 15 and 18 month old *Hdh*$^{Q150/Q150}$. HSP10 is the human homologue of the bacterial GroES and works in conjunction with the 60 kDa heat shock protein, homologue of the bacterial GroEL, which is required for the correct folding of many proteins. To function, the two HSPs need to work as a protein complex (Monzini *et al.* 1994; Hartl 1996). HSPs have been associated with insoluble polyglutamine protein aggregates, possibly in an attempt to remove them (Chai *et al.* 1999). This was also recognised in HD, where HSPs co-localised with perinuclear inclusions (Waelter *et al.* 2001). In addition, treating mammalian cells with geldanamycin induced the expression of several HSPs, whilst inhibiting HD exon 1 protein aggregation in a dose-dependent manner (Sittler *et al.* 2001). Subsequently, several studies recognised HSPs as aggregate-interacting proteins which suppress mutant huntingtin aggregation and neuronal cell death (Mitsui *et al.* 2002; Fujimoto *et al.* 2005; Cornett *et al.* 2006; Goswami *et al.* 2006; Kitamura *et al.* 2006). Others, however, could not detect this beneficial effect in R6/2 mice (Hansson *et al.* 2003; Zourlidou *et al.* 2007). Several proteins involved in the heat-

shock response pathway were shown to be upregulated in cells expressing mutant huntingtin, one of which was GroEL (Fan *et al.* 2008). On the other hand HSP70 expression was reduced in transgenic R6/1 and R6/2 brain, and it has been suggested that this was caused by the sequestration of the transcription factor for HSP70 by mutant huntingtin (Yamanaka *et al.* 2008). Hay *et al.* (2004) also reported a progressive decrease in protein levels of HSPs in transgenic R6/2, but subsequent quantification of mRNA levels showed no changes, so it was suggested that the decrease in protein levels could be a consequence of the sequestration of HSPs in aggregates (Hay *et al.* 2004). However, repeated experiments confirmed the decreased HSP levels in the transgenic R6/2 and showed comparable reductions of HSPs in $Hdh^{Q150/Q150}$ (Woodman *et al.* 2007). Only a few studies discuss HSP10/groEL in particular, although they too indicate that HSP10/groEL reduces aggregate formation and cell death in mammalian cell models of HD, and that HSP10/groEL requires HSP60/groES to function efficiently (Carmichael *et al.* 2000; Carmichael *et al.* 2002). In the present study, the increased level of HSP10 in $Hdh^{Q150/Q150}$ caudate-putamen may indicate an upregulation initiated by the cellular stress in the striatum.

6.2.3 Proteins involved in cell signalling changed in HD mouse brain

A number of proteins involved in calcium signalling were altered in HD mouse brain. Aberrant neuronal Ca^{2+} signalling has been connected with HD pathology, both in human patients and in HD mice, and is thought to occur early on in the disease process (Hodgson *et al.* 1999; Panov *et al.* 2002). Because of this, it has been suggested that Ca^{2+} dysregulation may be an initiating event in the pathogenesis of HD, and that high levels of Ca^{2+} could start the cascade of

events involving caspase activation (Zeron et al. 2002) and the catalysis of huntingtin proteolysis with the generation of toxic huntingtin fragments (section 1.7.4).

Calmodulin (CaM) was found to be decreased in 10 and 18 month $Hdh^{Q92/Q92}$, but increased in 18 month $Hdh^{Q150/Q150}$. CaM is a calcium-binding protein, which in turn binds a number of different proteins, many of them unable to bind calcium themselves. In this way, CaM mediates various processes, such as inflammation, metabolism, apoptosis, memory, and the immune response. CaM was found to interact with huntingtin, and this reaction appeared to be stronger with mutant than with wild type huntingtin in human HD brain (Bao *et al.* 1996). Further data suggested that CaM regulates the stabilisation of monomeric and aggregated huntingtin through transglutaminase 2. Longer mutant huntingtin proteins may be a trigger for transglutaminase cross-linking (section 1.6.4) and as such the calmodulin-huntingtin-transglutaminase complex could play a role in the formation of insoluble aggregates. This was corroborated by the finding that disrupting the CaM-huntingtin interaction decreases cytotoxicity in HD (Zainelli *et al.* 2004; Dudek *et al.* 2008).

Another protein involved in calcium messaging is the serine/threonine protein phosphatase 2B, generally known as calcineurin (CaN). CaN plays an essential role in T cell activation and the immune response, and is involved in the transduction of calcium signals. It is dependent on calmodulin for its activation. CaN is a heterodimer of CaN-A, the catalytic calmodulin-binding subunit, and CaN-B, the regulatory calcium binding subunit (Klee *et al.* 1998). In this study, the catalytic subunit was decreased in 18 month $Hdh^{Q150/Q150}$. CaN has already been

put forward as a player in the HD disease process, although some of the data reported are somewhat contradictory. In human post-mortem brain, CaN was detected only in neuronal cells and was highly concentrated in the striato-pallidal and striato-nigral pathways. This pattern of distribution was similar to the one found in rat brain (Goto *et al.* 1986). Some studies proposed a harmful effect of the downregulation of CaN. A decreased expression of CaN-B was found in R6/2 mice, and it was suggested that a deficiency in CaN might contribute to the defective neurotransmission process in HD (Lievens *et al.* 2002). Suppression of CaN also dramatically accelerated the neurological phenotype in R6/2 mice, putting forward the idea that CaN may play a protective role in HD (Hernandez-Espinosa & Morton 2006). In conflict with these reports are two studies proposing that CaN is detrimental for striatal neurons. The findings of one suggested that inhibition of CaN prevents mutant huntingtin mediated cell death of striatal neurons in HD (Pardo *et al.* 2006), while the other proposed that high levels of CaN-A could account for the increased vulnerability of striatal cells expressing mutant huntingtin to excitotoxicity (Xifro *et al.* 2008). Nevertheless, gene expression studies support the hypothesis that the lack of CaN contributes to the disease process in HD (Table 6.2) The current study also found a decrease of the α-isoform of CaN-A in 18 month $Hdh^{Q150/Q150}$.

FK506-binding protein 1A (FKBP-1A), also called immunophilin (FKBP12), is associated with the calcium release channel, which provides the pathway for calcium efflux required for the excitation-contraction coupling in skeletal muscle. It is also the binding protein for the immunosuppressant drug FK506, and this FKBP-1A/FK506 complex interacts with and inhibits calcineurin, and in this way inhibits T cell activation (Liu *et al.* 1991; Jayaraman *et al.* 1992). FKBP-1A was

decreased in 12 month *Hdh*$^{Q92/Q92}$. In the HD-74Q cell line, FKBP-1A was initially significantly reduced, but levels subsequently increased (Kita *et al.* 2002).

Research into the immunosuppressive drug FK506 demonstrated neuroprotective and neuroregenerative effects of the drug in animal models recapitulating a wide range of neurodegenerative diseases and conditions following brain injury (Gold 1997; Christner *et al.* 2001; Hamilton *et al.* 2002; Brecht *et al.* 2003). Initially, CaN inhibition was thought to lead not only to immunosuppression, but it was also the proposed basis for this FK506-mediated neuroprotection (Dawson *et al.* 1993). However, FK506-like inhibitors which had no influence on CaN activity kept their neuroprotective and neuroregenerative properties (Steiner *et al.* 1997). Although the neuroprotective effects of FKBP inhibitors imply an involvement of FKBP-1A in neuronal cell death, there is evidence that its inhibition does not affect neuronal protection and regeneration, as FK506 retained these properties in cell cultures from FKBP12 knock-out mice (Gold *et al.* 1999; Guo *et al.* 2001). It is evident that the full function of FKBP-1A and its involvement in neurodegenerative disease is still very uncertain and that, although a dysregulation of the protein may certainly have some harmful effect, the way in which the damage would be inflicted remains unclear.

The most substantial change detected in this study was a 75% decrease of carbonic anhydrase II (CA2) in 18 month *Hdh*$^{Q150/Q150}$. Carbonic anhydrases catalyse the conversion of carbon dioxide to bicarbonate and protons, to maintain the acid-base balance in blood and other tissues, and to help transport carbon dioxide out of the tissues. In the brain, CA2 was found in oligodendrocytes and GABAergic neurons (Kida *et al.* 2006). CA2 is thought to play a crucial role in signal transduction, long-term synaptic transformation and memory storage, and

CA dysfunction is associated with impaired cognition, mental retardation, Alzheimer's disease and ageing (Sun & Alkon 2002). There were conflicting reports on the level of CA2 in Alzheimer's disease brain. While some studies showed a significant reduction (Meier-Ruge *et al.* 1984; Sultana *et al.* 2006), some found no change (Vlkolinsky *et al.* 2001) and others reported the protein levels to be significantly increased (Sultana *et al.* 2007). In Pick's disease, CA was decreased (Meier-Ruge *et al.* 1984) and ageing was also associated with a significant decline of CA (Meier-Ruge *et al.* 1980). A decrease in CA certainly features in various forms of neurodegeneration and perhaps it contributes to the cognitive decline seen in HD patients.

Ubiquitin attaches to other proteins to label them for proteasomal degradation, a process called ubiquitination. As a consequence, ubiquitination has some control over the stability, function, and intracellular localisation of a wide variety of proteins. Ubiquitination also regulates DNA repair and endocytosis. Because of this, the ubiquitin proteasome pathway has been linked to diseases involving various types of cellular activity, and it has been suggested that the UPS is impaired in HD and contributes to HD pathology, although this is highly controversial (section 1.7.6). In the present study, ubiquitin was decreased in 15 month $Hdh^{Q150/Q150}$.

The last protein involved in signal processing and transduction, which has been identified in this study, is myelin basic protein (MBP). MBP is the second most abundant protein in myelin in the central nervous system, and it is essential in the myelination of nerves. In addition, it may be involved in cell signalling by regulating intracellular Ca^{2+} levels and by binding various proteins, one of which is

calmodulin. There are several splice variants of MBP, as well as a large number of post-translational modifications. Differential splicing generates a 21.5, 20.2, 18.5, 17.24, 17.22, and 14 kDa MBP in mouse, and a 21.5, 20.2, 18.5, and 17.2 kDa MBP in humans. The main isoform in the adult human central nervous system is 18.5 kDa MBP, whereas in adult mice it is 14 kDa MBP (Boggs 2006). MBP-knockout mice show decreased levels of myelination and experience tremors, seizures, and early death (Popko *et al.* 1987). MBP has been investigated for its role in demyelinating diseases, particularly multiple sclerosis (Musse & Harauz 2007).

In HD, an MRI study found loss of cerebral white matter in HD patients (Fennema-Notestine *et al.* 2004), while another study hypothesised that myelin breaks down early on in HD, followed by an attempt to remyelinate affected areas (Bartzokis *et al.* 2007). The 14 kDa MBP isoform was found to be increased in the 12 and 18 month $Hdh^{Q92/Q92}$. In the light of the Bartzokis study, this could agree with the remyelination theory. However, it is important to bear in mind that the alteration in the level of MBP in the $Hdh^{Q92/Q92}$ involves only the 14 kDa isoform, and that the other isoforms appeared to be unchanged. Although the 14 kDa MBP is the main isoform in mice, it is absent in humans, and as such this finding might well be mouse specific and not relevant to the human disease.

6.2.4 Proteins involved in ligand transport changed in HD mouse brain

The first ligand transporter changed in HD mouse caudate-putamen in this study is the α-subunit of haemoglobin (Hb). Hb is the iron-containing oxygen-transport metalloprotein in red blood cells, which carries oxygen from the lungs to

the rest of the body. In adults, Hb consists of two α and two β subunits. In Alzheimer's disease, reports on the contribution of Hb to the pathology differed, with some showing elevated and others lower levels of Hb in patients (Slemmon *et al.* 1994; Pandav *et al.* 2004).

In HD, knock-down of huntingtin expression in zebrafish gave rise to hypochromic blood due to decreased Hb production. Based on this, it was suggested that polyglutamine expansion disrupts the normal role of huntingtin in the iron pathway, and in this way contributes to HD pathology (Lumsden *et al.* 2007). In the present study, the α-subunit of Hb was decreased in 10 month $Hdh^{Q92/Q92}$ caudate-putamen, but increased in the 18 month $Hdh^{Q92/Q92}$ caudate-putamen. It is possible, however, that the increase observed in the older animals is the result of a relative increase of blood vessels in the sample, due to some degree of neuronal death in the striatum.

The apolipoprotein E (APOE) precursor was found to be decreased in the 18 month $Hdh^{Q150/Q150}$ in this study. APOE is an apoprotein found in the chylomicron, which transports exogenous lipids, fat-soluble vitamins and cholesterol from the intestines to other parts of the body. It is synthesised principally in the liver, but has also been found in other tissues, including the brain. It is essential for the normal catabolism of triglyceride-rich lipoproteins. APOE was initially recognised for its importance in lipoprotein metabolism and cardiovascular disease, but recently it has been studied for its role in Alzheimer's disease (AD), immunoregulation and cognition. The *APOE-ε4* isoform is the only confirmed risk factor for AD, but there is no conclusive theory to explain the mechanism by which *APOE-ε4* increases the susceptibility to this disease (Cedazo-Minguez 2007). In addition, *APOE-ε4* has been implicated in other

neurological disorders, including multiple sclerosis (Masterman & Hillert 2004) and Parkinson's disease (Martinez *et al.* 2005).

In parallel with these findings, several studies have looked into a possible effect of *APOE-ε4* on the age of onset in HD, with conflicting conclusions. *APOE-ε4* seemed to be a significant factor influencing the age of onset of HD in one study, but with the ε4 allele raising the age of onset rather than lowering it (Panas *et al.* 1999). In another, the *APOE-ε2/ε3* genotype was associated with significantly earlier age of onset in males than in females (Kehoe *et al.* 1999). However, further investigation failed to detect an association between the *APOE* genotypes and the age of onset in HD (Harrington *et al.* 1994; Rubinsztein *et al.* 1997; Kalman *et al.* 2000; Saft *et al.* 2004; Panegyres *et al.* 2006; Andresen *et al.* 2007).

6.2.5 A protein involved in the cell cycle changed in HD mouse brain

The last protein identified in this study is stathmin (STMN), which was increased in 18 month $Hdh^{Q150/150}$. STMN, also known as oncoprotein 18, plays a critical role in the regulation of the microtubule cytoskeleton (Rubin & Atweh 2004). When STMN is mutated or when it is not functioning properly, it can cause uncontrolled cell proliferation, characteristic of cancer cells (Cassimeris 2002). Disruption of the cytoskeleton and abnormal aggregation of cytoskeletal proteins often accompany neurodegenerative diseases (Richter-Landsberg 2008), and it has been suggested that the phosphorylation of STMN in the brain may be involved in neuropsychiatric and neurodegenerative disorders (Hayashi *et al.* 2006). It is not however clear just how STMN causes this harmful effect.

6.3 Comparison of the different mouse models

The SELDI-TOF study, reported in Chapter 3, showed that many of the protein changes were detected in more than one mouse model, the majority of which were found in the two knock-in models, *Hdh*^{Q92} and *Hdh*^{Q150}. However, Table 3.9 shows that about three quarters of these changes display a fold change in the opposite direction in the two models. Although it is possible that some of these apparent discrepancies are due to technical artifacts, subsequent western blot analysis, reported in Chapter 5, did overall not contradict the original SELDI results. This suggests that the differences between the *Hdh*^{Q92} and *Hdh*^{Q150} may well be genuine, which could indicate that the disease progresses at a different rate in the two models and that animals of the same age of both models could nevertheless be in another phase of the disease. As such, the difference in the direction of the changes could be the outcome of compensatory mechanisms at work at different stages of the disease process. Previous behavioural and neuropathological research into these mouse models has already indicated that the disease characteristics in the *Hdh*^{Q150}, and particularly in the *Hdh*$^{Q150/Q150}$, are more severe and present at a younger age than in the *Hdh*^{Q92}, which could correlate with our findings. The divergence between these two models could be attributable to the difference in length of the CAG repeat.

It would certainly be interesting to confirm these findings. Additional western blot analysis may provide some of the missing results for the proteins already assayed and it would be interesting to obtain and assay more samples of earlier timepoints for both models as well as assay some of the proteins identified from the SELDI-TOF analysis which have not yet been screened by immunoblot.

Analysis by immunohistochemistry of brain sections of both mouse models at different ages could provide further evidence of differences between the models as well as provide more detailed information on the localisation of specific changes.

Comparing the *Hdh*^{Q92} and *Hdh*^{Q150} mouse models should certainly go beyond the scope of the present study. One way to identify differences and similarities in these mice could be done by studying the phosphorylation state of huntingtin isolated from the brains of both *Hdh*$^{Q92/Q92}$ and *Hdh*$^{Q150/Q150}$ mice at different ages. Changes in the phosphorylation of huntingtin have been demonstrated to be relevant to the conformation and pathogenicity of the protein (Humbert *et al.* 2002; Pardo *et al.* 2006).

6.4 Conclusion

The majority of the proteins identified as differentially expressed in the brain of HD genetic mouse models in this study contribute to one of the pathological mechanisms recognised in HD, such as excitotoxicity, mitochondrial dysfunction, impaired cellular signalling, oxidative stress, impaired UPS and cell death. However, it is likely that the majority of the changes detected are secondary effects of an ongoing disease process, although in turn they may initiate the development of further disease characteristics.

By and large, the outcome of the SELDI-TOF and DIGE analysis suggests that the dysregulation at mRNA level correlates well with alterations at the protein level. However, analysis of the proteome, in addition to quantifying the levels of protein, can also reveal other more qualitative aspects of proteins. The post-translational alterations of proteins are important as they nearly always influence the actual function of proteins, which are the final effectors of events in cells and organisms. In this study, post-translational modifications were observed for three of the proteins detected by DIGE analysis. However, all the putative post-translationally modified versions of the same protein show very similar changes in expression. All of this suggests that it may be acceptable to concentrate on gene expression studies as a broad-based approach for the study of expression differences in disease, at any rate until more sophisticated proteomic techniques are available. Proteomics, as it stands, may be more suitable for conducting hypothesis-driven follow-up studies from gene expression results.

References

Adam B-L, Qu Y, Davis JW, Ward MD, Clements MA, Cazares LH, Semmes OJ, Schellhammer PF, Yasui Y, Feng Z and Wright GL, Jr. (2002). Serum protein fingerprinting coupled with a pattern-matching algorithm distinguishes prostate cancer from benign prostate hyperplasia and healthy men.[see comment]. *Cancer Res.* 62, 3609-3614.

Alban A, David SO, Bjorkesten L, Andersson C, Sloge E, Lewis S and Currie I (2003). A novel experimental design for comparative two-dimensional gel analysis: two-dimensional difference gel electrophoresis incorporating a pooled internal standard. *Proteomics.* 3, 36-44.

Almqvist EW, Elterman DS, MacLeod PM and Hayden MR (2001). High incidence rate and absent family histories in one quarter of patients newly diagnosed with Huntington disease in British Columbia. *Clin Genet.* 60, 198-205.

Ambrose CM, Duyao MP, Barnes G, Bates GP, Lin CS, Srinidhi J, Baxendale S, Hummerich H, Lehrach H and Altherr M (1994). Structure and expression of the Huntington's disease gene: evidence against simple inactivation due to an expanded CAG repeat. *Somatic Cell and Molecular Genetics.* 20, 27-38.

Anderson AN, Roncaroli F, Hodges A, Deprez M and Turkheimer FE (2008). Chromosomal profiles of gene expression in Huntington's disease. *Brain.* 131, 381-388.

Andrade MA and Bork P (1995). HEAT repeats in the Huntington's disease protein. *Nature Genet.* 11, 115-116.

Andresen JM, Gayan J, Cherny SS, Brocklebank D, Alkorta-Aranburu G, Addis EA, Group US-VCR, Cardon LR, Housman DE and Wexler NS (2007). Replication of twelve association studies for Huntington's disease residual age of onset in large Venezuelan kindreds. *J Medical Genetics.* 44, 44-50.

Andrew SE, Goldberg YP, Kremer B, Telenius H, Theilmann J, Adam S, Starr E, Squitieri F, Lin B, Kalchman MA, Graham RK and Hayden MR (1993). The relationship between trinucleotide (CAG) repeat length and clinical features of Huntington's disease. *Nature Genet.* 4, 398-403.

Andrich J, Saft C, Gerlach M, Schneider B, Arz A, Kuhn W and Muller T (2004). Coenzyme Q10 serum levels in Huntington's disease. *J Neural Transm* Suppl. Supplementum., 111-116.

Apraiz I, Mi J and Cristobal S (2006). Identification of proteomic signatures of exposure to marine pollutants in mussels (Mytilus edulis). *Molecular & Cellular Proteomics.* 5, 1274-1285.

Arning L, Kraus PH, Valentin S, Saft C, Andrich J and Epplen JT (2005). NR2A and NR2B receptor gene variations modify age at onset in Huntington disease. *Neurogenetics.* 6, 25-28.

Aronin N, Chase K, Young C, Sapp E, Schwarz C, Matta N, Kornreich R, Landwehrmeyer B, Bird E, Beal MF, Vonsattel JP, Smith T, Carraway R, Boyce FM, Young AB, Penney JB and DiFiglia M. (1995). CAG expansion affects the expression of mutant Huntingtin in the Huntington's disease brain. *Neuron.* 15, 1193-1201.

Arrasate M, Mitra S, Schweitzer ES, Segal MR and Finkbeiner S (2004). Inclusion body formation reduces levels of mutant huntingtin and the risk of neuronal death.[see comment]. *Nature.* 431, 805-810.

Augood SJ, Faull RL and Emson PC (1997). Dopamine D1 and D2 receptor gene expression in the striatum in Huntington's disease. *Ann Neurology.* 42, 215-221.

Backman L and Farde L (2001). Dopamine and cognitive functioning: brain imaging findings in Huntington's disease and normal aging. *Scand J Psychol.* 42, 287-296.

Bae B-I, Xu H, Igarashi S, Fujimuro M, Agrawal N, Taya Y, Hayward SD, Moran TH, Montell C, Ross CA, Snyder SH and Sawa A (2005). p53 mediates cellular dysfunction and behavioral abnormalities in Huntington's disease.[see comment]. *Neuron.* 47, 29-41.

Bae S-H, Harris AG, Hains PG, Chen H, Garfin DE, Hazell SL, Paik Y-K, Walsh BJ and Cordwell SJ (2003). Strategies for the enrichment and identification of basic proteins in proteome projects. *Proteomics.* 3, 569-579.

Bao J, Sharp AH, Wagster MV, Becher M, Schilling G, Ross CA, Dawson VL and Dawson TM (1996). Expansion of polyglutamine repeat in huntingtin leads to abnormal protein interactions involving calmodulin. *Proc Natl Acad Sci USA.* 93, 5037-5042.

Bartzokis G, Lu PH, Tishler TA, Fong SM, Oluwadara B, Finn JP, Huang D, Bordelon Y, Mintz J and Perlman S (2007). Myelin breakdown and iron changes in Huntington's disease: pathogenesis and treatment implications. *Neurochem Res.* 32, 1655-1664.

Beal MF, Brouillet E, Jenkins BG, Ferrante RJ, Kowall NW, Miller JM, Storey E, Srivastava R, Rosen BR and Hyman BT (1993). Neurochemical and histologic characterization of striatal excitotoxic lesions produced by the mitochondrial toxin 3-nitropropionic acid. *J Neuroscience.* 13, 4181-4192.

Beal MF, Kowall NW, Swartz KJ and Ferrante RJ (1990). Homocysteic acid lesions in rat striatum spare somatostatin-neuropeptide Y (NADPH-diaphorase) neurons. *Neuroscience Letters.* 108, 36-42.

Becher MW, Kotzuk JA, Sharp AH, Davies SW, Bates GP, Price DL and Ross CA (1998). Intranuclear neuronal inclusions in Huntington's disease and dentatorubral and pallidoluysian atrophy: correlation between the density of inclusions and IT15 CAG triplet repeat length. *Neurobiol Dis.* 4, 387-397.

Behrens PF, Franz P, Woodman B, Lindenberg KS and Landwehrmeyer GB (2002). Impaired glutamate transport and glutamate-glutamine cycling: downstream effects of the Huntington mutation. *Brain.* 125, 1908-1922.

Bence NF, Sampat RM and Kopito RR (2001). Impairment of the ubiquitin-proteasome system by protein aggregation.[see comment]. *Science.* 292, 1552-1555.

Bennett EJ, Bence NF, Jayakumar R and Kopito RR (2005). Global impairment of the ubiquitin-proteasome system by nuclear or cytoplasmic protein aggregates precedes inclusion body formation. *Mol Cell.* 17, 351-365.

Bett JS, Goellner GM, Woodman B, Pratt G, Rechsteiner M and Bates GP (2006). Proteasome impairment does not contribute to pathogenesis in R6/2 Huntington's disease mice: exclusion of proteasome activator REGgamma as a therapeutic target.[erratum appears in Hum Mol Genet. 2006 Feb 15;15(4):665]. *Hum Mol Genet.* 15, 33-44.

Boggs JM (2006). Myelin basic protein: a multifunctional protein. *Cell Mol Life Sci.* 63, 1945-1961.

Bolivar VJ, Manley K and Messer A (2004). Early exploratory behavior abnormalities in R6/1 Huntington's disease transgenic mice. *Brain Research.* 1005, 29-35.

Bonelli RM, Hodl AK, Hofmann P and Kapfhammer H-P (2004). Neuroprotection in Huntington's disease: a 2-year study on minocycline. *Int Clin Psychopharmacol.* 19, 337-342.

Bons JAP, de Boer D, van Dieijen-Visser MP and Wodzig WKWH (2006). Standardization of calibration and quality control using surface enhanced laser desorption ionization-time of flight-mass spectrometry. *Clin Chim Acta.* 366, 249-256.

Bouzidi MF, Schagger H, Collombet JM, Carrier H, Flocard F, Quard S, Mousson B and Godinot C (1993). Decreased expression of ubiquinol-cytochrome c reductase subunits in patients exhibiting mitochondrial myopathy with progressive exercise intolerance. *Neuromuscul Disord.* 3, 599-604.

Bradford MM (1976). A rapid and sensitive method for the quantitation of microgram quantities of protein utilizing the principle of protein-dye binding. *Anal Biochem.* 72, 248-254.

Brandt J, Bylsma FW, Gross R, Stine OC, Ranen N and Ross CA (1996). Trinucleotide repeat length and clinical progression in Huntington's disease. *Neurology.* 46, 527-531.

Brecht S, Schwarze K, Waetzig V, Christner C, Heiland S, Fischer G, Sartor K and Herdegen T (2003). Changes in peptidyl-prolyl cis/trans isomerase activity and FK506 binding protein expression following neuroprotection by FK506 in the ischemic rat brain. *Neuroscience.* 120, 1037-1048.

Brennan WA, Jr., Bird ED and Aprille JR (1985). Regional mitochondrial respiratory activity in Huntington's disease brain. *J Neurochemistry.* 44, 1948-1950.

Brignull HR, Morley JF, Garcia SM and Morimoto RI (2006). Modeling polyglutamine pathogenesis in C. elegans. *Methods Enzymol.* 412, 256-282.

Brigulla M, Thiele T, Scharf C, Breitner-Ruddock S, Venz S, Volker U and Greinacher A (2006). Proteomics as a tool for assessment of therapeutics in transfusion medicine: evaluation of prothrombin complex concentrates. *Transfusion.* 46, 377-385.

Brinkman RR, Mezei MM, Theilmann J, Almqvist E and Hayden MR (1997). The likelihood of being affected with Huntington disease by a particular age, for a specific CAG size. *Am.J.Hum.Genet.* 60, 1202-1210.

Brooks SP, Betteridge H, Trueman RC, Jones L and Dunnett SB (2006). Selective extra-dimensional set shifting deficit in a knock-in mouse model of Huntington's disease. *Brain Research Bulletin.* 69, 452-457.

Browne SE, Bowling AC, MacGarvey U, Baik MJ, Berger SC, Muqit MM, Bird ED and Beal MF (1997). Oxidative damage and metabolic dysfunction in Huntington's disease: selective vulnerability of the basal ganglia. *Annals of Neurology*. 41, 646-653.

Brune N, Andrich J, Gencik M, Saft C, Muller T, Valentin S, Przuntek H and Epplen JT (2004). Methyltetrahydrofolate reductase polymorphism influences onset of Huntington's disease. *J Neural Transm Suppl.* Supplementum., 105-110.

Brustovetsky N, LaFrance R, Purl KJ, Brustovetsky T, Keene CD, Low WC and Dubinsky JM (2005). Age-dependent changes in the calcium sensitivity of striatal mitochondria in mouse models of Huntington's Disease. *J Neurochemistry*. 93, 1361-1370.

Butterworth J (1986). Changes in nine enzyme markers for neurons, glia, and endothelial cells in agonal state and Huntington's disease caudate nucleus. *J Neurochemistry*. 47, 583-587.

Carmichael J, Chatellier J, Woolfson A, Milstein C, Fersht AR and Rubinsztein DC (2000). Bacterial and yeast chaperones reduce both aggregate formation and cell death in mammalian cell models of Huntington's disease. *Proc Natl Acad Sci USA*. 97, 9701-9705.

Carmichael J, Vacher C and Rubinsztein DC (2002). The bacterial chaperonin GroEL requires GroES to reduce aggregation and cell death in a COS-7 cell model of Huntington's disease. *Neuroscience Letters*. 330, 270-274.

Carrette O, Demalte I, Scherl A, Yalkinoglu O, Corthals G, Burkhard P, Hochstrasser DF and Sanchez J-C (2003). A panel of cerebrospinal fluid potential biomarkers for the diagnosis of Alzheimer's disease. *Proteomics.* 3, 1486-1494.

Carter CJ (1982). Glutamine synthetase activity in Huntington's disease. *Life Sci.* 31, 1151-1159.

Cassimeris L (2002). The oncoprotein 18/stathmin family of microtubule destabilizers. *Curr Opin Cell Biol.* 14, 18-24.

Cedazo-Minguez A (2007). Apolipoprotein E and Alzheimer's disease: molecular mechanisms and therapeutic opportunities.[see comment]. *J Cell Mol Med.* 11, 1227-1238.

Cepeda C, Ariano MA, Calvert CR, Flores-Hernandez J, Chandler SH, Leavitt BR, Hayden MR and Levine MS (2001). NMDA receptor function in mouse models of Huntington disease. *J Neuroscience Research.* 66, 525-539.

Cha JH, Frey AS, Alsdorf SA, Kerner JA, Kosinski CM, Mangiarini L, Penney JB, Jr., Davies SW, Bates GP and Young AB (1999). Altered neurotransmitter receptor expression in transgenic mouse models of Huntington's disease. *Philos Trans R Soc Lond B Biol Sci.* 354, 981-989.

Cha JH, Kosinski CM, Kerner JA, Alsdorf SA, Mangiarini L, Davies SW, Penney JB, Bates GP and Young AB (1998). Altered brain neurotransmitter receptors in transgenic mice expressing a portion of an abnormal human huntington disease gene. *Proc Natl Acad Sci USA.* 95, 6480-6485.

Chai Y, Koppenhafer SL, Bonini NM and Paulson HL (1999). Analysis of the Role of Heat Shock Protein (Hsp) Molecular Chaperones in Polyglutamine Disease. *J. Neurosci.* 19, 10338-10347.

Chan EYW, Luthi-Carter R, Strand A, Solano SM, Hanson SA, DeJohn MM, Kooperberg C, Chase KO, DiFiglia M, Young AB, Leavitt BR, Cha J-HJ, Aronin N, Hayden MR and Olson JM (2002). Increased huntingtin protein length reduces the number of polyglutamine-induced gene expression changes in mouse models of Huntington's disease. *Hum Mol Genet.* 11, 1939-1951.

Charvin D, Vanhoutte P, Pages C, Borrelli E and Caboche J (2005). Unraveling a role for dopamine in Huntington's disease: the dual role of reactive oxygen species and D2 receptor stimulation.[erratum appears in Proc Natl Acad Sci U S A. 2005 Nov 8;102(45):16530 Note: Borelli, Emiliana [Borrelli, Emilliana]. *Proc Natl Acad Sci USA.* 102, 12218-12223.

Chattopadhyay B, Ghosh S, Gangopadhyay PK, Das SK, Roy T, Sinha KK, Jha DK, Mukherjee SC, Chakraborty A, Singhal BS, Bhattacharya AK and Bhattacharyya NP (2003). Modulation of age at onset in Huntington's disease and spinocerebellar ataxia type 2 patients originated from eastern India. *Neuroscience Letters.* 345, 93-96.

Chen C-M, Wu Y-R, Cheng M-L, Liu J-L, Lee Y-M, Lee P-W, Soong B-W and Chiu DT-Y (2007). Increased oxidative damage and mitochondrial abnormalities in the peripheral blood of Huntington's disease patients. *Biochemical & Biophysical Research Comm.* 359, 335-340.

Chen M, Ona VO, Li M, Ferrante RJ, Fink KB, Zhu S, Bian J, Guo L, Farrell LA, Hersch SM, Hobbs W, Vonsattel JP, Cha JH and Friedlander RM (2000). Minocycline inhibits caspase-1 and caspase-3 expression and delays mortality in a transgenic mouse model of Huntington disease.[see comment]. *Nat Med.* 6, 797-801.

Chen N, Luo T, Wellington C, Metzler M, McCutcheon K, Hayden MR and Raymond LA (1999). Subtype-specific enhancement of NMDA receptor currents by mutant huntingtin. *J Neurochemistry.* 72, 1890-1898.

Choo YS, Johnson GVW, MacDonald M, Detloff PJ and Lesort M (2004). Mutant huntingtin directly increases susceptibility of mitochondria to the calcium-induced permeability transition and cytochrome c release. *Hum Mol Genet.* 13, 1407-1420.

Christner C, Herdegen T and Fischer G (2001). FKBP ligands as novel therapeutics for neurological disorders. *Mini Rev Med Chem.* 1, 377-397.

Ciammola A, Sassone J, Alberti L, Meola G, Mancinelli E, Russo MA, Squitieri F and Silani V (2006). Increased apoptosis, Huntingtin inclusions and altered differentiation in muscle cell cultures from Huntington's disease subjects. *Cell Death Differ.* 13, 2068-2078.

Clifford JJ, Drago J, Natoli AL, Wong JYF, Kinsella A, Waddington JL and Vaddadi KS (2002). Essential fatty acids given from conception prevent topographies of motor deficit in a transgenic model of Huntington's disease. *Neuroscience.* 109, 81-88.

Colin E, Regulier E, Perrin V, Durr A, Brice A, Aebischer P, Deglon N, Humbert S and Saudou F (2005). Akt is altered in an animal model of Huntington's disease and in patients. *Eur J Neurosci.* 21, 1478-1488.

Cornett J, Cao F, Wang CE, Ross CA, Bates GP and Li SH, Li XJ (2005). Polyglutamine expansion of huntingtin impairs its nuclear export. *Nature Genet.* 37, 198-204.

Cornett J, Smith L, Friedman M, Shin J-Y, Li X-J and Li S-H (2006). Context-dependent dysregulation of transcription by mutant huntingtin. *J Biological Chemistry.* 281, 36198-36204.

Corthals GL, Wasinger VC, Hochstrasser DF and Sanchez JC (2000). The dynamic range of protein expression: a challenge for proteomic research. *Electrophoresis.* 21, 1104-1115.

Coyle JT and Schwarcz R (1976). Lesion of striatal neurones with kainic acid provides a model for Huntington's chorea. *Nature.* 263, 244-246.

Craufurd D and Snowden J (2002). Neuropsychological and neuropsychiatric aspects of Huntington's Disease. In Huntington's Disease. (GP Bates, H P.S., AL Jones, eds). London: Oxford Univerity Press, pp. 62-94.

Cui L, Jeong H, Borovecki F, Parkhurst CN, Tanese N and Krainc D (2006). Transcriptional repression of PGC-1alpha by mutant huntingtin leads to mitochondrial dysfunction and neurodegeneration.[see comment]. *Cell.* 127, 59-69.

Davidsson P and Sjögren M (2006). Proteome studies of CSF in AD patients. *Mechanisms of Ageing and Development.* 127, 133-137.

Davies SW, Turmaine M, Cozens BA, DiFiglia M, Sharp AH, Ross CA, Scherzinger E, Wanker EE, Mangiarini L and Bates GP (1997). Formation of neuronal intranuclear inclusions underlies the neurological dysfunction in mice transgenic for the HD mutation. *Cell.* 90, 537-548.

Dawson TM, Steiner JP, Dawson VL, Dinerman JL, Uhl GR and Snyder SH (1993). Immunosuppressant FK506 enhances phosphorylation of nitric oxide synthase and protects against glutamate neurotoxicity.[see comment]. *Proc Natl Acad Sci USA.* 90, 9808-9812.

De Boer D, Wodzig WKWH and Van Dieijen-Visser MP (2006). 'Back to basics' with the energy-absorbing matrix in SELDI-TOF MS. *Ned Tijdschr Klin Chem Labgeneesk*, 201-202.

De Rooij KE, Dorsman JC, Smoor MA, Den Dunnen JT and Van Ommen GJ (1996). Subcellular localization of the Huntington's disease gene product in cell lines by immunofluorescence and biochemical subcellular fractionation. *Hum Mol Genet.* 5, 1093-1099.

Deckel AW, Gordinier A, Nuttal D, Tang V, Kuwada C, Freitas R and Gary KA (2001). Reduced activity and protein expression of NOS in R6/2 HD transgenic mice: effects of L-NAME on symptom progression. *Brain Research.* 919, 70-81.

Deckel AW, Tang V, Nuttal D, Gary K and Elder R (2002). Altered neuronal nitric oxide synthase expression contributes to disease progression in Huntington's disease transgenic mice. *Brain Research.* 939, 76-86.

del Hoyo P, Garcia-Redondo A, de Bustos F, Molina JA, Sayed Y, Alonso-Navarro H, Caballero L, Arenas J and Jimenez-Jimenez FJ (2006). Oxidative stress in skin fibroblasts cultures of patients with Huntington's disease. *Neurochem Res.* 31, 1103-1109.

Denovan-Wright EM and Robertson HA (2000). Cannabinoid receptor messenger RNA levels decrease in a subset of neurons of the lateral striatum, cortex and hippocampus of transgenic Huntington's disease mice. *Neuroscience.* 98, 705-713.

Desplats PA, Kass KE, Gilmartin T, Stanwood GD, Woodward EL, Head SR, Sutcliffe JG and Thomas EA (2006). Selective deficits in the expression of striatal-enriched mRNAs in Huntington's disease. *J Neurochemistry.* 96, 743-757.

Diamandis EP (2004a). Analysis of serum proteomic patterns for early cancer diagnosis: drawing attention to potential problems. *J Natl Cancer Inst.* 96, 353-356.

Diamandis EP (2004b). Mass spectrometry as a diagnostic and a cancer biomarker discovery tool: opportunities and potential limitations. *Mol & Cell Proteomics.* 3, 367-378.

Diaz-Hernandez M, Hernandez F, Martin-Aparicio E, Gomez-Ramos P, Moran MA, Castano JG, Ferrer I, Avila J and Lucas JJ (2003). Neuronal induction of the immunoproteasome in Huntington's disease. *J Neuroscience.* 23, 11653-11661.

DiFiglia M, Sapp E, Chase K, Schwarz C, Meloni A, Young C, Martin E, Vonsattel JP, Carraway R, Reeves SA, Boyce FM and Aronin N. (1995). Huntingtin is a cytoplasmic protein associated with vesicles in human and rat brain neurons. *Neuron.* 14, 1075-1081.

DiFiglia M, Sapp E, Chase KO, Davies SW, Bates GP, Vonsattel JP and Aronin N (1997). Aggregation of huntingtin in neuronal intranuclear inclusions and dystrophic neurites in brain. *Science.* 277, 1990-1993.

Ding Q, Lewis JJ, Strum KM, Dimayuga E, Bruce-Keller AJ, Dunn JC and Keller JN (2002). Polyglutamine expansion, protein aggregation, proteasome activity, and neural survival. *J Biological Chemistry.* 277, 13935-13942.

Dragatsis I, Levine MS and Zeitlin S (2000). Inactivation of Hdh in the brain and testis results in progressive neurodegeneration and sterility in mice. *Nature Genet.* 26, 300-306.

Dudek NL, Dai Y and Muma NA (2008). Protective effects of interrupting the binding of calmodulin to mutant huntingtin. *J Neuropathol Exp Neurol.* 67, 355-365.

Dunah AW, Jeong H, Griffin A, Kim Y-M, Standaert DG, Hersch SM, Mouradian MM, Young AB, Tanese N and Krainc D (2002). Sp1 and TAFII130 transcriptional activity disrupted in early Huntington's disease.[see comment]. *Science.* 296, 2238-2243.

Durr A, Hahn-Barma V, Brice A, Pecheux C, Dode C and Feingold J (1999). Homozygosity in Huntington's disease. *J Medical Genetics.* 36, 172-173.

Duyao M, Ambrose C, Myers R, Novelletto A, Persichetti F, Frontali M, Folstein S, Ross C, Franz M, Abbott M, Gray J, Conneally P, Young A, Penney J, Hollingsworth Z, Shoulson I, Lazzarini A, Falek A, Koroshetz W, Sax D, Bird E, Vonsattel J, Bonilla E, Alvir J, Bickham Conde J, Cha J-H, Dure L, Gomez F, Ramos M, Sanches-Ramos J, Snodgrass S, de Young M, Wexler N, Moscowitz C, Penchaszadeh G, MacFarlane H, Anderson M, Jenkins B, Srinidhi J, Barnes G, Gusella J and MacDonald M. (1993). Trinucleotide repeat length instability and age of onset in Huntington's disease. *Nature Genet.* 4, 387-392.

Duyao MP, Auerbach AB, Ryan A, Persichetti F, Barnes GT, McNeil SM, Ge P, Vonsattel JP, Gusella JF, Joyner AL and MacDonald ME. (1995). Inactivation of the mouse Huntington's disease gene homolog Hdh. *Science.* 269, 407-410.

Ekestern E and Lebhart G (2005). Long-term monitoring of the mortality trend of Huntington's disease in Austria. *Eur J Epidemiol.* 20, 169-172.

Engwegen JYMN, Gast M-CW, Schellens JHM and Beijnen JH (2006). Clinical proteomics: searching for better tumour markers with SELDI-TOF mass spectrometry. *Trends Pharmacol Sci.* 27, 251-259.

Faber PW, Alter JR, MacDonald ME and Hart AC (1999). Polyglutamine-mediated dysfunction and apoptotic death of a Caenorhabditis elegans sensory neuron. *Proc Natl Acad Sci USA.* 96, 179-184.

Fan MMY, Zhang H, Hayden MR, Pelech SL and Raymond LA (2008). Protective up-regulation of CK2 by mutant huntingtin in cells co-expressing NMDA receptors. *J Neurochemistry.* 104, 790-805.

Fennema-Notestine C, Archibald SL, Jacobson MW, Corey-Bloom J, Paulsen JS, Peavy GM, Gamst AC, Hamilton JM, Salmon DP and Jernigan TL (2004). In vivo evidence of cerebellar atrophy and cerebral white matter loss in Huntington disease. *Neurology.* 63, 989-995.

Ferrante RJ, Andreassen OA, Jenkins BG, Dedeoglu A, Kuemmerle S, Kubilus JK, Kaddurah-Daouk R, Hersch SM and Beal MF (2000). Neuroprotective Effects of Creatine in a Transgenic Mouse Model of Huntington's Disease. *J. Neuroscience.* 20, 4389-4397.

Fodor IK, Nelson DO, Alegria-Hartman M, Robbins K, Langlois RG, Turteltaub KW, Corzett TH and McCutchen-Maloney SL (2005). Statistical challenges in the analysis of two-dimensional difference gel electrophoresis experiments using DeCyder. *Bioinformatics.* 21, 3733-3740.

Fossale E, Wheeler VC, Vrbanac V, Lebel L-A, Teed A, Mysore JS, Gusella JF, MacDonald ME and Persichetti F (2002). Identification of a presymptomatic molecular phenotype in Hdh CAG knock-in mice. *Hum Mol Genet.* 11, 2233-2241.

Fountoulakis M, Takacs MF, Berndt P, Langen H and Takacs B (1999a). Enrichment of low abundance proteins of Escherichia coli by hydroxyapatite chromatography. *Electrophoresis.* 20, 2181-2195.

Fountoulakis M, Takacs MF and Takacs B (1999b). Enrichment of low-copy-number gene products by hydrophobic interaction chromatography. *J Chromatogr.* A. 833, 157-168.

Freeman WM and Hemby SE (2004). Proteomics for protein expression profiling in neuroscience. *Neurochem Res.* 29, 1065-1081.

Frey IM, Rubio-Aliaga I, Siewert A, Sailer D, Drobyshev A, Beckers J, de Angelis MH, Aubert J, Bar Hen A, Fiehn O, Eichinger HM and Daniel H (2007). Profiling at mRNA, protein, and metabolite levels reveals alterations in renal amino acid handling and glutathione metabolism in kidney tissue of Pept2-/- mice. *Physiol Genomics.* 28, 301-310.

Friedlander RM (2003). Apoptosis and caspases in neurodegenerative diseases. *N Engl J Med.* 348, 1365-1375.

Fujimoto M, Takaki E, Hayashi T, Kitaura Y, Tanaka Y, Inouye S and Nakai A (2005). Active HSF1 significantly suppresses polyglutamine aggregate formation in cellular and mouse models. *J Biological Chemistry.* 280, 34908-34916.

Gade D, Thiermann J, Markowsky D and Rabus R (2003). Evaluation of two-dimensional difference gel electrophoresis for protein profiling. Soluble proteins of the marine bacterium Pirellula sp. strain 1. *J Mol Microbiol Biotechnol.* 5, 240-251.

Gafni J and Ellerby LM (2002). Calpain activation in Huntington's disease. *J Neuroscience.* 22, 4842-4849.

Gafni J, Hermel E, Young JE, Wellington CL, Hayden MR and Ellerby LM (2004). Inhibition of calpain cleavage of huntingtin reduces toxicity: accumulation of calpain/caspase fragments in the nucleus. *J Biological Chemistry.* 279, 20211-20220.

Gauthier LR, Charrin BC, Borrell-Pages M, Dompierre JP, Rangone H, Cordelieres FP, De Mey J, MacDonald ME, Lessmann V, Humbert S and Saudou F (2004). Huntingtin controls neurotrophic support and survival of neurons by enhancing BDNF vesicular transport along microtubules.[see comment]. *Cell.* 118, 127-138.

Gizatullina ZZ, Lindenberg KS, Harjes P, Chen Y, Kosinski CM, Landwehrmeyer BG, Ludolph AC, Striggow F, Zierz S and Gellerich FN (2006). Low stability of Huntington muscle mitochondria against Ca2+ in R6/2 mice. *Annals of Neurology.* 59, 407-411.

Gold BG (1997). FK506 and the role of immunophilins in nerve regeneration. *Mol Neurobiol.* 15, 285-306.

Gold BG, Densmore V, Shou W, Matzuk MM and Gordon HS (1999). Immunophilin FK506-binding protein 52 (not FK506-binding protein 12) mediates the neurotrophic action of FK506. *J Pharmacol Exp Ther.* 289, 1202-1210.

Goldberg YP, Nicholson DW, Rasper DM, Kalchman MA, Koide HB, Graham RK, Bromm M, Kazemi-Esfarjani P, Thornberry NA, Vaillancourt JP and Hayden MR (1996). Cleavage of huntingtin by apopain, a proapoptotic cysteine protease, is modulated by the polyglutamine tract.[see comment]. *Nature Genet.* 13, 442-449.

Gonitel R, Moffitt H, Sathasivam K, Woodman B, Detloff PJ, Faull RLM and Bates GP (2008). DNA instability in postmitotic neurons. *Proc Natl Acad Sci USA.* 105, 3467-3472.

Gorg A, Obermaier C, Boguth G, Harder A, Scheibe B, Wildgruber R and Weiss W (2000). The current state of two-dimensional electrophoresis with immobilized pH gradients. *Electrophoresis.* 21, 1037-1053.

Goswami A, Dikshit P, Mishra A, Mulherkar S, Nukina N and Jana NR (2006). Oxidative stress promotes mutant huntingtin aggregation and mutant huntingtin-dependent cell death by mimicking proteasomal malfunction. *Biochemical & Biophysical Research Comm.* 342, 184-190.

Goto S, Matsukado Y, Mihara Y, Inoue N and Miyamoto E (1986). Calcineurin in human brain and its relation to extrapyramidal system. Immunohistochemical study on postmortem human brains. *Acta Neuropathol (Berl).* 72, 150-156.

Gourfinkel-An I, Vila M, Faucheux B, Duyckaerts C, Viallet F, Hauw J-J, Brice A, Agid Y and Hirsch EC (2002). Metabolic changes in the basal ganglia of patients with Huntington's disease: an in situ hybridization study of cytochrome oxidase subunit I mRNA. *J Neurochemistry.* 80, 466-476.

Gray M, Shirasaki DI, Cepeda C, Andre VM, Wilburn B, Lu X-H, Tao J, Yamazaki I, Li S-H, Sun YE, Li X-J, Levine MS and Yang XW (2008). Full-length human mutant huntingtin with a stable polyglutamine repeat can elicit progressive and selective neuropathogenesis in BACHD mice. *J Neuroscience.* 28, 6182-6195.

Green DR and Reed JC (1998). Mitochondria and apoptosis.(Special Section: Apoptosis). *Science.* v281, p1309(1304).

Gu M, Gash MT, Mann VM, Javoy-Agid F, Cooper JM and Schapira AH (1996). Mitochondrial defect in Huntington's disease caudate nucleus. *Annals of Neurology.* 39, 385-389.

Guo X, Dawson VL and Dawson TM (2001). Neuroimmunophilin ligands exert neuroregeneration and neuroprotection in midbrain dopaminergic neurons. *Eur J Neuroscience.* 13, 1683-1693.

Gusella JF, Wexler NS, Conneally PM, Naylor SL, Anderson MA, Tanzi RE, Watkins PC, Ottina K, Wallace MR, Sakaguchi AY, Young AB, Shoulson I, Bonilla E and Martin JB (1983). A polymorphic DNA marker genetically linked to Huntington's disease. *Nature.* 306, 234-238.

Gutekunst CA, Levey AI, Heilman CJ, Whaley WL, Yi H, Nash NR, Rees HD, Madden JJ and Hersch SM (1995). Identification and localization of huntingtin in brain and human lymphoblastoid cell lines with anti-fusion protein antibodies. *Proc Natl Acad Sci USA.* 92, 8710-8714.

Gutekunst CA, Li SH, Yi H, Mulroy JS, Kuemmerle S, Jones R, Rye D, Ferrante RJ, Hersch SM and Li XJ (1999). Nuclear and neuropil aggregates in Huntington's disease: relationship to neuropathology. *J Neuroscience.* 19, 2522-2534.

Gutekunst CA, Norflus F and Hersch SM (2002). The neuropathology of Huntington's disease. In Huntington's Disease. (GP Bates, PS Harper, AL Jones, eds): OUP, Oxford, UK, pp. 251-275.

Gygi SP, Corthals GL, Zhang Y, Rochon Y and Aebersold R (2000a). Evaluation of two-dimensional gel electrophoresis-based proteome analysis technology. *Proc Natl Acad Sci USA*. 97, 9390-9395.

Gygi SP, Corthals GL, Zhang Y, Rochon Y and Aebersold R (2000b). Evaluation of two-dimensional gel electrophoresis-based proteome analysis technology. *Proc Natl Acad Sci USA*. 97, 9390-9395.

Halliday GM, McRitchie DA, Macdonald V, Double KL, Trent RJ and McCusker E (1998). Regional specificity of brain atrophy in Huntington's disease. *Experimental Neurology*. 154, 663-672.

Hamilton GS, Wu Y-Q, Limburg DC, Wilkinson DE, Vaal MJ, Li J-H, Thomas C, Huang W, Sauer H, Ross DT, Soni R, Chen Y, Guo H, Howorth P, Valentine H, Liang S, Spicer D, Fuller M and Steiner JP (2002). Synthesis of N-glyoxyl prolyl and pipecolyl amides and thioesters and evaluation of their in vitro and in vivo nerve regenerative effects. *J Med Chem*. 45, 3549-3557.

Hansson O, Castilho RF, Korhonen L, Lindholm D, Bates GP and Brundin P (2001a). Partial resistance to malonate-induced striatal cell death in transgenic mouse models of Huntington's disease is dependent on age and CAG repeat length. *J Neurochemistry*. 78, 694-703.

Hansson O, Guatteo E, Mercuri NB, Bernardi G, Li XJ, Castilho RF and Brundin P (2001b). Resistance to NMDA toxicity correlates with appearance of nuclear inclusions, behavioural deficits and changes in calcium homeostasis in mice transgenic for exon 1 of the huntington gene. *Eur J Neuroscience*. 14, 1492-1504.

Hansson O, Nylandsted J, Castilho RF, Leist M, Jaattela M and Brundin P (2003). Overexpression of heat shock protein 70 in R6/2 Huntington's disease mice has only modest effects on disease progression. *Brain Research*. 970, 47-57.

Hansson O, Petersen A, Leist M, Nicotera P, Castilho RF and Brundin P (1999). Transgenic mice expressing a Huntington's disease mutation are resistant to quinolinic acid-induced striatal excitotoxicity. *Proc Natl Acad Sci USA*. 96, 8727-8732.

Harezlak J, Wang M, Christiani D and Lin X (2007). Quantitative quality-assessment techniques to compare fractionation and depletion methods in SELDI-TOF mass spectrometry experiments. *Bioinformatics*. 28, 2441-2448.

Harper P (2002a). Huntington's disease: a historical background. In Huntington's disease. (GP Bates, PS Harper, AL Jones, eds). London: Oxford Univerity Press; pp. 3-27.

Harper P (2002b). The epidemiology of Huntington's disease. In Huntington's disease. (GP Bates, H P.S., AL Jones, eds). London: Oxford Univerity Press, pp. 159-197.

Harper P and Jones AL (2002). Huntington's disease: genetic and molecular studies. In Huntington's disease. (GP Bates, H P.S., AL Jones, eds). London: Oxford Univerity Press, pp. 111-158.

Harrington CR, Louwagie J, Rossau R, Vanmechelen E, Perry RH, Perry EK, Xuereb JH, Roth M and Wischik CM (1994). Influence of apolipoprotein E genotype on senile dementia of the Alzheimer and Lewy body types. Significance for etiological theories of Alzheimer's disease. *Am J Pathol.* 145, 1472-1484.

Hartl D, Irmler M, Romer I, Mader MT, Mao L, Zabel C, de Angelis MH, Beckers J and Klose J (2008). Transcriptome and proteome analysis of early embryonic mouse brain development. *Proteomics.* 8, 1257-1265.

Hartl FU (1996). Molecular chaperones in cellular protein folding. *Nature.* 381, 571-579.

Hay DG, Sathasivam K, Tobaben S, Stahl B, Marber M, Mestril R, Mahal A, Smith DL, Woodman B and Bates GP (2004). Progressive decrease in chaperone protein levels in a mouse model of Huntington's disease and induction of stress proteins as a therapeutic approach. *Hum Mol Genet.* 13, 1389-1405.

Hayashi K, Pan Y, Shu H, Ohshima T, Kansy JW, White CL, 3rd, Tamminga CA, Sobel A, Curmi PA, Mikoshiba K and Bibb JA (2006). Phosphorylation of the tubulin-binding protein, stathmin, by Cdk5 and MAP kinases in the brain. *J Neurochemistry.* 99, 237-250.

Heinsen H, Rub U, Bauer M, Ulmar G, Bethke B, Schuler M, Bocker F, Eisenmenger W, Gotz M, Korr H and Schmitz C (1999). Nerve cell loss in the thalamic mediodorsal nucleus in Huntington's disease. *Acta Neuropathol (Berl).* 97, 613-622.

Heinsen H, Rub U, Gangnus D, Jungkunz G, Bauer M, Ulmar G, Bethke B, Schuler M, Bocker F, Eisenmenger W, Gotz M and Strik M (1996). Nerve cell loss in the thalamic centromedian-parafascicular complex in patients with Huntington's disease. *Acta Neuropathol (Berl).* 91, 161-168.

Heinsen H, Strik M, Bauer M, Luther K, Ulmar G, Gangnus D, Jungkunz G, Eisenmenger W and Gotz M (1994). Cortical and striatal neurone number in Huntington's disease. *Acta Neuropathol (Berl).* 88, 320-333.

Heng MY, Tallaksen-Greene SJ, Detloff PJ and Albin RL (2007). Longitudinal evaluation of the Hdh(CAG)150 knock-in murine model of Huntington's disease. *J Neuroscience.* 27, 8989-8998.

Hernandez-Espinosa D and Morton AJ (2006). Calcineurin inhibitors cause an acceleration of the neurological phenotype in a mouse transgenic for the human Huntington's disease mutation. *Brain Research Bulletin.* 69, 669-679.

Hersch SM and Ferrante RJ (2004). Translating therapies for Huntington's disease from genetic animal models to clinical trials. *NeuroRx.* 1, 298-306.

Hilditch-Maguire P, Trettel F, Passani LA, Auerbach A, Persichetti F and MacDonald ME (2000). Huntingtin: an iron-regulated protein essential for normal nuclear and perinuclear organelles. *Hum Mol Genet.* 9, 2789-2797.

Hodges A, Hughes G, Brooks S, Elliston L, Holmans P, Dunnett SB and Jones L (2008). Brain gene expression correlates with changes in behavior in the R6/1 mouse model of Huntington's disease. *Genes Brain Behav.* 7, 288-299.

Hodges A, Strand AD, Aragaki AK, Kuhn A, Sengstag T, Hughes G, Elliston LA, Hartog C, Goldstein DR, Thu D, Hollingsworth ZR, Collin F, Synek B, Holmans PA, Young AB, Wexler NS, Delorenzi M, Kooperberg C, Augood SJ, Faull RLM, Olson JM, Jones L and Luthi-Carter R (2006). Regional and cellular gene expression changes in human Huntington's disease brain. *Hum Mol Genet.* 15, 965-977.

Hodgson JG, Agopyan N, Gutekunst CA, Leavitt BR, LePiane F, Singaraja R, Smith DJ, Bissada N, McCutcheon K, Nasir J, Jamot L, Li XJ, Stevens ME, Rosemond E, Roder JC, Phillips AG, Rubin EM, Hersch SM and Hayden MR (1999). A YAC mouse model for Huntington's disease with full-length mutant huntingtin, cytoplasmic toxicity, and selective striatal neurodegeneration. *Neuron.* 23, 181-192.

Holbert S, Denghien I, Kiechle T, Rosenblatt A, Wellington C, Hayden MR, Margolis RL, Ross CA, Dausset J, Ferrante RJ and Neri C (2001). The Gln-Ala repeat transcriptional activator CA150 interacts with huntingtin: neuropathologic and genetic evidence for a role in Huntington's disease pathogenesis. *Proc Natl Acad Sci USA.* 98, 1811-1816.

Holmberg CI, Staniszewski KE, Mensah KN, Matouschek A and Morimoto RI (2004). Inefficient degradation of truncated polyglutamine proteins by the proteasome. *Embo J.* 23, 4307-4318.

Hoogeveen AT, Willemsen R, Meyer N, de Rooij KE, Roos RA, van Ommen GJ and Galjaard H (1993). Characterization and localization of the Huntington disease gene product. *Hum Mol Genet.* 2, 2069-2073.

Hu L, Ye M, Jiang X, Feng S and Zou H (2007). Advances in hyphenated analytical techniques for shotgun proteome and peptidome analysis--A review. *Analytica Chimica Acta.* 598, 193-204.

Huang H-L, Stasyk T, Morandell S, Dieplinger H, Falkensammer G, Griesmacher A, Mogg M, Schreiber M, Feuerstein I, Huck CW, Stecher G, Bonn GK , Huber LA (2006). Biomarker discovery in breast cancer serum using 2-D differential gel electrophoresis/ MALDI-TOF/TOF and data validation by routine clinical assays. *Electrophoresis.* 27, 1641-1650.

Humbert S, Bryson EA, Cordelieres FP, Connors NC, Datta SR, Finkbeiner S, Greenberg ME and Saudou F (2002). The IGF-1/Akt pathway is neuroprotective in Huntington's disease and involves Huntingtin phosphorylation by Akt. *Dev Cell.* 2, 831-837.

Huntington's Disease Collaborative Research Group (1993). A novel gene containing a trinucleotide repeat that is expanded and unstable on Huntington's disease chromosomes. The Huntington's Disease Collaborative Research Group. *Cell.* 72, 971-983.

Huntington G (1872). On chorea. *Medical and Surgical Reporter.* 26, 320-321.

Hutchens TW and Yip T-T (1993). New desorption strategies for the mass spectrometric analysis of macromolecules. *Rapid Comm Mass Spectrometry.* 7, 576-580.

Hye A, Lynham S, Thambisetty M, Causevic M, Campbell J, Byers HL, Hooper C, Rijsdijk F, Tabrizi SJ, Banner S, Shaw CE, Foy C, Poppe M, Archer N, Hamilton G, Powell J, Brown RG, Sham P, Ward M and Lovestone S (2006). Proteome-based plasma biomarkers for Alzheimer's disease. *Brain.* 129, 3042-3050.

Iannicola C, Moreno S, Oliverio S, Nardacci R, Ciofi-Luzzatto A and Piacentini M (2000). Early alterations in gene expression and cell morphology in a mouse model of Huntington's disease. *J Neurochemistry.* 75, 830-839.

Isacson O, Brundin P, Gage FH and Bjorklund A (1985). Neural grafting in a rat model of Huntington's disease: progressive neurochemical changes after neostriatal ibotenate lesions and striatal tissue grafting. *Neuroscience.* 16, 799-817.

Jackson GR, Salecker I, Dong X, Yao X, Arnheim N, Faber PW, MacDonald ME and Zipursky SL (1998). Polyglutamine-expanded human huntingtin transgenes induce degeneration of Drosophila photoreceptor neurons. *Neuron.* 21, 633-642.

Jayaraman T, Brillantes AM, Timerman AP, Fleischer S, Erdjument-Bromage H, Tempst P and Marks AR (1992). FK506 binding protein associated with the calcium release channel (ryanodine receptor). *J Biological Chemistry.* 267, 9474-9477.

Jech R, Klempir J, Vymazal J, Zidovska J, Klempirova O, Ruzicka E and Roth J (2007). Variation of selective gray and white matter atrophy in Huntington's disease. *Mov Disord.* 22, 1783-1789.

Jeste DV, Barban L and Parisi J (1984). Reduced Purkinje cell density in Huntington's disease. *Experimental Neurology.* 85, 78-86.

Johnston-Wilson NL, Sims CD, Hofmann JP, Anderson L, Shore AD, Torrey EF and Yolken RH (2000). Disease-specific alterations in frontal cortex brain proteins in schizophrenia, bipolar disorder, and major depressive disorder. The Stanley Neuropathology Consortium. *Mol Psychiatry.* 5, 142-149.

Jones AL (2002). The cell biology of Huntington's disease. In Huntington's disease. (GP Bates, H P.S., AL Jones, eds). London: Oxford Univerity Press, pp. 348-386.

Kahlem P, Green H and Djian P (1998). Transglutaminase action imitates Huntington's disease: selective polymerization of Huntingtin containing expanded polyglutamine. *Mol Cell.* 1, 595-601.

Kalchman MA, Graham RK, Xia G, Koide HB, Hodgson JG, Graham KC, Goldberg YP, Gietz RD, Pickart CM and Hayden MR (1996). Huntingtin is ubiquitinated and interacts with a specific ubiquitin-conjugating enzyme. *J Biological Chemistry.* 271, 19385-19394.

Kalman J, Juhasz A, Majtenyi K, Rimanoczy A, Jakab K, Gardian G, Rasko I and Janka Z (2000). Apolipoprotein E polymorphism in Pick's disease and in Huntington's disease. *Neurobiol Aging.* 21, 555-558.

Kaltenbach LS, Romero E, Becklin RR, Chettier R, Bell R, Phansalkar A, Strand A, Torcassi C, Savage J, Hurlburt A, Cha G-H, Ukani L, Chepanoske CL, Zhen Y, Sahasrabudhe S, Olson J, Kurschner C, Ellerby LM, Peltier JM, Botas J and Hughes RE (2007). Huntingtin interacting proteins are genetic modifiers of neurodegeneration. *PLoS Genet.* 3, e82.

Karp NA and Lilley KS (2005). Maximising sensitivity for detecting changes in protein expression: experimental design using minimal CyDyes. *Proteomics.* 5, 3105-3115.

Karp NA, McCormick PS, Russell MR and Lilley KS (2007). Experimental and statistical considerations to avoid false conclusions in proteomics studies using differential in-gel electrophoresis. *Mol & Cell Proteomics.* 6, 1354-1364.

Kasparova S, Sumbalova Z, Bystricky P, Kucharska J, Liptaj T, Mlynarik V and Gvozdjakova A (2006). Effect of coenzyme Q10 and vitamin E on brain energy metabolism in the animal model of Huntington's disease. *Neurochem Int.* 48, 93-99.

Kassubek J, Gaus W and Landwehrmeyer GB (2004b). Evidence for more widespread cerebral pathology in early HD: an MRI-based morphometric analysis.[comment]. *Neurology.* 62, 523-524; author reply 524.

Kassubek J, Juengling FD, Kioschies T, Henkel K, Karitzky J, Kramer B, Ecker D, Andrich J, Saft C, Kraus P, Aschoff AJ, Ludolph AC and Landwehrmeyer GB (2004a). Topography of cerebral atrophy in early Huntington's disease: a voxel based morphometric MRI study. *J Neurol Neurosurg Psychiatry.* 75, 213-220.

Kaufmann SH, Ewing CM and Shaper JH (1987). The erasable Western blot. *Anal Biochem.* 161, 89-95.

Kazantsev A, Preisinger E, Dranovsky A, Goldgaber D and Housman D (1999). Insoluble detergent-resistant aggregates form between pathological and nonpathological lengths of polyglutamine in mammalian cells. *Proc Natl Acad Sci USA.* 96, 11404-11409.

Kegel KB, Kim M, Sapp E, McIntyre C, Castano JG, Aronin N and DiFiglia M (2000). Huntingtin expression stimulates endosomal-lysosomal activity, endosome tubulation, and autophagy. *J Neuroscience.* 20, 7268-7278.

Kegel KB, Meloni AR, Yi Y, Kim YJ, Doyle E, Cuiffo BG, Sapp E, Wang Y, Qin ZH, Chen JD, Nevins JR, Aronin N and DiFiglia M (2002). Huntingtin is present in the nucleus, interacts with the transcriptional corepressor C-terminal binding protein, and represses transcription. *J Biological Chemistry.* 277, 7466-7476.

Kehoe P, Krawczak M, Harper PS, Owen MJ and Jones AL (1999). Age of onset in Huntington disease: sex specific influence of apolipoprotein E genotype and normal CAG repeat length. *J Medical Genetics.* 36, 108-111.

Kennedy L, Evans E, Chen CM, Craven L, Detloff PJ, Ennis M and Shelbourne PF (2003). Dramatic tissue-specific mutation length increases are an early molecular event in Huntington disease pathogenesis. *Hum Mol Genet.* 12, 3359-3367.

Kennedy L and Shelbourne PF (2000). Dramatic mutation instability in HD mouse striatum: does polyglutamine load contribute to cell-specific vulnerability in Huntington's disease? *Hum Mol Genet.* 9, 2539-2544.

Kida EMDP, Palminiello SP, Golabek AAP, Walus MM, Wierzba-Bobrowicz TMDP, Rabe AP, Albertini GMD and Wisniewski KEMDP (2006). Carbonic Anhydrase II in the Developing and Adult Human Brain. *J Neuropathol Exp Neurol.* 65, 664-674.

Kiechle T, Dedeoglu A, Kubilus J, Kowall NW, Beal MF, Friedlander RM, Hersch SM and Ferrante RJ (2002). Cytochrome C and caspase-9 expression in Huntington's disease. *Neuromolecular Med.* 1, 183-195.

Kita H, Carmichael J, Swartz J, Muro S, Wyttenbach A, Matsubara K, Rubinsztein DC and Kato K (2002). Modulation of polyglutamine-induced cell death by genes identified by expression profiling. *Hum Mol Genet.* 11, 2279-2287.

Kitamura A, Kubota H, Pack C-G, Matsumoto G, Hirayama S, Takahashi Y, Kimura H, Kinjo M, Morimoto RI and Nagata K (2006). Cytosolic chaperonin prevents polyglutamine toxicity with altering the aggregation state. *Nat Cell Biol.* 8, 1163-1170.

Klee CB, Ren H and Wang X (1998). Regulation of the calmodulin-stimulated protein phosphatase, calcineurin. *J Biological Chemistry.* 273, 13367-13370.

Klose J (1975). Protein mapping by combined isoelectric focusing and electrophoresis of mouse tissues. A novel approach to testing for induced point mutations in mammals. *Humangenetik.* 26, 231-243.

Klose J (1999). Genotypes and phenotypes. *Electrophoresis.* 20, 643-652.

Koroshetz WJ, Jenkins BG, Rosen BR and Beal MF (1997). Energy metabolism defects in Huntington's disease and effects of coenzyme Q10. *Annals of Neurology*. 41, 160-165.

Kremer B (2002). Clinical neurology of Huntington's Disease. In Huntington's Disease. (GP Bates, H P.S., AL Jones, eds). London: Oxford Univerity Press, pp. 28-61.

Kremer B, Almqvist E, Theilmann J, Spence N, Telenius H, Goldberg YP and Hayden MR (1995). Sex-dependent mechanisms for expansions and contractions of the CAG repeat on affected Huntington disease chromosomes. *Am J Hum Genet*. 57, 343-350.

Kremer HP, Roos RA, Dingjan GM, Bots GT, Bruyn GW and Hofman MA (1991). The hypothalamic lateral tuberal nucleus and the characteristics of neuronal loss in Huntington's disease. *Neuroscience Letters*. 132, 101-104.

Krobitsch S and Lindquist S (2000). Aggregation of huntingtin in yeast varies with the length of the polyglutamine expansion and the expression of chaperone proteins. *Proc Natl Acad Sci USA*. 97, 1589-1594.

Kuhn A, Goldstein DR, Hodges A, Strand AD, Sengstag T, Kooperberg C, Becanovic K, Pouladi MA, Sathasivam K, Cha J-HJ, Hannan AJ, Hayden MR, Leavitt BR, Dunnett SB, Ferrante RJ, Albin R, Shelbourne P, Delorenzi M, Augood SJ, Faull RLM, Olson JM, Bates GP, Jones L and Luthi-Carter R (2007). Mutant huntingtin's effects on striatal gene expression in mice recapitulate changes observed in human Huntington's disease brain and do not differ with mutant huntingtin length or wild-type huntingtin dosage. *Hum Mol Genet*. 16, 1845-1861.

Laforet GA, Sapp E, Chase K, McIntyre C, Boyce FM, Campbell M, Cadigan BA, Warzecki L, Tagle DA, Reddy PH, Cepeda C, Calvert CR, Jokel ES, Klapstein GJ, Ariano MA, Levine MS, DiFiglia M and Aronin N (2001). Changes in cortical and striatal neurons predict behavioral and electrophysiological abnormalities in a transgenic murine model of Huntington's disease. *J Neuroscience*. 21, 9112-9123.

Lazic SE, Goodman AOG, Grote HE, Blakemore C, Morton AJ, Hannan AJ, van Dellen A and Barker RA (2007). Olfactory abnormalities in Huntington's disease: decreased plasticity in the primary olfactory cortex of R6/1 transgenic mice and reduced olfactory discrimination in patients. *Brain Research*. 1151, 219-226.

Lazic SE, Grote HE, Blakemore C, Hannan AJ, van Dellen A, Phillips W and Barker RA (2006). Neurogenesis in the R6/1 transgenic mouse model of Huntington's disease: effects of environmental enrichment. *Eur J Neuroscience*. 23, 1829-1838.

Leavitt BR, Guttman JA, Hodgson JG, Kimel GH, Singaraja R, Vogl AW and Hayden MR (2001). Wild-type huntingtin reduces the cellular toxicity of mutant huntingtin in vivo. *Am J Hum Genet*. 68, 313-324.

Lee IN, Chen CH, Sheu JC, Lee HS, Huang GT, Chen DS, Yu CY, Wen CL, Lu FJ and Chow LP (2006). Identification of complement C3a as a candidate biomarker in human chronic hepatitis C and HCV-related hepatocellular carcinoma using a proteomics approach. *Proteomics*. 6, 2865-2873.

Lee W-CM, Yoshihara M and Littleton JT (2004). Cytoplasmic aggregates trap polyglutamine-containing proteins and block axonal transport in a Drosophila model of Huntington's disease. *Proc Nat Acad Sci USA*. 101, 3224-3229.

Leonard JV and Schapira AH (2000a). Mitochondrial respiratory chain disorders I: mitochondrial DNA defects. *Lancet*. 355, 299-304.

Leonard JV and Schapira AH (2000b). Mitochondrial respiratory chain disorders II: neurodegenerative disorders and nuclear gene defects. *Lancet*. 355, 389-394.

Levine MS, Klapstein GJ, Koppel A, Gruen E, Cepeda C, Vargas ME, Jokel ES, Carpenter EM, Zanjani H, Hurst RS, Efstratiadis A, Zeitlin S and Chesselet MF (1999). Enhanced sensitivity to N-methyl-D-aspartate receptor activation in transgenic and knockin mouse models of Huntington's disease. *J Neurosci Res*. 58, 515-532.

Li H, Li S-H, Cheng AL, Mangiarini L, Bates GP and Li X-J (1999). Ultrastructural localization and progressive formation of neuropil aggregates in Huntington's disease transgenic mice. *Hum. Mol. Genet*. 8, 1227-1236.

Li S-H and Li X-J (2004). Huntingtin-protein interactions and the pathogenesis of Huntington's disease. *Trends Genet*. 20, 146-154.

Li SH, Lam S, Cheng AL and Li XJ (2000). Intranuclear huntingtin increases the expression of caspase-1 and induces apoptosis. *Hum Mol Genet*. 9, 2859-2867.

Li SH, Schilling G, Young WS, 3rd, Li XJ, Margolis RL, Stine OC, Wagster MV, Abbott MH, Franz ML, Ranen NG, Folstein SI, Hedreen JC and Ross CA (1993). Huntington's disease gene (IT15) is widely expressed in human and rat tissues. *Neuron*. 11, 985-993.

Li W, Serpell LC, Carter WJ, Rubinsztein DC and Huntington JA (2006). Expression and characterization of full-length human huntingtin, an elongated HEAT repeat protein. *J Biological Chemistry*. 281, 15916-15922.

Li X-J, Friedman M and Li S (2007). Interacting proteins as genetic modifiers of Huntington disease. *Trends Genet*. 23, 531-533.

Li Y, Huang TT, Carlson EJ, Melov S, Ursell PC, Olson JL, Noble LJ, Yoshimura MP, Berger C, Chan PH, Wallace DC and Epstein CJ (1995). Dilated cardiomyopathy and neonatal lethality in mutant mice lacking manganese superoxide dismutase. *Nature Genet*. 11, 376-381.

Liang CRMY, Leow CK, Neo JCH, Tan GS, Lo SL, Lim JWE, Seow TK, Lai PBS and Chung MCM (2005). Proteome analysis of human hepatocellular carcinoma tissues by two-dimensional difference gel electrophoresis and mass spectrometry. *Proteomics*. 5, 2258-2271.

Lievens J-C, Woodman B, Mahal A and Bates GP (2002). Abnormal phosphorylation of synapsin I predicts a neuronal transmission impairment in the R6/2 Huntington's disease transgenic mice. *Mol Cell Neurosci*. 20, 638-648.

Lievens JC, Woodman B, Mahal A, Spasic-Boscovic O, Samuel D, Kerkerian-Le Goff L and Bates GP (2001). Impaired glutamate uptake in the R6 Huntington's disease transgenic mice. *Neurobiol Dis*. 8, 807-821.

Lin B, Nasir J, MacDonald H, Hutchinson G, Graham RK, Rommens JM and Hayden MR (1994). Sequence of the murine Huntington disease gene: evidence for conservation, alternate splicing and polymorphism in a triplet (CCG) repeat [corrected]. *Hum Mol Genet*. 3, 85-92.

Lin B, Rommens JM, Graham RK, Kalchman M, MacDonald H, Nasir J, Delaney A, Goldberg YP and Hayden MR (1993). Differential 3' polyadenylation of the Huntington disease gene results in two mRNA species with variable tissue expression. *Hum Mol Genet*. 2, 1541-1545.

Lin CH, Tallaksen-Greene S, Chien WM, Cearley JA, Jackson WS, Crouse AB, Ren S, Li XJ, Albin RL and Detloff PJ (2001). Neurological abnormalities in a knock-in mouse model of Huntington's disease. *Hum Mol Genet*. 10, 137-144.

Liu C-S, Cheng W-L, Kuo S-J, Li J-Y, Soong B-W and Wei Y-H (2008). Depletion of mitochondrial DNA in leukocytes of patients with poly-Q diseases. J *Neurol Sci.* 264, 18-21.

Liu J, Farmer JD, Lane WS, Friedman J, Weissman I and Schreiber SL (1991). Calcineurin is a common target of cyclophilin-cyclosporin A and FKBP-FK506 complexes. *Cell.* 66, 807-815.

Lodi R, Schapira AH, Manners D, Styles P, Wood NW, Taylor DJ and Warner TT (2000). Abnormal in vivo skeletal muscle energy metabolism in Huntington's disease and dentatorubropallidoluysian atrophy. *Annals of Neurology.* 48, 72-76.

Lumsden AL, Henshall TL, Dayan S, Lardelli MT and Richards RI (2007). Huntingtin-deficient zebrafish exhibit defects in iron utilization and development. *Hum Mol Genet.* 16, 1905-1920.

Luo S, Vacher C, Davies JE and Rubinsztein DC (2005). Cdk5 phosphorylation of huntingtin reduces its cleavage by caspases: implications for mutant huntingtin toxicity. *J Cell Biol.* 169, 647-656.

Luthi-Carter R and Cha JHJ (2003). Mechanisms of transcriptional dysregulation in Huntington's disease. *Clinical Neuroscience Research.* 3, 165-177.

Luthi-Carter R, Hanson SA, Strand AD, Bergstrom DA, Chun W, Peters NL, Woods AM, Chan EY, Kooperberg C, Krainc D, Young AB, Tapscott SJ and Olson JM (2002a). Dysregulation of gene expression in the R6/2 model of polyglutamine disease: parallel changes in muscle and brain. *Hum Mol Genet.* 11, 1911-1926.

Luthi-Carter R, Strand A, Peters NL, Solano SM, Hollingsworth ZR, Menon AS, Frey AS, Spektor BS, Penney EB, Schilling G, Ross CA, Borchelt DR, Tapscott SJ, Young AB, Cha JH and Olson JM (2000). Decreased expression of striatal signaling genes in a mouse model of Huntington's disease. *Hum Mol Gen.* 9, 1259-1271.

Luthi-Carter R, Strand AD, Hanson SA, Kooperberg C, Schilling G, La Spada AR, Merry DE, Young AB, Ross CA, Borchelt DR and Olson JM (2002b). Polyglutamine and transcription: gene expression changes shared by DRPLA and Huntington's disease mouse models reveal context-independent effects. *Hum Mol Genet.* 11, 1927-1937.

Lynch G, Kramar EA, Rex CS, Jia Y, Chappas D, Gall CM and Simmons DA (2007). Brain-derived neurotrophic factor restores synaptic plasticity in a knock-in mouse model of Huntington's disease. *J Neuroscience.* 27, 4424-4434.

Macdonald V, Halliday GM, Trent RJ and McCusker EA (1997). Significant loss of pyramidal neurons in the angular gyrus of patients with Huntington's disease. *Neuropathol Appl Neurobiol.* 23, 492-495.

Majumder P, Chattopadhyay B, Mazumder A, Das P and Bhattacharyya NP (2006). Induction of apoptosis in cells expressing exogenous Hippi, a molecular partner of huntingtin-interacting protein Hip1. *Neurobiol Dis.* 22, 242-256.

Maksimovic ID, Jovanovic MD, Colic M, Mihajlovic R, Micic D, Selakovic V, Ninkovic M, Malicevic Z, Rusic-Stojiljkovic M and Jovicic A (2001). Oxidative damage and metabolic dysfunction in experimental Huntington's disease: selective vulnerability of the striatum and hippocampus. *Vojnosanit Pregl.* 58, 237-242.

Mangiarini L, Sathasivam K, Seller M, Cozens B, Harper A, Hetherington C, Lawton M, Trottier Y, Lehrach H, Davies SW and Bates GP (1996). Exon 1 of the HD gene with an expanded CAG repeat is sufficient to cause a progressive neurological phenotype in transgenic mice. *Cell.* 87, 493-506.

Manley K, Shirley TL, Flaherty L and Messer A (1999). Msh2 deficiency prevents in vivo somatic instability of the CAG repeat in Huntington disease transgenic mice. *Nature Genet.* 23, 471-473.

Martinez M, Brice A, Vaughan JR, Zimprich A, Breteler MMB, Meco G, Filla A, Farrer MJ, Betard C, Singleton A, Hardy J, De Michele G, Bonifati V, Oostra BA, Gasser T, Wood NW and Durr A (2005). Apolipoprotein E4 is probably responsible for the chromosome 19 linkage peak for Parkinson's disease. *Am J Med Genet.* Part B, Neuropsychiatric Genetics: the Official Publication of the International Society of Psychiatric Genetics. 136, 72-74.

Masterman T and Hillert J (2004). The telltale scan: APOE [var epsilon]4 in multiple sclerosis. *The Lancet Neurology.* 3, 331-331.

McDonald T, Sheng S, Stanley B, Chen D, Ko Y, Cole RN, Pedersen P and Van Eyk JE (2006). Expanding the subproteome of the inner mitochondria using protein separation technologies: one- and two-dimensional liquid chromatography and two-dimensional gel electrophoresis. *Mol & Cell Proteomics.* 5, 2392-2411.

McGuire JR, Rong J, Li S-H and Li X-J (2006). Interaction of Huntingtin-associated protein-1 with kinesin light chain: implications in intracellular trafficking in neurons. *J Biological Chemistry.* 281, 3552-3559.

McLerran D, Grizzle WE, Feng Z, Bigbee WL, Banez LL, Cazares LH, Chan DW, Diaz J, Izbicka E, Kagan J, Malehorn DE, Malik G, Oelschlager D, Partin A, Randolph T, Rosenzweig N, Srivastava S, Srivastava S, Thompson IM, Thornquist M, Troyer D, Yasui Y, Zhang Z, Zhu L and Semmes OJ (2008a). Analytical validation of serum proteomic profiling for diagnosis of prostate cancer: sources of sample bias.[see comment]. *Clin Chem.* 54, 44-52.

McLerran D, Grizzle WE, Feng Z, Thompson IM, Bigbee WL, Cazares LH, Chan DW, Dahlgren J, Diaz J, Kagan J, Lin DW, Malik G, Oelschlager D, Partin A, Randolph TW, Sokoll L, Srivastava S, Srivastava S, Thornquist M, Troyer D, Wright GL, Zhang Z, Zhu L and Semmes OJ (2008b). SELDI-TOF MS whole serum proteomic profiling with IMAC surface does not reliably detect prostate cancer.[see comment]. *Clin Chem.* 54, 53-60.

Medina L, Figueredo-Cardenas G and Reiner A (1996). Differential abundance of superoxide dismutase in interneurons versus projection neurons and in matrix versus striosome neurons in monkey striatum. *Brain Research.* 708, 59-70.

Mei J, Kolbin D, Kao HT and Porton B (2006). Protein expression profiling of postmortem brain in schizophrenia. *Schizophr Res.* 84, 204-213.

Meier-Ruge W, Iwangoff P and Reichlmeier K (1984). Neurochemical enzyme changes in Alzheimer's and Pick's disease. *Arch Gerontol Geriatr.* 3, 161-165.

Meier-Ruge W, Iwangoff P, Reichlmeier K and Sandoz P (1980). Neurochemical findings in the aging brain. *Adv Biochem Psychopharmacol.* 23, 323-338.

Meldrum A, Dunnett SB and Everitt BJ (2001). Role of corticostriatal and nigrostriatal inputs in malonate-induced striatal toxicity. *Neuroreport.* 12, 89-93.

Menalled LB (2005). Knock-in mouse models of Huntington's disease. *NeuroRx.* 2, 465-470.

Menalled LB, Sison JD, Dragatsis I, Zeitlin S and Chesselet MF (2003). Time course of early motor and neuropathological anomalies in a knock-in mouse model of Huntington's disease with 140 CAG repeats. *J Comp Neurol.* 465, 11-26.

Menalled LB, Sison JD, Wu Y, Olivieri M, Li XJ, Li H, Zeitlin S and Chesselet MF (2002). Early motor dysfunction and striosomal distribution of huntingtin microaggregates in Huntington's disease knock-in mice. *J Neuroscience.* 22, 8266-8276.

Metzger S, Bauer P, Tomiuk J, Laccone F, Didonato S, Gellera C, Soliveri P, Lange HW, Weirich-Schwaiger H, Wenning GK, Melegh B, Havasi V, Baliko L, Wieczorek S, Arning L, Zaremba J, Sulek A, Hoffman-Zacharska D, Basak AN, Ersoy N, Zidovska J, Kebrdlova V, Pandolfo M, Ribai P, Kadasi L, Kvasnicova M, Weber BHF, Kreuz F, Dose M, Stuhrmann M and Riess O (2006). The S18Y polymorphism in the UCHL1 gene is a genetic modifier in Huntington's disease. *Neurogenetics.* 7, 27-30.

Metzger S, Rong J, Nguyen H-P, Cape A, Tomiuk J, Soehn AS, Propping P, Freudenberg-Hua Y, Freudenberg J, Tong L, Li S-H, Li X-J and Riess O (2008). Huntingtin-associated protein-1 is a modifier of the age-at-onset of Huntington's disease. *Hum Mol Genet.* 17, 1137-1146.

Metzler M, Chen N, Helgason CD, Graham RK, Nichol K, McCutcheon K, Nasir J, Humphries RK, Raymond LA and Hayden MR (1999). Life without huntingtin: normal differentiation into functional neurons. *J Neurochemistry.* 72, 1009-1018.

Metzler M, Helgason CD, Dragatsis I, Zhang T, Gan L, Pineault N, Zeitlin SO, Humphries RK and Hayden MR (2000). Huntingtin is required for normal hematopoiesis. *Hum Mol Genet.* 9, 387-394.

Mijalski T, Harder A, Halder T, Kersten M, Horsch M, Strom TM, Liebscher HV, Lottspeich F, de Angelis MH and Beckers J (2005). Identification of coexpressed gene clusters in a comparative analysis of transcriptome and proteome in mouse tissues. *Proc Natl Acad Sci USA.* 102, 8621-8626.

Mitsui K, Nakayama H, Akagi T, Nekooki M, Ohtawa K, Takio K, Hashikawa T and Nukina N (2002). Purification of polyglutamine aggregates and identification of elongation factor-1alpha and heat shock protein 84 as aggregate-interacting proteins. *J Neuroscience.* 22, 9267-9277.

Mizushima N, Ohsumi Y and Yoshimori T (2002). Autophagosome formation in mammalian cells. *Cell Struct Funct.* 27, 421-429.

Molloy MP (2000). Two-dimensional electrophoresis of membrane proteins using immobilized pH gradients. *Anal Biochem.* 280, 1-10.

Montoya A, Price BH, Menear M and Lepage M (2006). Brain imaging and cognitive dysfunctions in Huntington's disease. *J Psychiatry Neurosci.* 31, 21-29.

Monzini N, Legname G, Marcucci F, Gromo G and Modena D (1994). Identification and cloning of human chaperonin 10 homologue. *Biochim Biophys Acta.* 1218, 478-480.

Morton AJ, Hunt MJ, Hodges AK, Lewis PD, Redfern AJ, Dunnett SB and Jones L (2005). A combination drug therapy improves cognition and reverses gene expression changes in a mouse model of Huntington's disease. *Eur J Neuroscience.* 21, 855-870.

Musse AA and Harauz G (2007). Molecular "negativity" may underlie multiple sclerosis: role of the myelin basic protein family in the pathogenesis of MS. *Int Rev Neurobiol.* 79, 149-172.

Myers RH, Vonsattel JP, Stevens TJ, Cupples LA, Richardson EP, Martin JB and Bird ED (1988). Clinical and neuropathologic assessment of severity in Huntington's disease. *Neurology.* 38, 341-347.

Nagata E, Sawa A, Ross CA and Snyder SH (2004). Autophagosome-like vacuole formation in Huntington's disease lymphoblasts. *Neuroreport.* 15, 1325-1328.

Narain Y, Wyttenbach A, Rankin J, Furlong RA and Rubinsztein DC (1999). A molecular investigation of true dominance in Huntington's disease. *J Med Genet.* 36, 739-746.

Nasir J, Floresco SB, O'Kusky JR, Diewert VM, Richman JM, Zeisler J, Borowski A, Marth JD, Phillips AG and Hayden MR (1995). Targeted disruption of the Huntington's disease gene results in embryonic lethality and behavioral and morphological changes in heterozygotes. *Cell.* 81, 811-823.

Naver B, Stub C, Moller M, Fenger K, Hansen AK, Hasholt L and Sorensen SA (2003). Molecular and behavioral analysis of the R6/1 Huntington's disease transgenic mouse. *Neuroscience.* 122, 1049-1057.

Naze P, Vuillaume I, Destee A, Pasquier F and Sablonniere B (2002). Mutation analysis and association studies of the ubiquitin carboxy-terminal hydrolase L1 gene in Huntington's disease. *Neuroscience Letters.* 328, 1-4.

Nicniocaill B, Haraldsson B, Hansson O, O'Connor WT and Brundin P (2001). Altered striatal amino acid neurotransmitter release monitored using microdialysis in R6/1 Huntington transgenic mice. *Eur J Neuroscience.* 13, 206-210.

Nishimori T, Tomonaga T, Matsushita K, Oh-Ishi M, Kodera Y, Maeda T, Nomura F, Matsubara H, Shimada H and Ochiai T (2006). Proteomic analysis of primary esophageal squamous cell carcinoma reveals downregulation of a cell adhesion protein, periplakin. *Proteomics.* 6, 1011-1018.

O'Farrell PH (1975). High resolution two-dimensional electrophoresis of proteins. *J Biological Chemistry.* 250, 4007-4021.

Oh-Ishi M, Satoh M and Maeda T (2000). Preparative two-dimensional gel electrophoresis with agarose gels in the first dimension for high molecular mass proteins. *Electrophoresis.* 21, 1653-1669.

Ong SE and Pandey A (2001). An evaluation of the use of two-dimensional gel electrophoresis in proteomics. *Biomol Eng.* 18, 195-205.

Orr AL, Li S, Wang C-E, Li H, Wang J, Rong J, Xu X, Mastroberardino PG, Greenamyre JT and Li X-J (2008). N-terminal mutant huntingtin associates with mitochondria and impairs mitochondrial trafficking. *J Neuroscience.* 28, 2783-2792.

Panas M, Avramopoulos D, Karadima G, Petersen MB and Vassilopoulos D (1999). Apolipoprotein E and presenilin-1 genotypes in Huntington's disease. *J Neurology.* 246, 574-577.

Pandav RS, Chandra V, Dodge HH, DeKosky ST and Ganguli M (2004). Hemoglobin levels and Alzheimer disease: an epidemiologic study in India. *Am J Geriatr Psychiatry.* 12, 523-526.

Panegyres PK, Beilby J, Bulsara M, Toufexis K and Wong C (2006). A study of potential interactive genetic factors in Huntington's disease. *Eur Neurol.* 55, 189-192.

Panov AV, Gutekunst C-A, Leavitt BR, Hayden MR, Burke JR, Strittmatter WJ and Greenamyre JT (2002). Early mitochondrial calcium defects in Huntington's disease are a direct effect of polyglutamines.[see comment]. *Nat Neurosci.* 5, 731-736.

Pardo R, Colin E, Regulier E, Aebischer P, Deglon N, Humbert S and Saudou F (2006). Inhibition of calcineurin by FK506 protects against polyglutamine-huntingtin toxicity through an increase of huntingtin phosphorylation at S421. *J Neuroscience.* 26, 1635-1645.

Parker JA, Connolly JB, Wellington C, Hayden M, Dausset J and Neri C (2001). Expanded polyglutamines in Caenorhabditis elegans cause axonal abnormalities and severe dysfunction of PLM mechanosensory neurons without cell death. *Proc Natl Acad Sci USA.* 98, 13318-13323.

Patton WF (2000). A thousand points of light: the application of fluorescence detection technologies to two-dimensional gel electrophoresis and proteomics. *Electrophoresis*. 21, 1123-1144.

Perutz MF, Johnson T, Suzuki M and Finch JT (1994). Glutamine repeats as polar zippers: their possible role in inherited neurodegenerative diseases. *Proc Natl Acad Sci USA*. 91, 5355-5358.

Petricoin EF, Ardekani AM, Hitt BA, Levine PJ, Fusaro VA, Steinberg SM, Mills GB, Simone C, Fishman DA, Kohn EC and Liotta LA (2002). Use of proteomic patterns in serum to identify ovarian cancer.[see comment]. *Lancet*. 359, 572-577.

Picariello L, Sala SC, Martineti V, Gozzini A, Aragona P, Tognarini I, Paglierani M, Nesi G, Brandi ML and Tonelli F (2006). A comparison of methods for the analysis of low abundance proteins in desmoid tumor cells. *Anal Biochem*. 354, 205-212.

Popko B, Puckett C, Lai E, Shine HD, Readhead C, Takahashi N, Hunt SW, Sidman RL and Hood L (1987). Myelin deficient mice: Expression of myelin basic protein and generation of mice with varying levels of myelin. *Cell*. 48, 713-721.

Qu Y, Adam B-L, Yasui Y, Ward MD, Cazares LH, Schellhammer PF, Feng Z, Semmes OJ and Wright GL, Jr. (2002). Boosted decision tree analysis of surface-enhanced laser desorption/ionization mass spectral serum profiles discriminates prostate cancer from noncancer patients.[see comment]. *Clin Chem*. 48, 1835-1843.

Rae C, Digney AL, McEwan SR and Bates TC (2003). Oral creatine monohydrate supplementation improves brain performance: a double-blind, placebo-controlled, cross-over trial. *Proc Biol Sci*. 270, 2147-2150.

Raha S and Robinson BH (2000). Mitochondria, oxygen free radicals, disease and ageing. *Trends Biochemical Sciences*. 25, 502-508.

Ramos-Arroyo MA, Moreno S and Valiente A (2005). Incidence and mutation rates of Huntington's disease in Spain: experience of 9 years of direct genetic testing. *J Neurol Neurosurg Psychiatry*. 76, 337-342.

Ranen NG, Stine OC, Abbott MH, Sherr M, Codori AM, Franz ML, Chao NI, Chung AS, Pleasant N, Callahan C, Kasch LM, Ghaffari M, Chase GA, Kazazian HH, Brandt J, Folstein SE and Ross CA (1995). Anticipation and instability of IT-15 (CAG)n repeats in parent-offspring pairs with Huntington disease. *Am J Hum Genet*. 57, 593-602.

Ratovitski T, Nakamura M, D'Ambola J, Chighladze E, Liang Y, Wang W, Graham R, Hayden MR, Borchelt DR, Hirschhorn RR and Ross CA (2007). N-terminal proteolysis of full-length mutant huntingtin in an inducible PC12 cell model of Huntington's disease. *Cell Cycle.* 6, 2970-2981.

Ravikumar B, Acevedo-Arozena A, Imarisio S, Berger Z, Vacher C, O'Kane CJ, Brown SDM and Rubinsztein DC (2005). Dynein mutations impair autophagic clearance of aggregate-prone proteins. *Nature Genet.* 37, 771-776.

Reddy PH, Williams M, Charles V, Garrett L, Pike-Buchanan L, Whetsell WO, Jr., Miller G and Tagle DA (1998). Behavioural abnormalities and selective neuronal loss in HD transgenic mice expressing mutated full-length HD cDNA. *Nature Genet.* 20, 198-202.

Regulier E, Trottier Y, Perrin V, Aebischer P and Deglon N (2003). Early and reversible neuropathology induced by tetracycline-regulated lentiviral overexpression of mutant huntingtin in rat striatum. *Hum Mol Genet.* 12, 2827-2836.

Reiner A, Del Mar N, Meade CA, Yang H, Dragatsis I, Zeitlin S and Goldowitz D (2001). Neurons lacking huntingtin differentially colonize brain and survive in chimeric mice. *J Neuroscience.* 21, 7608-7619.

Reiner A, Dragatsis I, Zeitlin S and Goldowitz D (2003). Wild-type huntingtin plays a role in brain development and neuronal survival. *Mol Neurobiol.* 28, 259-276.

Richter-Landsberg C (2008). The cytoskeleton in oligodendrocytes. Microtubule dynamics in health and disease. *J Mol Neurosci.* 35, 55-63.

Rigamonti D, Bauer JH, De-Fraja C, Conti L, Sipione S, Sciorati C, Clementi E, Hackam A, Hayden MR, Li Y, Cooper JK, Ross CA, Govoni S, Vincenz C and Cattaneo E (2000). Wild-type huntingtin protects from apoptosis upstream of caspase-3. *J Neurosci.* 20, 3705-3713.

Rigamonti D, Sipione S, Goffredo D, Zuccato C, Fossale E and Cattaneo E (2001). Huntingtin's neuroprotective activity occurs via inhibition of procaspase-9 processing. *J Biological Chemistry.* 276, 14545-14548.

Rosenblatt A, Brinkman RR, Liang KY, Almqvist EW, Margolis RL, Huang CY, Sherr M, Franz ML, Abbott MH, Hayden MR and Ross CA (2001). Familial influence on age of onset among siblings with Huntington disease. *Am.J.Med.Genet.* 105, 399-403.

Rubin CI and Atweh GF (2004). The role of stathmin in the regulation of the cell cycle. *J Cell Biochem.* 93, 242-250.

Rubinsztein DC, Leggo J, Chiano M, Dodge A, Norbury G, Rosser E and Craufurd D (1997). Genotypes at the GluR6 kainate receptor locus are associated with variation in the age of onset of Huntington disease. *Proc Natl Acad Sci USA.* 94, 3872-3876.

Rubinsztein DC, Leggo J, Coles R, Almqvist E, Biancalana V, Cassiman JJ, Chotai K, Connarty M, Crauford D, Curtis A, Curtis D, Davidson MJ, Differ AM, Dode C, Dodge A, Frontali M, Ranen NG, Stine OC, Sherr M, Abbott MH, Franz ML, Graham CA, Harper PS, Hedreen JC, Jackson A, Kaplan J-C, Losekoot M, MaCMillan JC, Morrison P, Trottier Y, Novelletto A, Simpson SA, Theilmann J, Whittaker JL, Folstein SE, Ross CA and Hayden MR. (1996). Phenotypic characterization of individuals with 30-40 CAG repeats in the Huntington disease (HD) gene reveals HD cases with 36 repeats and apparently normal elderly individuals with 36-39 repeats. *Am J Hum Genet.* 59, 16-22.

Ruocco HH, Bonilha L, Li LM, Lopes-Cendes I and Cendes F (2008). Longitudinal analysis of regional grey matter loss in Huntington disease: effects of the length of the expanded CAG repeat. *J Neurol Neurosurg Psychiatry.* 79, 130-135.

Sadri-Vakili G and Cha J-HJ (2006a). Histone deacetylase inhibitors: a novel therapeutic approach to Huntington's disease (complex mechanism of neuronal death). *Curr Alzheimer Res.* 3, 403-408.

Sadri-Vakili G and Cha J-HJ (2006b). Mechanisms of disease: Histone modifications in Huntington's disease. *Nat Clin Pract Neurol.* 2, 330-338.

Saft C, Andrich JE, Brune N, Gencik M, Kraus PH, Przuntek H and Epplen JT (2004). Apolipoprotein E genotypes do not influence the age of onset in Huntington's disease. *J Neurol Neurosurg Psychiatry.* 75, 1692-1696.

Saft C, Zange J, Andrich J, Muller K, Lindenberg K, Landwehrmeyer B, Vorgerd M, Kraus PH, Przuntek H and Schols L (2005). Mitochondrial impairment in patients and asymptomatic mutation carriers of Huntington's disease. *Mov Disord.* 20, 674-679.

Sanchez-Pernaute R, Garcia-Segura JM, del Barrio Alba A, Viano J and de Yebenes JG (1999). Clinical correlation of striatal 1H MRS changes in Huntington's disease. *Neurology.* 53, 806-812.

Santamaria A, Perez-Severiano F, Rodriguez-Martinez E, Maldonado PD, Pedraza-Chaverri J, Rios C and Segovia J (2001). Comparative analysis of superoxide dismutase activity between acute pharmacological models and a transgenic mouse model of Huntington's disease. *Neurochem Res.* 26, 419-424.

Santoni V, Kieffer S, Desclaux D, Masson F and Rabilloud T (2000a). Membrane proteomics: use of additive main effects with multiplicative interaction model to classify plasma membrane proteins according to their solubility and electrophoretic properties. *Electrophoresis.* 21, 3329-3344.

Santoni V, Molloy M and Rabilloud T (2000b). Membrane proteins and proteomics: un amour impossible? *Electrophoresis.* 21, 1054-1070.

Sathasivam K, Hobbs C, Mangiarini L, Mahal A, Turmaine M, Doherty P, Davies SW and Bates GP (1999). Transgenic models of Huntington's disease. *Philos Trans R Soc Lond B Biol Sci.* 354, 963-969.

Saudou F, Finkbeiner S, Devys D and Greenberg ME (1998). Huntingtin acts in the nucleus to induce apoptosis but death does not correlate with the formation of intranuclear inclusions. *Cell.* 95, 55-66.

Schilling B, Gafni J, Torcassi C, Cong X, Row RH, LaFevre-Bernt MA, Cusack MP, Ratovitski T, Hirschhorn R, Ross CA, Gibson BW and Ellerby LM (2006). Huntingtin phosphorylation sites mapped by mass spectrometry. Modulation of cleavage and toxicity. *J Biological Chemistry.* 281, 23686-23697.

Schilling G, Becher MW, Sharp AH, Jinnah HA, Duan K, Kotzuk JA, Slunt HH, Ratovitski T, Cooper JK, Jenkins NA, Copeland NG, Price DL, Ross CA and Borchelt DR (1999). Intranuclear inclusions and neuritic aggregates in transgenic mice expressing a mutant N-terminal fragment of huntingtin. *Hum Mol Genet.* 8, 397-407.

Schwarcz R, Whetsell WO, Jr. and Mangano RM (1983). Quinolinic acid: an endogenous metabolite that produces axon-sparing lesions in rat brain. *Science.* 219, 316-318.

Selicharova I, Smutna K, Sanda M, Ubik K, Matouskova E, Bursikova E, Brozova M, Vydra J and Jiracek J (2007). 2-DE analysis of a new human cell line EM-G3 derived from breast cancer progenitor cells and comparison with normal mammary epithelial cells. *Proteomics.* 7, 1549-1559.

Semmes OJ, Feng Z, Adam B-L, Banez LL, Bigbee WL, Campos D, Cazares LH, Chan DW, Grizzle WE, Izbicka E, Kagan J, Malik G, McLerran D, Moul JW, Partin A, Prasanna P, Rosenzweig J, Sokoll LJ, Srivastava S, Srivastava S, Thompson I, Welsh MJ, White N, Winget M, Yasui Y, Zhang Z and Zhu L (2005). Evaluation of serum protein profiling by surface-enhanced laser desorption/ionization time-of-flight mass spectrometry for the detection of prostate cancer: I. Assessment of platform reproducibility.[see comment]. *Clin Chem.* 51, 102-112.

Seo H, Sonntag K-C and Isacson O (2004). Generalized brain and skin proteasome inhibition in Huntington's disease.[see comment]. *Annals of Neurology.* 56, 319-328.

Seong IS, Ivanova E, Lee J-M, Choo YS, Fossale E, Anderson M, Gusella JF, Laramie JM, Myers RH, Lesort M and MacDonald ME (2005). HD CAG repeat implicates a dominant property of huntingtin in mitochondrial energy metabolism. *Hum Mol Genet.* 14, 2871-2880.

Sharp AH, Loev SJ, Schilling G, Li SH, Li XJ, Bao J, Wagster MV, Kotzuk JA, Steiner JP, Lo A, Hedreen J, Sisodia S, Snyder SH, Dawson TM, Ryugo DK, and Ross CA (1995). Widespread expression of Huntington's disease gene (IT15) protein product. *Neuron.* 14, 1065-1074.

Shelbourne PF, Killeen N, Hevner RF, Johnston HM, Tecott L, Lewandoski M, Ennis M, Ramirez L, Li Z, Iannicola C, Littman DR and Myers RM (1999). A Huntington's disease CAG expansion at the murine Hdh locus is unstable and associated with behavioural abnormalities in mice. *Hum Mol Genet.* 8, 763-774.

Sieradzan KA and Mann DM (2001). The selective vulnerability of nerve cells in Huntington's disease. *Neuropathol Appl Neurobiol.* 27, 1-21.

Siesling S, Vegter-van de Vlis M, Losekoot M, Belfroid RD, Maat-Kievit JA, Kremer HP and Roos RA (2000). Family history and DNA analysis in patients with suspected Huntington's disease. *J Neurol Neurosurg Psychiatry.* 69, 54-59.

Sittler A, Lurz R, Lueder G, Priller J, Lehrach H, Hayer-Hartl MK, Hartl FU and Wanker EE (2001). Geldanamycin activates a heat shock response and inhibits huntingtin aggregation in a cell culture model of Huntington's disease.[erratum appears in Hum Mol Genet 2001 Aug 1;10(16):1719]. *Hum Mol Genet.* 10, 1307-1315.

Slemmon JR, Hughes CM, Campbell GA and Flood DG (1994). Increased levels of hemoglobin-derived and other peptides in Alzheimer's disease cerebellum. *J Neuroscience*. 14, 2225-2235.

Slow EJ, Graham RK, Osmand AP, Devon RS, Lu G, Deng Y, Pearson J, Vaid K, Bissada N, Wetzel R, Leavitt BR and Hayden MR (2005). Absence of behavioral abnormalities and neurodegeneration in vivo despite widespread neuronal huntingtin inclusions. *Proc Natl Acad Sci USA*. 102, 11402-11407.

Slow EJ, van Raamsdonk J, Rogers D, Coleman SH, Graham RK, Deng Y, Oh R, Bissada N, Hossain SM, Yang YZ, Li XJ, Simpson EM, Gutekunst CA, Leavitt BR and Hayden MR (2003). Selective striatal neuronal loss in a YAC128 mouse model of Huntington disease. *Hum Mol Genet*. 12, 1555-1567.

Smith KM, Matson S, Matson WR, Cormier K, Del Signore SJ, Hagerty SW, Stack EC, Ryu H and Ferrante RJ (2006). Dose ranging and efficacy study of high-dose coenzyme Q10 formulations in Huntington's disease mice. *Biochimica et Biophysica Acta*. 1762, 616-626.

Smith R, Brundin P and Li JY (2005). Synaptic dysfunction in Huntington's disease: a new perspective. *Cell Mol Life Sci*. 62, 1901-1912.

Snell RG, MacMillan JC, Cheadle JP, Fenton I, Lazarou LP, Davies P, MacDonald ME, Gusella JF, Harper PS and Shaw DJ (1993). Relationship between trinucleotide repeat expansion and phenotypic variation in Huntington's disease.[see comment]. *Nature Genet*. 4, 393-397.

Somiari RI, Sullivan A, Russell S, Somiari S, Hu H, Jordan R, George A, Katenhusen R, Buchowiecka A, Arciero C, Brzeski H, Hooke J and Shriver C (2003). High-throughput proteomic analysis of human infiltrating ductal carcinoma of the breast. *Proteomics*. 3, 1863-1873.

Sotrel A, Paskevich PA, Kiely DK, Bird ED, Williams RS and Myers RH (1991). Morphometric analysis of the prefrontal cortex in Huntington's disease. *Neurology*. 41, 1117-1123.

Sowell J, Strekowski L and Patonay G (2002). DNA and protein applications of near-infrared dyes. *J Biomed Opt*. 7, 571-575.

Spargo E, Everall IP and Lantos PL (1993). Neuronal loss in the hippocampus in Huntington's disease: a comparison with HIV infection. *J Neurol Neurosurg Psychiatry*. 56, 487-491.

Spires TL, Grote HE, Garry S, Cordery PM, Van Dellen A, Blakemore C and Hannan AJ (2004a). Dendritic spine pathology and deficits in experience-dependent dendritic plasticity in R6/1 Huntington's disease transgenic mice. *Eur J Neuroscience*. 19, 2799-2807.

Spires TL, Grote HE, Varshney NK, Cordery PM, van Dellen A, Blakemore C and Hannan AJ (2004b). Environmental enrichment rescues protein deficits in a mouse model of Huntington's disease, indicating a possible disease mechanism. *J Neuroscience*. 24, 2270-2276.

Squitieri F, Cannella M, Sgarbi G, Maglione V, Falleni A, Lenzi P, Baracca A, Cislaghi G, Saft C, Ragona G, Russo MA, Thompson LM, Solaini G and Fornai F (2006). Severe ultrastructural mitochondrial changes in lymphoblasts homozygous for Huntington disease mutation. *Mech Ageing Dev*. 127, 217-220.

Stack EC, Dedeoglu A, Smith KM, Cormier K, Kubilus JK, Bogdanov M, Matson WR, Yang L, Jenkins BG, Luthi-Carter R, Kowall NW, Hersch SM, Beal MF and Ferrante RJ (2007). Neuroprotective effects of synaptic modulation in Huntington's disease R6/2 mice. *J Neuroscience*. 27, 12908-12915.

Stack EC, Smith KM, Ryu H, Cormier K, Chen M, Hagerty SW, Del Signore SJ, Cudkowicz ME, Friedlander RM and Ferrante RJ (2006). Combination therapy using minocycline and coenzyme Q10 in R6/2 transgenic Huntington's disease mice. *Biochimica et Biophysica Acta*. 1762, 373-380.

Steffan JS, Agrawal N, Pallos J, Rockabrand E, Trotman LC, Slepko N, Illes K, Lukacsovich T, Zhu YZ, Cattaneo E, Pandolfi PP, Thompson LM and Marsh JL (2004). SUMO modification of Huntingtin and Huntington's disease pathology. *Science*. 304, 100-104.

Steffan JS, Bodai L, Pallos J, Poelman M, McCampbell A, Apostol BL, Kazantsev A, Schmidt E, Zhu YZ, Greenwald M, Kurokawa R, Housman DE, Jackson GR, Marsh JL and Thompson LM (2001). Histone deacetylase inhibitors arrest polyglutamine-dependent neurodegeneration in Drosophila.[see comment]. *Nature*. 413, 739-743.

Steiner JP, Connolly MA, Valentine HL, Hamilton GS, Dawson TM, Hester L and Snyder SH (1997). Neurotrophic actions of nonimmunosuppressive analogues of immunosuppressive drugs FK506, rapamycin and cyclosporin A. *Nat Med.* 3, 421-428.

Strand AD, Aragaki AK, Shaw D, Bird T, Holton J, Turner C, Tapscott SJ, Tabrizi SJ, Schapira AH, Kooperberg C and Olson JM (2005). Gene expression in Huntington's disease skeletal muscle: a potential biomarker. *Hum Mol Genet*. 14, 1863-1876.

Strand AD, Baquet ZC, Aragaki AK, Holmans P, Yang L, Cleren C, Beal MF, Jones L, Kooperberg C, Olson JM and Jones KR (2007). Expression profiling of Huntington's disease models suggests that brain-derived neurotrophic factor depletion plays a major role in striatal degeneration. *J Neuroscience*. 27, 11758-11768.

Strong TV, Tagle DA, Valdes JM, Elmer LW, Boehm K, Swaroop M, Kaatz KW, Collins FS and Albin RL (1993). Widespread expression of the human and rat Huntington's disease gene in brain and nonneural tissues. *Nature Genet*. 5, 259-265.

Sultana R, Boyd-Kimball D, Cai J, Pierce WM, Klein JB, Merchant M and Butterfield DA (2007). Proteomics analysis of the Alzheimer's disease hippocampal proteome. *J Alzheimers Dis*. 11, 153-164.

Sultana R, Boyd-Kimball D, Poon HF, Cai J, Pierce WM, Klein JB, Merchant M, Markesbery WR and Butterfield DA (2006). Redox proteomics identification of oxidized proteins in Alzheimer's disease hippocampus and cerebellum: an approach to understand pathological and biochemical alterations in AD. *Neurobiol Aging*. 27, 1564-1576.

Sun M-K and Alkon DL (2002). Carbonic anhydrase gating of attention: memory therapy and enhancement. *Trends Pharmacol Sci*. 23, 83-89.

Sun X-J, Wei J, Wu X-Y, Hu M, Wang L, Wang H-H, Zhang Q-H, Chen S-J, Huang Q-H and Chen Z (2005). Identification and characterization of a novel human histone H3 lysine 36-specific methyltransferase. *J Biological Chemistry*. 280, 35261-35271.

Sun Y, Savanenin A, Reddy PH and Liu YF (2001). Polyglutamine-expanded huntingtin promotes sensitization of N-methyl-D-aspartate receptors via post-synaptic density 95. *J Biological Chemistry*. 276, 24713-24718.

Swatton JE, Prabakaran S, Karp NA, Lilley KS and Bahn S (2004). Protein profiling of human postmortem brain using 2-dimensional fluorescence difference gel electrophoresis (2-D DIGE). *Mol Psychiatry*. 9, 128-143.

Tabrizi SJ, Workman J, Hart PE, Mangiarini L, Mahal A, Bates G, Cooper JM and Schapira AH (2000). Mitochondrial dysfunction and free radical damage in the Huntington R6/2 transgenic mouse. *Annals of Neurology*. 47, 80-86.

Tallaksen-Greene SJ, Crouse AB, Hunter JM, Detloff PJ and Albin RL (2005). Neuronal intranuclear inclusions and neuropil aggregates in HdhCAG(150) knockin mice. *Neuroscience*. 131, 843-852.

Tang T-S, Chen X, Liu J and Bezprozvanny I (2007). Dopaminergic signaling and striatal neurodegeneration in Huntington's disease. J Neuroscience. 27, 7899-7910.

Tang T-S, Slow E, Lupu V, Stavrovskaya IG, Sugimori M, Llinas R, Kristal BS, Hayden MR and Bezprozvanny I (2005). Disturbed Ca2+ signaling and apoptosis of medium spiny neurons in Huntington's disease. Proc Natl Acad Sci USA. 102, 2602-2607.

Tao T and Tartakoff AM (2001). Nuclear relocation of normal huntingtin. *Traffic.* 2, 385-394.

Taylor JP, Hardy J and Fischbeck KH (2002). Toxic proteins in neurodegenerative disease. *Science.* 296, 1991-1995.

Telenius H, Kremer HP, Theilmann J, Andrew SE, Almqvist E, Anvret M, Greenberg C, Greenberg J, Lucotte G, Squitieri F, Starr E, Goldberg YP and Hayden MR (1993). Molecular analysis of juvenile Huntington disease: the major influence on (CAG)n repeat length is the sex of the affected parent. *Hum Mol Genet.* 2, 1535-1540.

Trueman RC, Brooks SP, Jones L and Dunnett SB (2007). The operant serial implicit learning task reveals early onset motor learning deficits in the Hdh knock-in mouse model of Huntington's disease. *Eur J Neuroscience.* 25, 551-558.

Trueman RC, Brooks SP, Jones L and Dunnett SB (2008). Time course of choice reaction time deficits in the Hdh(Q92) knock-in mouse model of Huntington's disease in the operant Serial Implicit Learning Task (SILT). *Behav Brain Res.* 189, 317-324.

Trushina E, Dyer RB, Badger JD, 2nd, Ure D, Eide L, Tran DD, Vrieze BT, Legendre-Guillemin V, McPherson PS, Mandavilli BS, Van Houten B, Zeitlin S, McNiven M, Aebersold R, Hayden M, Parisi JE, Seeberg E, Dragatsis I, Doyle K, Bender A, Chacko C and McMurray CT (2004). Mutant huntingtin impairs axonal trafficking in mammalian neurons in vivo and in vitro. *Mol Cell Biol.* 24, 8195-8209.

Turmaine M, Raza A, Mahal A, Mangiarini L, Bates GP and Davies SW (2000). Nonapoptotic neurodegeneration in a transgenic mouse model of Huntington's disease. Proc Natl Acad Sci USA. 97, 8093-8097.

Turner C, Cooper JM and Schapira AHV (2007). Clinical correlates of mitochondrial function in Huntington's disease muscle. *Mov Disord.* 22, 1715-1721.

Unlu M, Morgan ME and Minden JS (1997). Difference gel electrophoresis: a single gel method for detecting changes in protein extracts. *Electrophoresis*. 18, 2071-2077.

van Dellen A, Blakemore C, Deacon R, York D and Hannan AJ (2000). Delaying the onset of Huntington's in mice. *Nature*. 404, 721-722.

van Dellen A, Cordery PM, Spires TL, Blakemore C and Hannan AJ (2008). Wheel running from a juvenile age delays onset of specific motor deficits but does not alter protein aggregate density in a mouse model of Huntington's disease. *BMC Neurosci*. 9, 34.

Van Raamsdonk JM, Pearson J, Slow EJ, Hossain SM, Leavitt BR and Hayden MR (2005). Cognitive dysfunction precedes neuropathology and motor abnormalities in the YAC128 mouse model of Huntington's disease. *J Neuroscience*. 25, 4169-4180.

Veenstra TD, Prieto DA and Conrads TP (2004). Proteomic patterns for early cancer detection. *Drug Discov Today*. 9, 889-897.

Vlkolinsky R, Cairns N, Fountoulakis M and Lubec G (2001). Decreased brain levels of 2',3'-cyclic nucleotide-3'-phosphodiesterase in Down syndrome and Alzheimer's disease. *Neurobiol Aging*. 22, 547-553.

von Horsten S, Schmitt I, Nguyen HP, Holzmann C, Schmidt T, Walther T, Bader M, Pabst R, Kobbe P, Krotova J, Stiller D, Kask A, Vaarmann A, Rathke-Hartlieb S, Schulz JB, Grasshoff U, Bauer I, Vieira-Saecker AM, Paul M, Jones L, Lindenberg KS, Landwehrmeyer B, Bauer A, Li XJ and Riess O (2003). Transgenic rat model of Huntington's disease. *Hum Mol Genet*. 12, 617-624.

Vonsattel JP and DiFiglia M (1998). Huntington disease. *J Neuropathol Exp Neurol*. 57, 369-384.

Vonsattel JP, Myers RH, Stevens TJ, Ferrante RJ, Bird ED and Richardson EP, Jr. (1985). Neuropathological classification of Huntington's disease. *J Neuropathol Exp Neurol*. 44, 559-577.

Waelter S, Boeddrich A, Lurz R, Scherzinger E, Lueder G, Lehrach H and Wanker EE (2001). Accumulation of mutant huntingtin fragments in aggresome-like inclusion bodies as a result of insufficient protein degradation. *Mol Biol Cell*. 12, 1393-1407.

Wan J, Sun W, Li X, Ying W, Dai J, Kuai X, Wei H, Gao X, Zhu Y, Jiang Y, Qian X and He F (2006). Inflammation inhibitors were remarkably up-regulated in plasma of severe acute respiratory syndrome patients at progressive phase. *Proteomics*. 6, 2886-2894.

Wang X, Zhu S, Drozda M, Zhang W, Stavrovskaya IG, Cattaneo E, Ferrante RJ, Kristal BS and Friedlander RM (2003). Minocycline inhibits caspase-independent and -dependent mitochondrial cell death pathways in models of Huntington's disease. *Proc Natl Acad Sci USA*. 100, 10483-10487.

Wanker E and Droge A (2002). Structural biology of Huntington's disease. In Huntington's disease. (GP Bates, H P.S., AL Jones, eds). London: Oxford Univerity Press, pp. 327-347.

Wanker EE, Rovira C, Scherzinger E, Hasenbank R, Walter S, Tait D, Colicelli J and Lehrach H (1997). HIP-I: a huntingtin interacting protein isolated by the yeast two-hybrid system. *Hum Mol Genet*. 6, 487-495.

Warby SC, Doty CN, Graham RK, Carroll JB, Yang Y-Z, Singaraja RR, Overall CM and Hayden MR (2008). Activated caspase-6 and caspase-6-cleaved fragments of huntingtin specifically colocalize in the nucleus. *Hum Mol Genet*. 17, 2390-2404.

Weeks RA, Piccini P, Harding AE and Brooks DJ (1996). Striatal D1 and D2 dopamine receptor loss in asymptomatic mutation carriers of Huntington's disease. *Annals of Neurology*. 40, 49-54.

Welin J, Wilkins JC, Beighton D and Svensater G (2004). Protein Expression by Streptococcus mutans during Initial Stage of Biofilm Formation. *Appl. Environ. Microbiol.* 70, 3736-3741.

Wellington CL, Ellerby LM, Gutekunst C-A, Rogers D, Warby S, Graham RK, Loubser O, van Raamsdonk J, Singaraja R, Yang Y-Z, Gafni J, Bredesen D, Hersch SM, Leavitt BR, Roy S, Nicholson DW and Hayden MR (2002). Caspase cleavage of mutant huntingtin precedes neurodegeneration in Huntington's disease. *J Neuroscience*. 22, 7862-7872.

Wellington CL, Ellerby LM, Hackam AS, Margolis RL, Trifiro MA, Singaraja R, McCutcheon K, Salvesen GS, Propp SS, Bromm M, Rowland KJ, Zhang T, Rasper D, Roy S, Thornberry N, Pinsky L, Kakizuka A, Ross CA, Nicholson DW, Bredesen DE and Hayden MR (1998). Caspase cleavage of gene products associated with triplet expansion disorders generates truncated fragments containing the polyglutamine tract. *J Biological Chemistry*. 273, 9158-9167.

Wellington CL, Singaraja R, Ellerby L, Savill J, Roy S, Leavitt B, Cattaneo E, Hackam A, Sharp A, Thornberry N, Nicholson DW, Bredesen DE and Hayden MR (2000). Inhibiting caspase cleavage of huntingtin reduces toxicity and aggregate formation in neuronal and nonneuronal cells. *J Biological Chemistry.* 275, 19831-19838.

Weydt P, Pineda VV, Torrence AE, Libby RT, Satterfield TF, Lazarowski ER, Gilbert ML, Morton GJ, Bammler TK, Strand AD, Cui L, Beyer RP, Easley CN, Smith AC, Krainc D, Luquet S, Sweet IR, Schwartz MW and La Spada AR (2006). Thermoregulatory and metabolic defects in Huntington's disease transgenic mice implicate PGC-1alpha in Huntington's disease neurodegeneration. *Cell Metab.* 4, 349-362.

Wheeler VC, Auerbach W, White JK, Srinidhi J, Auerbach A, Ryan A, Duyao MP, Vrbanac V, Weaver M, Gusella JF, Joyner AL and MacDonald ME (1999). Length-dependent gametic CAG repeat instability in the Huntington's disease knock-in mouse. *Hum Mol Genet.* 8, 115-122.

Wheeler VC, Gutekunst C-A, Vrbanac V, Lebel L-A, Schilling G, Hersch S, Friedlander RM, Gusella JF, Vonsattel J-P, Borchelt DR and MacDonald ME (2002). Early phenotypes that presage late-onset neurodegenerative disease allow testing of modifiers in Hdh CAG knock-in mice. *Hum Mol Genet.* 11, 633-640.

Wheeler VC, White JK, Gutekunst CA, Vrbanac V, Weaver M, Li XJ, Li SH, Yi H, Vonsattel JP, Gusella JF, Hersch S, Auerbach W, Joyner AL and MacDonald ME (2000). Long glutamine tracts cause nuclear localization of a novel form of huntingtin in medium spiny striatal neurons in HdhQ92 and HdhQ111 knock-in mice. *Hum Mol Genet.* 9, 503-513.

White JK, Auerbach W, Duyao MP, Vonsattel JP, Gusella JF, Joyner AL and MacDonald ME (1997). Huntingtin is required for neurogenesis and is not impaired by the Huntington's disease CAG expansion. *Nature Genet.* 17, 404-410.

Wong-Riley MT (1989). Cytochrome oxidase: an endogenous metabolic marker for neuronal activity. *Trends in Neurosciences.* 12, 94-101.

Wood JD, MacMillan JC, Harper PS, Lowenstein PR and Jones AL (1996). Partial characterisation of murine huntingtin and apparent variations in the subcellular localisation of huntingtin in human, mouse and rat brain. *Hum Mol Genet.* 5, 481-487.

Woodman B, Butler R, Landles C, Lupton MK, Tse J, Hockly E, Moffitt H, Sathasivam K and Bates GP (2007). The Hdh(Q150/Q150) knock-in mouse model of HD and the R6/2 exon 1 model develop comparable and widespread molecular phenotypes. *Brain Res Bull.* 72, 83-97.

Wu D, Tomonaga T, Sogawa K, Satoh M, Sunaga M, Nezu M, Oh-Ishi M, Kodera Y, Maeda T, Ochiai T and Nomura F (2007). Detection of biomarkers for alcoholism by two-dimensional differential gel electrophoresis. *Alcohol Clin Exp Res.* 31, S67-71.

Xia J, Lee DH, Taylor J, Vandelft M and Truant R (2003). Huntingtin contains a highly conserved nuclear export signal. *Hum Mol Genet.* 12, 1393-1403.

Xifro X, Garcia-Martinez JM, Del Toro D, Alberch J and Perez-Navarro E (2008). Calcineurin is involved in the early activation of NMDA-mediated cell death in mutant huntingtin knock-in striatal cells. J Neurochemistry. 105, 1596-1612.

Yamamoto A, Lucas JJ and Hen R (2000). Reversal of neuropathology and motor dysfunction in a conditional model of Huntington's disease. *Cell.* 101, 57-66.

Yamanaka T, Miyazaki H, Oyama F, Kurosawa M, Washizu C, Doi H and Nukina N (2008). Mutant Huntingtin reduces HSP70 expression through the sequestration of NF-Y transcription factor. *Embo J.* 27, 827-839.

Yang S-H, Cheng P-H, Banta H, Piotrowska-Nitsche K, Yang J-J, Cheng ECH, Snyder B, Larkin K, Liu J, Orkin J, Fang Z-H, Smith Y, Bachevalier J, Zola SM, Li S-H, Li X-J and Chan AWS (2008). Towards a transgenic model of Huntington's disease in a non-human primate.[see comment]. *Nature.* 453, 921-924.

Yu KH, Rustgi AK and Blair IA (2005). Characterization of proteins in human pancreatic cancer serum using differential gel electrophoresis and tandem mass spectrometry. *J Proteome Res.* 4, 1742-1751.

Yu Z-X, Li S-H, Evans J, Pillarisetti A, Li H and Li X-J (2003). Mutant huntingtin causes context-dependent neurodegeneration in mice with Huntington's disease. *J Neuroscience.* 23, 2193-2202.

Zabel C, Chamrad DC, Priller J, Woodman B, Meyer HE, Bates GP and Klose J (2002). Alterations in the mouse and human proteome caused by Huntington's disease. *Mol Cell Proteomics.* 1, 366-375.

Zainelli GM, Ross CA, Troncoso JC, Fitzgerald JK and Muma NA (2004). Calmodulin regulates transglutaminase 2 cross-linking of huntingtin. *J Neuroscience.* 24, 1954-1961.

Zeitlin S, Liu JP, Chapman DL, Papaioannou VE and Efstratiadis A (1995). Increased apoptosis and early embryonic lethality in mice nullizygous for the Huntington's disease gene homologue. *Nature Genet.* 11, 155-163.

Zeron MM, Chen N, Moshaver A, Lee AT, Wellington CL, Hayden MR and Raymond LA (2001). Mutant huntingtin enhances excitotoxic cell death. *Mol Cell Neurosci.* 17, 41-53.

Zeron MM, Hansson O, Chen N, Wellington CL, Leavitt BR, Brundin P, Hayden MR and Raymond LA (2002). Increased sensitivity to N-methyl-D-aspartate receptor-mediated excitotoxicity in a mouse model of Huntington's disease.[see comment]. *Neuron.* 33, 849-860.

Zhang Y, Leavitt BR, van Raamsdonk JM, Dragatsis I, Goldowitz D, MacDonald ME, Hayden MR and Friedlander RM (2006). Huntingtin inhibits caspase-3 activation. *Embo J.* 25, 5896-5906.

Zourlidou A, Gidalevitz T, Kristiansen M, Landles C, Woodman B, Wells DJ, Latchman DS, de Belleroche J, Tabrizi SJ, Morimoto RI and Bates GP (2007). Hsp27 overexpression in the R6/2 mouse model of Huntington's disease: chronic neurodegeneration does not induce Hsp27 activation. *Hum Mol Genet.* 16, 1078-1090.

Zuccato C and Cattaneo E (2007). Role of brain-derived neurotrophic factor in Huntington's disease. *Prog Neurobiol.* 81, 294-330.

Zuccato C, Ciammola A, Rigamonti D, Leavitt BR, Goffredo D, Conti L, MacDonald ME, Friedlander RM, Silani V, Hayden MR, Timmusk T, Sipione S and Cattaneo E (2001). Loss of huntingtin-mediated BDNF gene transcription in Huntington's disease.[see comment]. *Science.* 293, 493-498.

Zuccato C, Tartari M, Crotti A, Goffredo D, Valenza M, Conti L, Cataudella T, Leavitt BR, Hayden MR, Timmusk T, Rigamonti D and Cattaneo E (2003). Huntingtin interacts with REST/NRSF to modulate the transcription of NRSE-controlled neuronal genes.[see comment]. *Nature Genet.* 35, 76-83.

Zucker B, Luthi-Carter R, Kama JA, Dunah AW, Stern EA, Fox JH, Standaert DG, Young AB and Augood SJ (2005). Transcriptional dysregulation in striatal projection- and interneurons in a mouse model of Huntington's disease: neuronal selectivity and potential neuroprotective role of HAP1. *Hum Mol Genet.* 14, 179-189.